CRANFIELD UNIVERSITY

SCHOOL OF INDUSTRIAL AND MANUFACTURING SCIENCE

PhD THESIS

Academic Year 1998-9

S.A.WILSON

ELECTRIC-FIELD STRUCTURING OF PIEZOELECTRIC COMPOSITE MATERIALS

Supervisor: PROFESSOR R.W.WHATMORE

September 1999

Abstract

Piezoelectric composite materials, consisting of a ferroelectric ceramic in an electrically-inactive polymer matrix, have been shown to greatly outperform single phase materials for certain applications. A new assembly technique, which electrically controls the spatial distribution of the ceramic within the polymer, promises to enhance the sensitivity of 0-3 type piezoelectric composites. The materials so-produced have a quasi 1-3 structure and it is intended that they will exhibit some of the advantages of 1-3 piezoelectric composites, whilst retaining the simplicity of 0-3 manufacturing.

The electric field structuring technique exploits the electrokinetic phenomenon of dielectrophoresis, which is responsible for the electrorheological effect. When a suspension of ceramic particles in an insulating fluid is exposed to a moderate AC electric field, the particles polarize and as a result they exhibit a mutually attractive force. Under suitable conditions the particles assemble into 'pearl-chains', 'fibrils' or columns, oriented parallel to the applied field. If the fluid is a resin pre-polymer, this can then be cured and the newly formed structures frozen into place to form a composite material with anisotropic properties. The key process parameters are explored and the implications of employing this method to produce technologically useful materials are discussed.

It is demonstrated, for the first time, that dielectrophoresis can be used to induce anisotropic dielectric and piezoelectric properties in 55%vol. fraction ceramic / polymer composites. A model composite system of pure lead titanate in an epoxy resin is considered in basic detail. A method of producing a lead zirconate titanate (PZT) powder with a narrow particle size distribution, by flux growth, has been shown to be effective. New concepts in multiphase composites are introduced, whereby chains are formed within the confines of a second immiscible fluid or where particles of two different materials are mixed in a suspension, each material having its own 'polarization signature'.

Acknowledgements

My heartfelt thanks to all of those people who have helped me to complete this study. To Roger Whatmore, for giving me the opportunity to study at Cranfield and for his support, his advice, his patient supervision and many words of encouragement. To George Maistros for his lasting support and his technical expertise in dielectrics. To Harry Block for his inspiration and his enthusiasm. To the technical staff in the School of Industrial and Manufacturing Science and most especially to Andrew Stallard, who have contributed to this research in so many ways. To the academic and research staff in the Advanced Materials Group for their help and advice and to my colleagues in the Nanotechnology Group.

The work detailed in this thesis was undertaken on an EPSRC Case Studentship and supported financially by DERA. Particular thanks must go to my industrial supervisor at the Structural Materials Centre, Steve Mahon for his support, for his experience and guidance, for providing materials and test facilities. I am grateful for his faith in my ability.

Special thanks to Dan Campbell of the Open University who got me started in materials and to my friend Hil, who has been there throughout my academic career.

Finally I must also thank my family for the love and support that they have given me over the years.

E ferro ferrum temperatum

After the fire, the fire still burns.

Contents

List of Figures

List of Tables

1. Introduction

Piezoelectric composite materials, consisting of a ferroelectric ceramic in an electrically-inactive polymer matrix, have been extensively researched in recent years and have been shown to greatly outperform single phase materials for certain applications. In particular they have brought about significant advances in the field of underwater sound generation and detection. Appropriate composite structures also have advantages for acoustic imaging and medical ultrasound.

In developing such a material, a key consideration concerns the spatial distribution of the ceramic within the polymer and in recent years many different structural arrangements or 'connectivity patterns' [1] have been explored to suit a variety of applications. The two types of composite which show the most promise for underwater applications are: i) a composite of rods of ceramic material embedded in a polymeric matrix, by convention termed a 1-3 composite and ii) a uniform dispersion of unconnected ceramic particles in a continuous polymeric matrix, termed a 0-3 composite (Figure 1.1). 1-3 type materials have the advantage of greater sensitivity and are preferred for active applications such as sound generation. 0-3 type materials can provide adequate sensitivity for passive applications such as sound detection. Their relatively low production cost, allied to their greater flexibility and formability, make them the preferred choice for large area applications.

The current project aims to explore the possibility of using a new processing technique, electric-field structuring, to enhance the properties of 0-3 type piezoelectric composites. The materials so produced will have a quasi 1-3 structure and it is intended that they will exhibit some of the advantages of 1-3 piezoelectric composites whilst retaining the simplicity of 0-3 manufacturing. In addition, this processing technique is of academic interest and a better understanding may well lead to new types of useful dual-phase and multi-phase materials.

The electric field structuring technique exploits the electrokinetic phenomenon of dielectrophoresis, which is responsible for the electrorheological effect. When a suspension of ceramic particles in an insulating fluid is exposed to a moderate AC electric field, the particles polarize and as a result they exhibit a mutually attractive force. Under suitable conditions the particles assemble into 'pearl-chains', 'fibrils' or columns, oriented parallel to the applied field. If the fluid is a resin pre-polymer, this can then be cured and the new-formed structures frozen into place to form a composite material with anisotropic properties. Although it has previously been demonstrated that a wide variety of filler/matrix combinations can be structured in this way [2], there is no published work yet available that considers the full implications of employing this method to produce technologically useful materials. It is intended that the findings of the current project will also test the validity of this new technique in the context of materials processing.

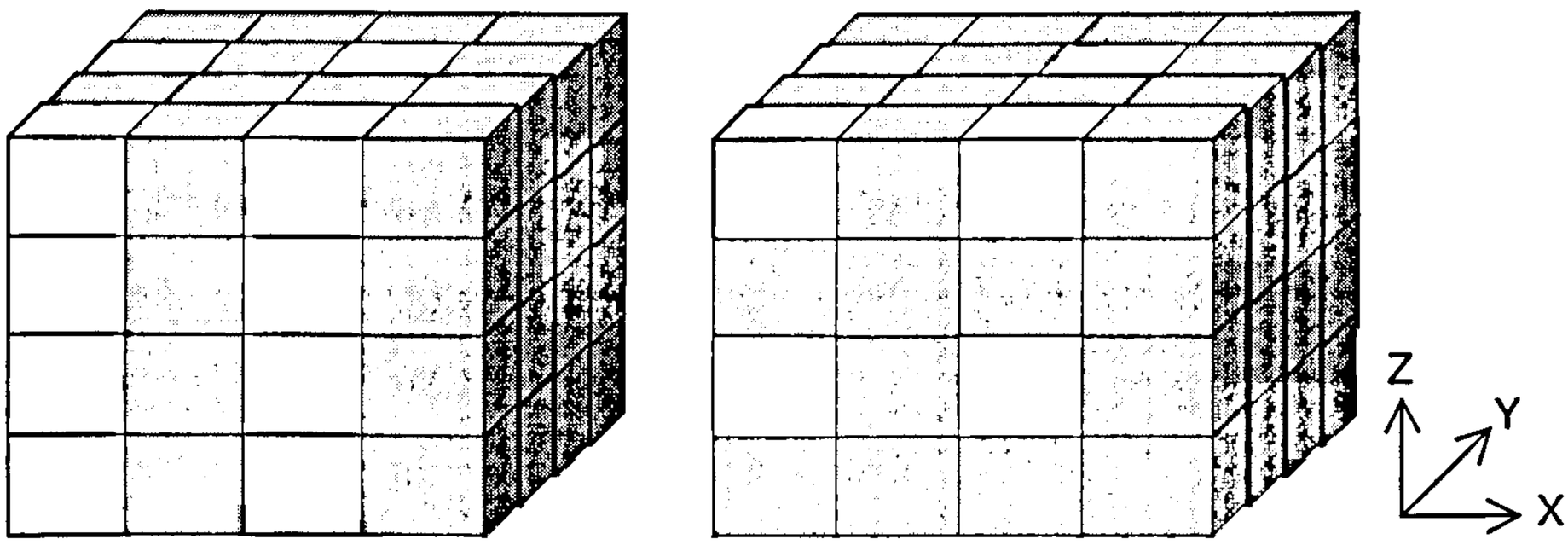

Figure 1.1 Schematic diagram of 1-3 type (left) and 0-3 type connectivity patterns for two-phase composites (see note).

Note: 'Connectivity' is a descriptive term, which is used to classify the distribution of the constituent phases in composite materials. An index number is assigned to each phase according to the number of dimensions in which it is physically self-connected. In the above diagram (left) the white-phase is self-connected in one dimension, along the z-axis, and in no other. The grey-phase is self-connected in three dimensions. Hence this structure is assigned 1-3 connectivity. In the same way, the white-phase in the 0-3 composite is not self-connected in any direction.

2. Overview of Dielectrophoresis and Piezoelectric Composites

2.1 Dielectrophoresis

2.1.1 Definition

'Dielectrophoresis is the translational motion of neutral matter caused by polarization effects in a non-uniform electric field.' - H.A.Pohl (1951) [4]. It is distinct from the motion of a charged body in an electric field, which is described by the term electrophoresis.

2.1.2 Dielectrophoresis or Electrophoresis?

Dielectrophoresis and electrophoresis can be contrasted as follows:-

a) Dielectrophoresis by definition requires a non-uniform field. Electrophoresis occurs in both uniform and non-uniform fields.

b) Dielectrophoresis requires moderate to high field strengths. The dielectrophoretic force depends on the dielectric permittivities of both the suspended particles and the surrounding fluid and on the mismatch between them. Higher field strengths are required for fluids of low dielectric permittivity. Electrophoresis operates under relatively low fields.

c) Dielectrophoresis causes particles to move in a direction which is independent of the sign of the field. Accordingly, either a.c. or d.c. fields can be used. Electrophoresis brings about movement which is dependent on the sign of the charge on the particle and the field direction, hence reversing the field reverses the direction of travel.

d) Dielectrophoresis gives rise to a force that is directly proportional to particle volume and is therefore more pronounced with larger particles. Electrophoresis is observable with particles of any size.

The dielectrophoretic force is discussed more fully in the section : (8.1) 'Review of structure formation in ER fluids'.

2.2 Electric-field Structuring - Schematic

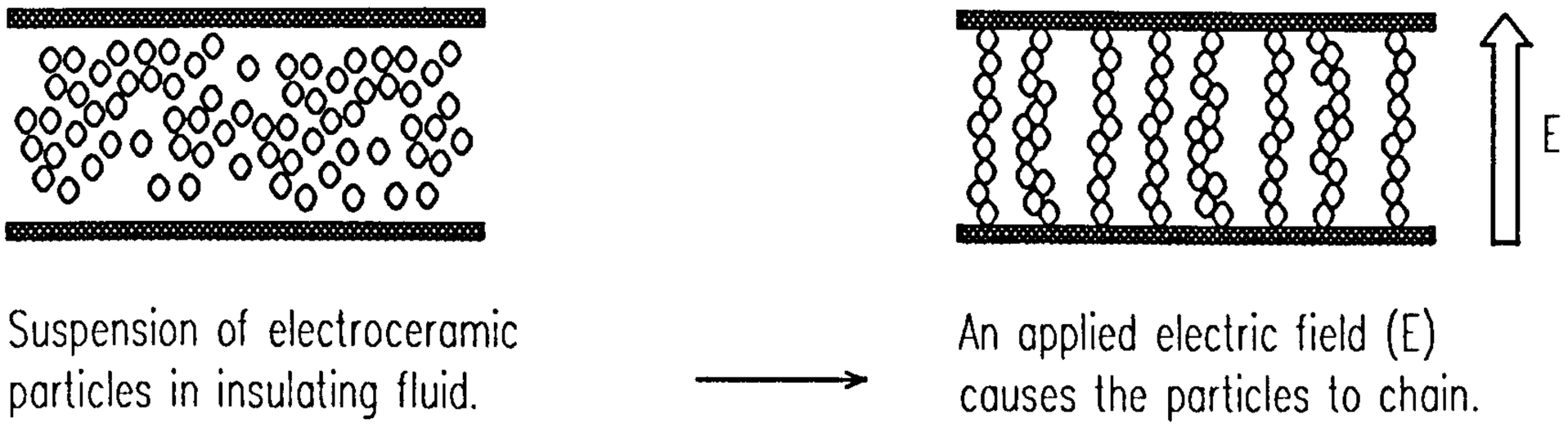

Figure 2.1 When a suspension of ceramic particles in a low conductivity fluid is exposed to a moderate electric field, the particles will often polarize and as a result they experience a mutual attraction. Over time they assemble into structures between the electrodes, these are referred to as 'pearl chains', 'fibrils' or columns.

2.3 Ferroelectric Materials

Ferroelectrics are polar dielectrics in which the direction of polarization can be reoriented between equivalent stable positions by the application of an electric field, without any change in crystal structure. All ferroelectric materials exhibit both pyroelectric behaviour, whereby a net dipole moment is produced in response to a change in temperature and also piezoelectric behavior, whereby a net dipole moment is produced in response to an applied stress.

The key to understanding these phenomena lies in a study of the ferroelectric crystal structure. Each of these materials possesses a unique axis along which there exists a permanent electric dipole, even in the absence of an applied electric field. The dipole due to this spontaneous polarization is normally compensated within the crystal lattice, to retain overall neutrality. Straining the lattice, however, disturbs this equilibrium. The dipole moment changes in magnitude to compensate and this leads to a macroscopic

polarization of the crystal and a net surface charge results. The surface charge can be measured as a change in electrical potential. An associated phenomenon known as the converse piezoelectric effect also exists, whereby an externally applied electric field induces a lattice strain.

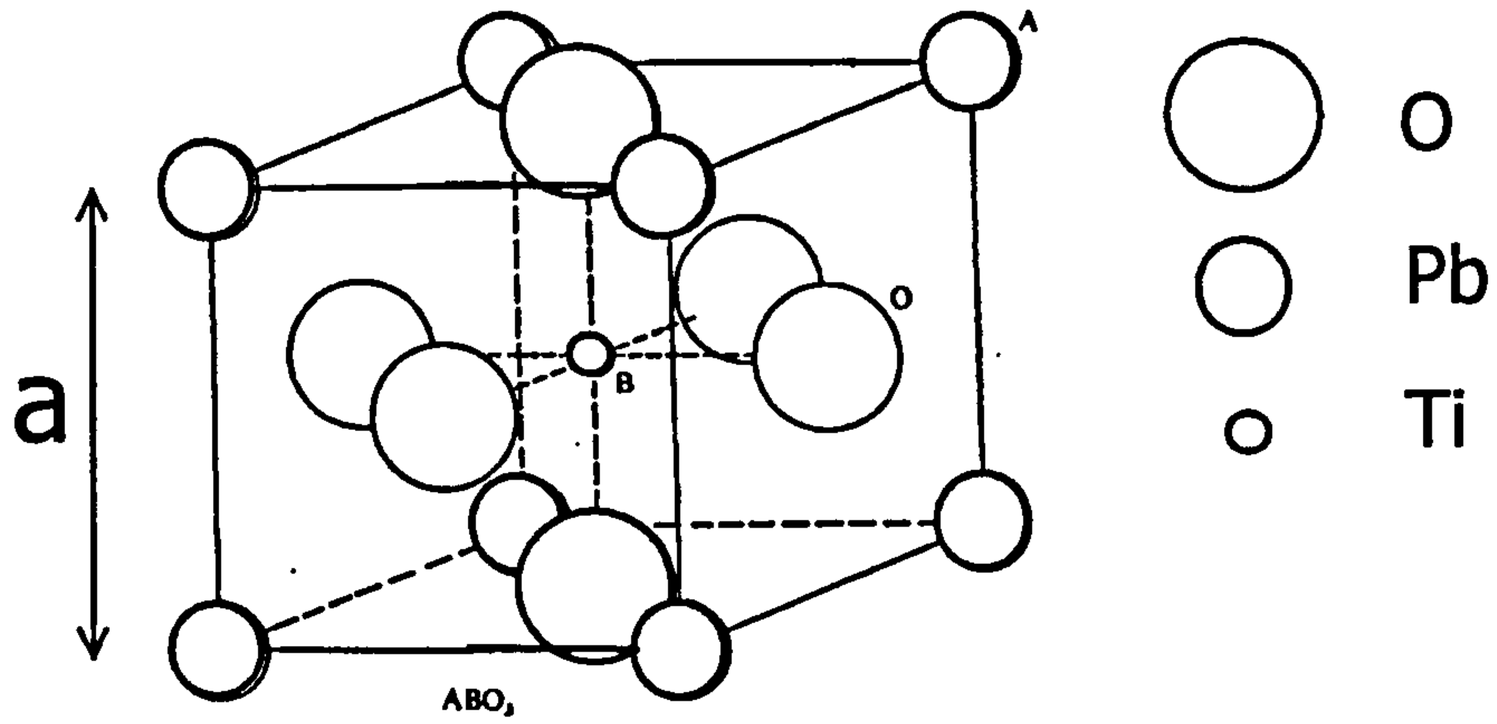

Figure 2.2: The perovskite unit cell for lead titanate ($PbTiO_3$)

Many of the technologically useful ferroelectrics are oxides, having the general formula ABO_3 and adopting the 'perovskite' crystal structure. (Perovskite being a mineral form of calcium titanate). The unit cell is shown in Figure 2.2. In this, the A-site cations are centred in cuboctahedral cages and are 12-fold coordinate with the oxygen (O^{2-}) ions. The B-site cations are 8-fold coordinate and occupy octahedral cages of oxygen ions. Above a critical temperature, the Curie temperature, the unit cell is able to maintain a prototype cubic symmetry. Below this temperature the unit cell becomes distorted, the metal cations are displaced from their symmetry positions relative to the oxygen anions thereby accounting for the electrical dipole moment. In barium titanate, $BaTiO_3$, the relative displacements for Ba^{+2}, Ti^{+4} and O^{-2} along the c-axis are respectively +0.06Å, +0.12Å and –0.03Å; in lead titanate, $PbTiO_3$, the relative displacements along the c-axis are +0.47Å for Pb^{+2} and +0.30Å for Ti^{+4} [38]. Some commercially important ferroelectric oxides which have the perovskite structure are $PbTiO_3$, $PbZrO_3$, $BaTiO_3$, $LaMnO_3$ and $Pb(Mg_{1/3}Nb_{2/3})O_3$.

Polycrystalline ferroelectrics adopt a domain structure. Each domain is a region of net polarization and each individual crystal may have many of these, distributed so as to achieve an overall minimum energy balance. The domains are normally restricted in size by grain boundaries. However, if some degree of grain orientation exists then domains in neighbouring grains may affect each other, either through mechanical strain or electric polarization coupling; this may extend over several crystals.

Ferroelectrics exhibit spontaneous polarization only below a certain critical temperature, known as their Curie temperature and this represents the upper limit of their usefulness as transducer materials.

2.4 Piezoelectric Definitions

Piezoelectric properties are defined in the ANSI/IEEE Standard on Piezoelectricity [4], which also prescribes methods for the determination of piezoelectric and dielectric constants

When a piezoelectric material is strained by an external force, electrical charge is displaced and can be measured in an electrical circuit. This is the direct piezoelectric effect. A converse effect is observed, whereby the same material placed in an electric field exhibits a structural deformation. The magnitude of the observed effect is dependent on the orientation of the applied force, or conversely the applied field, in relation to the crystallographic axes of the material.

The piezoelectric charge coefficient is given by the expression:

$$d_{ij} = \frac{\text{strain developed}}{\text{applied field}} = \frac{\text{charge density}}{\text{applied stress}} \qquad [\text{ units C/N }]$$

The piezoelectric voltage coefficient is given by:

$$g_{ij} = \frac{\text{strain developed}}{\text{applied charge density}} = \frac{\text{field developed}}{\text{applied mechanical stress}} \qquad [\text{ units Vm/N }]$$

The electromechanical coupling coefficient is given by:

$$k_{ij} = \sqrt{\frac{\text{mechanical energy stored}}{\text{electrical energy applied}}} = \sqrt{\frac{\text{electrical energy stored}}{\text{mechanical energy applied}}}$$

By convention the first subscript (i) refers to the direction of the applied stress (or conversely the applied field) and the second subscript (j) refers to the direction of the response. The subscripts can take any value from 1 to 3 for the orthogonal axes and from 4 to 6 for the shear planes.

The sensitivity of a piezoelectric transducer material operating underwater can be described in terms of its electrical response to a hydrostatic pressure wave. The hydrostatic voltage coefficient (g_h) relates the electric field appearing across the transducer to the applied hydrostatic stress. The hydrostatic charge coefficient (d_h) describes the polarization that results from hydrostatic stress. The two terms are related by the expression:

$$d_h = g_h.\varepsilon_r$$

where ε_r is the relative permittivity of the material.

The hydrostatic piezoelectric coefficients are related to their triaxial components by the expressions:

$$d_h = d_{33} + 2d_{31} \quad (= d_{33} + d_{32} + d_{31})$$

and

$$g_h = g_{33} + 2g_{31} \quad (= g_{33} + g_{32} + g_{31})$$

where subscript 3 denotes the poled direction, 1 and 2 are orthogonal axes.

2.5 Piezoelectric Materials for Hydrostatic Applications

Amongst conventional electroceramics, the most sensitive piezoelectric transducer materials are the morphotropic phase boundary PZT's (lead zirconate titanate). These materials, however, are found to have relatively low hydrostatic coefficients. The reason for this lies in their anisotropic charge response, in effect d_{33} and a negative

transverse component ($2d_{31}$) act to cancel each other out. Moreover, the high permittivity of PZT acts to produce very low values for the piezoelectric voltage coefficient (g_h). Lead titanate (PT), particularly in its calcium-modified form, exhibits some advantages for hydrostatic applications.

Processing difficulties make ceramic materials unsuitable for the large area conformal arrays used in modern sonar systems. They are dense and brittle and this results in poor acoustic impedance matching to water and a low resistance to explosive shock. Piezoelectric polymers, such as poly(vinylidene fluoride) (PVDF), on the other hand, have greatly improved formability relative to ceramics and can be made to cover large areas. They combine this with both a lower density and lower relative permittivity. However, they are relatively insensitive in terms of their hydrostatic charge response. A low Curie temperature gives the materials a strong temperature dependence. This can lead to problems with depoling and the irreversible degradation of properties with time.

In contrast, piezoelectric composite materials can be made which exhibit very high hydrostatic piezoelectric coefficients. The polymer phase lowers density, providing a better acoustic impedance match to water and more easily adjusted buoyancy than that obtained for an homogenous ceramic. The low dielectric permittivity of the polymer phase effectively increases the piezoelectric voltage coefficients. The high elastic compliance of the polymer phase provides better resistance to mechanical shock and exhibits the high damping required for a good passive device. Finally, the piezoelectric properties can be tailored by changing the way the ceramic is distributed within the polymer.

The coupling of the ceramic and polymer phase is termed the connectivity [1]. This is of key importance because it controls the electric flux patterns which will exist within the composite, as well as its mechanical properties. The two types of composite, as previously stated, most favoured for underwater applications are: i) a composite of rods of ceramic material embedded in a polymeric matrix (1-3 composite) and ii) a

uniform dispersion of unconnected ceramic particles in a polymeric matrix (0-3 composite). Typical properties of these two types are included in Table 2.1, where ε_r refers to relative dielectric permittivity. A more extensive range of published values is to be found in Appendix A. Table 2.2 lists measured dielectric properties of the materials used for experimental work in the current study.

Table 2.1 - Comparison of the properties of candidate transducer materials for hydrophone devices.

Material	Density kg m^{-3}	ε_r	d_{33} pCN^{-1}	g_{33} mVN^{-1}	d_h pCN^{-1}	g_h mVm^{-1}	$d_h.g_h.10^{15}$ m^2N^{-1}	Ref. No.
PZT	7900	1800	450	28	40	2.5	100	[5]
$PbTiO_3$	7500	230	53	26	47	23	1080	[6]
$PbNb_2O_6$	6330	225	85	42	67	33	2200	[7]
PVDF	1800	12	-30	-280	-10	-100	1000	[8]
1-3 Composite PZT/Epoxy	1370	54	150	313	27	56	1536	[9]
1-3 Composite PZT/ PU foam	930	41	180	495	73	210	15330	[10]
0-3 Composite PZT/PU		26	10	43	2	8	10	[15]
0-3 Composite PT/Epoxy		48	60	141	42	96	4032	[17]

Table 2.2 – Dielectric properties of materials used in the current study.

Material	Relative permittivity (ε_r)	Dielectric loss (tan δ)
Lead titanate (PT)	149.9	0.043
Vernitron PZT5H	888.5	0.047
Vernitron PZT5H (PbO-PbF_2 flux grown (page 42)	638.1	0.079
Epotek 302-3M resin	3.94	0.009

2.5.1 Figures of Merit

Table 2.1 includes a figure of merit (the $d_h.g_h$ product) which is widely quoted as a means to compare piezoelectric transducer materials. When considering materials for a particular application, however, it is useful to note that the response of a system depends on the value of the open-circuit capacitance. If the capacitance of the sensing element is very much greater than that of its cable and associated circuitry then the appropriate figure of merit is g_h. In the reverse case, d_h should be used. PVDF has a good voltage response but a low permittivity (and hence a low element capacitance). As a result there is a problem with stray capacitance and a signal pre-amplifier must be positioned close to the element. Garner et al [20] note that in most cases it is insufficient to simply consider response and that signal-to-noise ratio is more important. Sources of noise may be environmental (Sea-state Zero) or component related. Which of these dominates depends on frequency. They suggest that for low background conditions or at low frequencies, a figure of merit of $(d_h.g_h/ \tan \delta)^{1/2}$ is appropriate, otherwise g_h can suffice.

2.6 1-3 Composites

Klicker [9] developed 1-3 composites of PZT rods embedded in a continuous polymeric matrix and, in so doing, achieved major improvements in g_h compared to conventional ceramics. In this configuration the stress on the polymer, which is more compliant than the PZT rods, is transferred to the rods. Loading the material in this way increases its efficiency, but at the same time the Poissons' expansion of the polymer introduces an unwanted transverse stress on the rods. To overcome this, foamed polymers with, typically 45% porosity were successfully used. While this increased the $d_h.g_h$ product by an order of magnitude, the materials' properties were found to be highly dependent on pressure above 1.3 MPa . Stiffening the matrix in the transverse direction with continuous glass fibres has been found to decrease d_{31} without appreciably lowering d_{33} and these materials are reported to have the highest hydrostatic piezoelectric coefficients of all [11]. Savakus [12] introduced a simplified procedure for forming 1-3 composites. A horizontal grid was cut in solid PZT ceramic to form an array of rectangular square columns. The material removed by cutting was

replaced by back-filling with polymer to form the composite. The dielectric properties of these materials were found to compare favourably with composites prepared using ceramic rods.

2.7 0-3 Composites

The advantage of 0-3 composites lies in their simplicity. While still having useful piezoelectric properties, 0-3 composites can be easily formed into a large variety of shapes, including thin sheets and at low cost. This makes them more suitable for mass-production.

2.7.1 Ceramic Phase

The piezoelectric ceramic phase most often used in this type of composite is based on lead titanate, which has superior hydrostatic properties to PZT. A large anisotropy in the electromechanical coupling factors, that for thickness dilational vibration is very much larger than that for planar extensional vibration, makes it possible for these ceramics to be used for high frequency applications.

Pure lead titanate has a high coercive field which presents particular problems when poling. A useful modification is to replace 24% Pb with Ca, which reduces the Curie temperature [21]. Manganese is used to improve poling and reduce losses [5]. B-site modifications of Ti,Co,W are used to tailor the mechanical properties [22]. Takeuchi et al. also report that the dielectric permittivity and d_{33} can be increased, while retaining a large electromechanical anisotropy, by increasing the calcium content to 36 mol.%. A variety of rare-earth substitutions has also been studied, particularly with regard to ultrasonic applications.

In lead titanate the high axial ratio (c/a =1.07) of the unit cell can be exploited effectively in powder production. Cooling through the Curie point engenders high internal stresses in polycrystalline ceramic bodies, which then crack into small fragments. A means of powder production to produce 'virtually single-domain particles' and their use in a composite material is detailed in a U.S. Patent [23]. It is

noted that the powder preparation route has a major influence on the sensitivity of the final composite. In particular, ball-milling is found to diminish piezoelectric response.

2.7.2 Polymer Phase

Although the polymer phase is not usually electroactive, it heavily influences the composite properties and can determine the ultimate sensitivity of a device. Electrical and dielectric properties are particularly important. The conductivity of the polymer greatly influences composite poling and is susceptible to changes both in temperature and in absorbed moisture. Dielectric loss in the polymer generates heat in active mode and can limit the upper frequency of operation of a device. Properties such as elasticity, strength, toughness and resilience are subject to variation with temperature, time and environment.

2.7.3 Ceramic-Polymer Interface

The coupling at the ceramic-polymer interface is of prime importance to composite properties. Factors which influence the extent of coupling are: 1) the fabrication procedure, which must allow for the polymer to wet the entire ceramic surface, 2) particle size and concentration, which dictate the total surface area of the interface, 3) powder surface roughness and/or contamination [8]. Galgoci and Runt [24] found that interfacial adhesion in PZT/epoxy composites was far from optimum. Silane and titanium alkoxide coupling agents were tested and found to increase adhesion beyond the cohesive limit of the epoxy. Coupling agents may also inhibit the ingress of moisture to the composite and hence reduce long term ageing.

2.7.4 Composite Preparation

Both mechanical and piezoelectric properties of the composite depend on there being a uniform dispersion of particles. Initial forced mixing is aimed at achieving an optimum distribution while avoiding air-entrapment, which will introduce voids into the cured material. Particle agglomeration is a further source of voiding. One option to facilitate mixing is to raise the mixing temperature, though in the case of thermosetting polymers this must be done with due regard to the rate of cure, which will accelerate and there

will be an associated increase in chemoviscosity. Hot pressing [25] or warm rolling [26] can be used to form the mixture into sheets. It should be noted that although the piezoelectric sensitivity of the composite increases with increasing volume fraction of the ceramic, the practical limit lies at around 60% loading. Above this limit the material lacks mechanical strength.

2.7.5 Poling of Composites

The sensitivity of a piezoelectric material is dependent on effective poling of the ceramic. In 0-3 composites this presents a particular problem. The respective resistivities of the ceramic and polymer phases are very different, such that the potential developed across the ceramic is a small fraction of the total applied voltage [8]. This makes complete poling of the ceramic difficult to achieve. Chilton et al [27] [28] have addressed this problem and suggest two techniques which may be used: 1) Increased temperature is found to facilitate domain switching; 2) Moisture diffused into the polymeric matrix can be used to reduce the effective resistivity of the polymer. This can then be expelled after poling. A technique of introducing a small volume fraction of carbon black into the polymer [14] to produce the same effect is rejected as this greatly increases dielectric losses in the composite.

3. Assembly of composite materials using the dielectrophoretic effect – a review

To-date relatively little published work exists concerning this new method of assembling composite materials. Randall [29] used the dielectrophoretic effect to produce composites of nano-scale $BaTiO_3$ in a silicone elastomer. The constituents were mixed manually followed by a vacuum degas. An electric field was applied of 0.1kV/mm r.m.s. at 40Hz and the mixture was allowed to cure at 60-80°C. The process took 1hr. to complete. Randall observed that chaining of the particles into discontinuous fibrils occurred. The dielectric permittivities of the composite were measured, both perpendicular and parallel to the direction of the applied field. These revealed dielectric anisotropy.

Miller [30] studied suspensions of $BaTiO_3$ in silicone oil. He showed that above a certain critical d.c. field strength the electrorheological response, as measured by fluid viscosity, diminished drastically and electrically-induced turbulence prevented chain formation. The cause of this effect was unknown. Alternating fields of much higher strength could be applied without turbulence appearing. The ER response was then found to be strongly frequency dependent. He reported that the suspensions exhibited a linear relationship between yield stress and the square of the applied field, a characteristic of dipole-dipole interaction. He also noted the weak ER response of hydrothermally-prepared nano-scale powder under d.c. conditions. At high field strengths the fibrillar networks which formed tended to coarsen with time, leading to an increase in viscosity. At high field strength there was also an observed increase in the number of chains being formed. Randall[60] aligned Ag-coated acrylic fibres and SiC fibres parallel to an applied field.

Randall [2] listed some potential applications for the technique. He highlighted some of the factors which must be considered if dielectrophoresis is to be used as a means

to assemble composites. i). The matrix material must be insulating with a lower dielectric permittivity than the filler and with a low dielectric loss. A number of different particulate materials are listed which have successfully been aligned in a silicone elastomer. ii). It must be fast-polymerizing in order to limit sedimentation. A viscous liquid may also be used, but the viscosity must not be so high as to limit the dielectrophoretic assembly. iii). The uncured polymer must have a high dielectric breakdown strength. The choice of filler is limited by conductivity. If a conducting or semi-conducting filler is allowed to form chains between the electrodes then a conducting pathway is formed and the polarization effect is lost. If a layer of insulating polymer is retained in a gap between particles then a large field-gradient is created which can exceed the breakdown strength of the polymer and a slowing down of the curing process will result.

Randall [2] noted that an electric field applied to a polymer/ceramic particulate suspension will induce both electrophoresis and dielectrophoresis. Electrophoresis can result in a net migration of the filler to one of the electrodes. In order to nullify the electrophoretic effect, alternating fields can be used. He suggested that the optimum frequency for dielectrophoretic assembly can be identified by two techniques. Firstly by direct observation, fibrillation in low volume fraction dispersions (under 5%) can be inspected by light microscopy. The particle size limit for this technique is around 2microns diameter. Secondly, the frequency and field strength dependence of the shear stress, at a fixed shear-rate, can be examined using a rotational viscometer. From these measurements the relationship between shear stress and field strength can be determined for any fixed volume-fraction and alternating field frequency. An 'optimum alignment' condition is revealed at the field frequency which gives the strongest electrorheological response.

Randall infers that the strongest electrorheological effect occurs for $SrTiO_3$ in a silicone elastomer polymer at a field frequency of 10Hz and this corresponds to the coarsest fibrils found by direct observation. Similarly, an ideal electrorheological

effect for epoxy thermosets was found at around 650-750Hz. No dielectrophoretic alignment was observed for epoxy thermosets under direct or low frequency alternating fields. This is explained as being due to ionic space-charge polarization dominating at low frequencies leading to a high dielectric constant and loss. The 'ideal alignment frequency' is said to be independent of volume fraction.

Bowen [31] continues this theme stating that, under a.c. field conditions a critical field must be established for fibril formation but, in addition, there is also a critical field frequency for maximum fibril formation.

Bowen [32] studied the frequency dependence of the dielectrophoretic effect in thermosetting polymers. He concluded that at low frequencies where space charge polarization dominates, polarization of the particles will not be possible. 'The coarseness of the chains is very sensitive to the magnitude of the loss tangent and the characteristic relaxation times, because polarizability of the particles may be a rate dependent process.'

Bowen [33] compared the dielectric permittivities of dielectrophoretically-aligned composites with equivalent random-structured composites. He showed that aligned composites have dielectric anisotropy and used simple mixing rules to predict their dielectric properties.

4. Modus Operandi

4.1 Critique of Published Work

The recent work of Randall, Bowen et al. (2, 29-33) has shown that the dielectrophoretic effect can be used to assemble a wide range of filler/matrix combinations into composite materials. To-date little information has been published regarding the properties of these materials. In order to carry this work forward, it is necessary to say that some of the interpretations of the above authors are open to question. The most significant point that needs to be addressed is their concept of an 'ideal alignment frequency' for an applied alternating field. This is identified as the frequency at which an applied field produces the strongest electrorheological effect, as measured by a rotational viscometer. This is also said to be the frequency at which the coarsest fibrils form. What is unclear is the time-scale of these events. Elsewhere it has been observed that fibrils can coarsen or, more exactly, that they can coalesce into larger structures over a period of time. Blackwood et al. [34] investigated the different structures formed in an ER fluid by rapidly applying d.c. fields of different strength and by applying the same fields in a stepwise fashion. They found that, up to a certain limit, the number of fibrils increased with increasing field strength. The same field applied gradually in a stepwise manner led to a coarser network of fibrils; the implication being that field strength is the critical parameter in controlling the number of chains formed. With time these chains may coarsen into columnar structures. This can arise either by individual chains coalescing or by the movement of individual particles from one chain to another. Halsey [35] ascribes this phenomenon to thermal (Brownian) motion or to fluctuations in the field. Fluctuations may arise when particles in close proximity to each other, jostle to find an equilibrium separation. The question then arises, why use alternating fields at all? It seems that a pulsed d.c. field of sufficient strength may also find some use in forming particulate structures.

A further concern, regarding previous work, lies in the assumption that the electrorheological behaviour of the suspension measured by a rotational viscometer

can be directly related to what is, in essence, its dielectric behaviour under assembly conditions, where the fluid is relatively static. Maistros [36], in his work on dielectric monitoring of curing rubber-modified epoxy resin blends, isolated the interfacial component of the complex permittivity. Interestingly, the permittivity due to this component was high and dielectric loss showed a strong maximum peak at 650Hz. This corresponds to Randalls' 'optimum alignment frequency' for epoxy resin matrix materials. Above the frequency in question interfacial polarization drops rapidly to a very low level and this is consistent with the observed fall in viscosity. However, below this frequency, interfacial permittivity and hence polarization is as high or higher and would, therefore, be expected to play its full role in the assembly process. Further, the flow of the dispersion in the viscometer causes a change in dielectric behaviour known as flow-modified permittivity (FMP) and this is shear-rate dependent. As particles rotate, the time taken to re-establish polarization relative to the applied field frequency becomes significant. Block [37], in his review, explains three possible mechanisms for interfacial polarization under a field: 1) Carrier migration through the bulk of the particle; 2) Surface charge migration; 3) Charge migration in the double-layer. For each of these time is clearly a factor. If particles are rotating faster than migration can occur then polarization will not reach its maximum, resulting in weaker particle interactions and hence a lower observed viscosity. If this argument holds true, then a measurement of viscosity may not directly correlate to one of dielectrophoretic activity. In addition, a degree of mechanical rather than dielectrophoretic structuring is taking place as chains are continually broken up by the viscometer. It may be that attractive forces between chain segments or agglomerations are observed rather than true interparticle forces.

4.2 Overview of the Current Project

It seems clear that further studies should incorporate a knowledge of the dielectric properties of the constituent phases and also of the particle dispersions. This would provide the means to assess the role of particle surface and interfacial chemistry on the assembly process and its influence on the properties of composites so produced. It

has been noted that the bulk permittivity varies according to the type and number of chains formed [34]. This may provide a means of assessing the repeatability of the process under given assembly conditions.

It is proposed that a model electroceramic/polymer system be studied. Suitable conditions will be found to assemble structured composites and these will be related to the electrical and physical properties of the components. A range of process variables will be tested, as will alternative filler / matrix combinations. Optimisation of the properties of the composites will be studied and the validity of this technique as a means of producing technologically useful materials will be explored.

4.3 Notes on Practical Aspects of the Project

Preliminary attempts and initial consideration of the field structuring process have highlighted the following:

4.3.1 Filler Materials

a) Choice of filler. Affects the active piezoelectric coefficients and their magnitudes.

b) Powder production route. Influences surface chemistry, surface energy, roughness.

c) Particle size. Influences properties of the finished composite. Affects the viscosity of the initial dispersion. Influences settling rate/ sedimentation.

d) Volume fraction. The dielectrophoretic process may be effective only up to a certain ceramic loading.

e) Density. Influences settling rate and the time available for the assembly process.

f) Conductivity. Greatly influences poling.

g) Impurities. Moisture content, in particular, affects conductivity.

4.3.2 Matrix

a) Choice of polymer. Influences the whole range of composite materials properties.

b) Preparation. The need to degas the polymer may limit the time available for assembly.

c) Cure cycle. The assembly process must be completed before gelation occurs. After this particles are effectively immobilised.

d) Viscosity. Viscous forces retard the assembly process and influence settling rate.

e) Conductivity. Limits the field which may be applied.

f) Impurities. These may be responsible for unwanted electrophoretic activity. They may influence charge migration in the polarizing stage.

g) Coupling agents. Act as adhesion promoters to improve composite performance. They may also have an influence on the assembly process. Additives such as foaming agents or rubber may be used effectively to enhance properties once the structuring process is better understood.

h) Air entrapment. Porosity will lead to variability in the properties of the finished material.

4.3.3 Processing

a) Temperature. Raising the temperature reduces the viscosity of the polymer. It thus facilitates the migration of particles. However, reducing viscosity leads to an increase in the rate of sedimentation and hence places a limit on the nature and size of particles which can be used. Raising temperature accelerates the rate of cure.

b) Time. Assembly must be matched to the cure cycle and sedimentation.

c) Field strength and frequency. Has been discussed earlier and requires further investigation to establish its precise influence on the assembly process.

d) Release agents. Are at present needed to recover samples from the mould. These may increase electrical resistance between the electrodes and the curing polymer.

4.4 Project Strategy

4.4.1 Process

The viscosity of a model filler / polymer system should be measured. This can subsequently be related to the fibrillar network structure, its variation with time and the range of processing parameters. The time-persistence of chain structures is of interest, as is chain coarsening. The dielectric behaviour of a particular dispersion can be measured in parallel to establish permittivity, loss and conductivity during the assembly process. Rapidly-applied d.c. fields, pulsed fields and alternating fields can be tried. The object of this is to gain a further insight into the assembly process and to provide experimental data to compare with the analysis of other workers. Various volume fractions can tested, as can particle size dependence. A range of particle sizes, prepared in-house and all by a similar route, could be used. The properties of materials made can be tested and compared to similar unaligned composites. The use of coupling agents and their influence on processing and properties needs to be explored. Impurities deliberately added to the uncured polymer may be of interest. It may be found that a useful material can be made by applying an initial strong field pulse, followed by a weaker a.c. holding field whilst the polymer cures.

4.4.2 Materials

Well characterised lead titanate powders made according to U.S. Patent [23] have been prepared in-house. These are 'virtually single domain' and said to give optimum piezoelectric properties in 0-3 composite materials. Barium titanate powders have also been prepared via a mixed oxide route. The effect of using surface etched powders on the assembly process is of interest. Lead titanate, however, is not an ideal filler material to use for study because of its high density, which promotes sedimentation.

Powders with a mean particle diameter of less than about 4μm diameter cannot be made by the above route. A range of commercial ferroelectric powders is also available.

The matrix material used in preliminary work is a low conductivity epoxy resin (Dow DER 332, a DGEBA diglycidyl ether of bisphenol A), having a Mol.Wt. of 340 and a hydroxy/ epoxy ratio of 0.015. The hardener is BASF Laromin C260 (4.4'-diamino-3.3'-dimethyl dicyclohexylmethane). The first composites have been found to be very brittle and difficult to handle. Epoxy/ rubber blends are possibly a better alternative. These can be made initially more viscous which would have the advantage of limiting sedimentation. Blends made using BF Goodrich Hycar CTBN 1300X have recently been studied at Cranfield. To-date this has been prepared by direct mixing, giving a more viscous fluid pre-polymer. A further option is to source an alternative epoxy resin. A variety of mould release agents have been successfully used including PTFE aerosol spray, silicone oil and 'Freekote'.

Useful characterisation techniques will include X-ray diffraction, microtomy, optical and electron microscopy of polished sections and fracture surfaces.

5. Studies in Electroceramic Powder Preparation

5.1 Lead Titanate

The mixed-oxide preparation of lead titanate, from PbO and TiO_2, has a number of variables and these were explored by experimentation in order to derive an optimal processing route. The aim was to produce a powder consisting of electroactive, equiaxed grains with a narrow particle size distribution, which would be suitable for the ceramic phase of a model composite system. A further aim was to develop the ability to produce a range of such powders with different median particle sizes, which could be used to explore the dielectrophoretic assembly process.

5.1.1 Background

In defining a processing route, reference has been made to the methods outlined in U.S. Patent No.5169551 [23]. An essential feature of this patent is the use of rapid cooling to achieve dissociation between the grains of the solid-phase reaction product. Lead titanate is well suited to this method given its relatively large axial ratio (c/a = 1.063:1) in the crystalline state. Thermal shock is induced in the reaction product by plunging it into water direct from the furnace. The resultant internal strain causes it to shatter along grain boundaries. It has also been found that the requisite effect can be produced in lead titanate, albeit to a lesser degree, simply by cooling in air. The major advantage of rapid cooling is that it averts the necessity for ball-milling as the final stage of powder preparation. Ball-milling is said to damage the particles, introducing structural fractures and distorted phases. This leads to an increase in the number of domains, it makes subsequent poling difficult to achieve and reduces piezo-activity. This behaviour has been observed elsewhere and is known to our group at Cranfield from previous studies.

An essential departure from methods outlined in the above patent was the absence of a lead oxide atmosphere in the furnace. Substantially the same effect is achieved in this

study by adding an excess of lead oxide to the initial mix. Unreacted lead oxide is effectively removed when the powder is subsequently etched.

To form a powder the step sequence of operations is as follows:

1. Mill together the component oxides. (Variables - time, composition).
2. Dry and sieve.
3. Press into 5g pellets. (Variables - applied load, pellet size).
4. Calcine. (Variables - time and temperature).
5. Remove from furnace and pulverize. (Variables - cooling rate, method of pulverization).
6. Etch. (Variables - etchant, time, temperature).

The solid phase reaction (calcining) takes place by a process of ionic diffusion and experimental work has shown that the formation of lead titanate is mainly attributable to the diffusion of Pb^{+2} ions into particles of TiO_2 [38]. This implies that an intimate mixture of small particles is favoured and that there will be optimal conditions associated with milling and pellet forming. Longer milling times produce smaller particles and a finer grained ceramic can result.

The combination reaction involves four processes:

i) thermal expansion of the particles, below 400°C;
ii) ionic diffusion - solid phase reaction, 400°C - 750°C;
iii) contraction of the reaction product, 750°C - 850°C;
iv) grain growth, above 800°C.

The melting point of PbO is at 880°C. Significant vaporization can be expected, therefore, at the calcining temperature. Hence it is essential to provide a lead oxide atmosphere to counteract the expected loss. We have chosen here to include an excess of lead oxide in the initial mixture of reactants. It should be noted that lead oxide vapour is highly corrosive and capable of attacking furnace linings and crucibles alike, hence it requires tight control. A platinum crucible is preferred.

5.1.2 Experimental

Details of the study and the information it produced are presented below. An optimal processing route was then defined which is laid out in section 5.1.3.

Step 1. a) Milling the reactants.

A sample consisting of a 1:1 molar ratio (PbO: TiO_2) of the reactants was divided into two parts. One part was ball-milled in acetone using zirconia elements for 5hrs. The second part was milled under the same conditions for 18hrs. The two parts were then calcined under identical conditions. The products are illustrated in Figures 5.1 and 5.2 respectively. As expected, the longer milling time has led to greater comminution of the reactants and crucially to a more uniform particle size distribution. The product is then much finer grained and does not exhibit large irregular agglomerations.

b) Initial composition.

Lead titanate was prepared under identical conditions from mixtures containing: i) no excess lead oxide (PbO: TiO_2 = 1:1 molar ratio); ii) 10% excess lead oxide by percentage of total weight of reactants; and iii) 20% excess lead oxide. The products are illustrated in Figure 5.3, representing no excess PbO and Figure 5.4, representing 10% excess PbO. Images of crystallites formed with 10% excess PbO and with 20% excess PbO were indistinguishable. Compare the ill-defined agglomerates in Figure 5.1 with that in Figure 5.5, which has 20% excess PbO.

Step 2. Dry and sieve.

Step 3. Pellet pressing.

Two identical 5g samples of the reactants were pressed into a 20mm diameter die, at loads of 11.6MPa and 20.6MPa respectively, and held for 5mins. After processing, no differences were detected in the powders so formed.

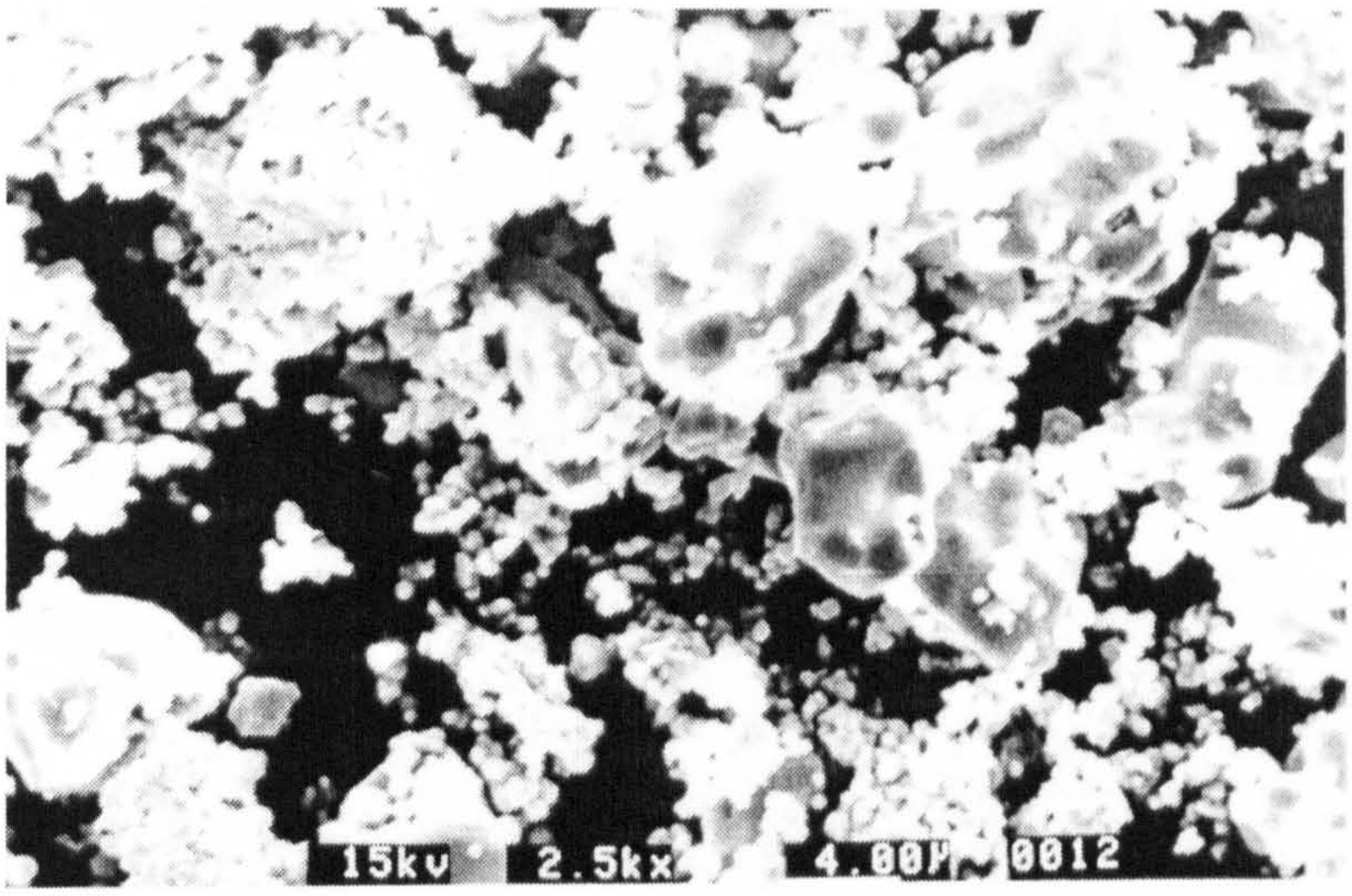

Figure 5.1 - $PbTiO_3$ + 0% excess PbO. Milled 5hrs, calcined at 850°C.

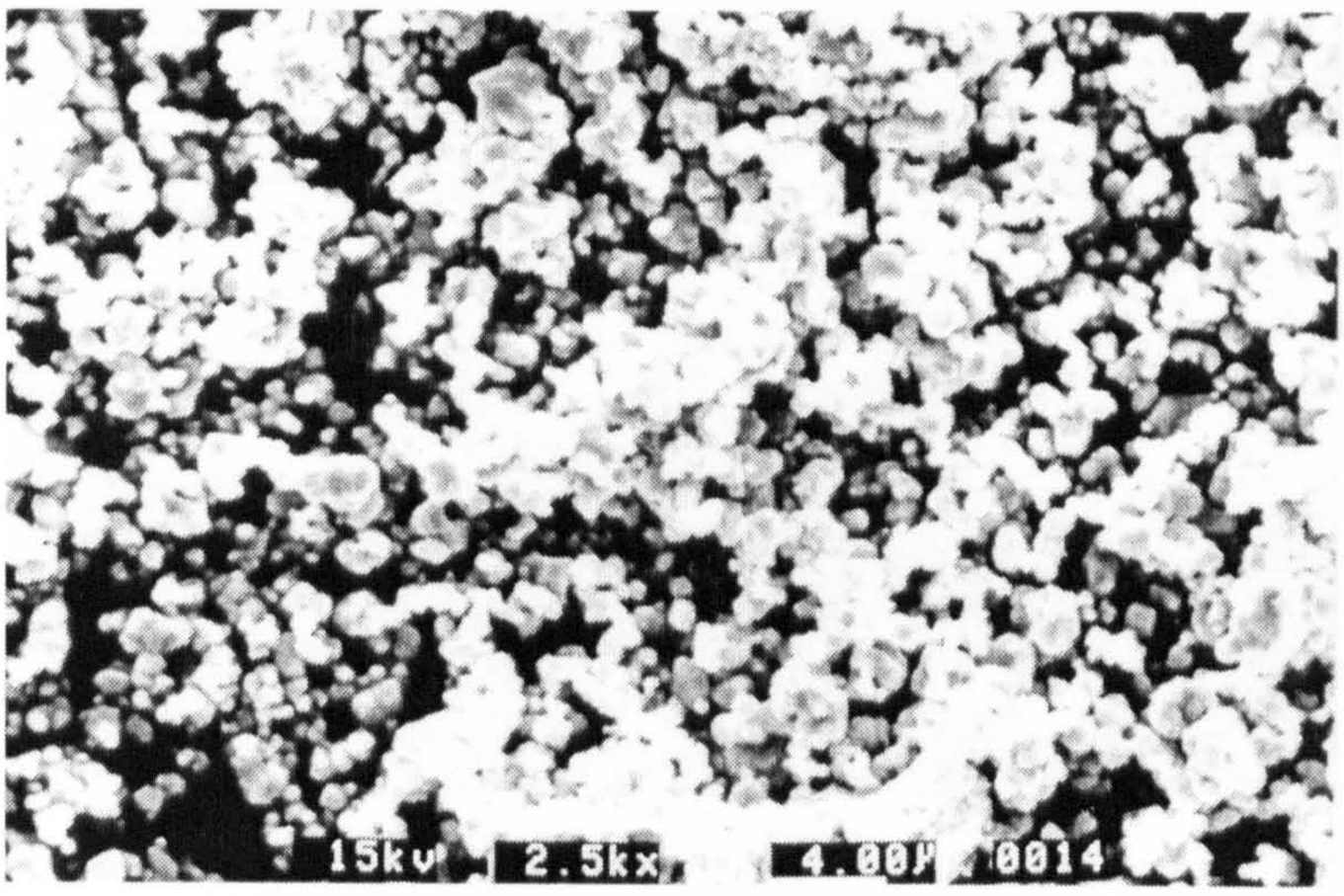

Figure 5.2 - $PbTiO_3$ + 0% excess PbO. Milled 18hrs, calcined at 850°C.

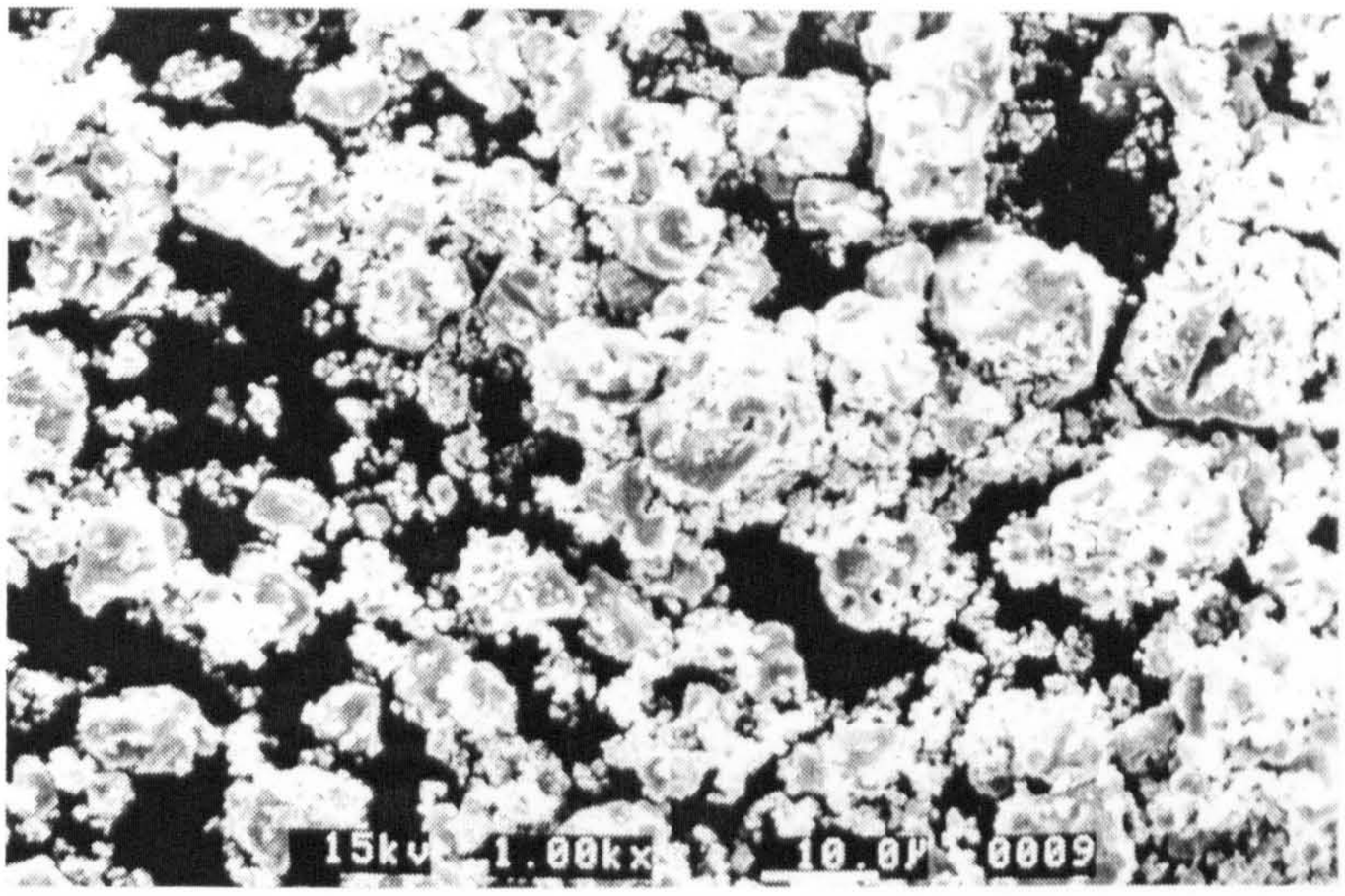

Figure 5.3 - $PbTiO_3$ + 0% excess PbO (x1000)

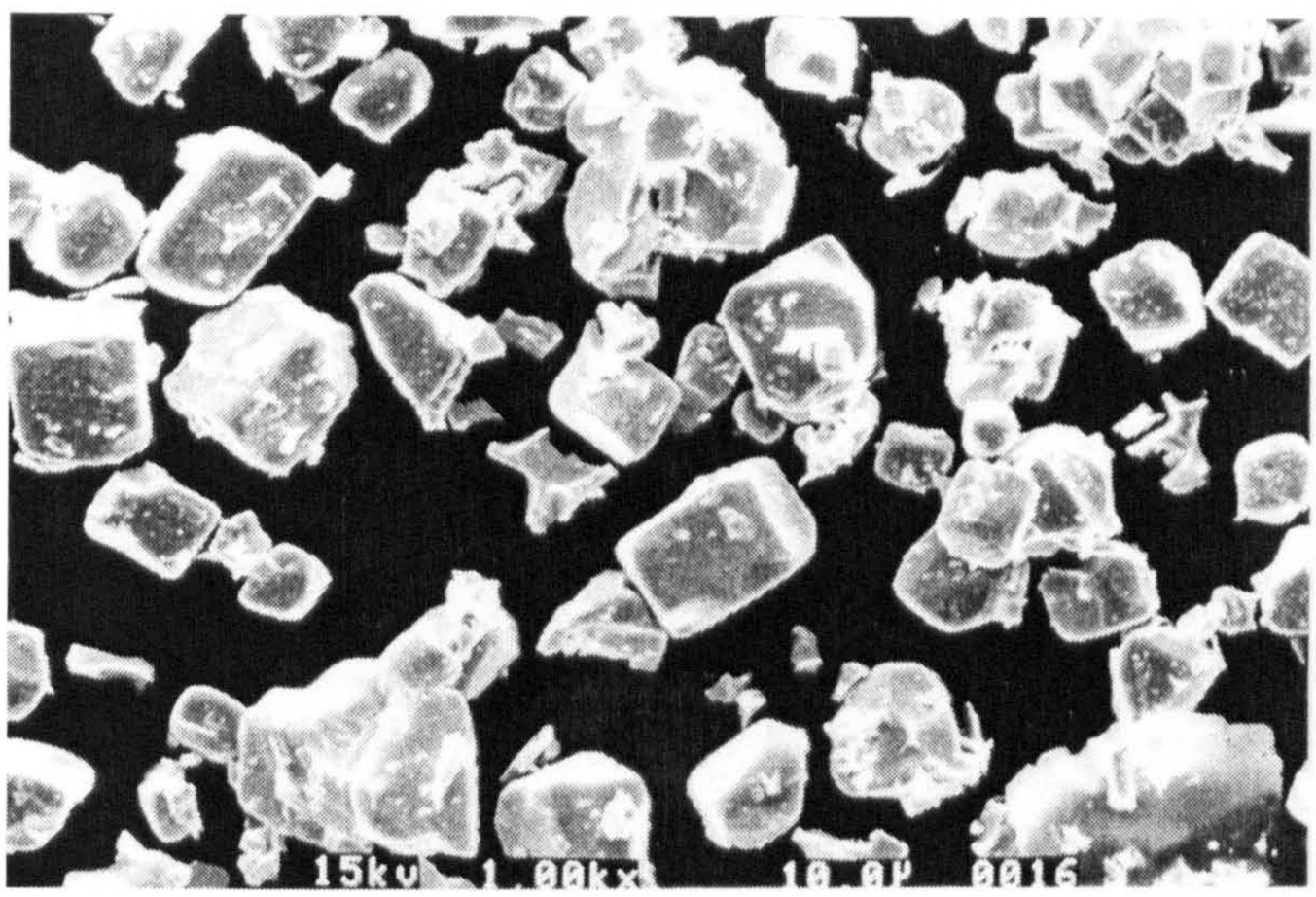

Figure 5.4 - $PbTiO_3$ + 10% excess PbO (x1000)

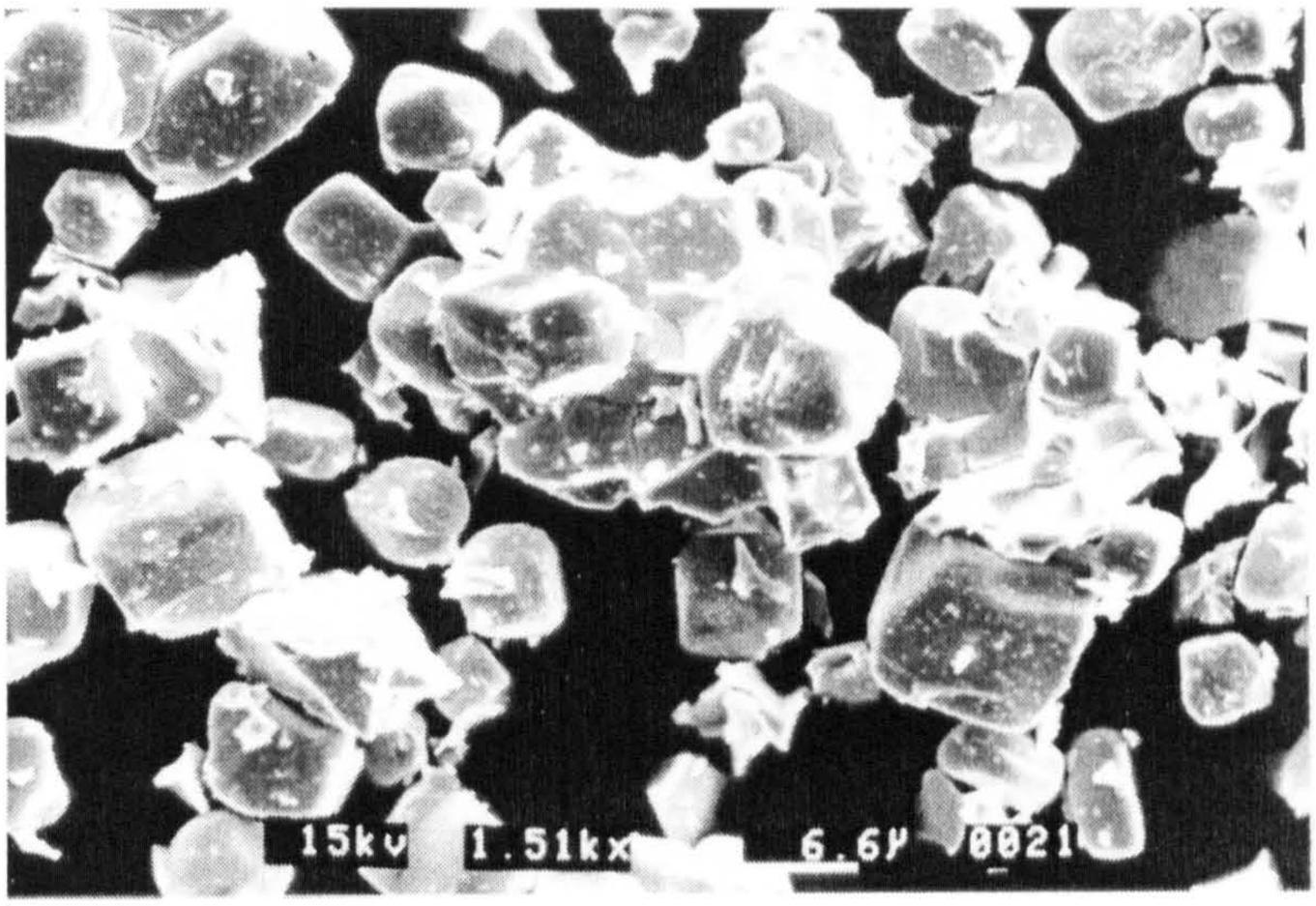

Figure 5.5 - $PbTiO_3$ + 20% excess PbO (x1500)

Step 4. Calcining.

The calcining temperature was in all cases 850°C, just below the melting point of PbO. In order to define the optimum time period for this step, identical samples containing 20% by weight excess PbO, were calcined for 1, 2, 4, 8 and 24hrs. The products were etched and a particle size analysis was performed using an x-ray Sedigraph (Table 5.1). The samples were further examined by x-ray diffraction and visually with a scanning electron microscope.

Table 5.1: Effect of calcining time on the particle size distribution for lead titanate powders as determined by X-ray Sedigraph.

Time at 850°C	Particle diameter (µm) median	modal	% wt particles (<5 µm)	% wt particles (5 - 15µm)	% wt particles (>15µm)
1hr	7.99	7.97	15.1	79.9	5.0
2hrs	9.51	9.25	7.6	78.1	14.2
4hrs	9.06	9.10	13.2	75.1	11.7
8hrs	9.66	10.05	12.2	71.7	16.1
24hrs	8.51	6.61	20.2	56.4	23.4

Inspection of the particle size data and SEM images reveals the following information:

After 1hour the solid phase reaction is incomplete. The Sedigraph calculates particle sizes as an equivalent spherical diameter and in this case the data are misleading. Photographs (Figure 5.2) show that the product does not consist primarily of individual grains but rather of clusters of smaller particles.

After 2hours the reaction is complete and in fact, 92.9% by weight of the product exists as individual grains with equivalent diameters in the interval (4 - 20μm). Again, because of the method of calculation, this implies that there are relatively few of the larger grains.

After 4hours the measurements are inconclusive.

After 8hours and more particularly after 24hours , a trend emerges which shows evidence of grain growth, probably by Ostwald ripening. The outcome is a relative increase in the number of larger (>15μm) grains and also an increase in the number of smaller (< 5μm) grains in the product.

Step 5. Rapid cooling.

Direct from the furnace, identical samples were either quenched in de-ionised water at room temperature or allowed to air-cool. Where excess lead oxide had been used the product was dark yellow in colour and both the air-cooled and water quenched samples broke up into a fine-grained powder very easily. Quenching instantly pulverises the product and is preferred. Where no excess lead oxide had been included the product was greyish in colour; samples were much more difficult to break down and fragmented unevenly.

Step 6. Etching.

Two powder samples were etched in nitric acid. Etching was performed at 80°C for 1 hour and the etchant was one part conc. HNO_3 : nine parts distilled water by volume. The quantities were 400mg powder to 10ml etchant. The effect of this is to dissolve

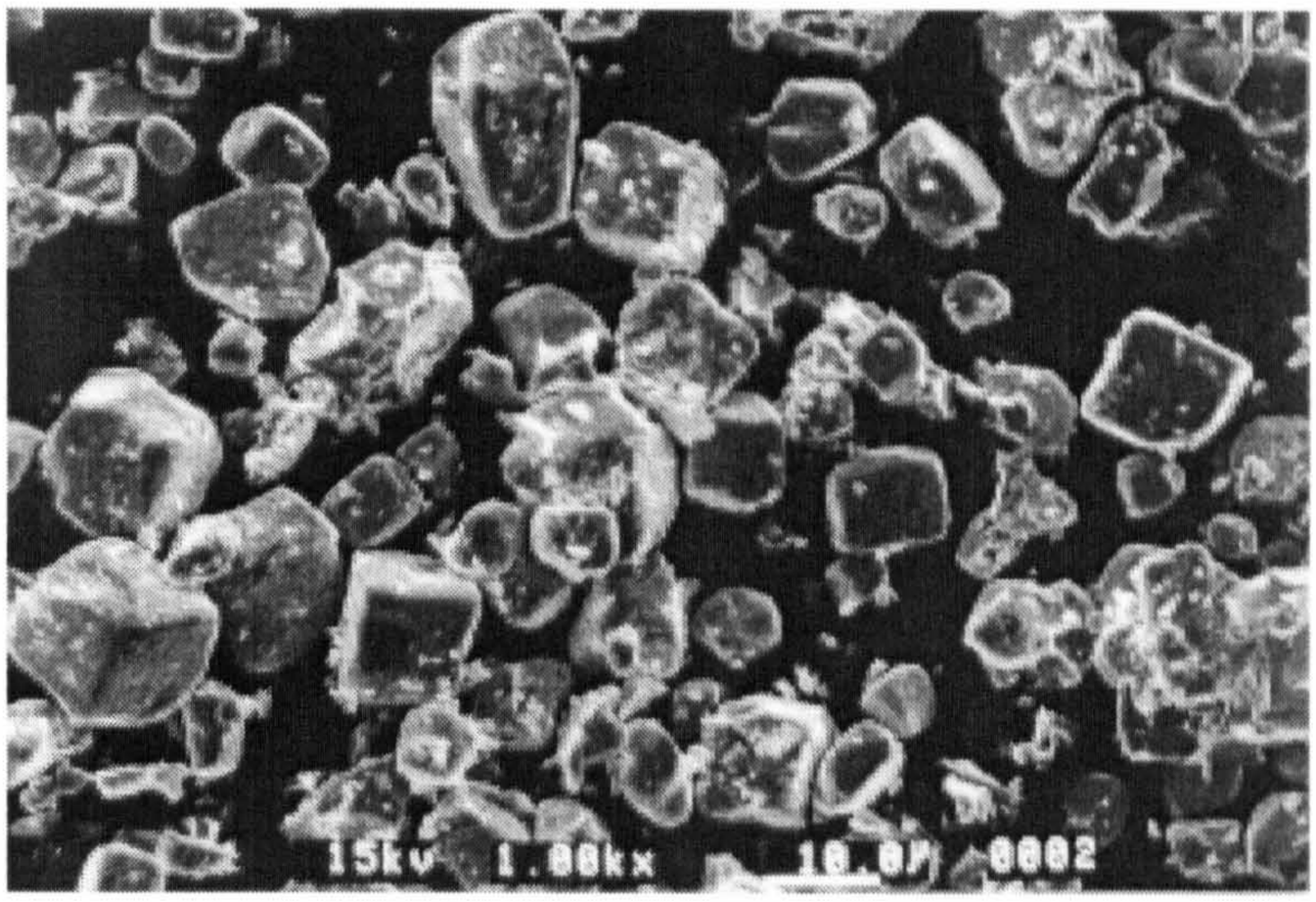

Figure 5.6 - $PbTiO_3$ + 10% excess PbO, quenched (x1000)

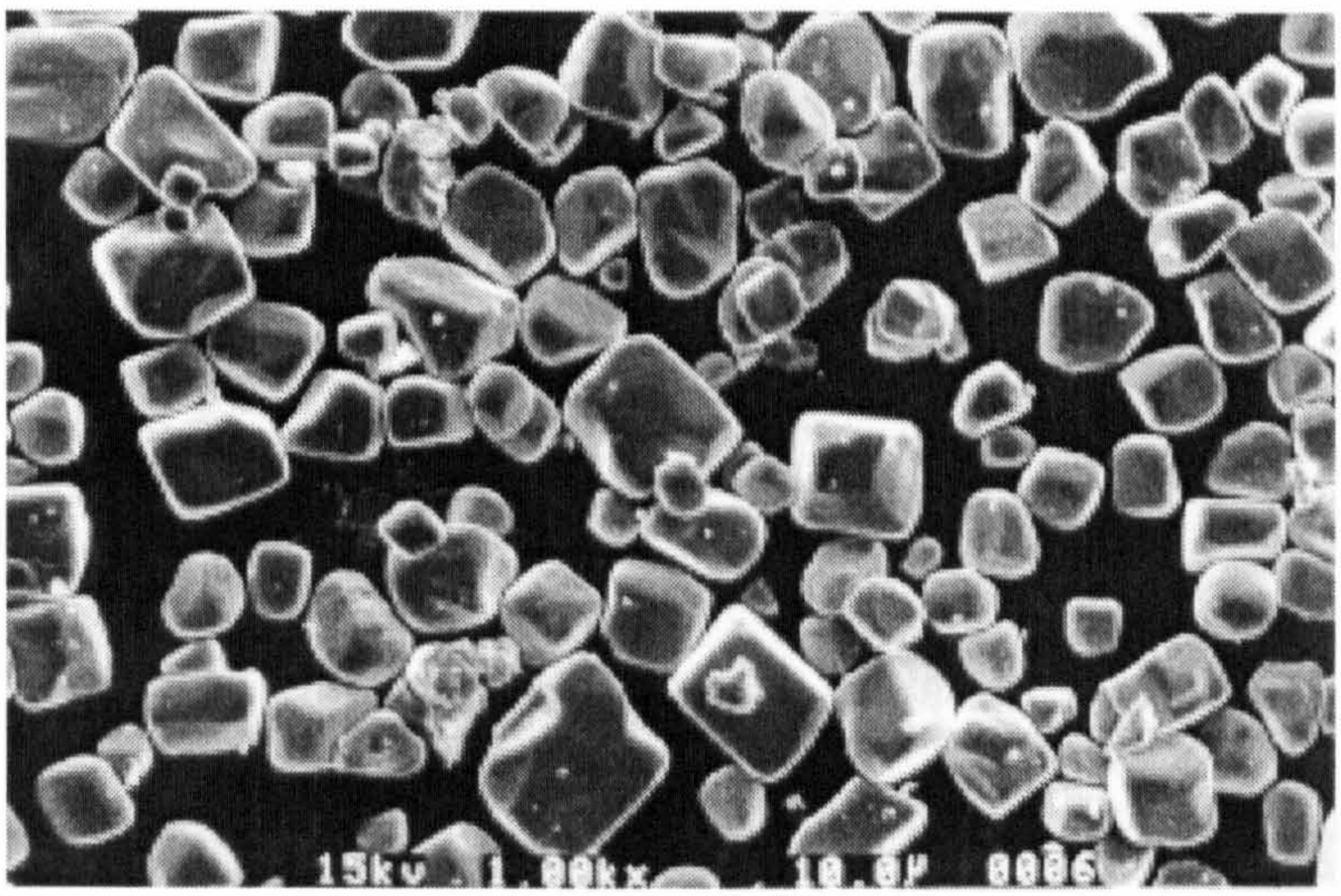

Figure 5.7 - $PbTiO_3$ + 10% excess PbO etched in nitric acid (x1000)

the tiny fragments which result from rapid cooling, to break up any agglomerates which may be present and to remove surface damage from the grains. The yield for the process is around 82% by weight and it is illustrated in Figure 5.6, which shows the quenched powder and Figure 5.7, showing the powder after etching. A further benefit of this process is that it effectively removes unreacted excess PbO from the product. Figure 5.8 shows XRD traces of the reaction product a). before and b). after etching. These were compared to data from a powder simulation (Crystallographica©,

Oxford Cryosystems,1995),which confirmed the reaction product to be tetragonal $PbTiO_3$. The peak at $2\theta = 29.00°$ is the most distinctive feature to be absent in the etched sample. This is a characteristic of the powder x-ray diffraction pattern of orthorhombic PbO.

Peak No.	Angle (2Θ)	D-spacing (10^{-10} m)	Relative Intensity	hkl
1	21.50	4.133	31	001
2	22.89	3.885	61	100
3	31.51	2.839	96	101
4	32.54	2.752	94	110
5	39.28	2.294	100	111
6	43.67	2.073	32	002
7	46.62	1.948	99	200
8	49.80	1.831	39	102
9	51.83	1.764	36	201
10	52.50	1.743	36	210
11	55.42	1.658	57	112
12	57.34	1.607	98	211
13	65.72	1.421	46	202
14	68.00	1.379	30	003,220
15	70.52	1.335	29	212
16	72.46	1.304	45	221,103,300
17	77.06	1.238	28	301
18	77.36	1.234	37	113

Table 5.2: X-ray diffraction data for the etched sample of lead titanate (Cu:Kα_1).

Crystallographic analysis of the x-ray diffraction data is shown in Table 5.2. The unit cell dimensions are shown to be:

$a = 2 \times d_{200} = 2 \times 1.948 = 3.896$ Angstroms (Crystallographica° a = 3.904 Å)

$c = 2 \times d_{002} = 2 \times 2.073 = 4.146$ Angstroms (Crystallographica° c = 4.152 Å)

The volume of a unit cell is: $a^2c = 6.293 \times 10^{-29}$ m^3

Given the M.W. of $PbTiO_3$ = 303.06 and the atomic mass unit is 1.66053×10^{-24} g , then the mass of the unit cell is 5.0324×10^{-22} g

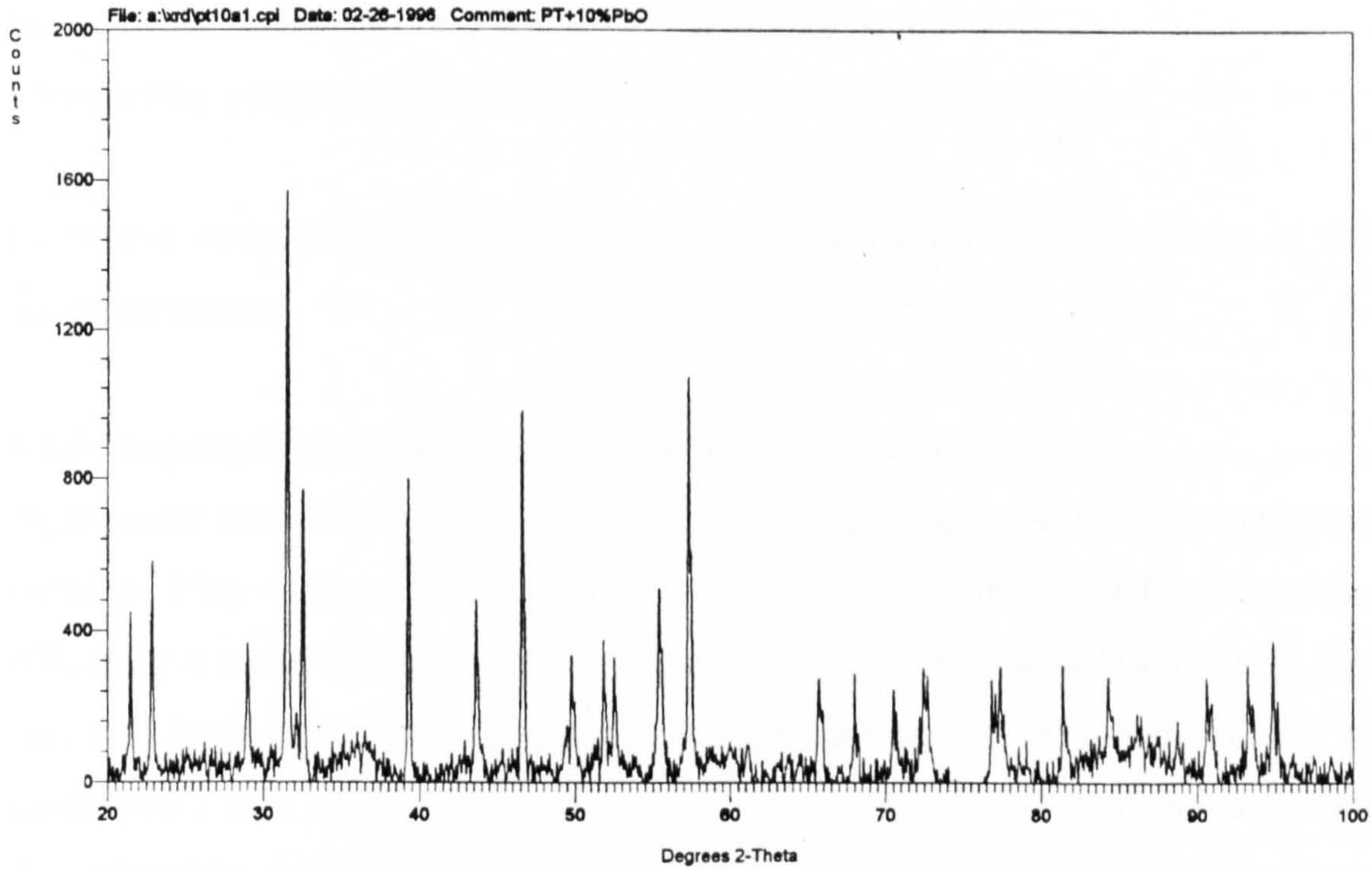

Figure 5.8a) - Lead titanate with 10% excess PbO

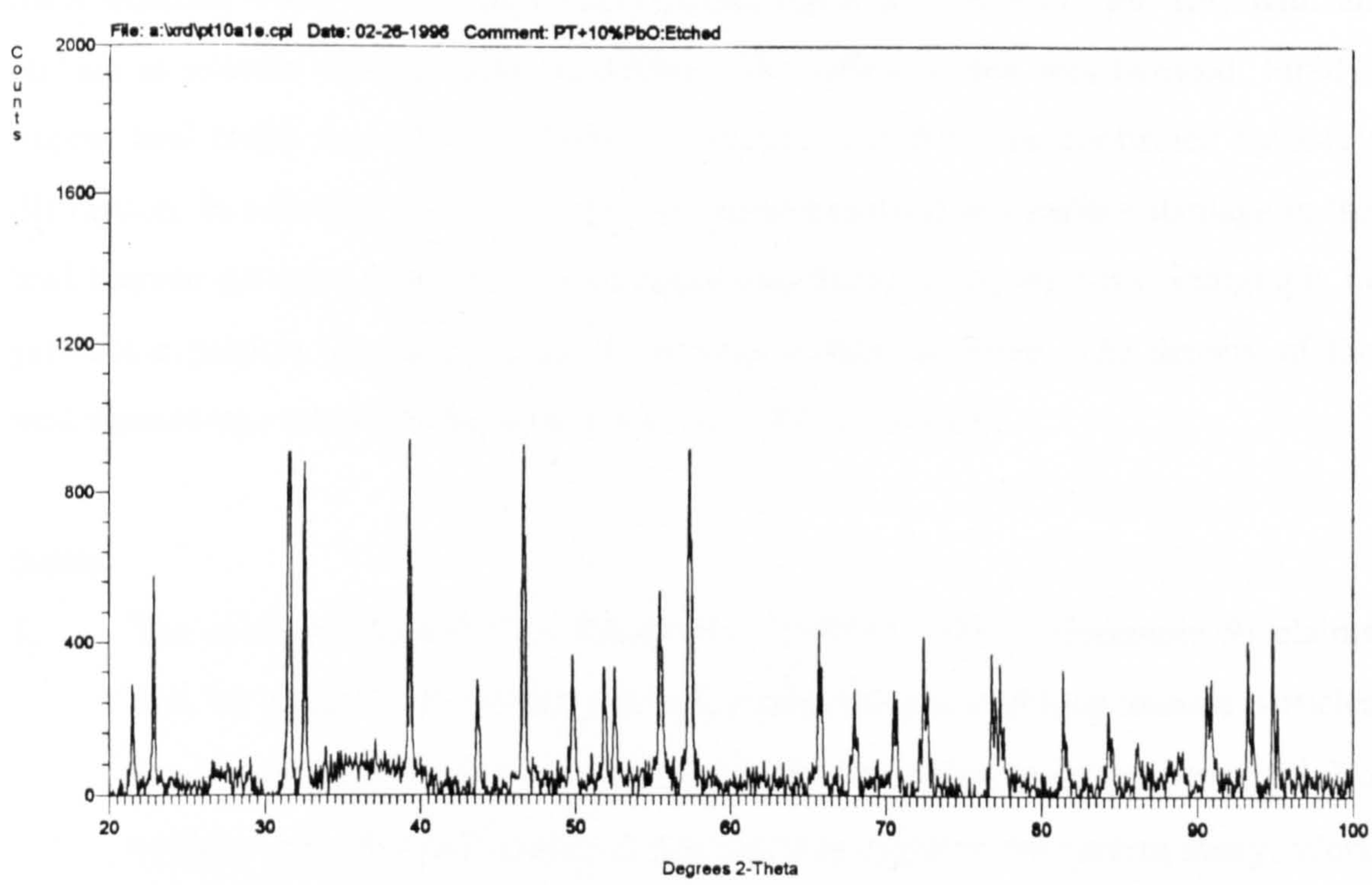

Figure 5.8b) - Lead titanate with 10% excess PbO, etched.

Hence the x-ray density of the product is: 7.997×10^3 kg m^{-3}

Measured by pycnometry the density was found to be: 7.771×10^3 kg m^{-3}

From this study an optimal processing route was defined. This is set out in the following section

5.1.3 Preparation of Lead Titanate Powder (Summary)

High purity lead titanate (PT) was prepared by solid phase reaction of lead oxide (Aldrich: PbO <10μm, 99.9%+) and titanium dioxide (Aldrich , TiO_2 325 mesh, 99%min.) in molar quantities of 11:10. The addition of 10% excess lead oxide in this way was found to produce a powder having a narrow particle size distribution. The oxides were first ball-milled in acetone for 4hrs with zirconia elements and then formed into 5g. pellets by holding at a pressure of 20MPa for 5mins. The pellets were then fired at 800°C for 2hrs and immediately pulverized by quenching in distilled water at room temperature. The powder so formed was etched in a solution of nine parts distilled water to one part concentrated nitric acid at 80°C for 1hr, with an etchant to powder ratio of 10ml to 400mg. The effect of this was twofold. Firstly, excess lead oxide was removed from the surface and this was confirmed by x-ray diffraction. In addition, nanosized particles were dissolved and surface damage to the lead titanate particles removed. This process was found, using an x-ray Sedigraph, to produce a particle size distribution of between 2-8μm diameter. The density of the lead titanate was measured by pycnometry as 7.771×10^3 kg/m^3.

Notes:

1. The afore-mentioned U.S. Patent No. 5169551 [23] in (Example 9) claims that, by using a very similar method, a preponderance of lead titanate particles having equivalent spherical diameters in the 40 - 60μm range are produced. No evidence of individual grains of this size was found in the current study. Work by the patent-holder was carried out on a much larger scale, batch sizes of 200g as opposed to 5g, which may explain the discrepancy.

2. There have been attempts by many workers to grow single crystals of lead titanate both from flux and from melt. Flux systems employing combinations of PbO, PbO-B_2O_3, KF, Pb_3O_4-PbF_2, and KF-KBF_4-PbF_2 have been used [39] with some success. Perhaps the most promising method, for the purposes of the current work is described by Sun et al. [40], who have studied a technique of using a PbO self-flux, combined with a precise slow thermal cycle. It is possible that this technique could be adapted to produce a range of lead titanate powders of increasing particle sizes.
3. Alternative methods of preparing lead titanate powders exist, notably by the sol-gel technique [41] and by co-precipitation. 0-3 composites have been made by Lee et al. [42] using powders prepared by different routes and their properties compared. Gel-spinning has been used by Kamiya et al.[43], Kim et al [44] and others to prepare lead titanate fibres.
4. Etching of the powder can also be performed using acetic acid. It should be noted that acetic acid effectively accelerates the curing of epoxy resins and is difficult to completely remove from the particles' surface.

5.2 Lead Zirconate - PZT5H

The above-mentioned techniques, solid-phase reaction, sol-gel and co-precipitation can also be adapted to prepare lead zirconate titanate (PZT) and a number of reviews are available, for example those of Xu [38] and of Jaffe, Cook and Jaffe [45].

For the current study a commercial PZT, PZT5H from Vernitron plc was selected. This is a 'soft' PZT, ie. dopants are included to lower the coercive field, making it relatively easy to pole. Figure 5.9 shows the x-ray diffraction pattern of the powder, as received. The lack of definition shows that the PZT is not, at this stage, in a useable form. Furthermore, it also contains a polymeric binding agent, between 5 - 20% wt. of which is added to the ceramic to promote green strength. For our purposes this is not required and it must first be removed. The remainder can then be sintered, followed by rapid cooling and etching to produce an electroactive powder.

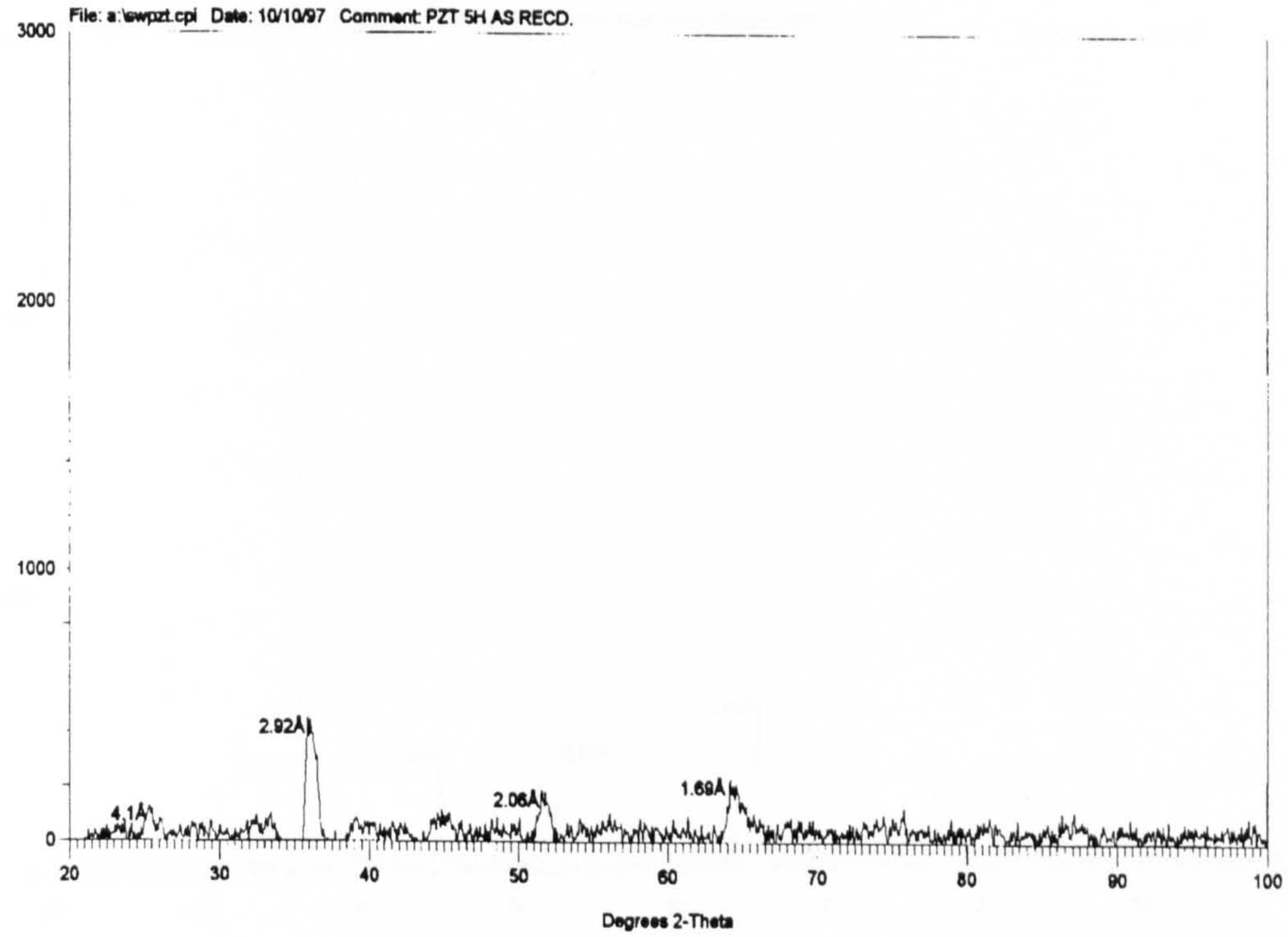

Figure 5.9 - X-ray diffraction trace of PZT5H powder as received

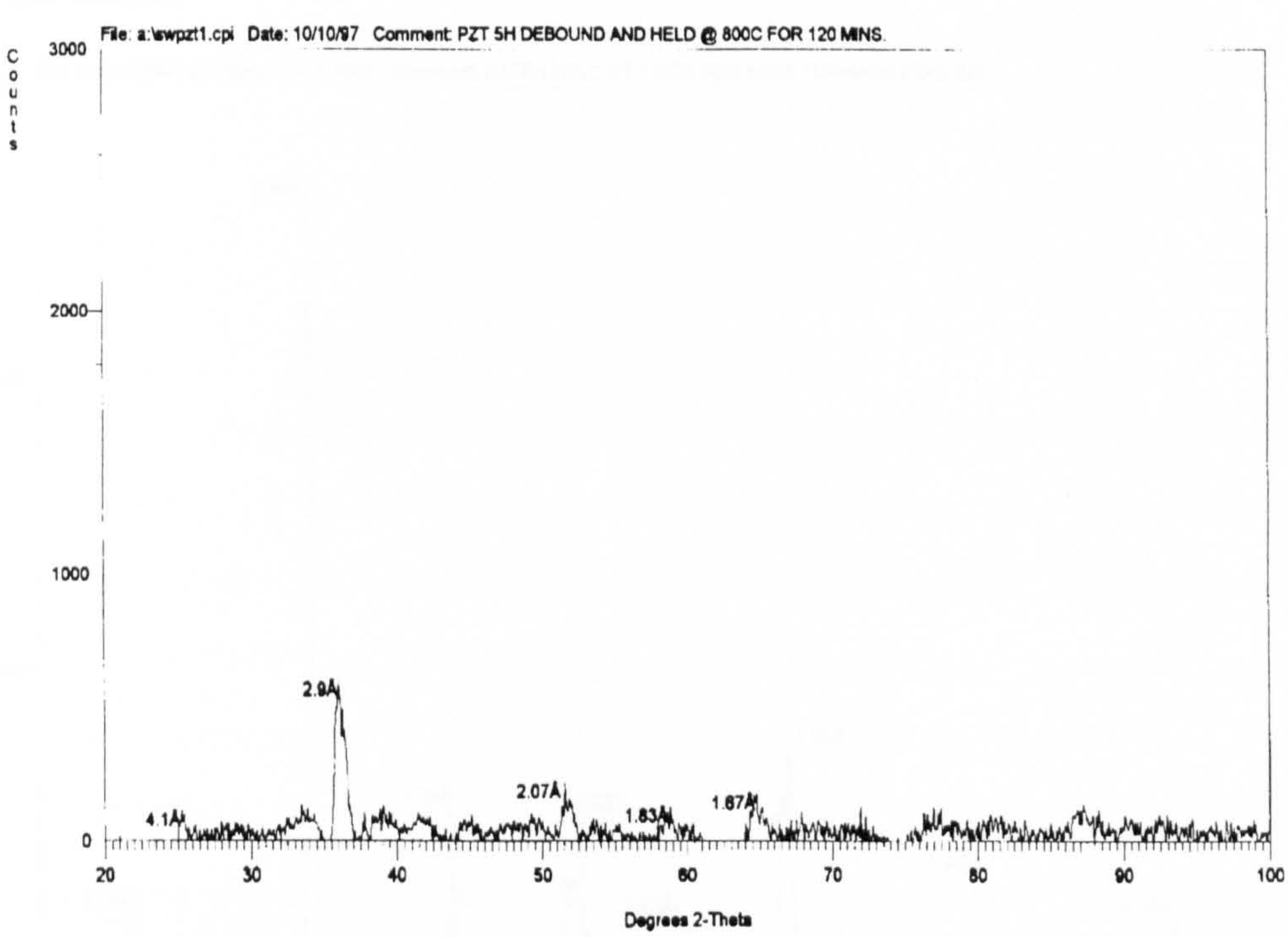

Figure 5.10a) - X-ray diffraction trace of PZT5H sintered at 800°C for 2hrs

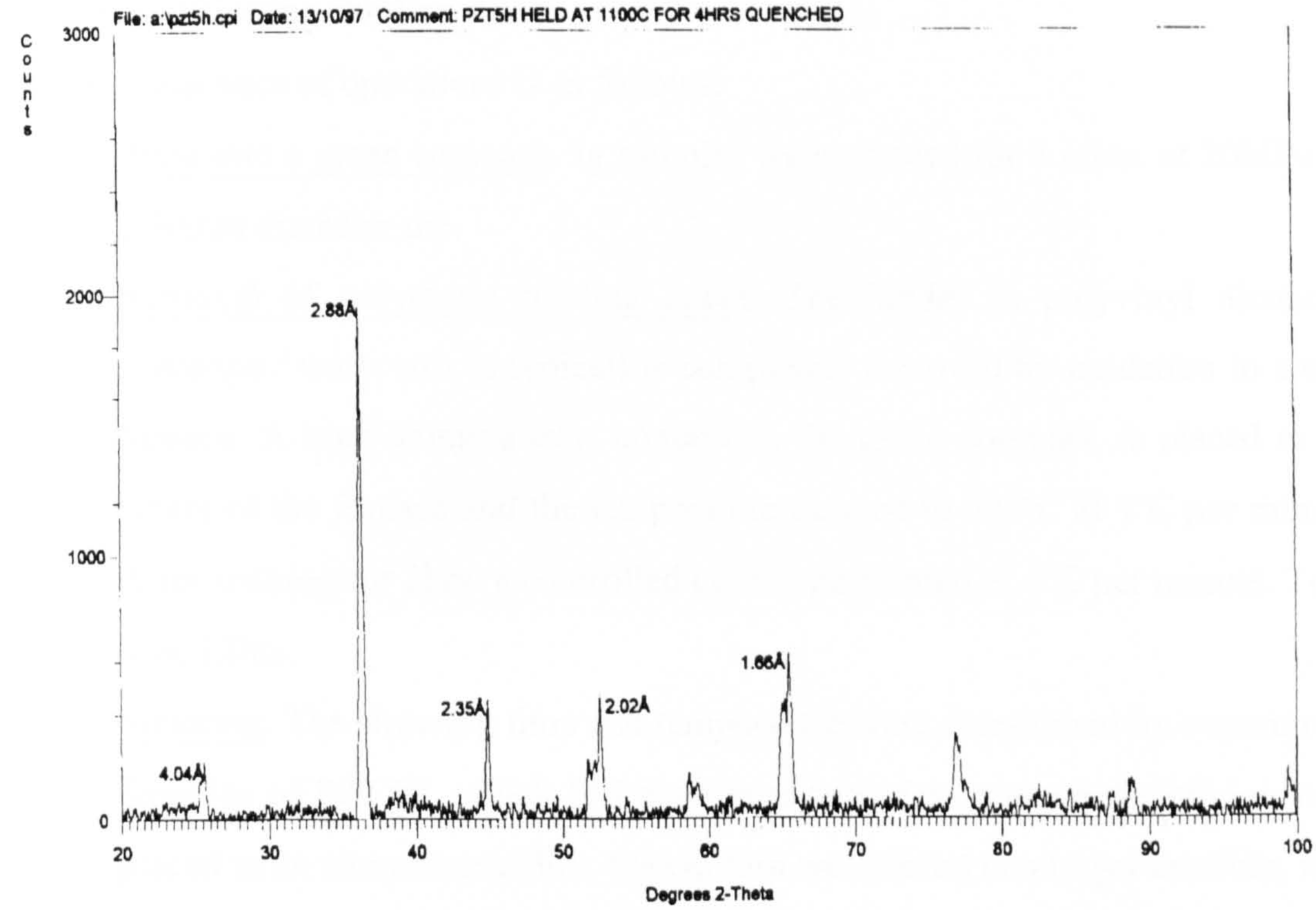

Figure 5.10b) - X-ray diffraction trace of PZT5H sintered at 1100°C for 4hrs. and quenched

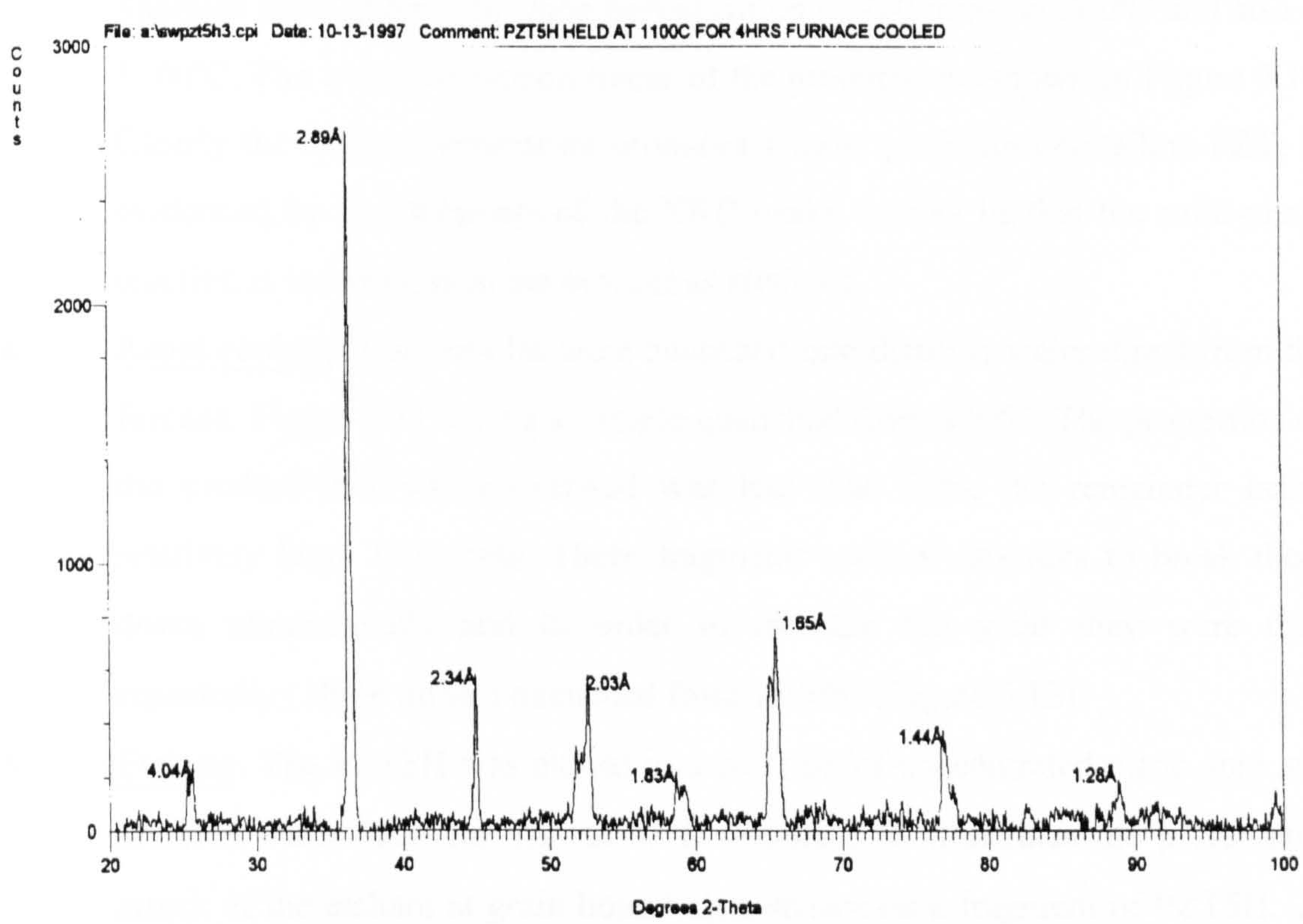

Figure 5.10c) - X-ray diffraction trace of PZT5H sintered at 1100°C for 4hrs. and furnace-cooled

5.2.1 Conditioning the Powder

The step sequence of operations is as follows:

1. Press into a green compact. 5g samples were pressed for 5 mins. at 20MPa in a 30mm diameter die.
2. Removal of polymeric binding agent. The binder (a polyvinyl alcohol / glycerine / water mix is typical) is completely removed by oxidation in a tube furnace. A high alumina tray, containing the green compact, is placed in the centre of the furnace and the temperature ramped to 500°C at 1°C per minute. After soaking for 2hrs. a controlled cool is performed at 4°C per minute. Total time 12hrs.
3. Sintering. The sintering time and temperature were determined by experiment. Samples of PZT5H, which had been heat-treated to remove the binder, were placed in an alumina crucible. This in turn was placed in a larger crucible, with a tight fitting lid, and surrounded by a spacer powder of PZT5H + 5%wt excess PbO. A spacer powder was used to restrict lead loss in the samples. Samples were sintered for time periods of up to 240 mins. at 800°C and also at 1100°C. The x-ray diffraction traces of the products are shown in Figure 5.10. Clearly the higher temperature produces a more perfectly crystalline PZT, as evidenced by the sharpness of the XRD peaks. It may be that the solid-phase reaction is incomplete in the powder as received.
4. Rapid cooling. The samples were quenched into distilled water direct from the furnace. Figure 5.11 shows a sample quenched from 800°C. The proportion of the product that was pulverised was less than 50%, the remainder being relatively large fragments. These fragments resisted attempts to break them down ultrasonically and in order to increase the yield they were then repeatedly (three times) quenched from 1100°C (Figure 5.12).
5. Etching. The PZT5H was etched in a solution of concentrated nitric acid and distilled water (1:8) for 1hr. at 65°C. Figure 5.13 illustrates the preferential attack of the etchant at grain boundaries, shown on a fragment of PZT5H. To achieve a high yield such fragments must be broken down prior to etching.

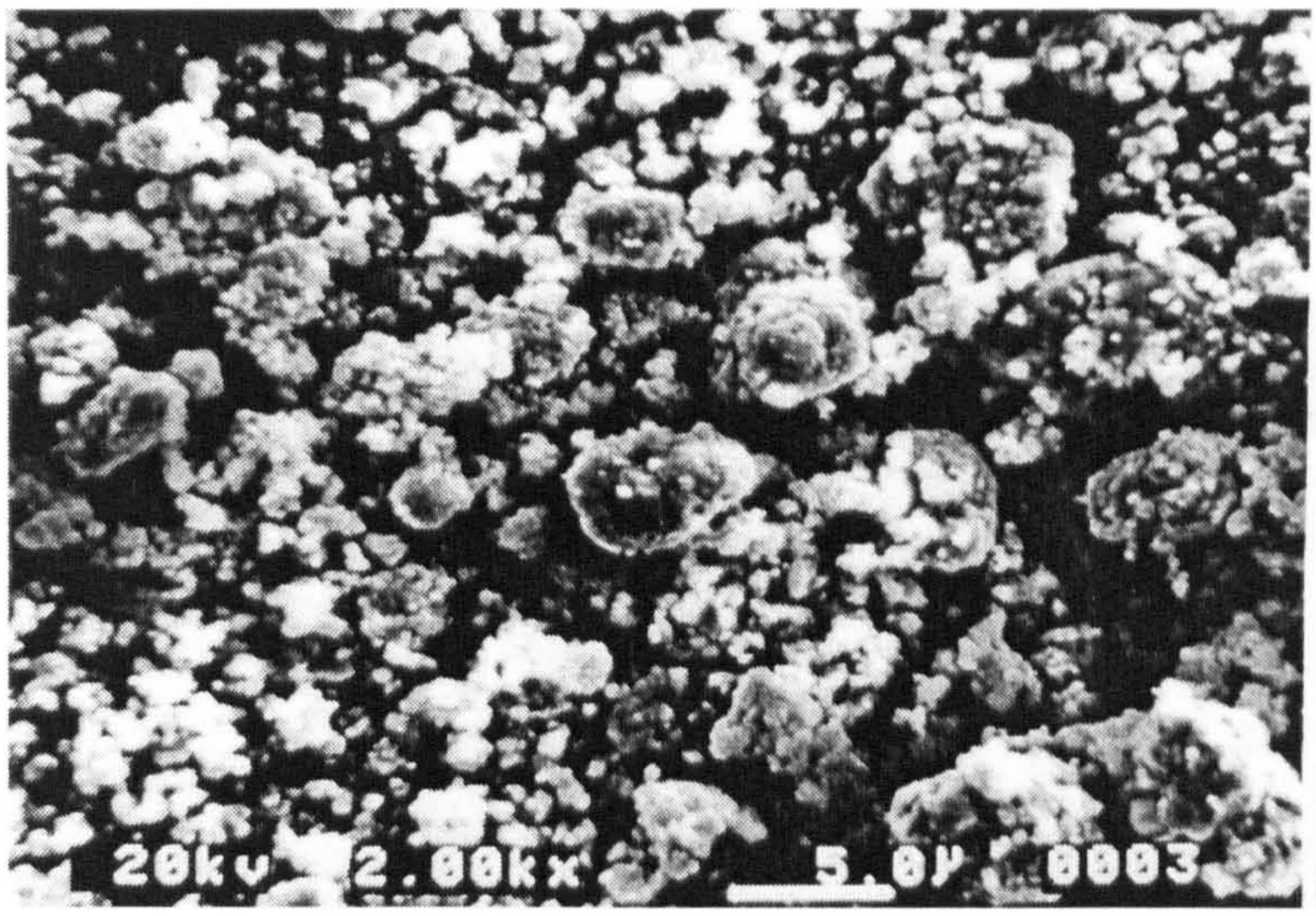

Figure 5.11 - PZT5H quenched from 800°C (x 2000)

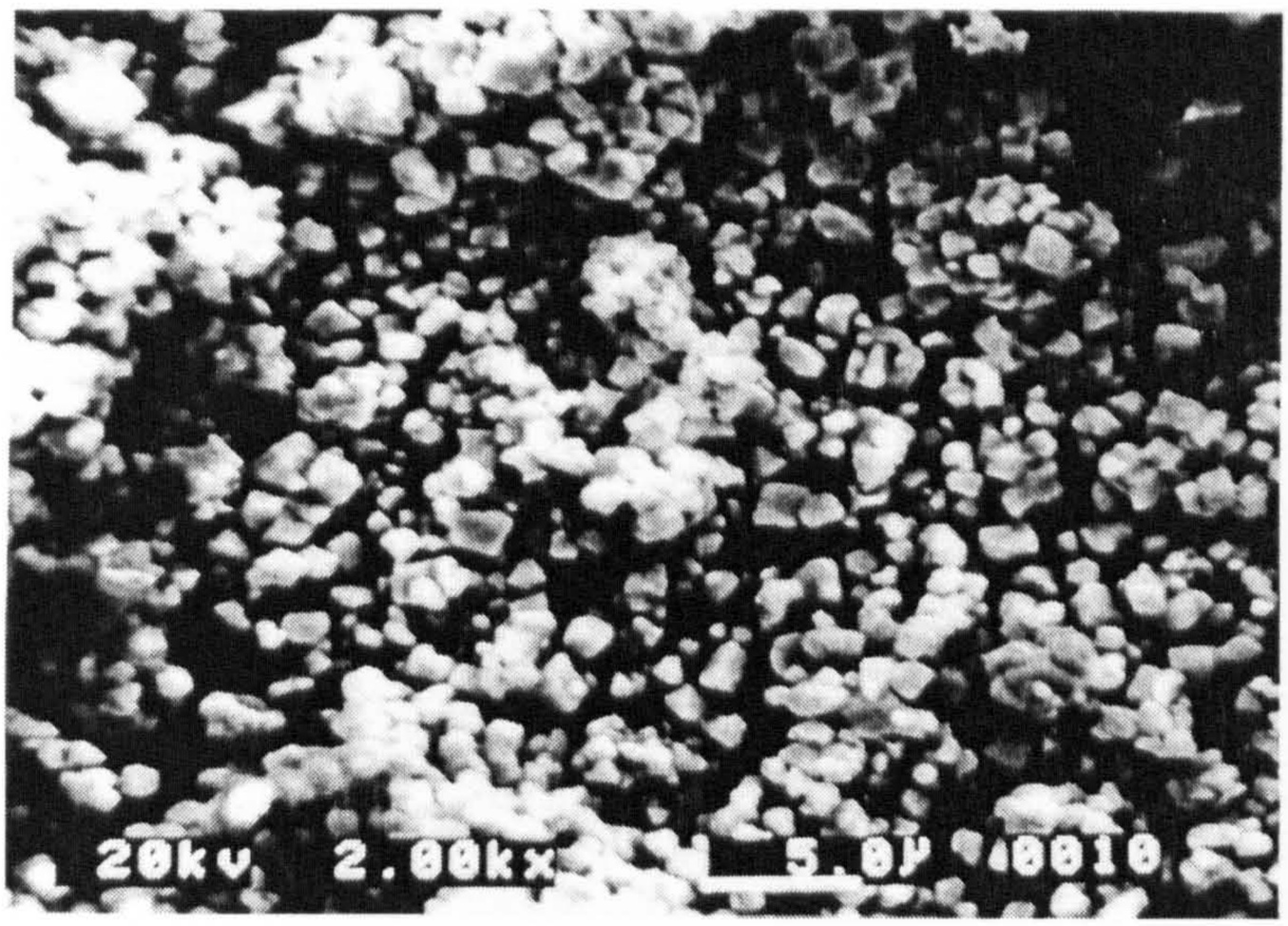

Figure 5.12 - PZT5H repeatedly quenched from 1100°C (x 2000)

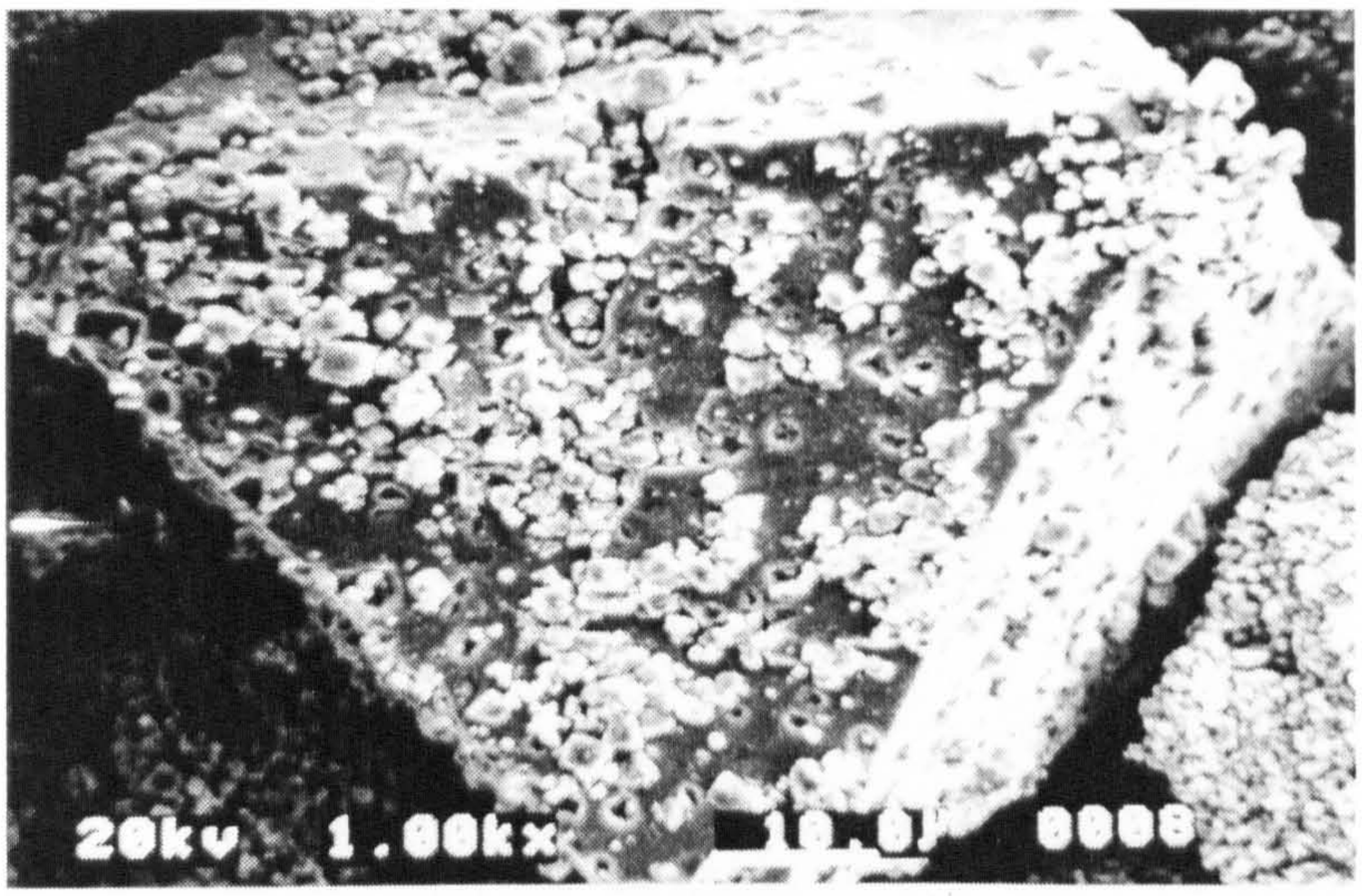

Figure 5.13 - Surface attack of nitric acid on a fragment of PZT5H (x 1000)

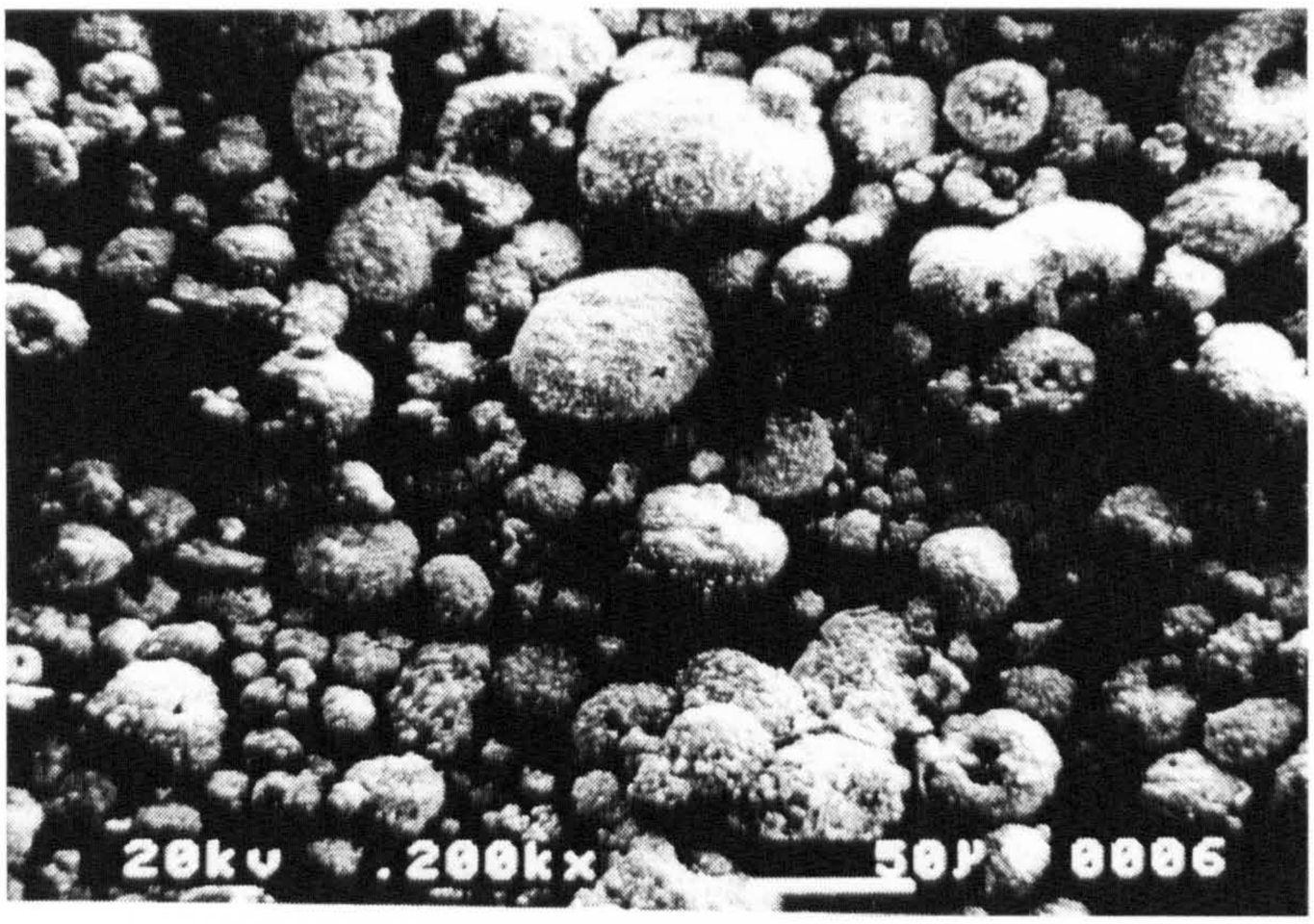

Figure 5.14 - PZT5H agglomerates after etching (x 200)

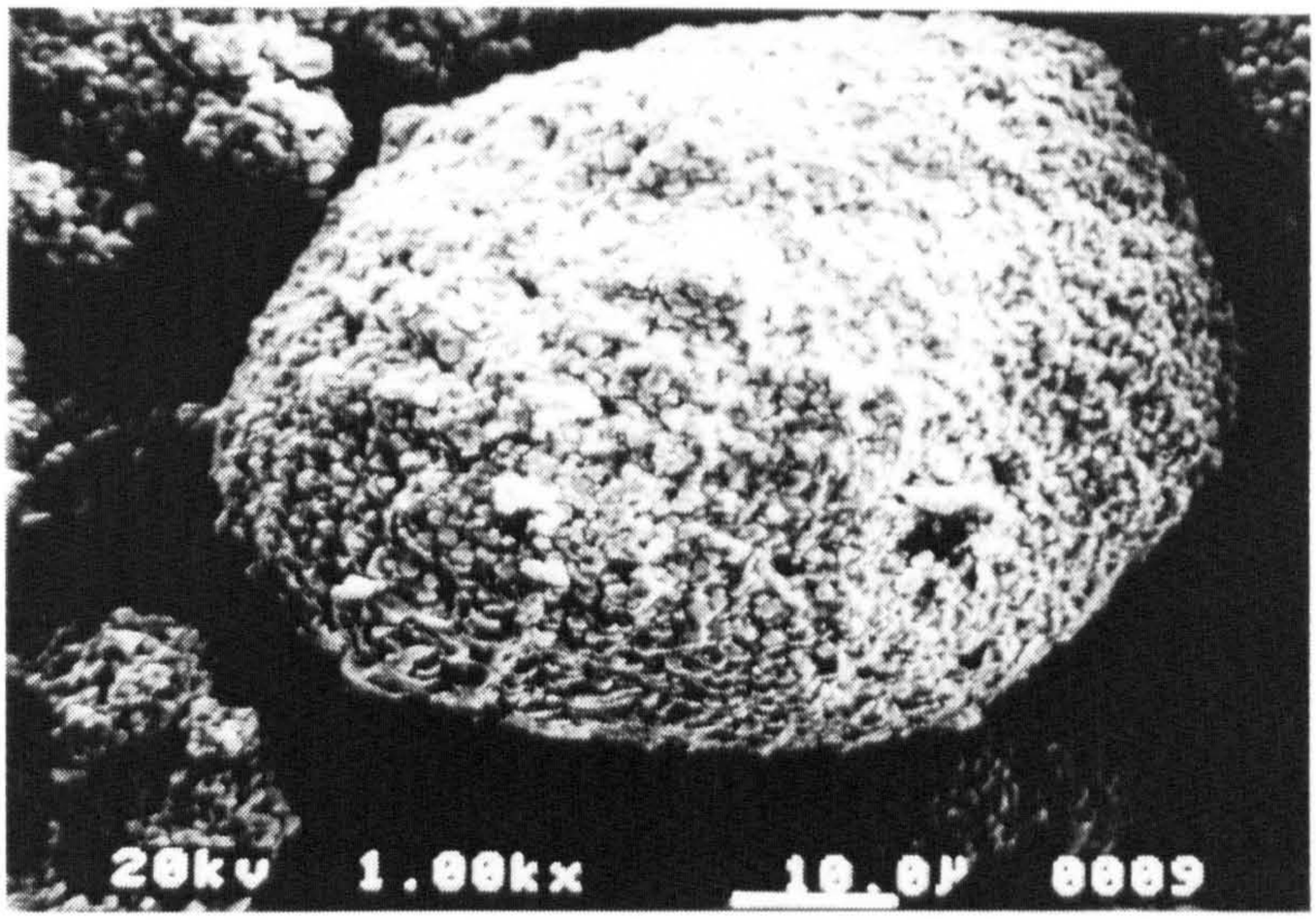

Figure 5.15 - PZT5H single agglomerate after etching (x 1000)

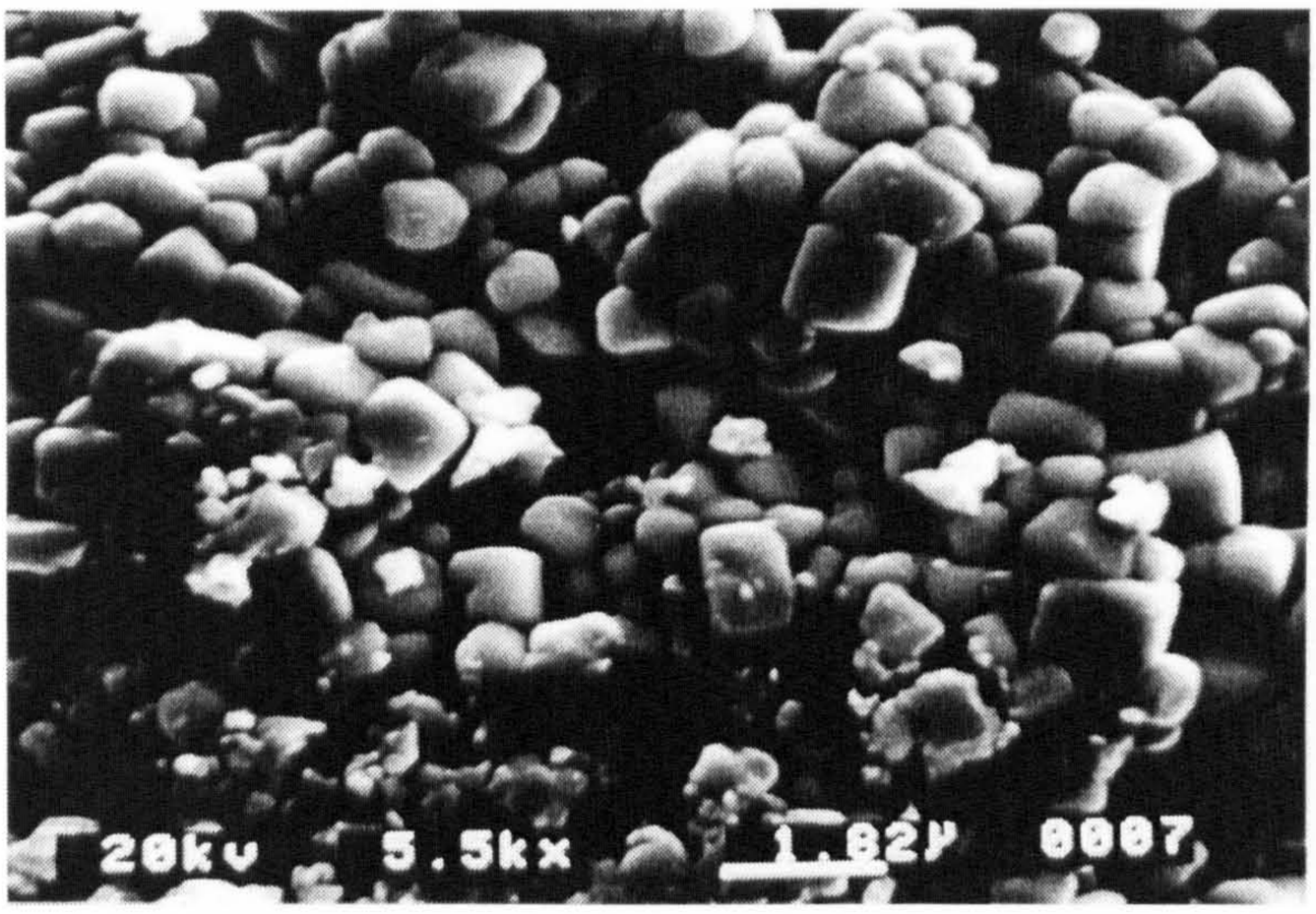

Figure 5.16 - PZT5H agglomerate structure after etching (x 5500)

Figures 5.14 to 5.16 show agglomerates after etching at different magnifications. The exposed individual regular crystallites are around 1μm in diameter.

Note: Particle size distribution can be improved by decanting the supernatant fluid containing sub-micron sized particles in suspension, when the etchant is rinsed from the product.

5.2.2 Growth of PZT Crystallites.(Background)

For the purposes of this study, it is desirable to have a larger mean particle size. This would correlate more closely with the work on lead titanate, as well as giving composites with improved piezoelectric properties. A way to achieve this is by flux-growth and this has been widely reported, usually with the aim of growing large single crystals. There is also considerable interest in using the technique to lower the sintering temperature of PZT ceramics. A variety of fluxes has been used, most notably KF-PbF_2 [46], $2PbF_2$ - NaF [47], PbO and PbO-PbF_2 [48,49]. The first two of these have been shown to have limitations with certain PZT compositions, either in terms of crystal growth or in their effect on the final properties of the crystals so-produced. The importance of PbO atmosphere control and its essential role in the sintering of PZT ceramics is discussed by Kingon and Clarke [50]. Boron oxide (B_2O_3) is commonly added to a flux system to control PbO volatilization. A private communication to this group, taken from recent work, has suggested an optimum flux ratio of Pb0 : PbF_2 (40:15 mol). This compares to the eutectic composition of %Pb0:PbF_2 (46:54 mol) shown in the phase diagram Figure 5.17

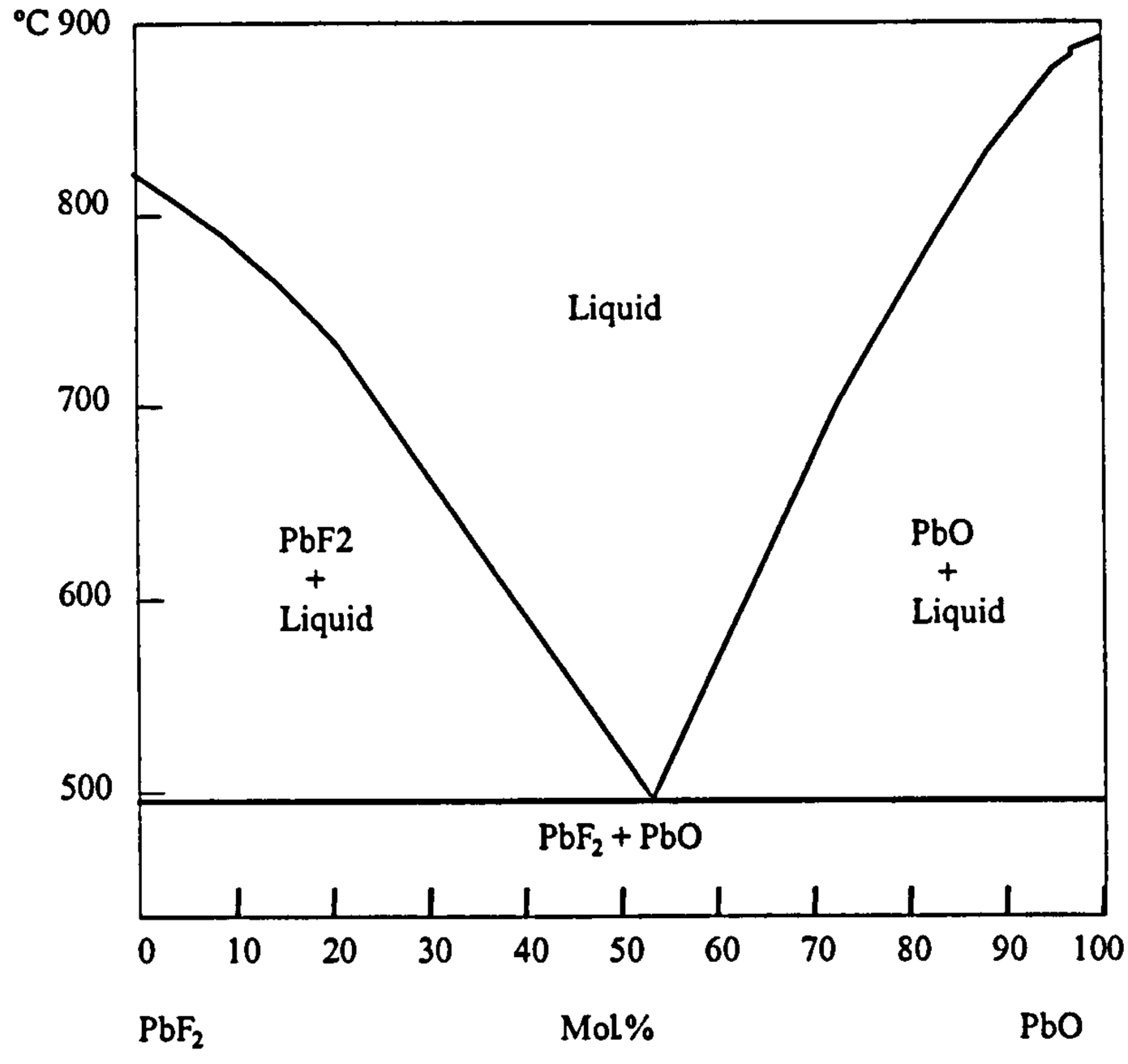

Figure 5.17 - Phase diagram of the PbF_2 - PbO system

5.2.3 Growth of PZT Crystallites (Experimental)

Experiments were carried out to determine the possibility of integrating both PbO and PbO- PbF_2 fluxes into the powder preparation route to achieve a larger median particle size. The variables which were explored were flux composition, the PZT to flux ratio and sintering time.

Flux composition a). Two samples of PZT5H with 20%mol. of flux were sintered at 1100°C for 4hrs. Both were repeatedly quenched and etched as previously described. In one sample a pure PbO flux was used in the other a PbO : PbF_2 (40:15 mol) flux. Some grain growth was evident from the PbO : PbF_2 flux which produced particles having a narrow size distribution in the range 1-4 μm range. In addition the yield was improved. Fewer agglomerates were present and these were loose and relatively easy

to break down in the etching process. In contrast no grain growth was observed from the PbO flux. There was a much lower yield of good particles and more agglomerates. These were markedly harder and more difficult to break down. Figure 5.18 shows x-ray diffraction traces of the two flux-grown samples. The peaks are significantly sharper than those in Figure 5.10, indicating more perfect crystals and probably some variation in the dopant concentration. Some peaks are notably absent from the flux-grown trace and the indication is that the crystal structure appears to have moved from tetragonal with some rhombohedral to a more cubic structure.

Sintering time. Samples of PZT5H with 20%mol. flux in the composition PbO : PbF_2 (40:15 mol) were sintered for periods of 2hrs, 4hrs, 8hrs and 16hrs. After quenching and etching the following observations were made:

After 2hrs - the powder had a particle size distribution in the range 1-6 μm, and there were some agglomerates.

After 4hrs - as above with fewer agglomerates and fewer small (1μm) particles.

After 8hrs - little change, a few small agglomerates, significant numbers of particles in the 8-10 μm range.

After 16hrs - very few agglomerates and these on a par with the largest grains, size distribution ~90% of particles in the 2-5 μm range.

Total amount of flux. Two samples containing 20%mol. and 40%mol. of PbO : PbF_2 (40 : 15) flux were processed under identical conditions. Examination by SEM and x-ray diffraction failed to highlight any differences in the product.

5.2.4 Preparation of Lead Zirconate Titanate Powder - PZT5H (Concise)

A sample was prepared where the flux composition was PbO : PbF_2 (1:1) which closely approximates to the eutectic composition. The sintering temperature was 1100°C, the dwell time 16hrs, the product was repeatedly quenched and etched in nitric acid. The powder so produced showed significant grain growth with a narrow particle size distribution in 5-10 μm range. The x-ray diffraction trace of the product showed a more complex structure than had been evident in the previous flux-grown

samples and this closely resembled the original (Figure 5.10c). This route was adopted to produce PZT5H powder for the model composite materials. Comparison of Figures 5.19 and 5.20 illustrates the improvement in grain-size that the modified processing route can achieve.

The density of the PZT5H was measured by pycnometry to be 7.349×10^3 kg m^{-3}.

Note: Some novel methods exist for the preparation of PZT which may well be useful in the current context. Yoshikawa et al. [52] have produced PZT fibres by gel-spinning; Kimura et al. [53] have made 'needle-like' PZT by reaction of PbO with a form of $TiZrO_4$; Wen et al. [54] have produced PZT microspheres by flame-treating a powder.

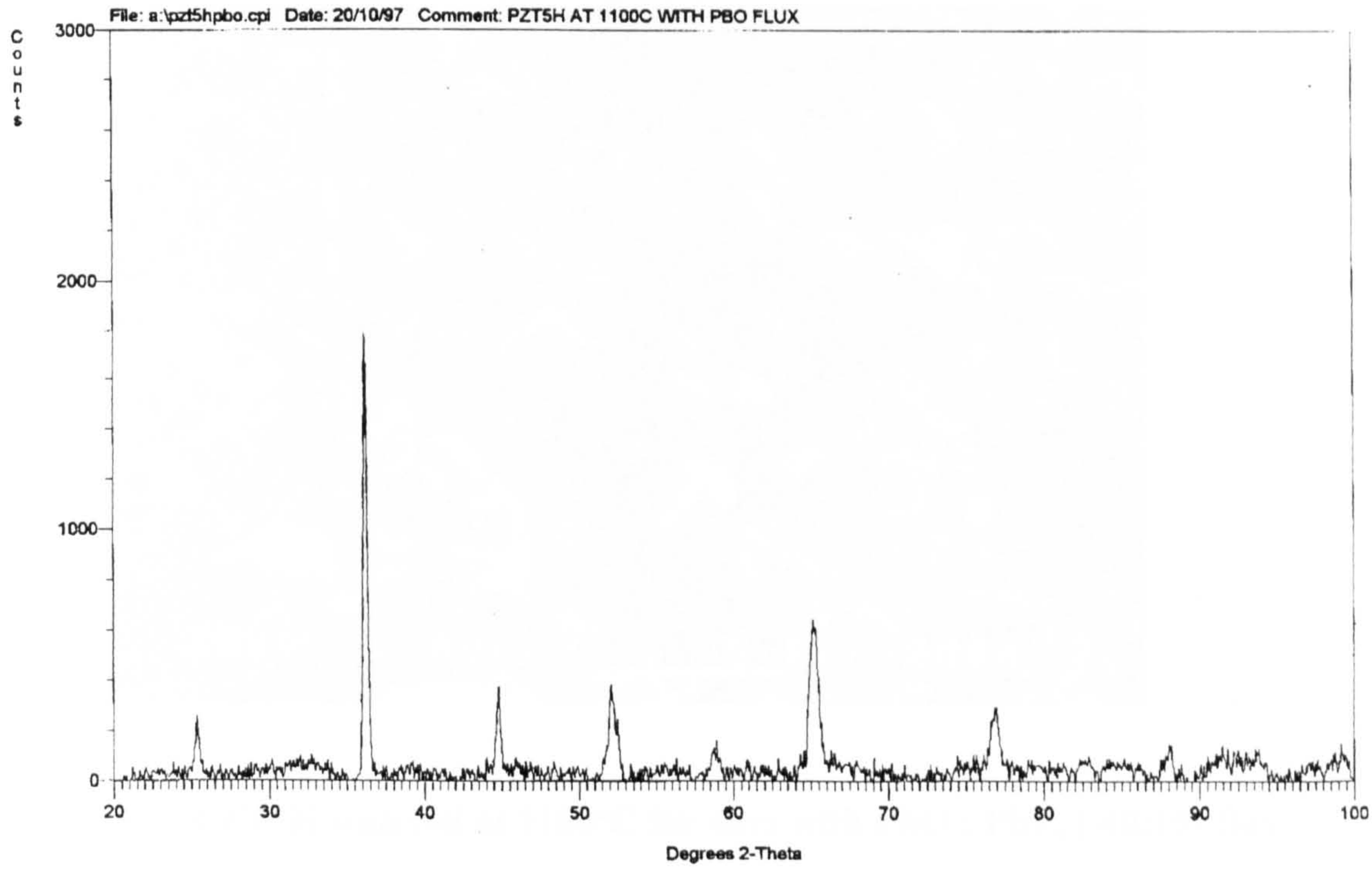

Figure 5.18a) - X-ray diffraction trace of PZT5H grown from 20%mol. PbO flux

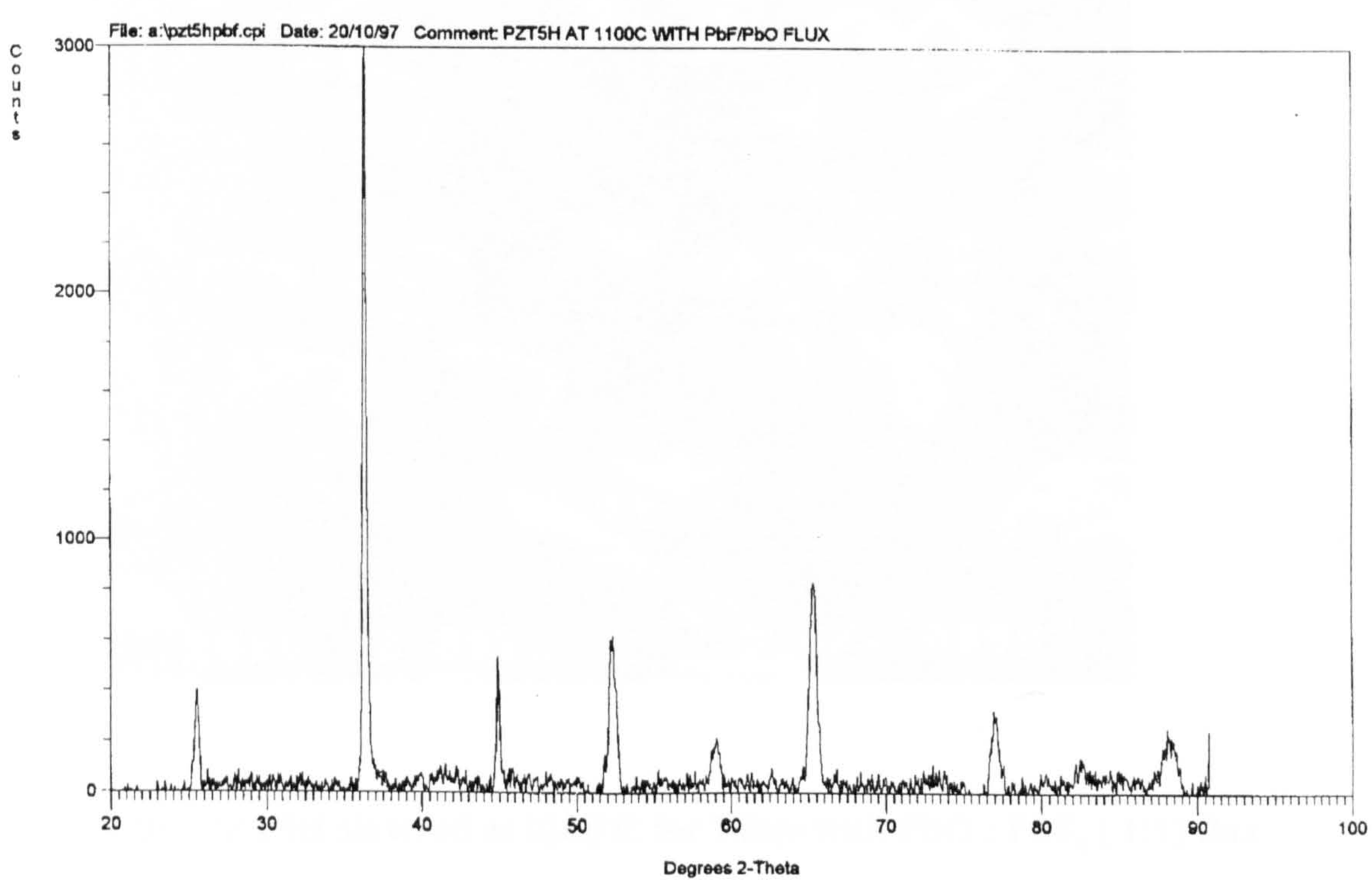

Figure 5.18b) - X-ray diffraction trace of PZT5H grown from 20%mol. flux - PbO : PbF_2 (40 : 15)

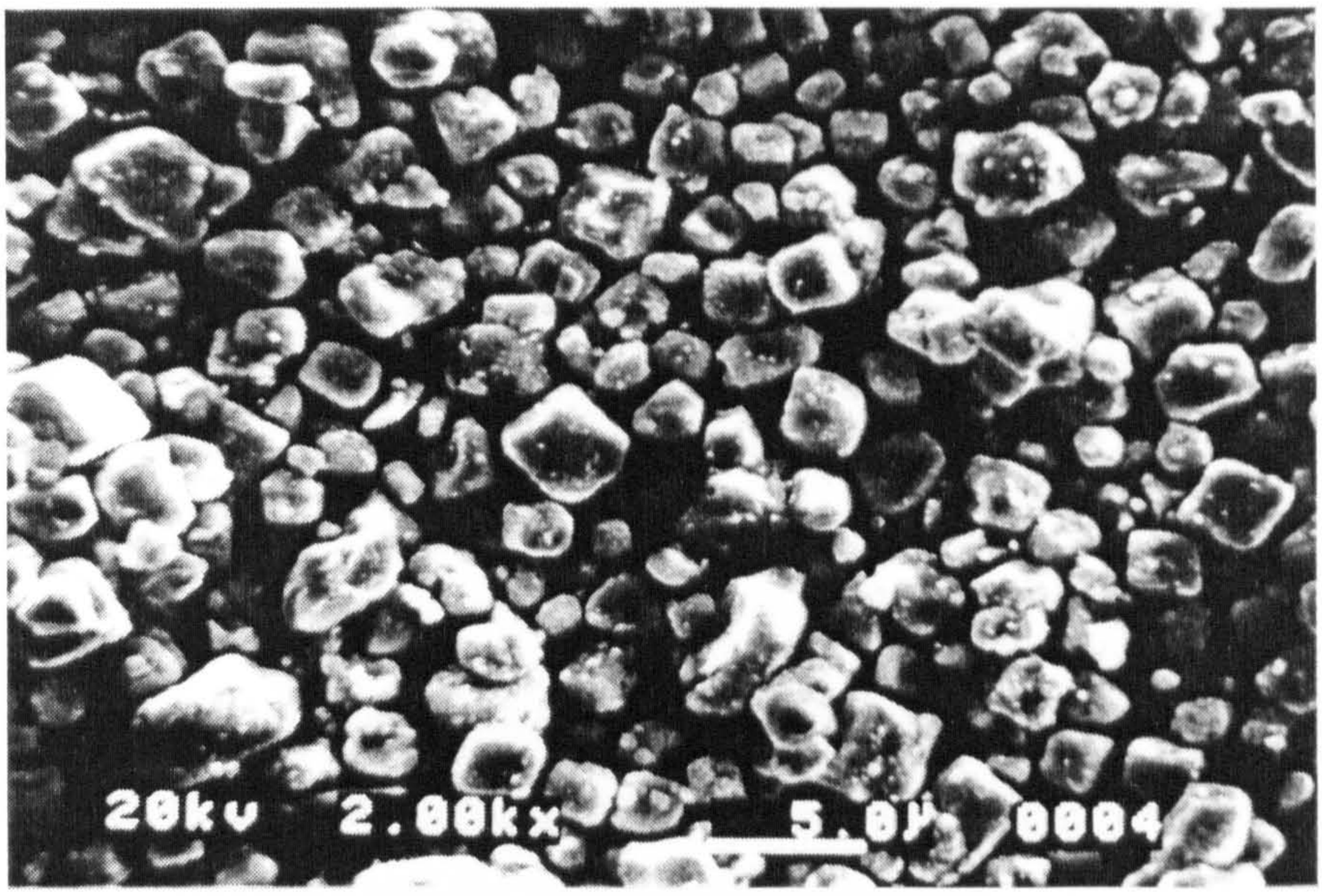

Figure 5.19 - PZT5H sintered at 1100°C for 4hrs with PbO : PbF_2 (40:15) flux

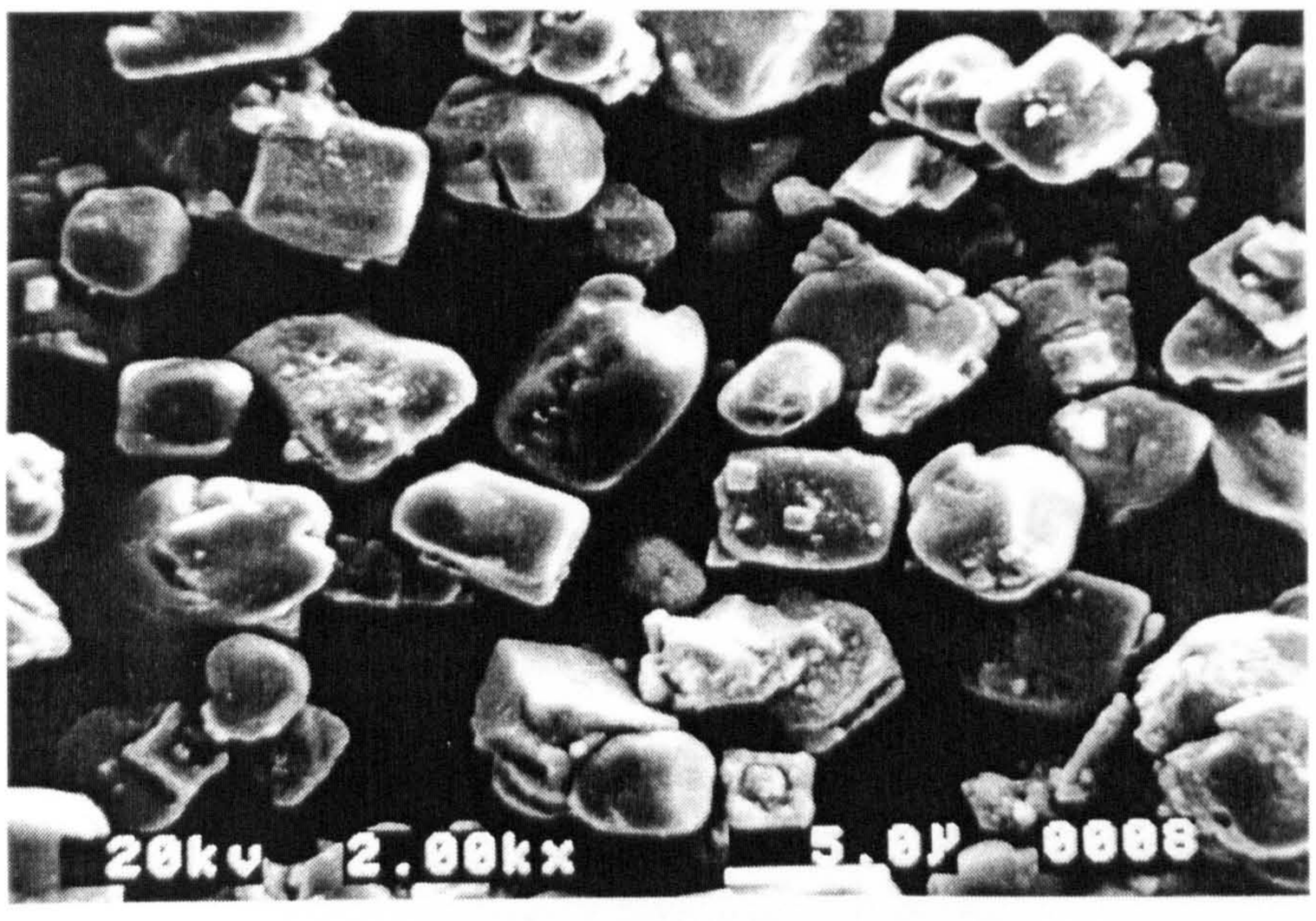

Figure 5.20 - PZT5H sintered at 1100°C for 16hrs with PbO : PbF_2 (1:1) flux

6. Polymer Phase

6.1 Material – Epotek 302-3M

Piezoelectric composites with a thermosetting polymer matrix have been widely studied and several are available commercially as transducer materials. They are therefore of technological interest and an epoxy-resin matrix composite was selected as the model for the current study.

The compound chosen was a low conductivity, optically clear two-part epoxy (Epotek 302-3M, from Epoxy Technology Inc., Billerica, MA, USA). This is predominantly a resin based on diglycidyl ether of bisphenol-A (DGEBA):

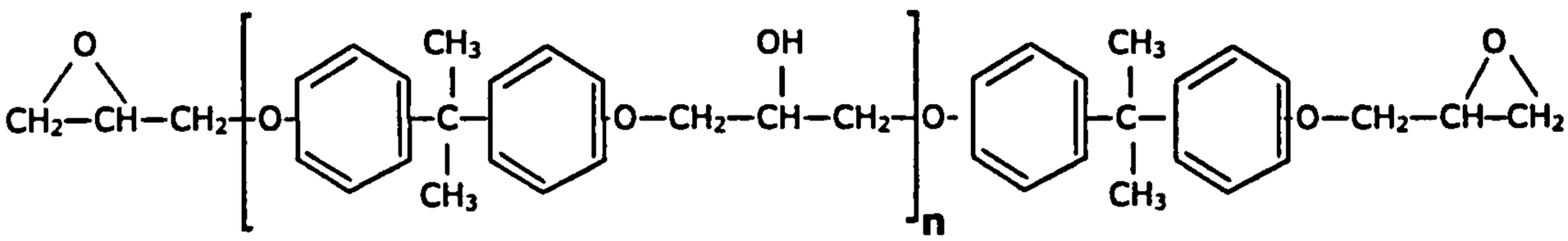

DGEBA is the most commonly available epoxy prepolymer. In addition to the reactive epoxy groups on the chain ends, there are also hydroxyl groups in the repeat units which are available for crosslinking by amines or by reaction with epoxy groups (etherification). Values of n, in commercial resins, usually lie in the range 0 to ca.10 (molecular weights in the approximate range 340 to 3000).

The curing agent is based on the multi-functional aliphatic amine, poly(oxypropyl)-diamine:

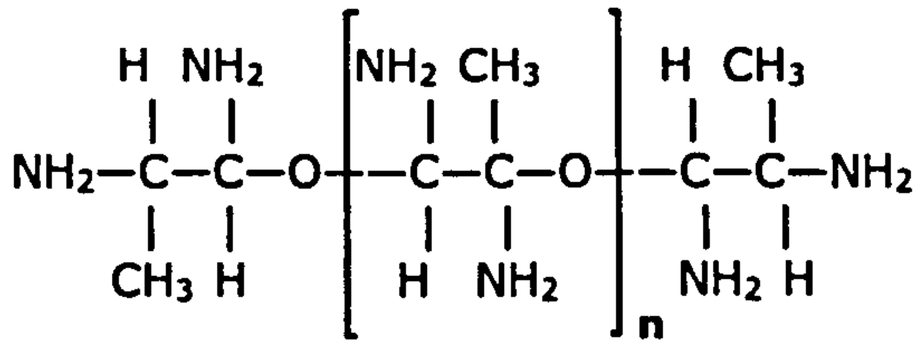

Both parts of Epotek 302-3M are clear liquids at room temperature. The manufacturers' data shows the resin to have a typical viscosity of 1600cps after mixing at 25°C. This is relatively high among commercial epoxies and gives an advantage in the current context, in that it will serve to inhibit sedimentation of the dense ceramic powder during the field structuring process. The resin is said to have a glass-rubber transition temperature (T_g) of 52°C when cured at 65°C for 90mins. Post-curing the resin at 150°C for 1hr. raises T_g to 96°C. Refractive index is given as 1.5340 and transmission of light at optical frequencies is >96%. Pot-life is around 90mins at room temperature.

6.1.1 Epoxy Resins - Cure Cycle.

The two liquid components of the resin system are designed to react chemically to produce a high molecular-weight network polymer. Initially, at a typical cure temperature, the reaction is kinetically controlled. As the polymer network begins to form, there is an associated increase in local viscosity and the liquid becomes a rubbery gel. This physical change progressively affects the reaction kinetics by inhibiting the mobility of the reactants. The network continues to form until the resin solidifies into a glass. Near this point, mobility of the reactants is hindered to such an extent that the reaction cannot be described solely in terms of chemical kinetics. The reaction effectively becomes diffusion-controlled. Consequently, a situation may arise whereby the reaction is fully quenched, even though a complete conversion of the reactants has not been achieved. In that event the temperature could subsequently be raised for a period to drive the reaction to completion and this would be accompanied by an increase in T_g.

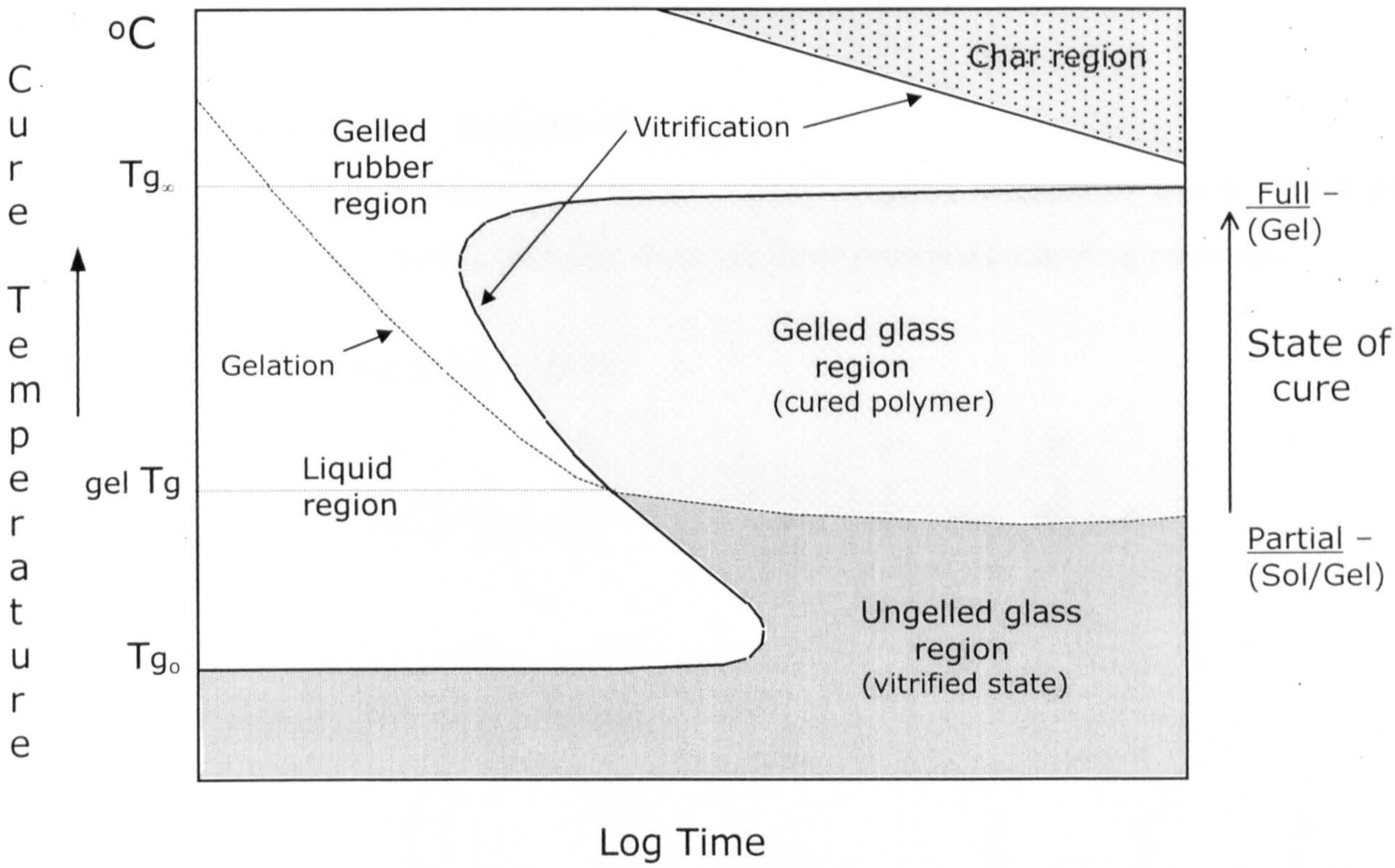

Figure 6.1: Generalized time-temperature transformation diagram for a thermosetting resin curing under isothermal conditions (adapted from J.B. Enns and J.K. Gillham [55]).

The characteristic time-temperature transformation diagram for this type of reaction is shown in Figure 6.1. This a general scheme, adapted from the work of Enns and Gillham [55], which illustrates the physical changes displayed by the material, under isothermal conditions, as the cure reaction progresses. Changes in physical properties are directly governed by the extent of chemical conversion. The marked temperatures are: Tg_0 - the glass transition temperature of the uncured reactants; gel Tg - the temperature at which gelation and vitrification occur simultaneously and Tg_∞ - the maximum glass transition temperature of the fully cured network. Significantly, it has been shown that there is a direct correlation between the value of Tg and the extent of conversion of the reactants, which is independent of cure temperature [56].

Note: it is common that a resin held at Tg_∞ for an extended period of time will revert to a rubbery state, so-called 'devitrification'. The maximum continuous-service temperature of the resin would then be somewhat lower.

6.1.2 Epoxy Resins - Reaction Mechanism

The mechanism of the primary amine - epoxy reaction mechanism was a subject of debate for many years. Essentially there are three principal competing reactions:

a) Primary amine-epoxy addition

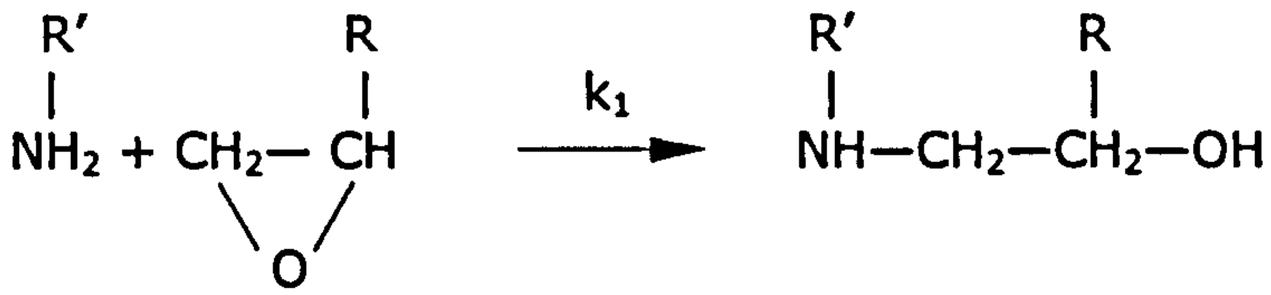

b) Secondary amine-epoxy addition

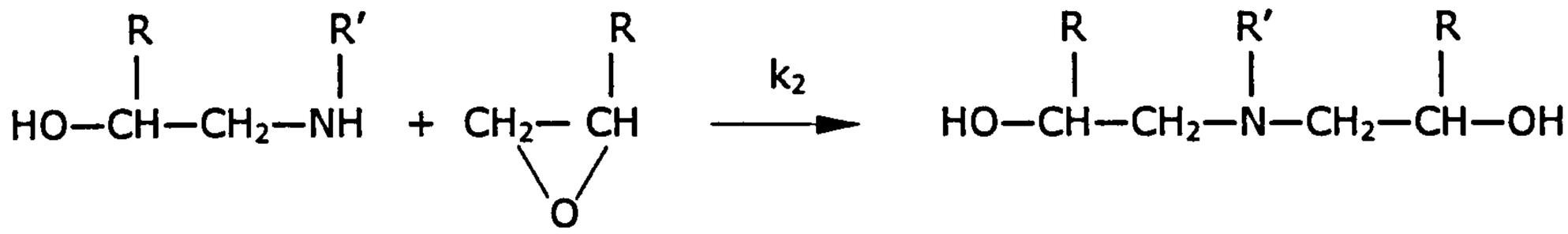

c) Hydroxyl - epoxy (etherification)

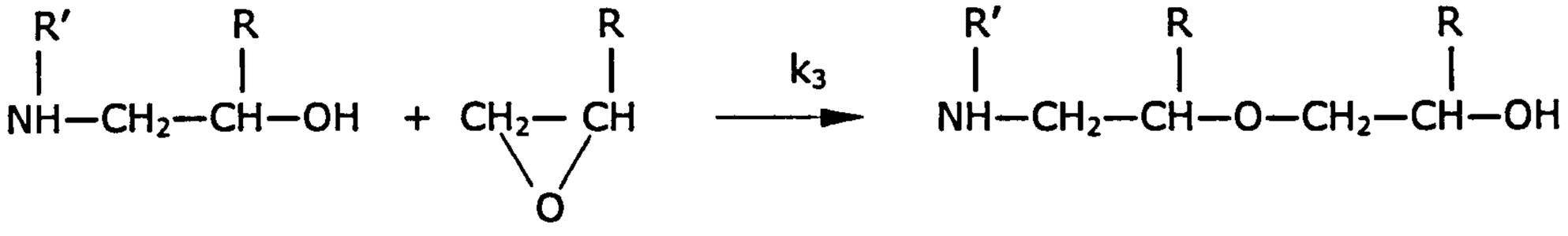

Of these the primary and secondary amine-epoxy additions assume greatest significance. Both of these reactions are found to be catalysed by the hydroxyl groups formed in the product (autocatalysis) [57]. This autocatalytic action has led to the following scheme being proposed as a reaction mechanism:

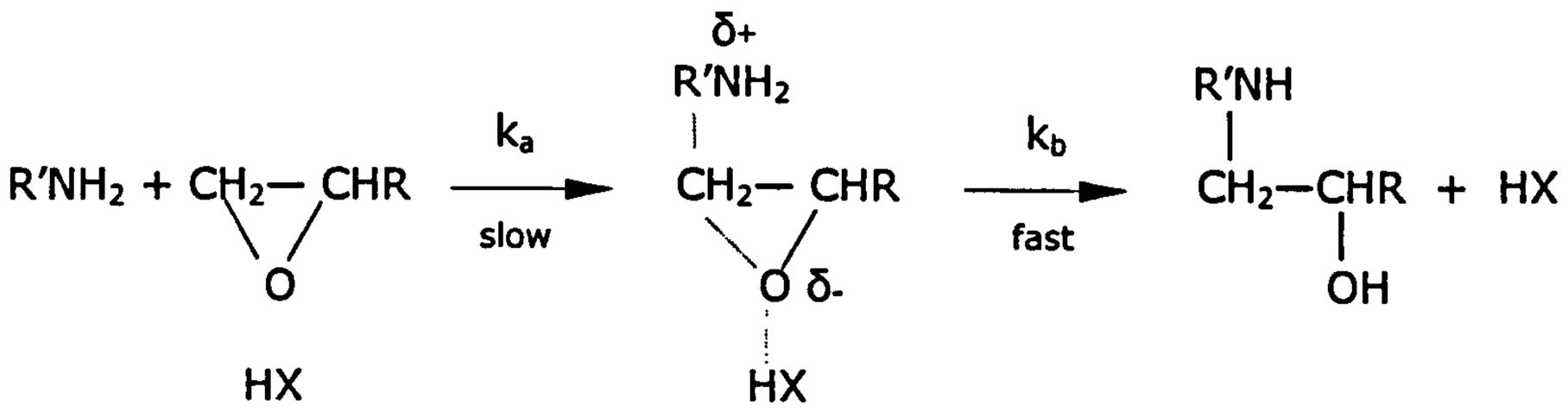

Where HX is any hydrogen bond donor, typically hydroxyl groups on the reaction products, impurities or an added catalyst. Shechter et al. [58] noted that cross-linking of low molecular weight epoxy resins with polyamines was accelerated by a large number of chemicals capable of acting as hydrogen bond donors, eg. alcohols, phenols, acids, amides, sulphonamides.

6.1.3 Epoxy Resins - Kinetics

The autocatalytic model has been analysed and developed by several groups and it has successfully been used to characterise the chemical kinetics of the cure reaction. Wisanrakkit and Gillham [59], in their comprehensive study, showed that although the autocatalytic model suggests third order kinetics, it can in fact be satisfactorily expressed using a single overall rate constant with an Arrhenius type temperature dependence.

In the diffusion-controlled regime, ie. close to vitrification, the diffusion of chemical reactants limits the rate of reaction. Here the Williams-Landel-Ferry (WLF) equation [60], which is based on free-volume considerations and is a widely accepted model of diffusion-controlled processes in the region of T_g in amorphous polymers, has been adapted to closely describe the reaction rate [59].

The overall rate constant (k_a) for the curing process therefore, has the form suggested by Havlicek and Dusek [61]:

$$\frac{1}{k_a(\alpha,T)} = \frac{1}{k_T(T)} + \frac{1}{k_d(\alpha,T)},$$

here k_a is the overall rate constant, k_T is the kinetic (Arrhenius) rate constant and k_d is the diffusion rate constant, α represents the extent of conversion and T is temperature. The equation shows that overall rate is dominated at one extreme by the Arrhenius rate constant, where ($k_d >> k_T$) and at the other by diffusion, which is the case after vitrification, here ($k_T >> k_d$).

6.1.4 Epoxy Resins - Viscosity

Changes in the physical properties of the curing polymer, such as viscosity, are directly linked to the extent of conversion of the reactants which, in turn, is a function of both time and temperature. A prediction of viscosity, therefore, requires information not only about chemical kinetics but also about the temperature dependence of viscosity.

Before gelation takes place, the zero-shear bulk viscosity is directly proportional to the weight average molecular weight M_w. Increase in M_w can be described by an Arrhenius-type expression and therefore the viscosity-temperature relationship also has this form. Roller [62] also views flow to be an energy-activated process and has developed the following chemorheological expression by correlating viscosity with cure time at fixed temperature:

$$\ln \eta = \ln \eta_\infty + \left(\frac{\Delta E_\eta}{RT}\right) + k_\infty \int_0^t \exp\left(\frac{\Delta E_k}{RT}\right) . dt$$

where ΔE_η is the activation energy for viscous flow, η_∞ is a constant and k_∞ , ΔE_k are kinetic parameters of the cure reaction. Tajima and Crozier [63,64] have criticised this approach and found that better results are achieved by relating viscosity to temperature for a given extent of conversion. Their expression resembles the Williams-Landel-Ferry equation [60].

Maistros and Bucknall [36] have recognised the intrinsic non-linearity of the viscosity - extent of conversion relationship. They point to the standard gelation theory of Flory [65], which uses probability to estimate the extent of cure at gelation. According to this theory, it is found that a difunctional epoxy resin and a tetrafunctional amine

curing agent, in stoichiometric ratio, will gel when 58% of the reactants have been converted. At this conversion the resin has a Tg = gel Tg , the point at which gelation and vitrification coincide. Plotting log η against extent of conversion shows that the relationship is linear up until 35% of reactants have been converted. Beyond this point chain entanglement becomes significant and viscosity rises according to an empirical second order polynomial equation until gelation occurs.

6.1.5 Epoxy Resins - Industrial Practice

In many practical situations, notably the industrial production of composites, it is desirable to apply pressure to a curing thermoset. This prevents the formation of voids due to shrinkage or gas entrapment. Applied pressure, in a sense, acts contrary to an increase in temperature and brings about a non-linear increase in viscosity. On a molecular level, however, whereas an increase in temperature will reduce viscosity by increasing free-volume and hence segmental mobility, an increase in pressure is not found to significantly reduce free volume; it is occupied volume that is reduced and this restriction serves to increase viscosity [66]. Similarly it is expected that the overall rate of reaction will have a pressure dependence in both the kinetically-controlled and the diffusion-controlled regimes.

The properties of the finished composite are dictated by processing, which makes precise control of the cure cycle desirable. This is by no means an easy task, as can be appreciated from the above discussion. In an industrial setting the picture is clouded by large variations in part geometry and the exothermic nature of the cure reaction, which make even curing throughout an entire component difficult to achieve.

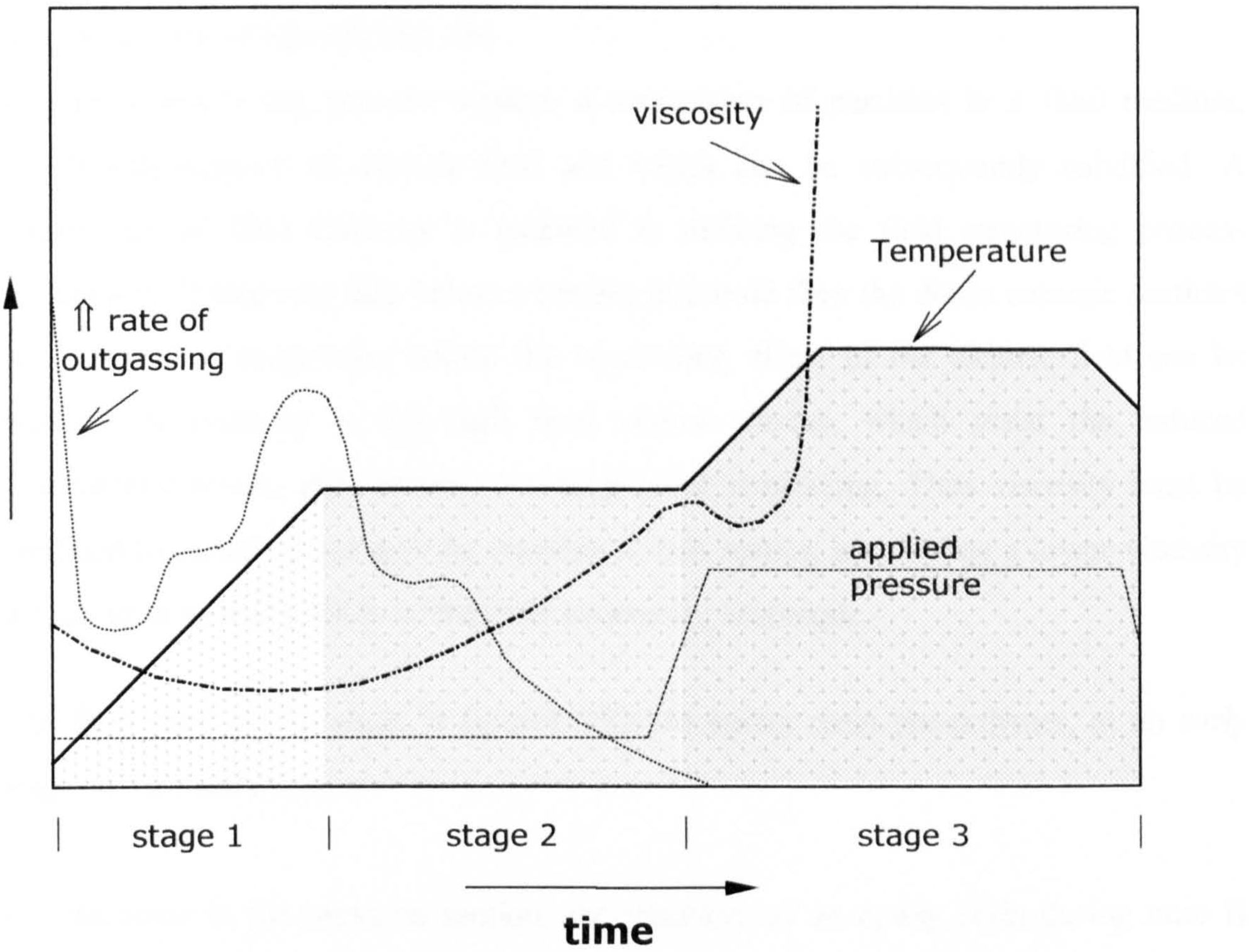

Figure 6.2: Schematic diagram of an epoxy-composite cure cycle. The relationship between the critical process parameters (temperature and pressure) and resin viscosity is shown, as is the rate of degassing (adapted from Tajima and Crozier [63]).

Figure 6.2 is a schematic diagram of a typical industrial cure cycle for an epoxy-composite:

Stage 1 is designed to allow de-gassing of the resin (removal of dissolved air), which progresses more quickly at lower viscosity. The reaction rate is adjusted by means of a chemical accelerant to permit sufficient time for this to happen.

Stage 2 - the cure reaction proceeds.

Stage 3 - before the resin has gelled, pressure is applied. Resin is still able to flow around the filler to prevent voids forming as the composite is compacted. The reaction proceeds to completion.

6.2 Viscosity of Epotek 302-3M

The field structuring process requires a suspension of particles in a fluid medium, which will support an electric field and which can be subsequently solidified. A knowledge of fluid viscosity is essential in defining the field structuring process parameters. If viscosity falls below a certain threshold then the dense ceramic particles will fall out of suspension before the structuring effect of the electric field can be realised. If viscosity is too high then viscous forces, which resist the induced electrostatic forces, may retard or even prevent structuring. Thus viscosity must be confined to certain limits and the purpose of this section is to define a lower viscosity threshold to permit a study of the field structuring technique.

The fluid used in this study is Epotek 302-3M epoxy resin pre-polymer, at an early stage of the cure cycle.

As discussed in the previous section, the viscosity of an epoxy resin during cure is dependent both on temperature and on the extent of conversion of the reactants. Because of this complexity, a complete assessment of a particular system can be a substantial undertaking. In the context of this work, we required only sufficient information to enable the study to move forward. This was gathered by continuously monitoring the viscosity of the resin, as it cured under isothermal conditions. The measurement was then repeated over a series of several fixed cure temperatures.

The two components of the resin were mixed according to manufacturers' recommendations and measurements were made with a rotational viscometer (Contraves Rheomat 115). The system used was a narrow gap concentric cylinder arrangement conforming to DIN norm 53019. A fixed shear rate was selected for all temperatures and this was chosen in the light of previous experience as 100 s^{-1}. Constant temperature was maintained by a Rheotherm 15 oil-bath with an accuracy of ±0.2°C. The maximum viscosity that could be measured with this arrangement was 60Pas and it was found that the resin had not completely gelled by the time this point

was reached. One benefit of this in practice was that it was still possible, at the end of a run, to remove the rotating bob from the disposable aluminium cups that were used. The bob could then be cleaned off chemically for future use. If curing were allowed to reach completion, the alternative would be to burn the then-vitrified epoxy off in a furnace to reclaim the bob.

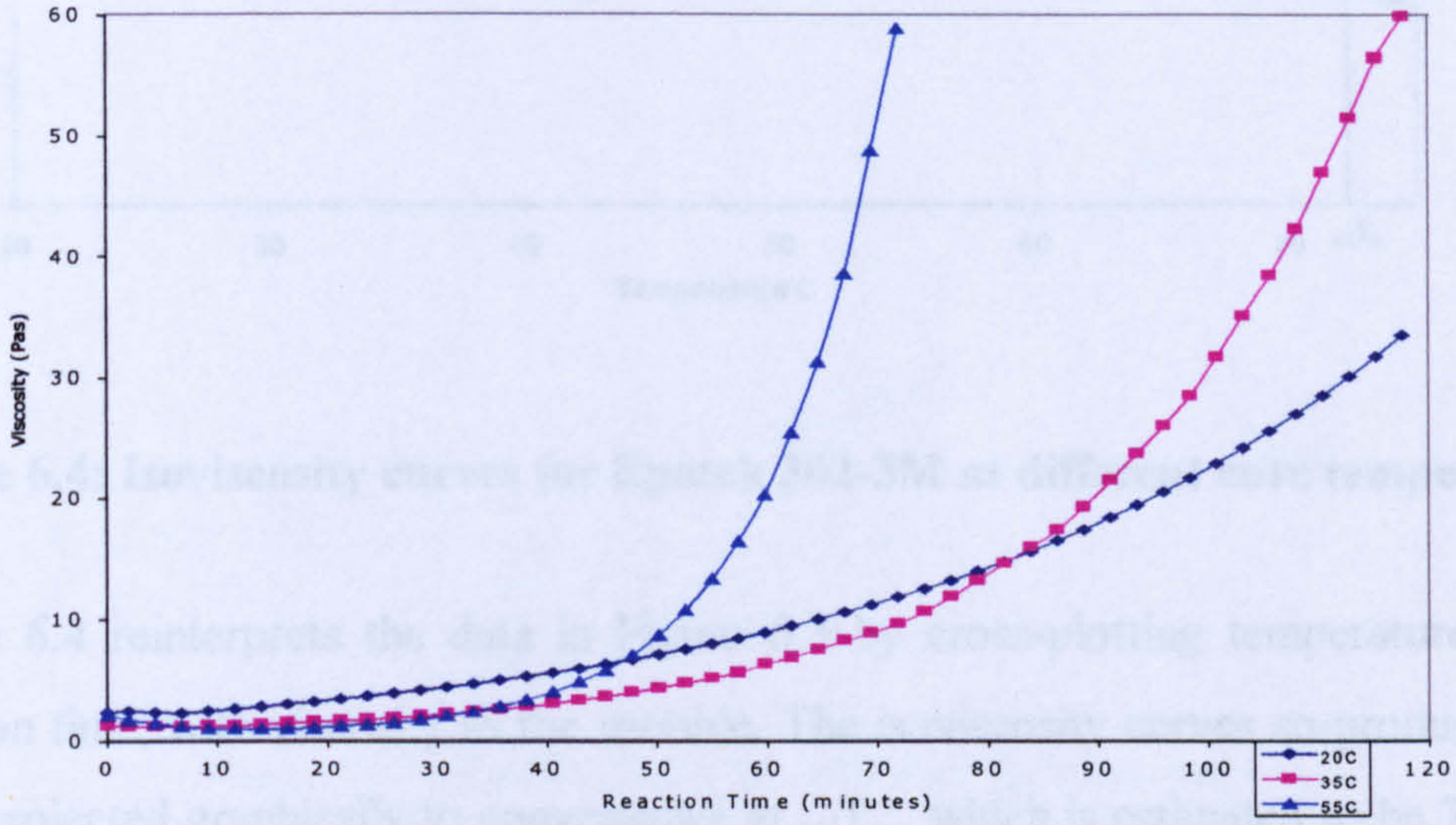

Figure 6.3: Epotek 302-3M – variation in viscosity as a function of reaction time.

Figure 6.3 shows the rise in viscosity of the resin with time at three temperatures. The interplay between viscosity changes which are due to temperature and those due to increase in molecular weight is evident. For example, at 55°C initial viscosity is lower than it is at 20°C, but this situation is reversed after around 45mins owing to the higher rate of chemical conversion.

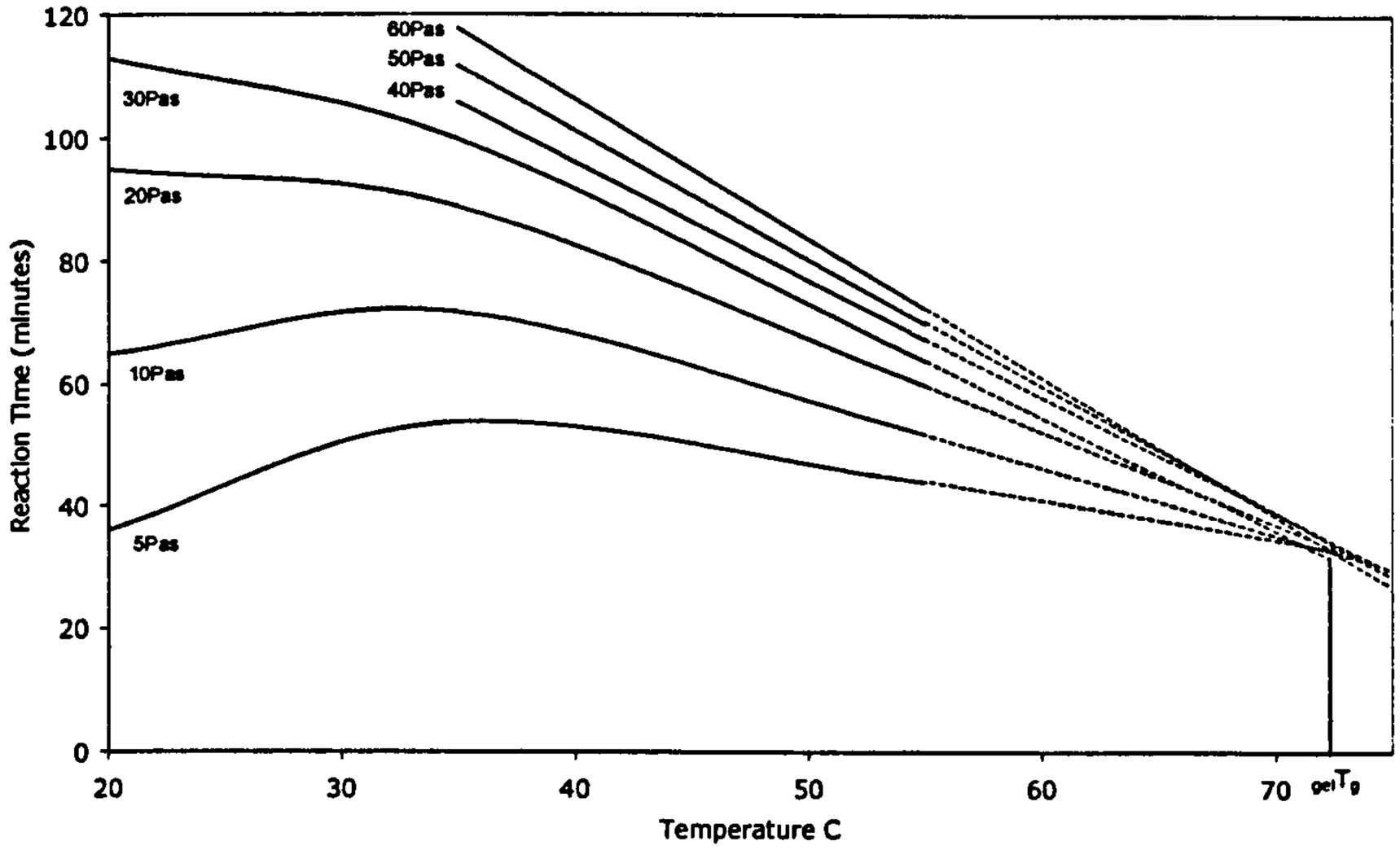

Figure 6.4: Isoviscosity curves for Epotek 302-3M at different cure temperatures.

Figure 6.4 reinterprets the data in Figure 6.3 by cross-plotting temperature against reaction time, with viscosity as the variable. The isoviscosity curves so-produced have been projected graphically to convergence at $_{gel}T_g$, which is estimated to be 72°C at a reaction time of 36mins. Note: The manufacturers' data suggest a typical cure of 90mins. at 65°C to achieve a T_g of 56°C.

6.2.1 Effect of Step-Curing on Measured Viscosity

For the purposes of this study, experimental conditions dictate that the resin will not be cured at a continuous fixed temperature. The resin will be allowed to partially cure with ceramic particles in suspension, it must then be stirred to achieve a uniform particle distribution, transferred to a mould and only then will an electric field be applied. It is not expected that the introduction of ceramic particles will invalidate the viscosity data gathered here. However, the step-wise nature of the overall process may be a factor to consider. In order to gain some insight into the practical significance of the above results, two samples of resin were studied. One sample was monitored continuously as before, while curing at 35°C. After mixing, the second sample was

allowed to stand at room temperature (21°C) for 1 hour; its temperature was then raised to 35°C and monitoring of viscosity began. The results are shown in Figure 6.5.

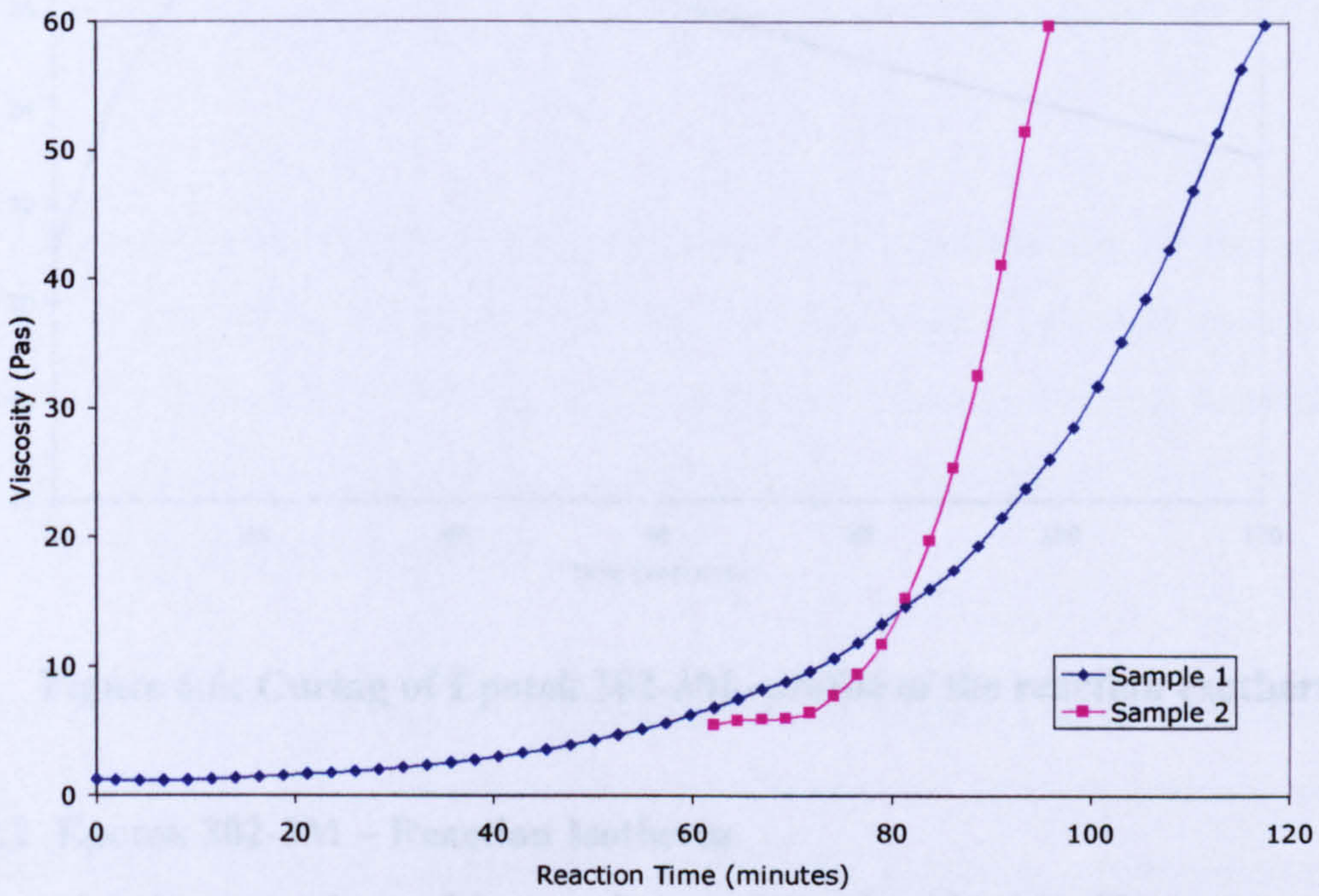

Figure 6.5: Epotek 302-3M effect of step-curing.

As expected Sample 2, which had been held at room temperature, initially showed a lower viscosity than Sample 1, which had been held at 35°C throughout. However, its rate of cure thereafter was very much faster. Total time (to 60 Pas) for the step-cured sample was reduced to 95mins compared to 120mins for Sample 1.

These results appear contrary to the accepted norm, that physical properties are directly related to the extent of chemical conversion. The inference is that the shearing action of the viscometer, in this case, has an influence on the property being measured. Therefore, the above measurements may not accurately reflect the variation in viscosity of the resin under motionless conditions and are treated only as a useful guide.

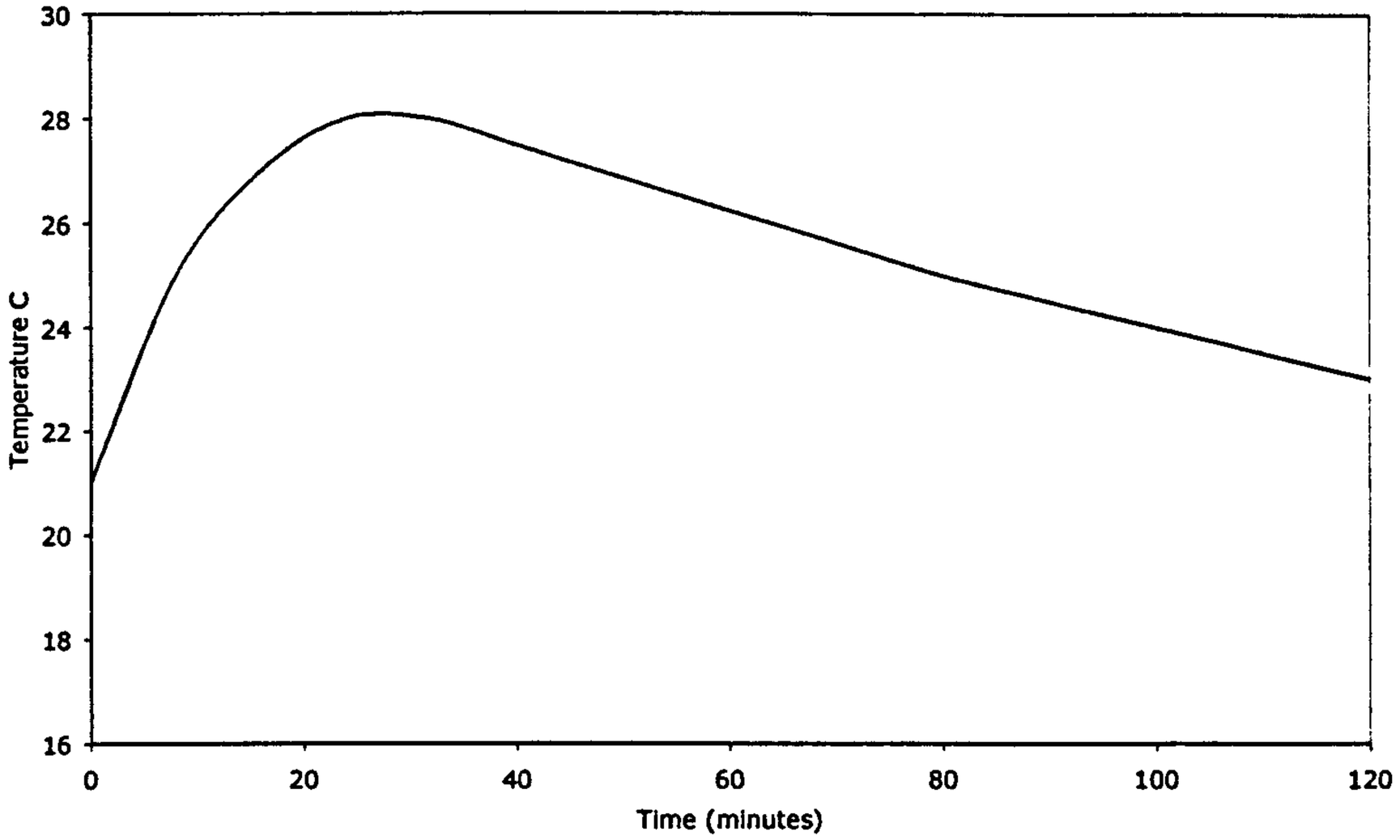

Figure 6.6: Curing of Epotek 302-3M -profile of the reaction exotherm.

6.2.2 Epotek 302-3M – Reaction Isotherm

Figure 6.6 shows the form of the reaction exotherm for this resin. The temperature of a small (10g) sample of resin was monitored after mixing with the diamine curing agent at room temperature. Initially there was an abrupt rise in temperature, which reached a maximum after 24 minutes.

6.3 Suspensions of Particulate Lead Titanate in Epotek 302-3M - Control of Sedimentation.

The expression which most accurately describes the settling of small particles (<50μm diameter) in a fluid is Stokes' Law. This assumes that the drag on a spherical particle is due entirely to viscous forces. This is the case when particle velocity is insufficient to cause turbulence in the surrounding fluid. Accordingly, a Stokes' Law approximation was used to estimate the settling time for lead titanate particles in the curing resin:

$$\text{Settling time} = \frac{18\mu s}{g d^2 (D_s - D_p)}$$

where μ is the fluid viscosity; s is distance; d is the particle diameter; D_s and D_p are the densities of the solid and the fluid respectively.

The results were plotted graphically. Figure 6.7 is a plot showing the time taken for particles of various sizes (4-32μm) to fall a nominal 0.1mm. A range of fluid viscosities is considered. Figure 6.8 shows the same information for a range of smaller particles (1-4μm).

For this study lead titanate powders are used, with a particle size distribution in the range 2-8 μm. Figure 6.7 shows that the time taken for a spherical particle with a diameter of 8 microns to settle 0.1mm in a fluid of viscosity 10Pas is expected to be around 72mins. The time taken to settle through a distance equal to one particle diameter is therefore around 6mins.

In the above approximation, settling time is directly proportional to fluid viscosity. It follows that the fluid viscosity can be adjusted to exercise control over the sedimentation of the dense ceramic particles. For example, cross-referencing with Figure 6.4 at 55°C the curing epoxy will have reached a viscosity of 10Pas after 52mins. At this point it is still quite fluid and any suspended particles can be uniformly dispersed by stirring. From this point, at 55°C, viscosity increases rapidly and sedimentation is effectively suppressed. Thus it should be possible to define a step-sequence of operations which will allow a uniform suspension to be exposed to an electric field for sufficient time for particle chains to form and for the structured composite to be solidified, whilst avoiding the problem of sedimentation.

In order to finalise the composites processing route more information is required regarding the amount of time that is required for particle chaining to be completed. The electrical parameters must be explored and this is the subject of Chapter 8.

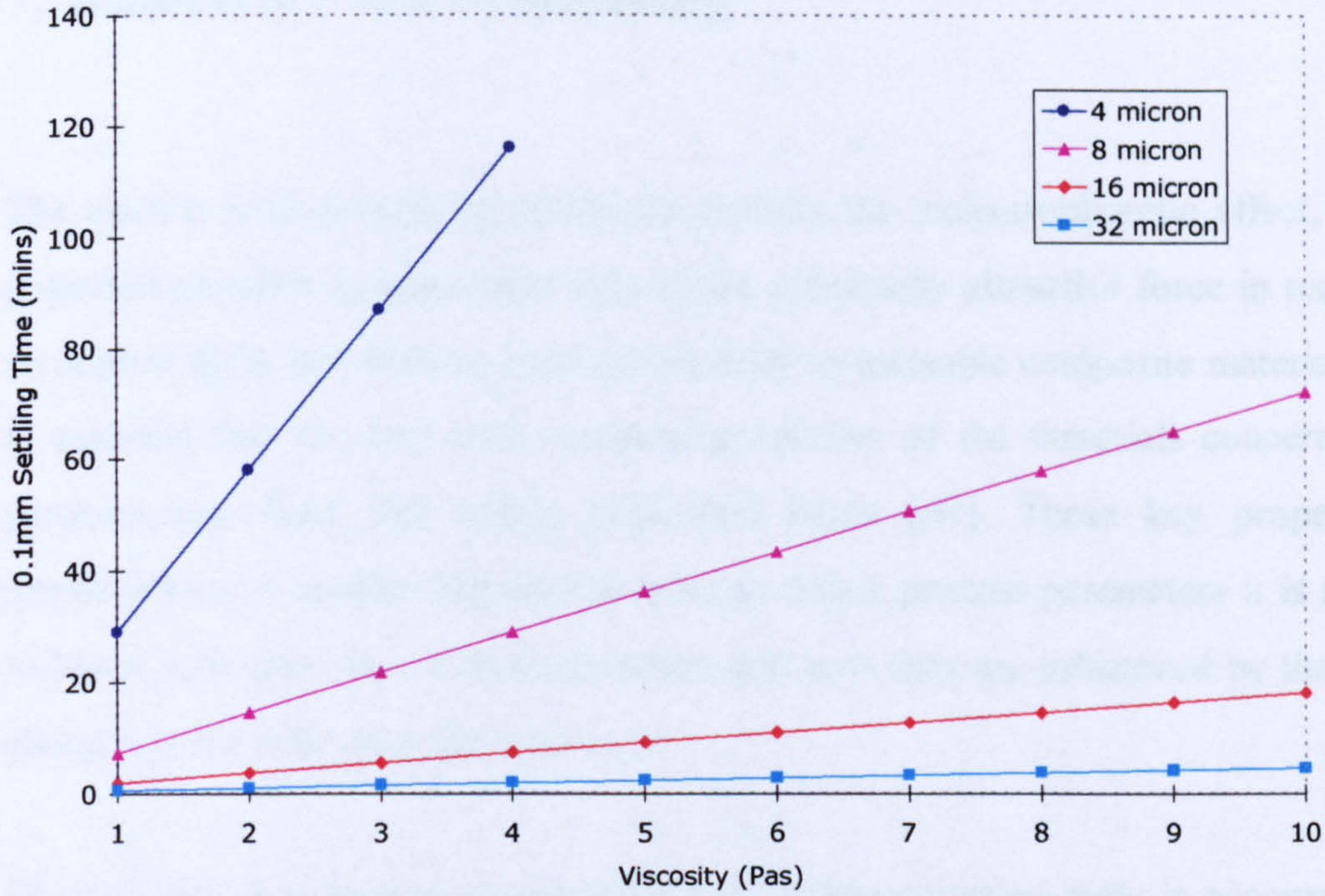

Figure 6.7: Time for lead titanate particles (4 to 32 microns diameter) to settle in a fluid -variation with viscosity. (Stokes' Law approximation)

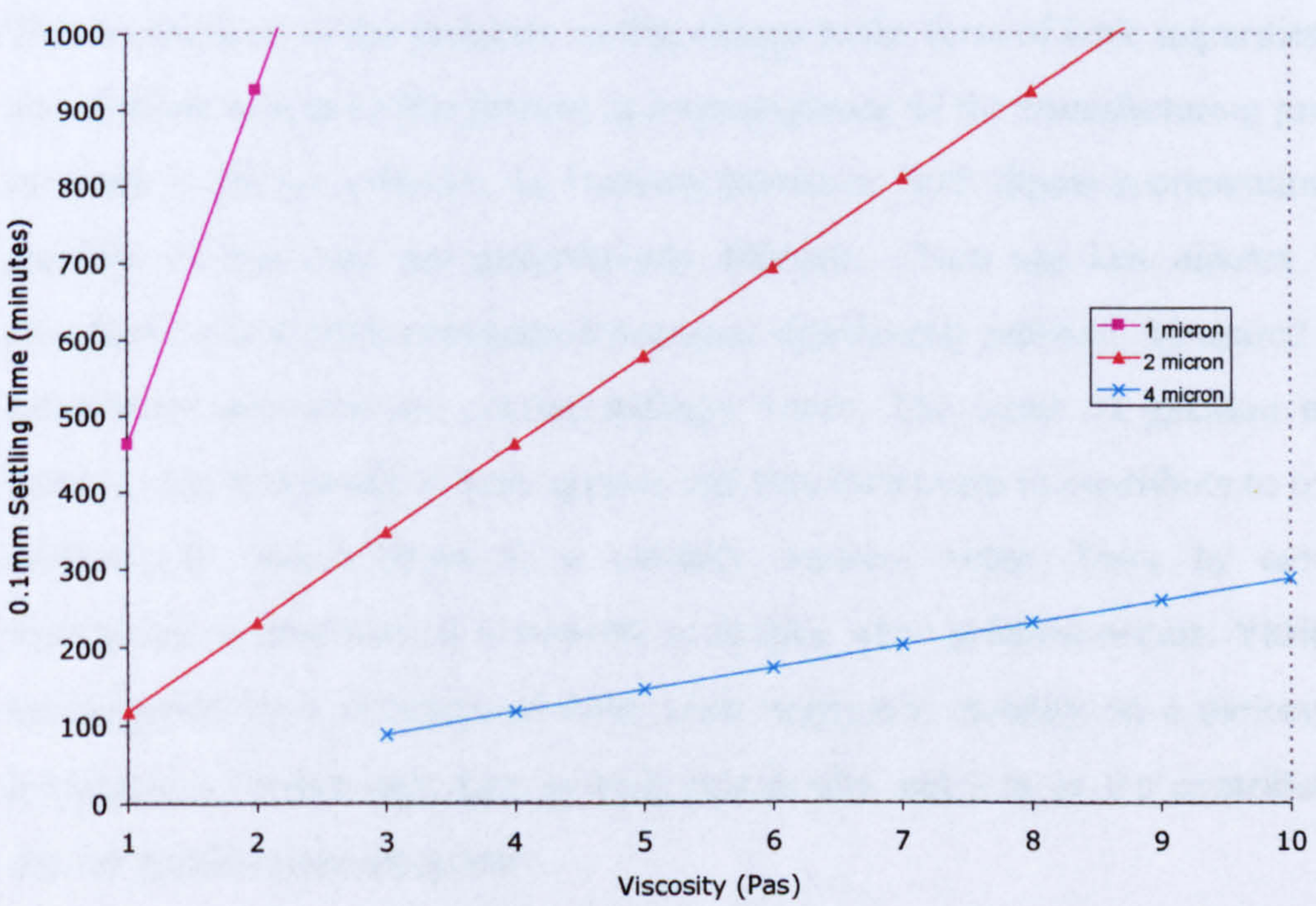

Figure 6.8: Time for lead titanate particles (1 to 4 microns diameter) to settle in a fluid - variation with viscosity. (Stokes' Law approximation)

7. Dielectric Cure Monitoring

The electric field structuring technique exploits the dielectrophoretic effect, whereby polarized particles in suspension experience a mutually attractive force in response to an applied field. If it is to be used successfully to assemble composite materials then it is essential that the key bulk electrical properties of the materials concerned, both particles and fluid, fall within prescribed limits [67]. These key properties are permittivity and conductivity and in order to define process parameters it is necessary to know how they vary with temperature and how they are influenced by the physical changes in the resin over the cure cycle.

During cure, the physical transformation of a thermosetting resin is accompanied by characteristic changes in its electrical properties. In the liquid phase, the pre-polymer and curing agent both contain polar groups and an applied electric field causes the dipoles to rotate relatively freely into alignment, producing a high dielectric response. This is enhanced by the presence of free charge in the form of ionic impurities. Sodium and chloride ions are often present as a consequence of the manufacturing process and moisture is always a factor. As viscosity increases, both dipole reorientation and the mobility of free ions are progressively inhibited. There are less dipoles and their contribution to overall polarization becomes significantly reduced. Measured values of permittivity and loss are correspondingly lower. The onset of gelation effectively prevents the movement of ionic species and they then cease to contribute to overall DC conductivity, which drops to a virtually constant value. Thus, by continuously monitoring conductivity, it is possible to deduce when gelation occurs. Vitrification is accompanied by a cessation of large scale segmental mobility on a molecular scale, leading to a further reduction in both permittivity and loss as the contribution from dipolar reorientation disappears.

This pattern of behaviour has been investigated by several groups, who see it as a useful tool in the fabrication of polymer-composite components [36,68-72]. They have

developed the technique of 'dielectric cure monitoring', whereby strategically placed capacitive sensors in the resin measure complex permittivity directly, across a range of frequencies, throughout the cure cycle. This data can subsequently be compared against an analogue model to achieve some degree of closed-loop control. Potentially this avoids the problems associated with predictive modeling and this theme is a continuing topic of research at Cranfield University.

In contrast to the intricate changes in the electrical properties of the resin during cure, the dielectric properties of the ceramic phase are expected to remain virtually constant over the relatively narrow temperature range encountered. However, in assessing the overall behaviour of a suspension of ceramic powder in the resin, it must be recognised that the dielectric properties are also markedly influenced by polarization of the interface between the two phases. The purpose of the work described in this section is to use the dielectric cure monitoring technique to investigate the electrical properties of suspensions of lead titanate in a curing epoxy resin and to explore the effects of changes in ceramic volume fraction, time and temperature.

7.1 Permittivity and Loss in Epoxy Resins

The complex relative permittivity of a resin (ε^*) has a number of constituent parts, each representing a different polarization mechanism and each contributing to the measured value. The components are: (ε_e^*) due to electronic polarization; (ε_a^*) due to atomic polarization; (ε_d^*) due to alignment of molecular dipole moments; (ε_c^*) due to conduction and (ε_b^*) due to electrode polarization. Where more than one phase exists there is a contribution due to interfacial polarization (ε_i^*).

For the purposes of this study it is useful to group these components into two groups according to whether they are dipolar or ionic in nature:

i). **Dipolar effects** are due to the reorientation of bound charges. They include electronic polarization, which is due to the small displacement of electron clouds relative to nuclei, and atomic polarization, which is due to the shift of atomic groups

relative to each other. These two effects together are termed *deformation polarization.* In epoxy resins the contribution of electronic polarization to overall permittivity is an order of magnitude greater than that of atomic polarization [71]. Both effects exhibit resonant behaviour at near optical frequencies, electronic polarization at around 10^{15} Hz which corresponds to the ultraviolet region of the electromagnetic spectrum and atomic polarization at between 10^{12} Hz and 10^{14} Hz which is the frequency of infrared radiation. Note: The refractive index (n) of the resin used in the current study, Epotek 302-3M, is given by the manufacturer as 1.5340. Hence a permittivity (ε_e') of around 2.353 is expected at optical frequencies (where $\varepsilon_e' = n^2$).

A further dipolar effect, which assumes much greater importance in the current context, is the alignment of molecular dipole moments in response to an applied electric field. These are permanent dipoles which are due to asymmetric charge distribution and which exist in the absence of any external field. Alignment takes place by rotational diffusion and is termed *orientation polarization.* Initially the dipole moments of polar molecules are randomly oriented by thermal energy. They are able to interact with an external alternating field and follow it only by physical rotation, vibrating about the field direction. In doing this, the resistance of the surrounding medium must be overcome and as a result the induced polarization lags behind the external field. A characteristic frequency is associated with each rotation, indicative of the time required for the system to reach equilibrium. When the applied field exceeds this frequency the dipole will be unable to follow the field and will cease to contribute to the overall polarization. This phenomenon is referred to as *dielectric relaxation* and its effect on observed permittivity and loss can be described mathematically by the Debye equations:

$$\varepsilon' = \varepsilon_\infty + \frac{\varepsilon_s - \varepsilon_\infty}{1+\omega^2\tau^2}$$

$$\varepsilon'' = \frac{\left(\varepsilon_s - \varepsilon_\infty\right).\omega\tau}{1+\omega^2\tau^2}$$

where ε'_∞ and ε''_s are the limiting high frequency and static values of permittivity.

Figure 7.1 shows the graphical form of the Debye expressions. The parameter (τ) is known as the relaxation time and is associated with a strong energy absorption, which appears as a peak in the observed dielectric loss. Substances whose permittivity is frequency dependent are said to exhibit *dielectric dispersion.*

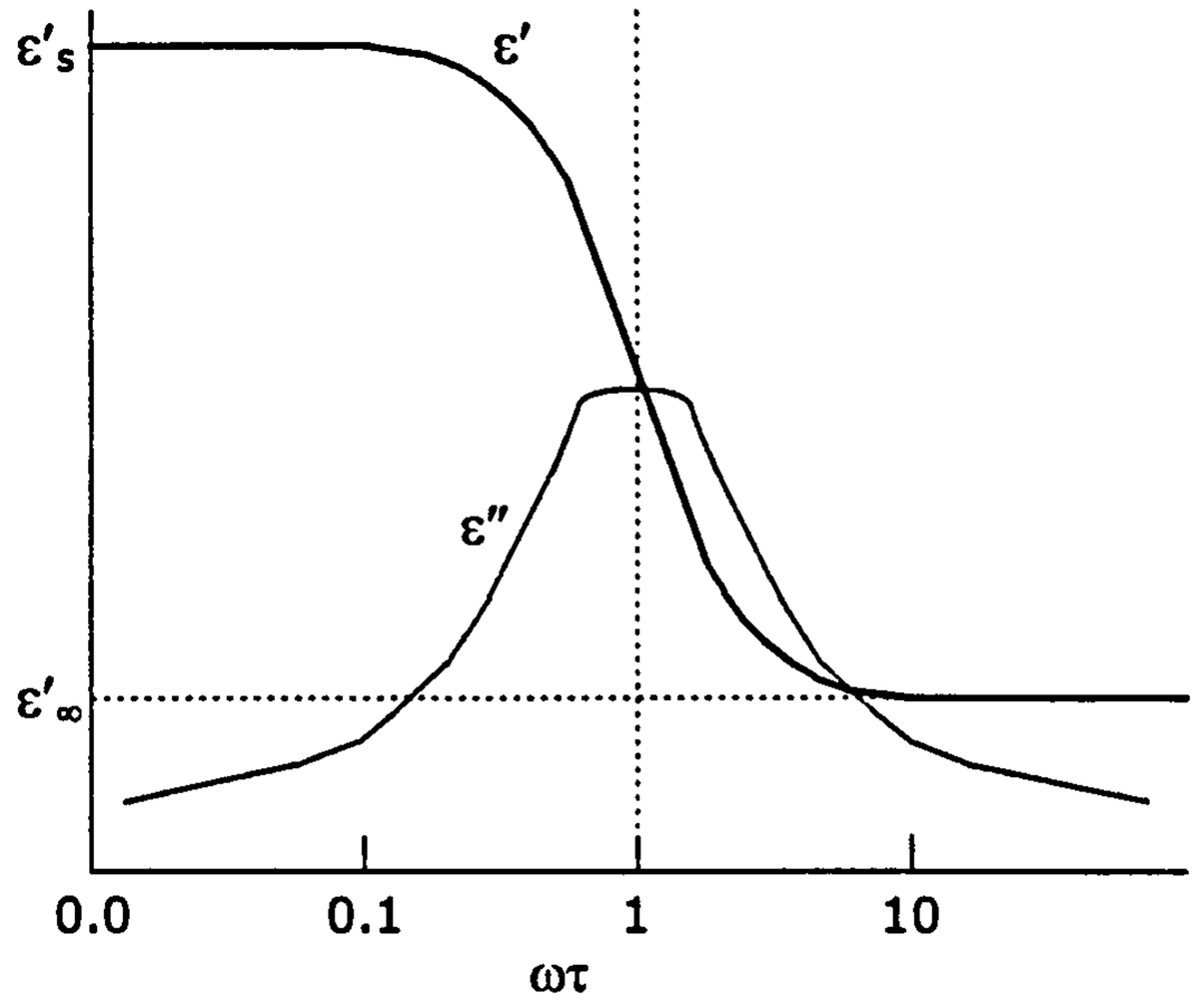

Figure 7.1: Dielectric relaxation. Geometric representation of the Debye expressions showing the variation of permittivity (ε') and loss (ε") as a function of angular frequency (ω) and relaxation time (τ).

In practice a large number of inter- and intra-molecular conformations exist in a resin, which contribute cumulatively to the overall dielectric response. As a consequence, dielectric spectra can be difficult to model strictly in terms of the underlying molecular processes and the ideal Debye response is rarely observed. The theories of Onsager, Kirkwood and Fröhlich and more recently Kubo provide an insight into the dependence of the dielectric relaxation strength in terms of the molecular dipole moment [73]. In the uncured resin, dipole activity is associated with the amine, bridging ether and epoxy ring groups. The development of the relaxation spectrum in terms of its molecular components, as the resin cures, has been discussed among others by Tabellout et al [68].

In the amorphous state, a strong dielectric response is associated with cooperative motion of main chain segments. This occurs in many polymers at or above T_g and is commonly used as a comparative tool. This is the α-relaxation, defined as the relaxation observed at the highest temperature (at fixed frequency) or the lowest frequency (at fixed temperature) [74]. The terms β- and γ- then refer to relaxations observed at lower temperatures (or at increasing frequency).

ii). **Ionic Effects** are due to the diffusion of charged species (ions) in response to an electric field and are most pronounced at lower frequencies. An important phenomenon, which is observed in all dielectric experiments on curing resins, is the polarization which occurs at the electrodes caused by a build-up of ions. Ions accumulate at the electrode surfaces whenever conductivity is large enough and frequency is low enough and form a charged blocking layer. The observed experimental value of permittivity is then very much increased and values in excess of 10^4 are quite possible. In addition, observed dielectric loss may be lower than its true value [75]. Increases due to *electrode polarization* diminish at higher frequencies and also as the resin cures, which progressively limits ionic mobility. In the cured resin the now relatively fixed ions continue to influence the dielectric properties of the polymer as they provide trapping sites for the charge carriers which can markedly affect conduction [76].

7.1.1 Interfacial Polarization

Charges accumulate at the interface of two phases or materials which have different conductivity and this 'blocked' charge can lead to very high values of measured permittivity. The effect is known as *interfacial polarization*, often referred to as MWS (Maxwell-Wagner-Sillars) polarization in recognition of their work on heterogeneous dielectrics [73]. Block et al., in their review [37], suggest three different mechanisms which could contribute to charge separation at an interface.

These are:

1) bulk transport of charge carriers within a higher conductivity second phase;
2) surface migration of charge carriers;

3) migration of charge carriers (counterions) within the double layer of a liquid phase. To these must be added the observation that frequently in solid phase polymer composites an interlayer exists which has dielectric properties unlike either of the adjacent bulk phases. This may result from an accumulation of impurities at the interface or from changes in local polymer morphology. A discussion of available models of interfacial polarization has been presented by North et al. [77].

7.1.2 Interpretation of Dielectric Spectra

Cole and Cole (1941) [73] proposed a useful method of displaying the frequency dependence of complex permittivity for systems that show a distribution of relaxation times. Their expression has the form:

$$\varepsilon^*(\varpi) = \left(\varepsilon'_s - \varepsilon'_\infty\right).\frac{1}{1+\left(i\varpi\tau_0\right)^{1-\alpha}} + \varepsilon'_\infty \quad ; \quad 0 \le \alpha \le 1$$

where α is an empirical factor known as the distribution parameter. Graphically the Cole-Cole equation has the form of a circle with the centre below the abscissa. To use the technique, a plot is made of ε' versus ε'' at a number of frequencies. The circular arc formed cuts the abscissa at ε'_∞ and at ε'_s and the angle subtended at the centre from these points is $\alpha\pi / 2$. For a single Debye relaxation $\alpha = 0$ and the arc formed is a semi-circle with its centre lying on the x-axis. Where α takes on higher values, an increasingly broad distribution of relaxation times is indicated. Other related functions, which are used to model in the frequency domain, are the Cole-Davidson, Fuoss-Kirkwood and Havriliak-Negami. The Kohlrausch-Williams-Watt function operates in the time domain. A full discussion of these various treatments has been given by Böttcher [78]. A number of workers have found that there are advantages in performing analyses using the *electric modulus*, which is a term introduced by McCrum et al. to describe the inverse of complex permittivity [74]. Tsangaris et al. [79] have transposed the Debye, Cole-Cole, Cole-Davidson, Havriliak-Negami and Sillars expressions into their electric modulus equivalents. They have found that interfacial polarization in low volume-fraction binary composites is best revealed by the

Cole-Davidson approach. For higher order composites or high volume-fraction composites the Havriliak-Negami equation is favoured.

7.2 Dielectric Cure Monitoring of Epotek 302-3M

An essential feature of dielectric cure monitoring is the ability to separate out and monitor parameters governing both ionic and dipolar mobility. A way to do this is to measure the frequency dependence of complex permittivity (ε*). Figure 7.2 is a block diagram of the equipment used in this study. A sample of the resin (4g) is placed in a glass test-tube in a brass cell with an insulating lid. The temperature of the cell is closely controlled and feedback is provided from a thermocouple mounted close to the sample. A capacitive sensor is placed in the resin and enameled copper wires connect it into a bridge circuit. An AC voltage is applied to the sensor from a computer-controlled Solartron SI 1260 Impedance / Gain-Phase Analyser. The resulting current is compared to the applied voltage in respect of amplitude ratio and phase difference. The analyser is set to scan over a selected frequency range, at regular intervals, and the capacitance and loss data are recorded on a PC for subsequent analysis. The analyser scans twenty-six individual frequencies, in the range 10 Hz - 1MHz, each sweep taking 30s. A second thermocouple, carefully placed at the back of the sensor where it will not interfere with the electrical measurements, monitors the resin temperature directly. The temperature profile of the curing resin is also recorded.

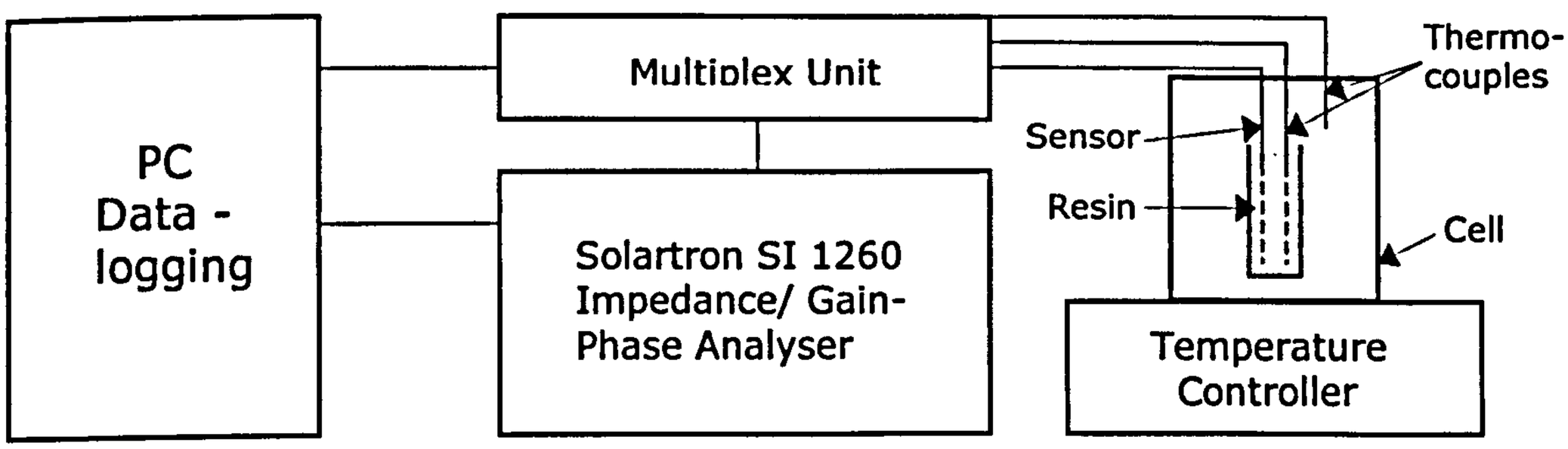

Figure 7.2: Block diagram showing the equipment used for dielectric cure monitoring of Epotek 302-3M and epoxy resin / lead titanate suspensions.

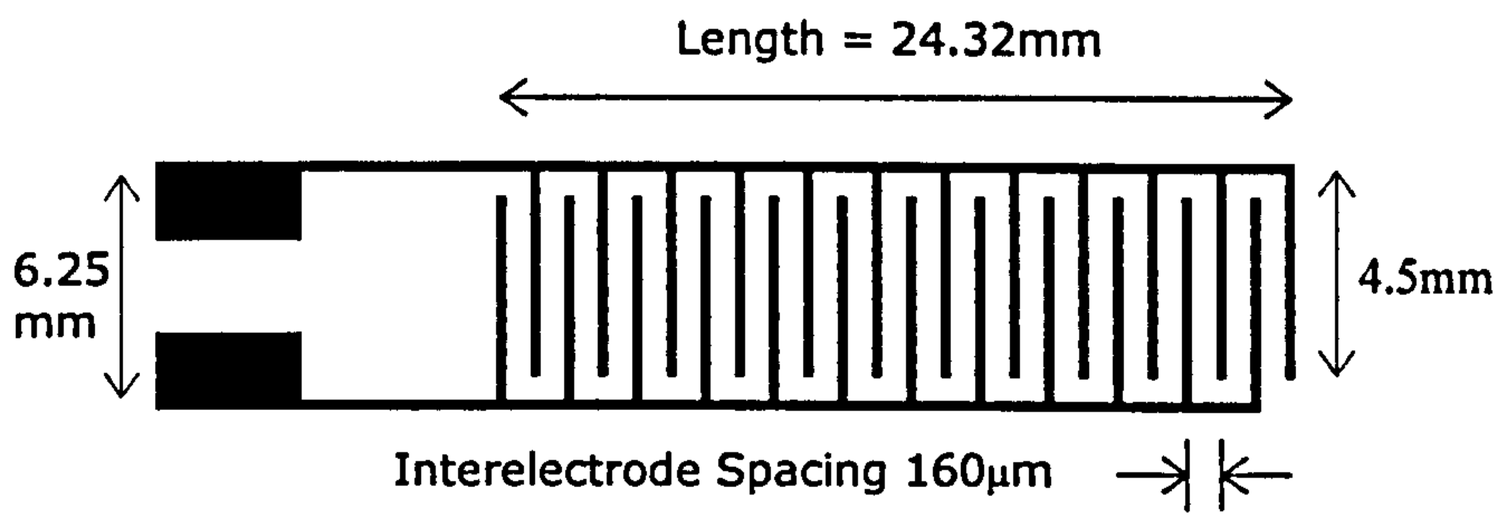

Figure 7.3: Interdigited, coplanar capacitive sensor (Gelnorm DE).

The sensors used in this study are coplanar and have the interdigitated pattern shown in Figure 7.3. The substrate of this type of sensor is a woven glass / epoxy composite having a predictable, very low permittivity. In addition, the electrodes are designed to be thin in comparison to the gap width, so that the flux passing between them will be negligible. The greater part of the capacitance will therefore be due to the fringing field passing through the resin (Figure 7.4). The extent to which the fringing field penetrates into the surrounding resin, which is dependent on the inter-electrode spacing, is anticipated to be 300μm for the Gelnorm DE sensor. A more precise type of sensor (Dek-Dyne) was used to gather the results presented here. The Dek-Dyne has a penetration of 25μm and is thus more suited to the suspensions under consideration. The precise calculation of the capacitance of the sensors is complex and involves a calibration function supplied by the manufacturer. This is incorporated in the customised software to convert the electrical signals received into a measure of resin permittivity.

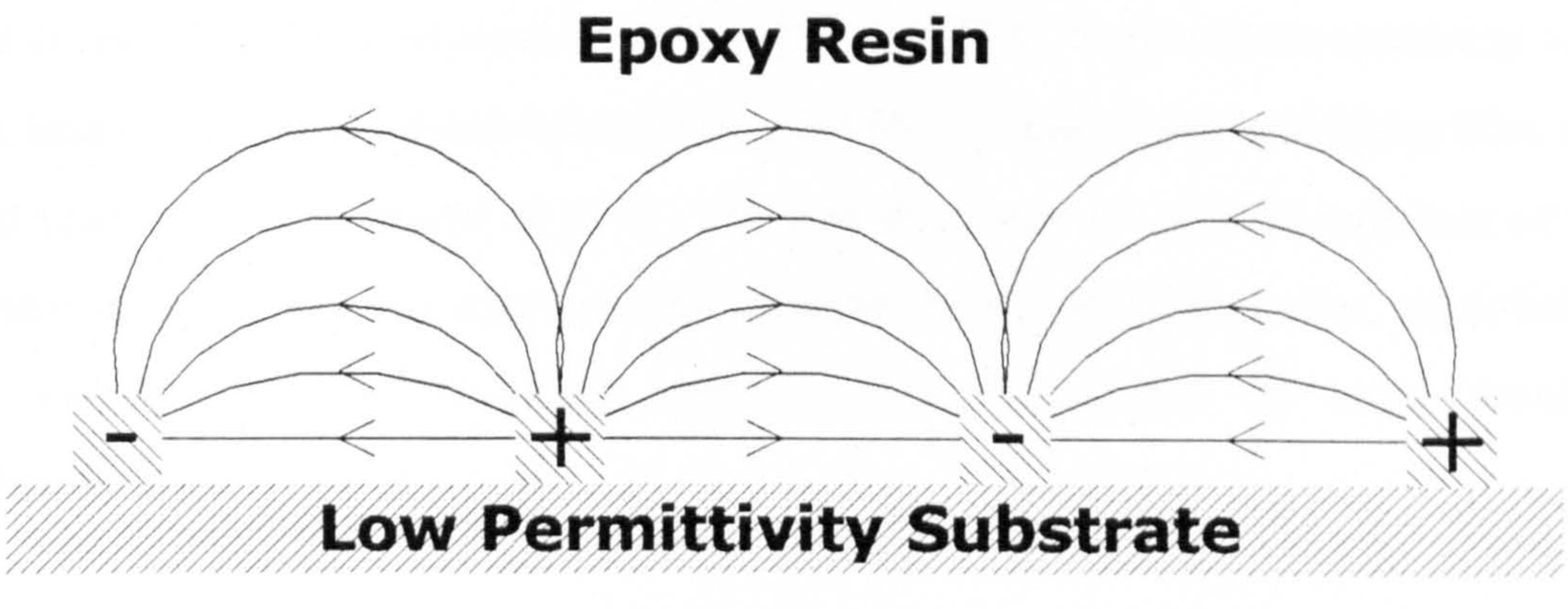

Figure 7.4: Fringing field - flux pattern between coplanar electrodes.

7.2.1 Procedure

The experimental procedure is as follows:

1. Both resin and the lead titanate powder are dried in a vacuum oven for a minimum of 16hrs. Lead titanate was prepared in-house, as described previously.
2. The cure temperature is preset and the cell allowed to warm up. Stability is reached after around 30 mins.
3. Open and closed circuit values are measured and the bridge is zeroed.
4. The sensor is placed in a glass test-tube and connected into the bridge circuit. Air capacitance is measured for each of the thirty-one frequencies used in a typical sweep. Software subsequently incorporates this value in calculations to deduce relative permittivity and dielectric loss.
5. The two components of the resin system are mixed thoroughly and the mixture is transferred into the test-tube. In each case, measurements begin 5 minutes after mixing.
6. The chosen frequency range of 1Hz - 1MHz is scanned at two-minute intervals over a specified cure time of 5hrs. The temperature of the resin is monitored continuously to ensure that it remains within ± 1°C of the preset value. Data are collected for each sweep in the form of a text file.

In the first instance, measurements were carried out using low-cost (Gelnorm) sensors. The curing resin was monitored at 35°C, 45°C and 65°C. Suspensions containing 10% vol. lead titanate were monitored at 35°C and 65°C. A suspension containing 40% vol. lead titanate was monitored at 35°C. The low frequency (< 150Hz) response of the particular brand of sensor used for these runs was known to be imprecise, nevertheless the exercise provided a useful approximation in advance of more accurate measurements.

Higher quality, finely calibrated sensors were subsequently employed for greater precision and the measurements are taken as reliable at frequencies above c.20Hz. A cure temperature of 40°C was chosen in order to achieve a relatively slow cure. By doing this the key features of the capacitance data are more pronounced and therefore easier to detect. The procedure was repeated for suspensions of 10% vol. and 40% vol. lead titanate in the resin. Subsequently, all samples were subjected to a ramped temperature of 1°C per minute for 50 minutes and the dielectric measurements were then resumed.

7.3 Results and Discussion

7.3.1 Epoxy Resin

Figure 7.5a) shows relative permittivity plotted as a function of both cure time and frequency for Epotek 302-3M epoxy resin curing at 40°C. A concurrent plot of dielectric loss is show in Figure 7.5b) The plots show the following general features which will be discussed in more detail in the following section:-

Initial permittivity is seen to reach very high values below 400Hz (log f = 2.6). Beyond 400Hz there is a sharp decline and at 4kHz it levels off to a constant value ($\varepsilon' = 6$). This behaviour is paralleled by dielectric loss and is due to free movement of ionic species leading to electrode polarization, which dominates completely over dipolar effects.

Note: As previously discussed, measurements below c.20Hz are taken to be beyond the reliable range of the current set-up.

Cure time = 0 to 120 mins. Electrode polarization is very much in evidence, however as the cure reaction proceeds ionic mobility is inhibited by rising viscosity. The dielectric response is then reduced and relaxation is seen at progressively lower frequencies. At the same time there is a distinct relaxation in permittivity at the upper frequency limit (log f = 6) having a mid-point at a cure time of 45mins. The associated dielectric loss peak is clearly visible. This is the α-relaxation and is due to motion of the polymer backbone. Again as the reaction proceeds this dipolar effect is seen to move to lower frequencies.

Cure time = 120 to 300 mins. Electrode polarization ceases to be a significant feature. Permittivity and loss drop gradually to their final values of 2.4 and <0.13 respectively at 1MHz). The α-relaxation peak, with the onset of vitrification, has moved out of the detectable range. The cured resin shows a small dipolar relaxation at 250kHz (log f = 5.4). Examination of the data reveals that there is a further small relaxation at c.110Hz.

7.3.2 Suspensions of Lead Titanate in Epoxy Resin

Figures 7.6 and 7.7 show relative permittivity and loss plotted as functions of both cure time and frequency for suspensions of 10% vol. and 40% vol. of lead titanate in Epotek 302-3M epoxy resin curing at 40°C. The plots have the same general form as for the resin alone, however some significant differences emerge.

Permittivity data are replotted in Figure 7.8 to reveal the additional contribution that the ceramic powder makes to overall permittivity. Of particular interest is the dielectric increment ($\Delta\varepsilon'_u$) between initial and final permittivity at the upper frequency limit (1MHz). For the resin $\Delta\varepsilon'_u = (6 - 2.4) = 3.6$. For the 40% suspension $\Delta\varepsilon'_u = (12.4 - 6.4) = 6$. This discrepancy reflects the substantial interactions between neighbouring ceramic particles, which produce a non-uniform charge distribution in the presence of an electric field. The presence of an electrical double layer at the liquid - ceramic interface is a significant factor. In such circumstances the observed measurement of

permittivity is strongly dependent on the distribution of the ceramic phase and modeling is beyond the scope of this study. Günther and Heinrich have used Rayleigh's theory to model a disordered arrangement of identical spheres in a second dielectric medium, however their expression requires some knowledge of the spatial distribution of phases, which in the current experiment is uncertain [73]. This and other models are discussed in Chapter 10

The simultaneous dielectric loss is re-plotted in Figure 7.9 Dielectric loss (ε'') is

$$\varepsilon'' = \varepsilon_d'' + \frac{\sigma}{2\pi f \varepsilon_o}$$

generally represented as the sum of two components, a dipolar contribution (ε_d'') and that due to conduction, which has the form $\sigma.(\varepsilon_o.2\pi f)^{-1}$.

When dielectric loss is dominated overwhelmingly by conduction, then the term (ε_d'') becomes insignificant and dielectric loss is then inversely proportional to frequency (f). In this event, a plot of log (ε'') v. log (f) has a slope of -1. Figure 7.10 shows this to be true, in the initial stage of cure, at frequencies between 10^2 and 10^5Hz. The dominant role of ionic conduction in this region is confirmed.

The above relationship can be used to calculate initial values of conductivity for the resin and suspensions (Table 7.1). Note that a suspension of 10% lead titanate in resin has a lower conductivity than the plain resin and that conductivity is enhanced in the 40% suspension. [Note: Conductivity of dry, pure lead titanate is less than 10^{-11} S/m].

Table 7.1 - Initial conductivity of Epotek 302-3M epoxy resin and suspensions.

	@ 1kHz	@ 10kHz	@ 63kHz
Resin	6.11 $\mu S\ m^{-1}$	6.44 $\mu S\ m^{-1}$	7.09 $\mu S\ m^{-1}$
Resin+10%PT	4.28 $\mu S\ m^{-1}$	4.48 $\mu S\ m^{-1}$	5.12 $\mu S\ m^{-1}$
Resin+40%PT	8.82 $\mu S\ m^{-1}$	11.47 $\mu S\ m^{-1}$	13.55 $\mu S\ m^{-1}$

Conductivity can also be expressed as:

$$\sigma = \sum_i z_i q n_i \mu_i$$

where z_i is the valency of the *i*th ionic species; q is the electronic charge; n_i is the concentration of charge carriers and μ_i is the charge mobility. Hence it can be said that where the number of charge carriers does not vary then conductivity is directly proportional to ionic mobility.

Theoretical expressions that relate increments in permittivity to the dipole moments present in a material have been made by Onsager and subsequently modified by Fröhlich. A full treatment of these and related theories is to be found in Scaife [73]

Figures 7.11 and 7.12 monitor the curing resin at fixed frequency and illustrate the movement of the α-relaxation peak to lower frequencies as curing progresses. At 100kHz the peak dielectric loss, for resin and suspensions alike occurs after 55mins.

$$\alpha \approx \frac{\varepsilon_{max}''}{\Delta\varepsilon'}$$

At10kHz the same peak has shifted to 112mins and, furthermore, has become much broader as a consequence of cross-linking. This effect can be quantified by evaluating the ratio of maximum dielectric loss (ε_{max}'') to the dielectric increment of permittivity associated with the relaxation ($\Delta\varepsilon$'). This closely approximates to the distribution parameter (α) in the Cole-Cole equation:

Where α = 0 the Cole-Cole expression reduces to the Debye equation, indicating a single relaxation time. When α = 1 then a very broad symmetrical distribution of times is indicated. Table 7.2 uses the above expression to indicate the increase in the spread of relaxation times associated with main-chain motion (α-relaxation) as the cure reaction progresses.

Table 7.2 - Values of the Cole-Cole distribution parameter for curing Epotek 302-3M epoxy resin and suspensions.

Distribution parameter (α)	At 55 mins.	At 112 mins.
Resin	0.231	0.267
Resin+10%PT	0.258	0.300
Resin+40%PT	0.293	0.369

It is interesting to note that there appears to be no relative movement in the position of the α-relaxation peaks for the resin and the suspensions. Therefore it can be said that presence of the ceramic phase appears to have no influence on the speed of the cure reaction.

Figures 7.13 and 7.14 which monitor the complex permittivity of the curing resin and suspensions after 60 mins. and 120 mins. respectively, are included for completeness.

7.3.3 Interfacial Polarization

The dielectric spectra have revealed a number of characteristic features which can be related directly to the physical transformation of the curing resin and suspensions. A complete quantitative analysis of the values obtained, however, requires that all of the following factors be considered: i) the dielectric properties of the two component materials; ii) the relative amounts of each material; iii) electrostatic interactions between the particles, which in turn are functions of particle shape and spatial distribution and iv) interfacial effects, which include surface or boundary conductivity and the accumulation of space charge. A model of this is necessarily highly complex and much of the appropriate information is not available directly from fixed-temperature measurements. For example, whilst it is possible to quantify an increase in permittivity shown by the suspensions over that of the resin, the contributions of the ceramic phase and any interfacial effects are uncertain. One reason for this is that the relative volume fractions of the ceramic and polymer in the detectable range, close to the sensor, may differ from the bulk values. Furthermore, a difference in conductivity between the two phases is essential if interfacial polarization is to be observed. As the

resin cures its conductivity changes markedly from a value which is considerably higher than that of the ceramic to one which is lower (4 x 10^{-16} S/m - bulk value). Clearly, as a result, the electrical properties of the interface will change dynamically as cure progresses. The interface itself has a finite thickness and has dielectric properties that are different from either of the pure phases. There have been several attempts to incorporate this into a mathematical model, with some success, and the more important of these are discussed more fully in Chapter 10.

Some of the factors to consider are:

i) the degree to which the diffuse interface is able to shield a build-up of charge at the ceramic surface and, hence, the effect of space charge;

ii) the mobility of surface charge - where conductivity is high then interfacial polarization may be virtually frequency independent, where surface charge is redistributed by ion hopping then some temperature and frequency dependence is expected;

iii) whether charge is localised at the surface or whether there is a possibility of an exchange between bound charge carriers in the filler and the bulk of the matrix. [77].

There are several ways in which the interfacial region can be investigated experimentally –a) by monitoring the decay current after a step removal of voltage and its variation with temperature (DC-transient experiments), which can reveal thermally activated relaxations and discharges; b) by monitoring DC conductivities and absorption currents, which can identify the role of space charges; c) by resolved low frequency dielectric spectroscopy. In the current work, more information can be gained by repeating the dielectric measurements on the finished composites and the base material, as the temperature is slowly ramped up. The previously examined samples were ramped from room temperature at 1C min^{-1} over a period of 1hour. Plots of permittivity and dielectric loss are shown for the resin and suspensions in Figures 7.15 to 7.17. A comparison of the dielectric loss observed for each sample at 1kHz is shown in Figures 7.18. The observed increases are due to a resurgence of cooperative dipolar

motion of chain segments as the material passes through the glass transition. Over a longer period it is expected that a decrease in overall dielectric activity will be observed as the cure proceeds toward completion.

Knowledge of the development of the ceramic - polymer interface would be valuable in the current context because of the critical influence it has on the electrical properties of the composite and hence on its effectiveness as a transducer material. By studying this aspect of the field structuring process, it may be possible to identify surface active agents or ionic dopants that could be used to enhance performance.

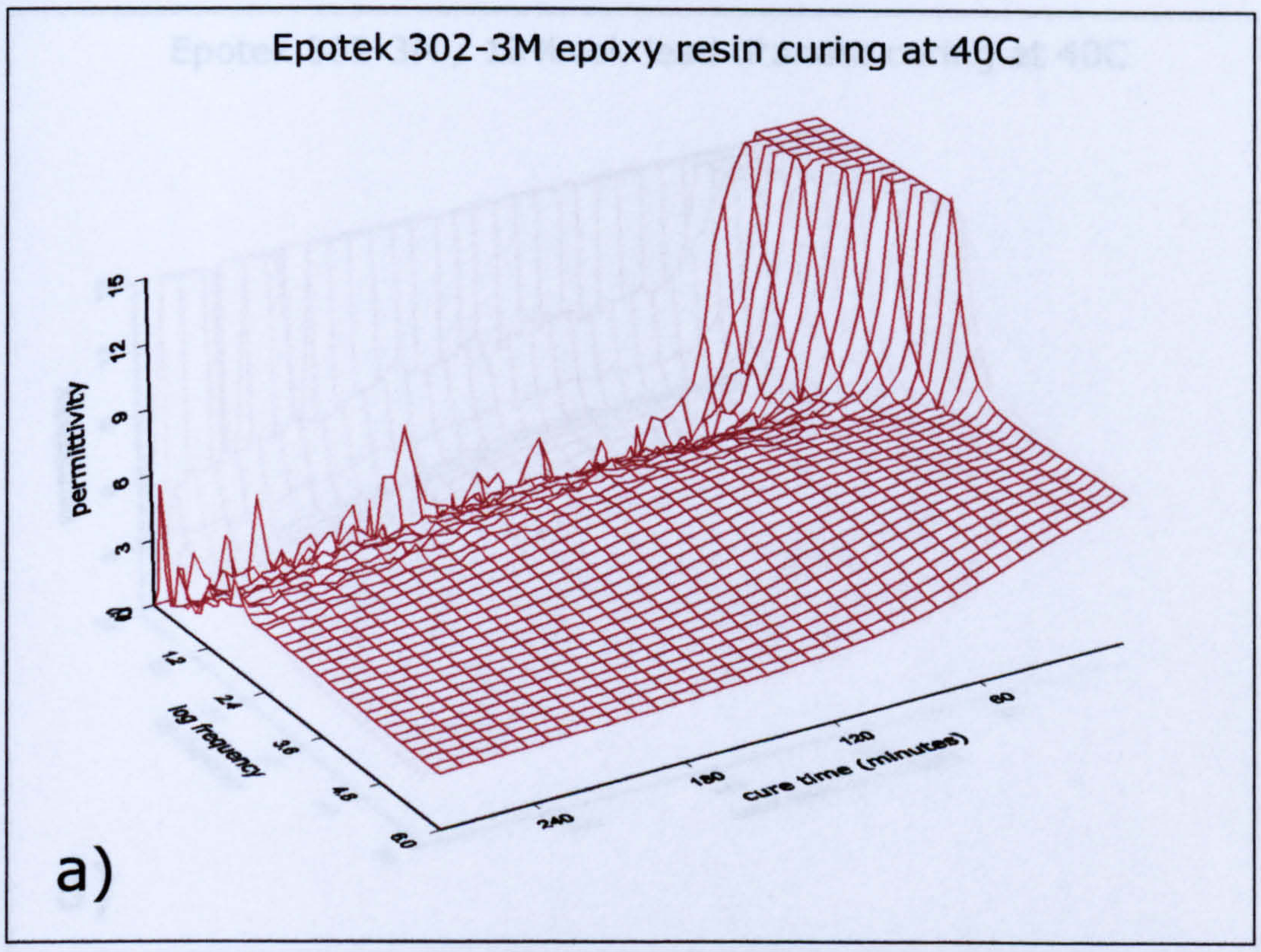

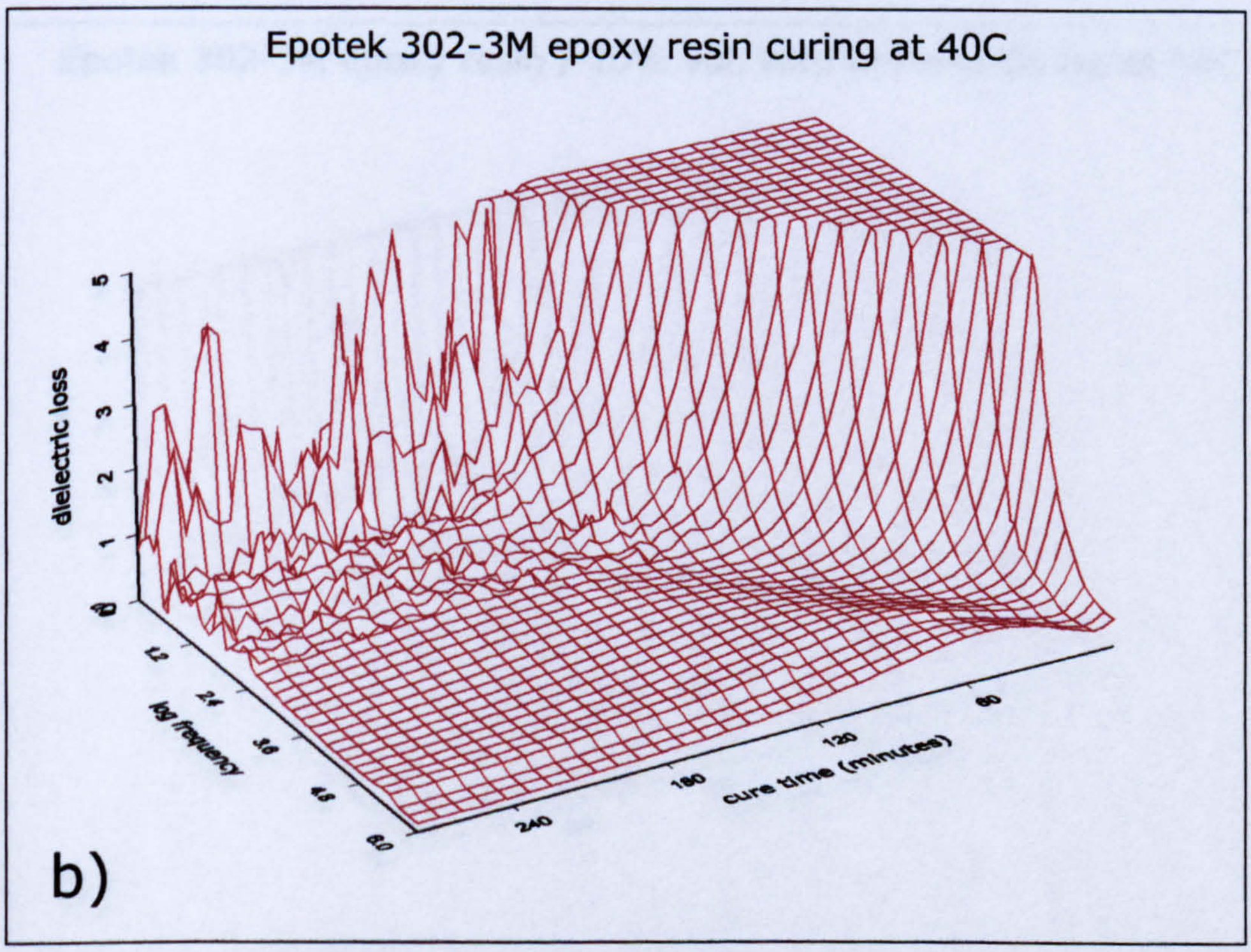

Figure 7.5: Dielectric cure monitoring of Epotek 302-3M epoxy resin.

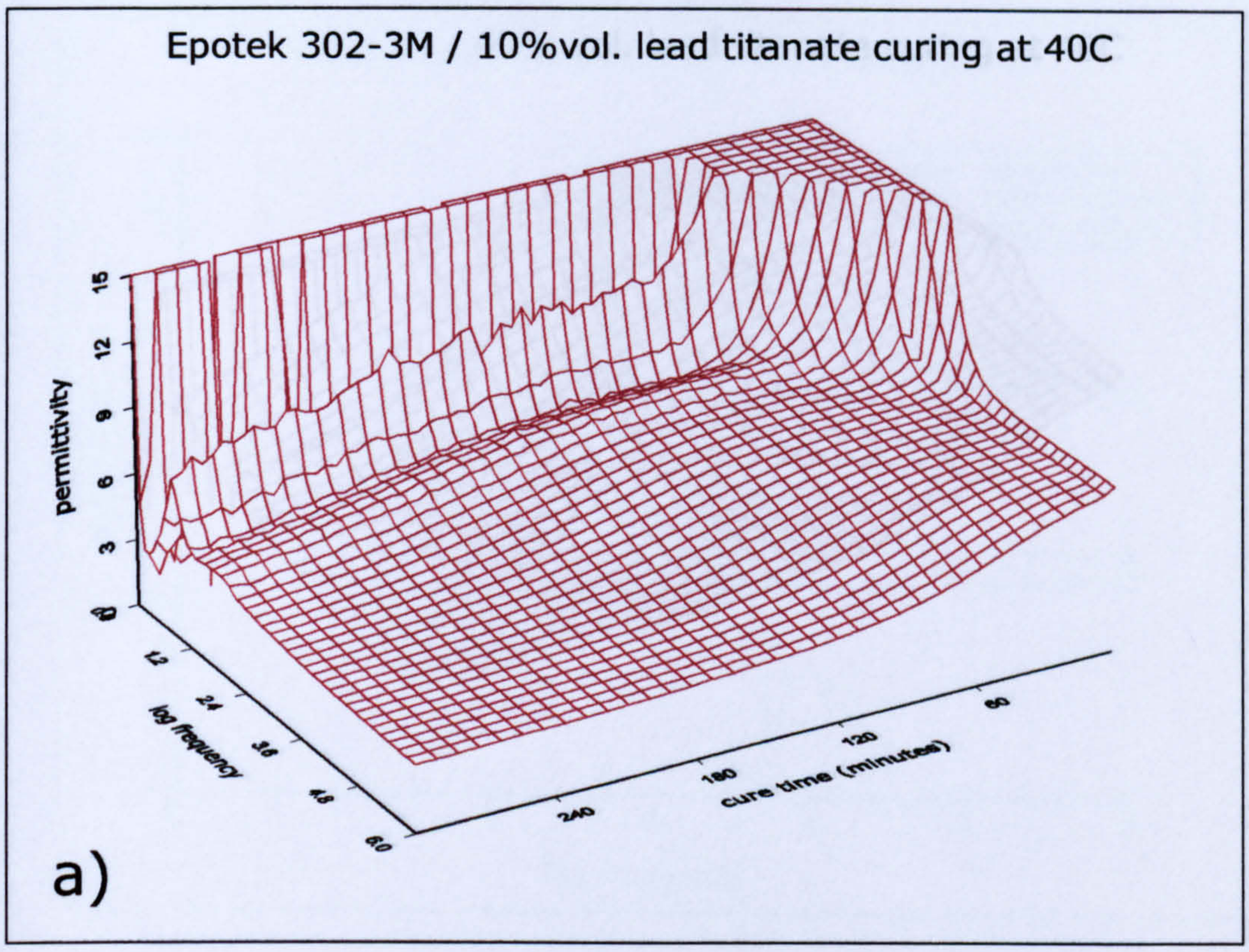

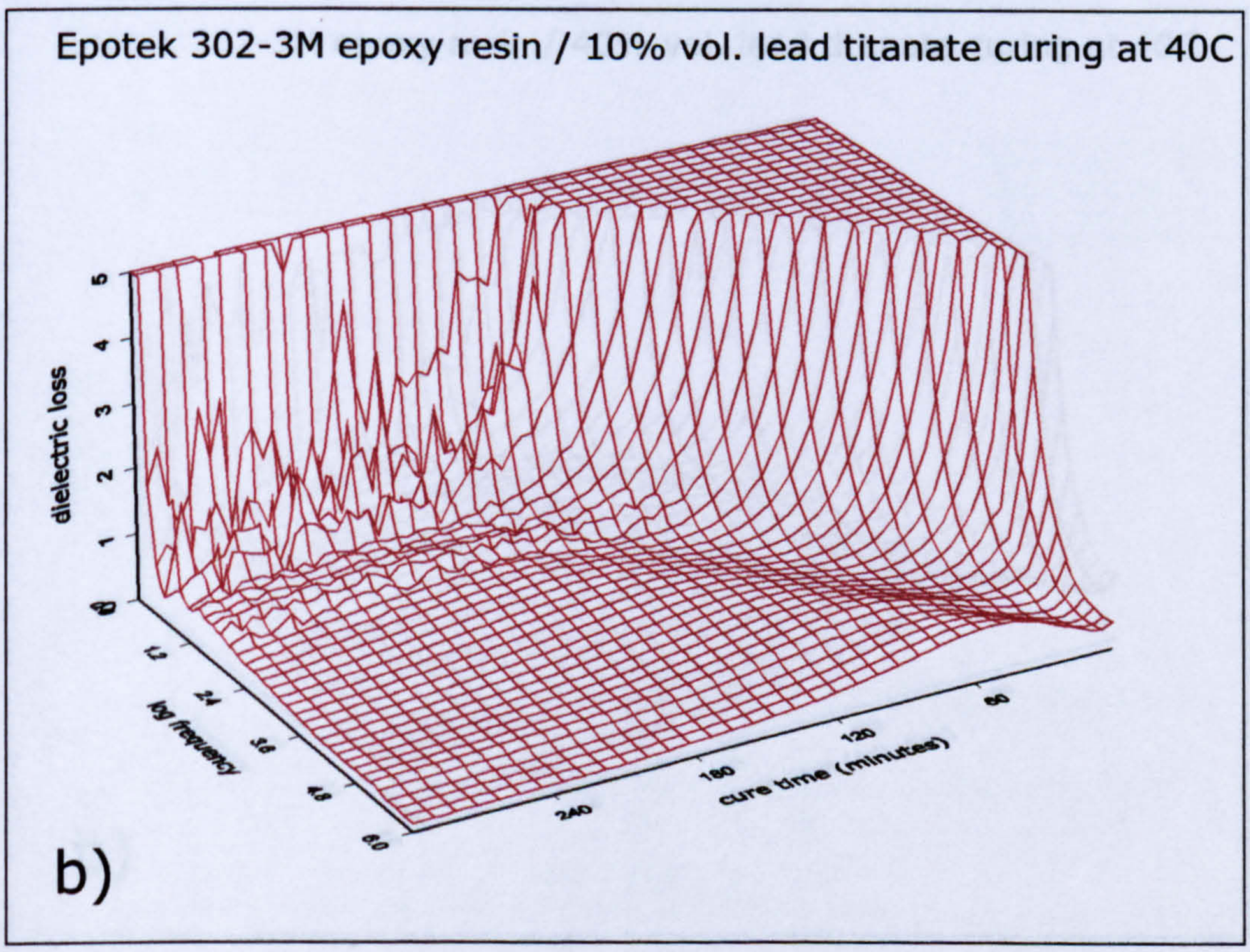

Figure 7.6: Dielectric cure monitoring of Epotek 302-3M epoxy resin + 10% vol. lead titanate.

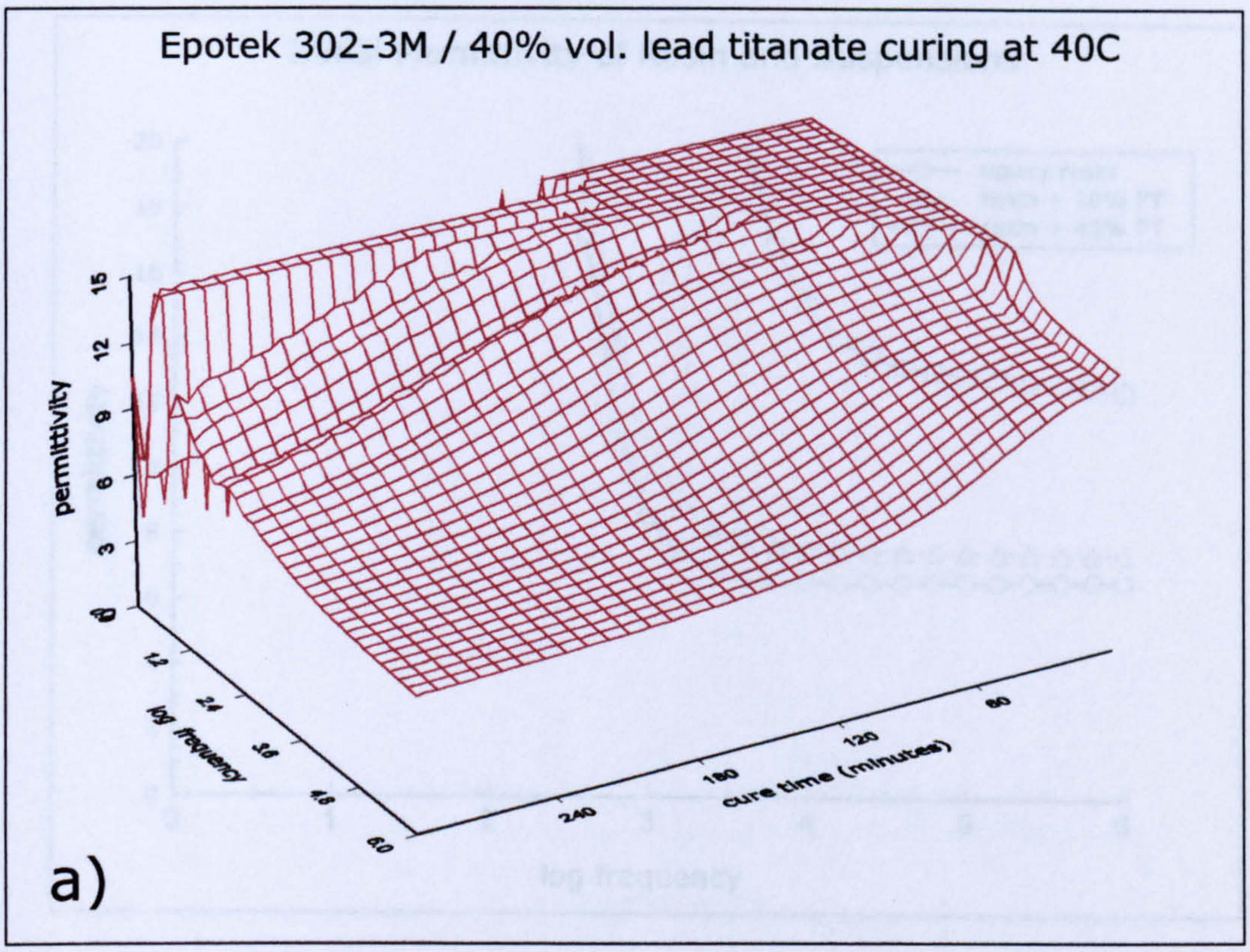

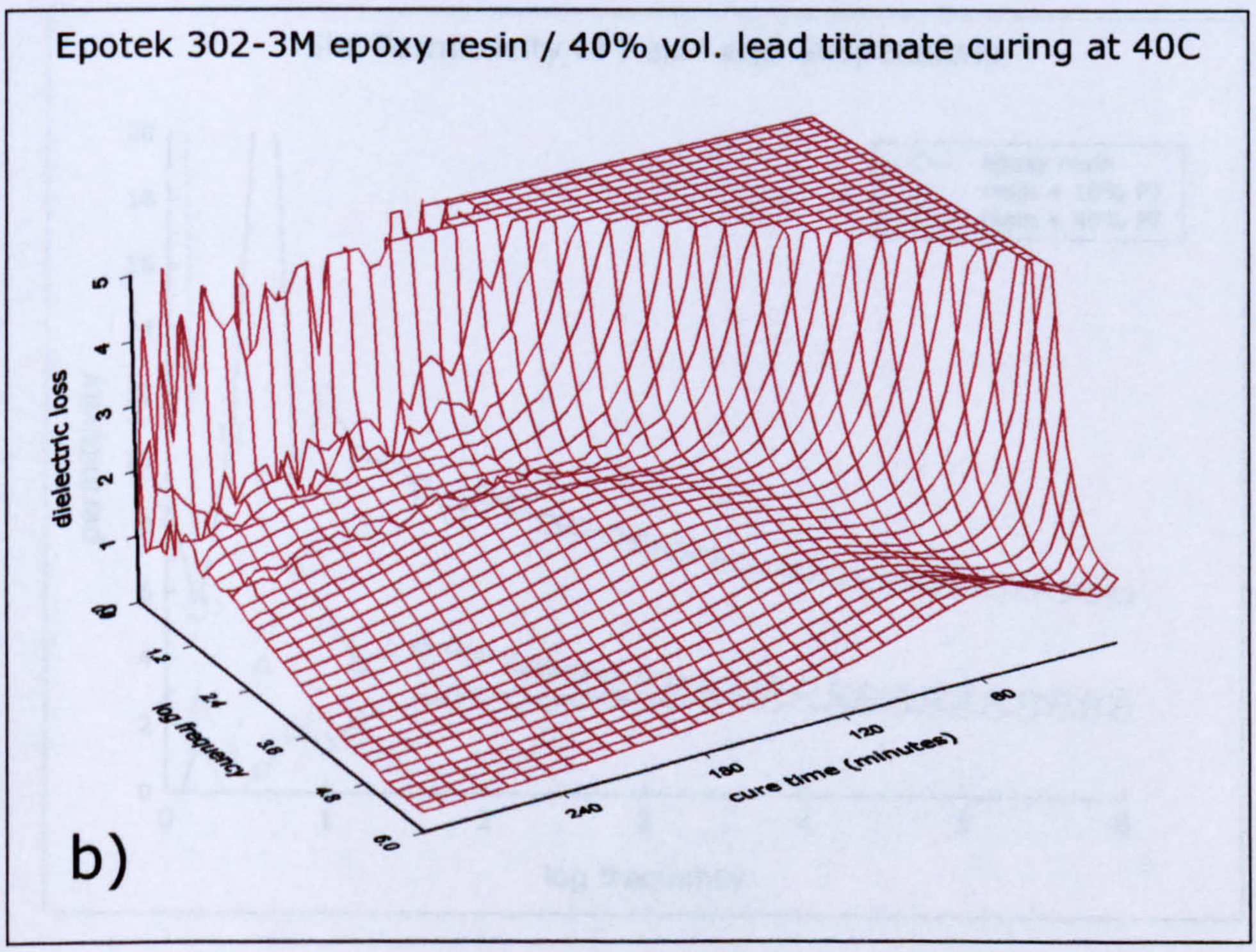

Figure 7.7: Dielectric cure monitoring of Epotek 302-3M epoxy resin + 40% vol. lead titanate.

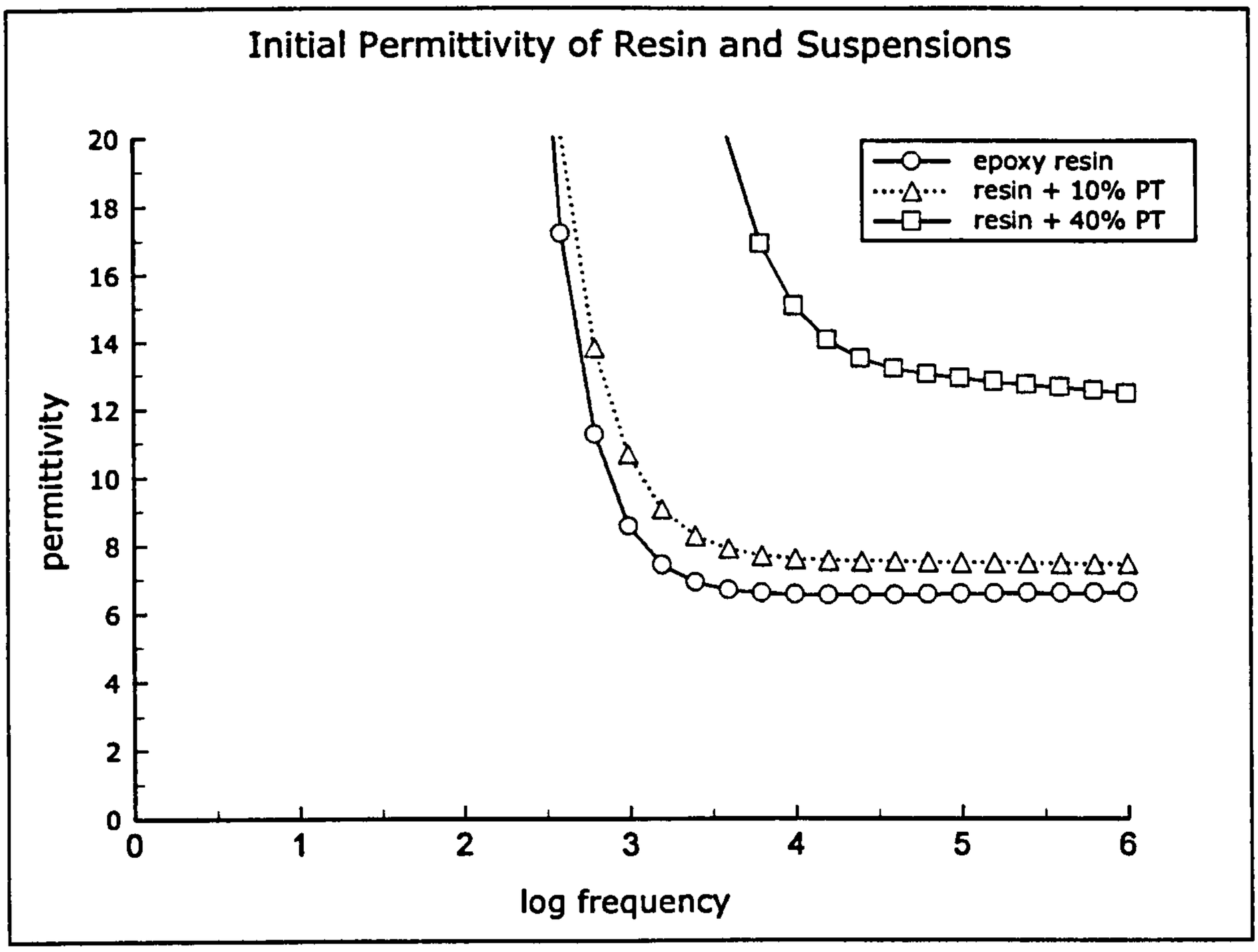

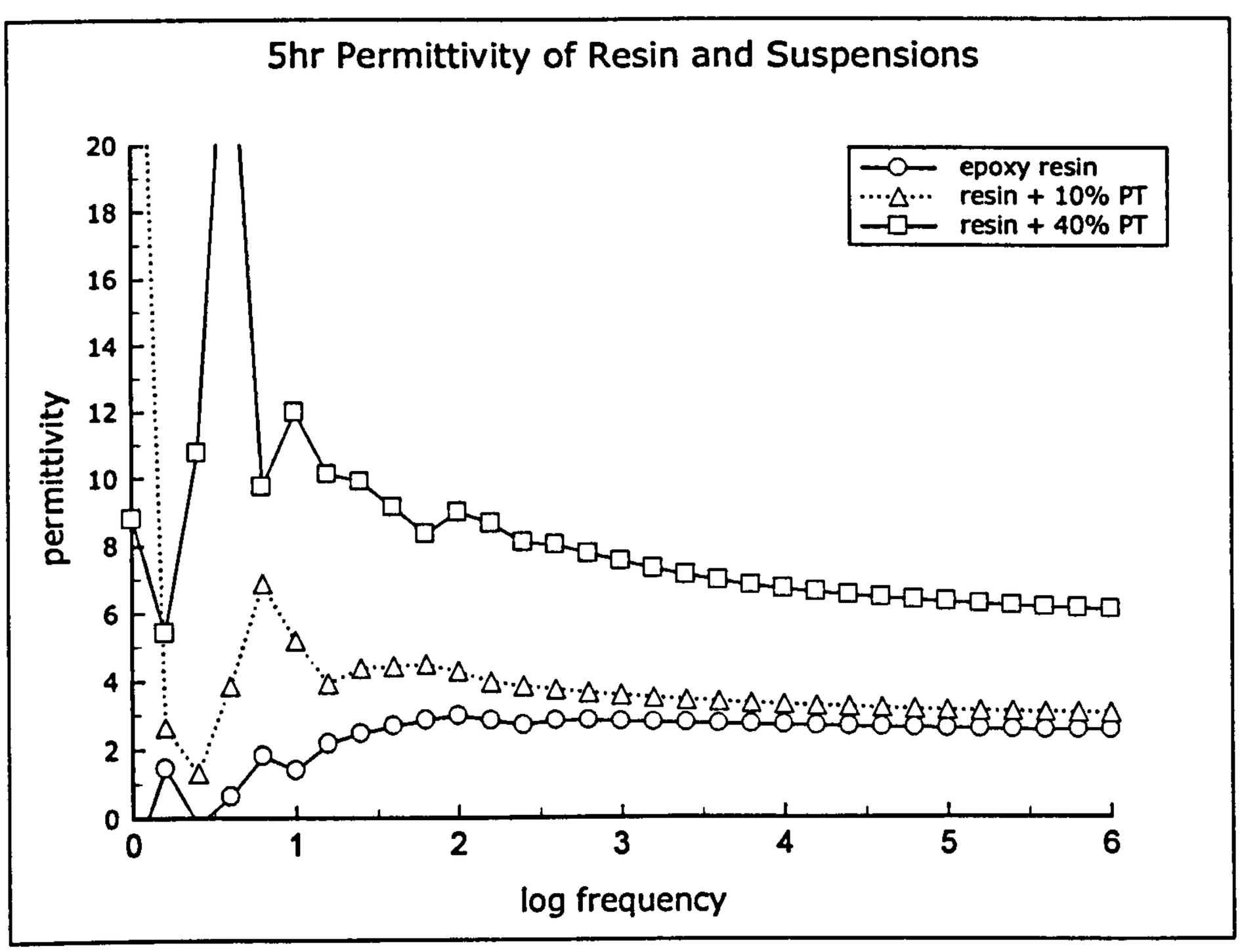

Figure 7.8: Dielectric cure monitoring of Epotek 302-3M epoxy resin and suspensions – initial and 5hr. permittivity at 40°C.

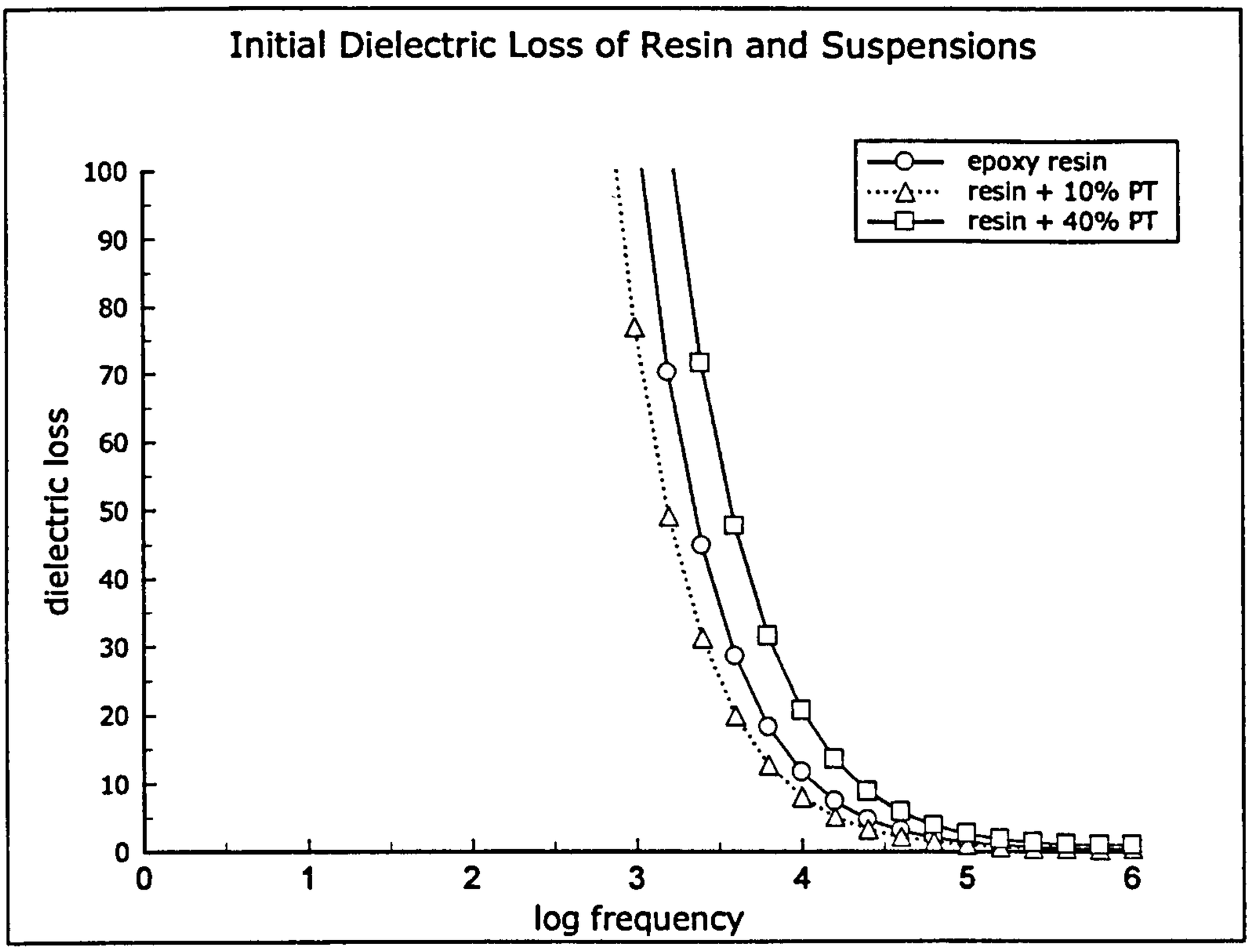

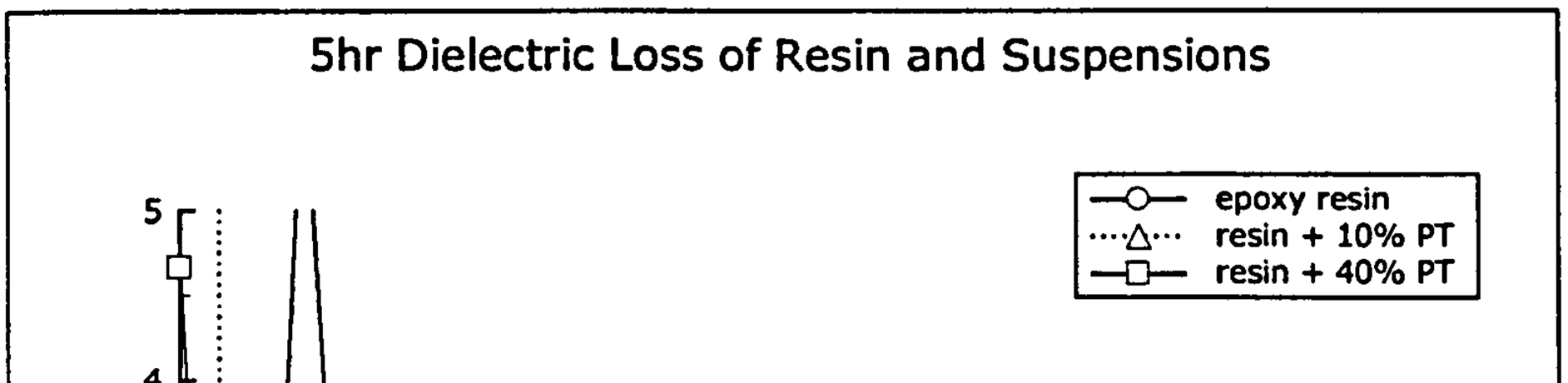

Figure 7.9: Dielectric cure monitoring of Epotek 302-3M epoxy resin and suspensions - initial and 5hr. dielectric loss at 40°C.

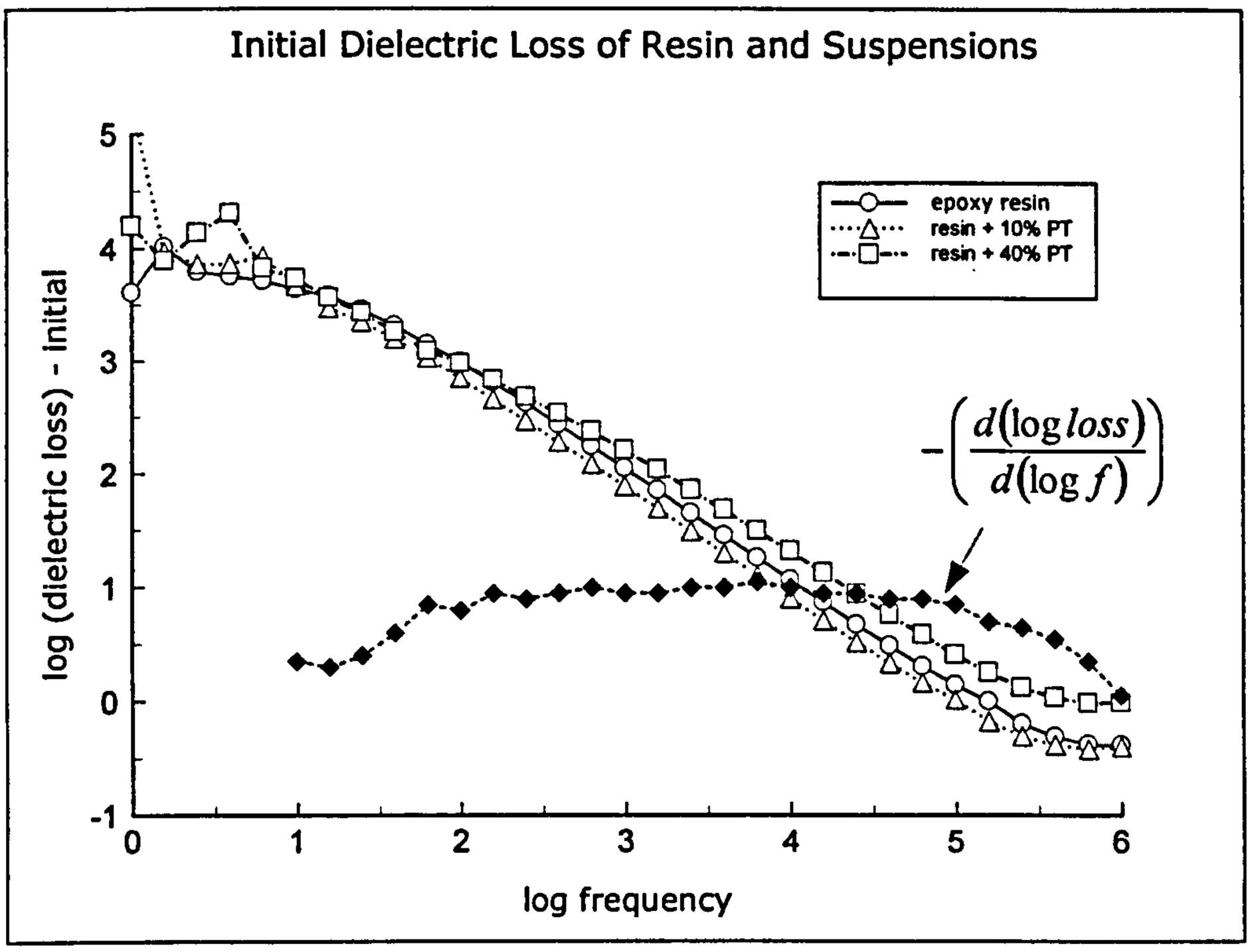

Figure 7.10: Dielectric cure monitoring of Epotek 302-3M epoxy resin and suspensions - initial and 5hr. log (dielectric loss) at 40°C.

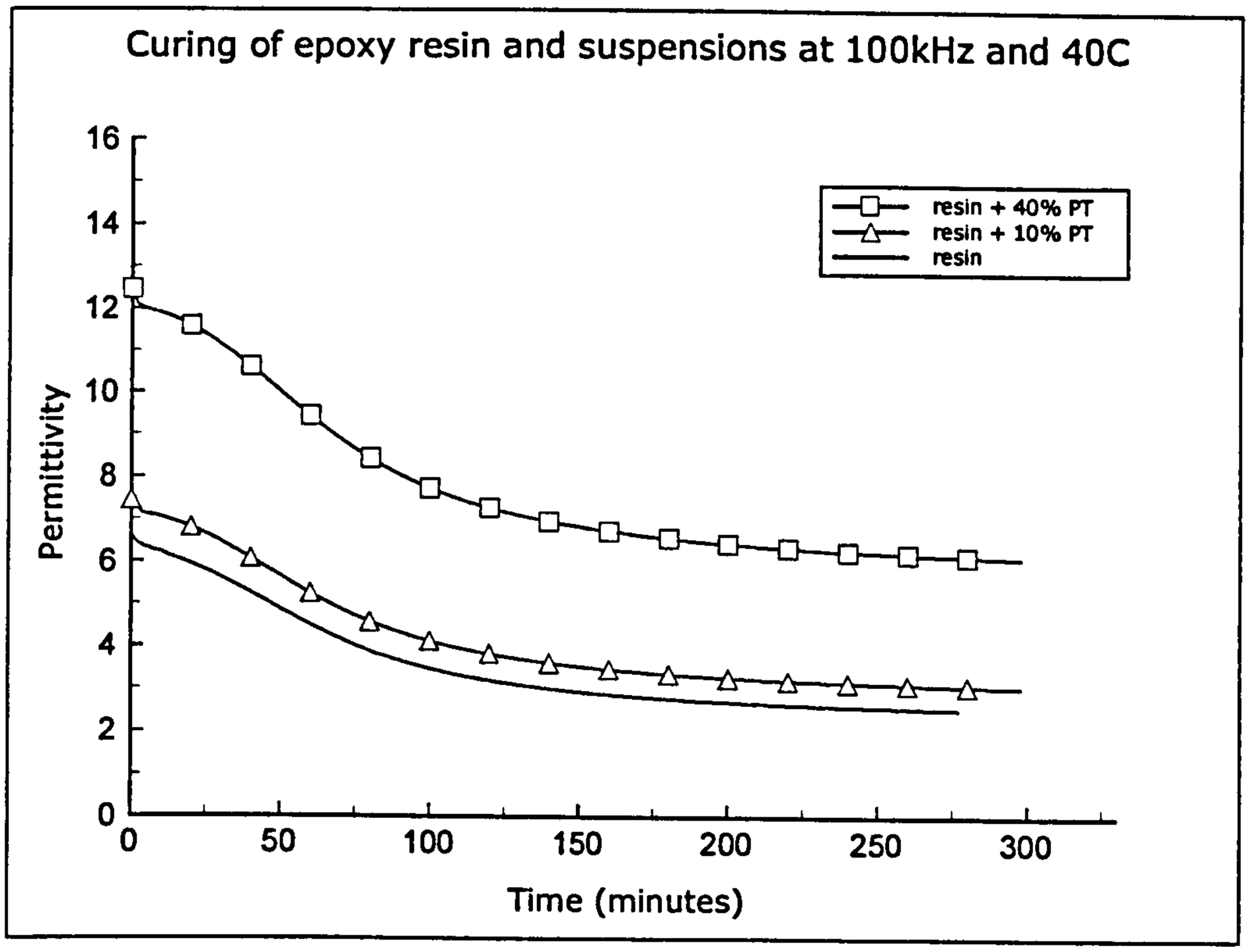

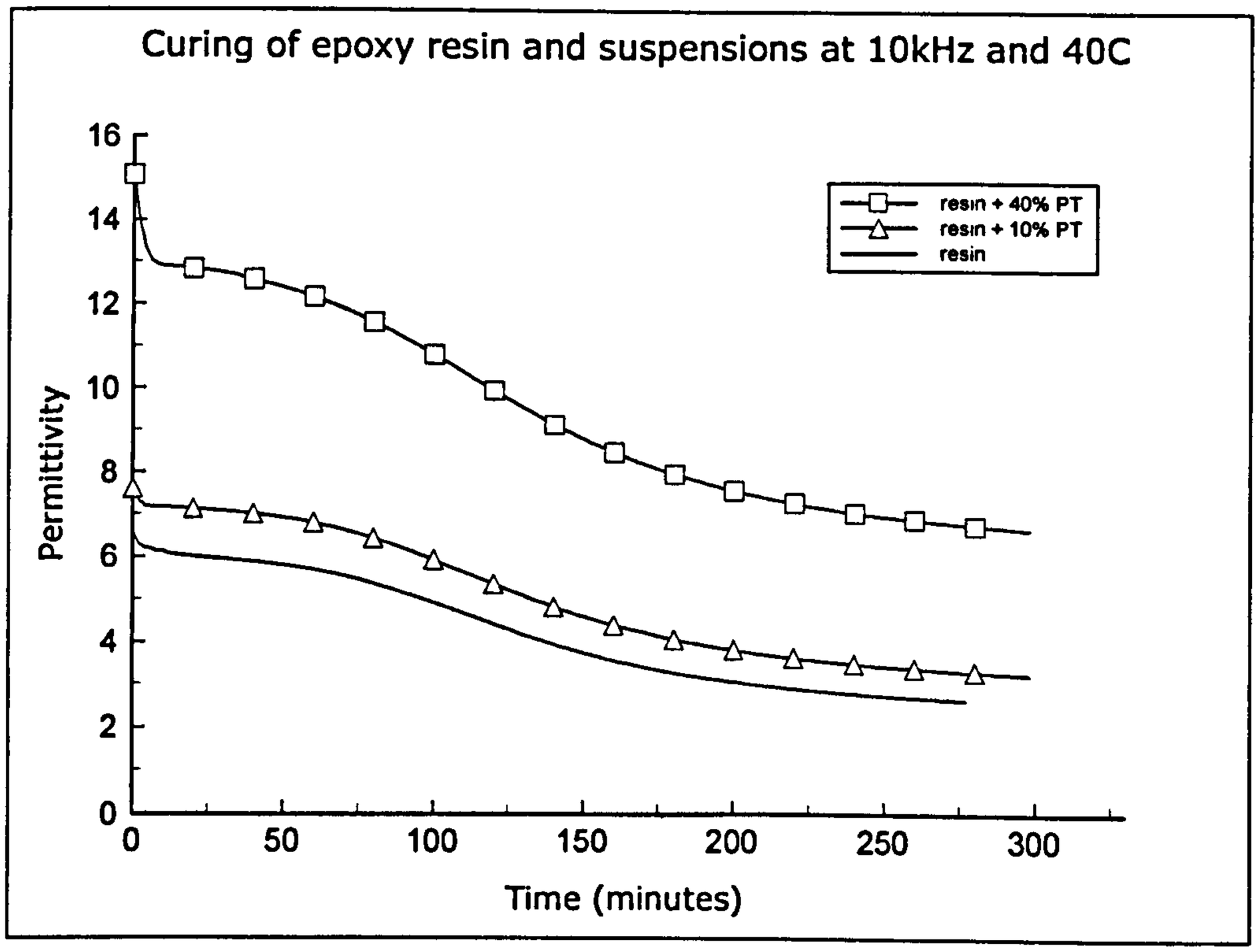

Figure 7.11: Dielectric cure monitoring of Epotek 302-3M epoxy resin and suspensions – time variation of permittivity at 10kHz and 100kHz.

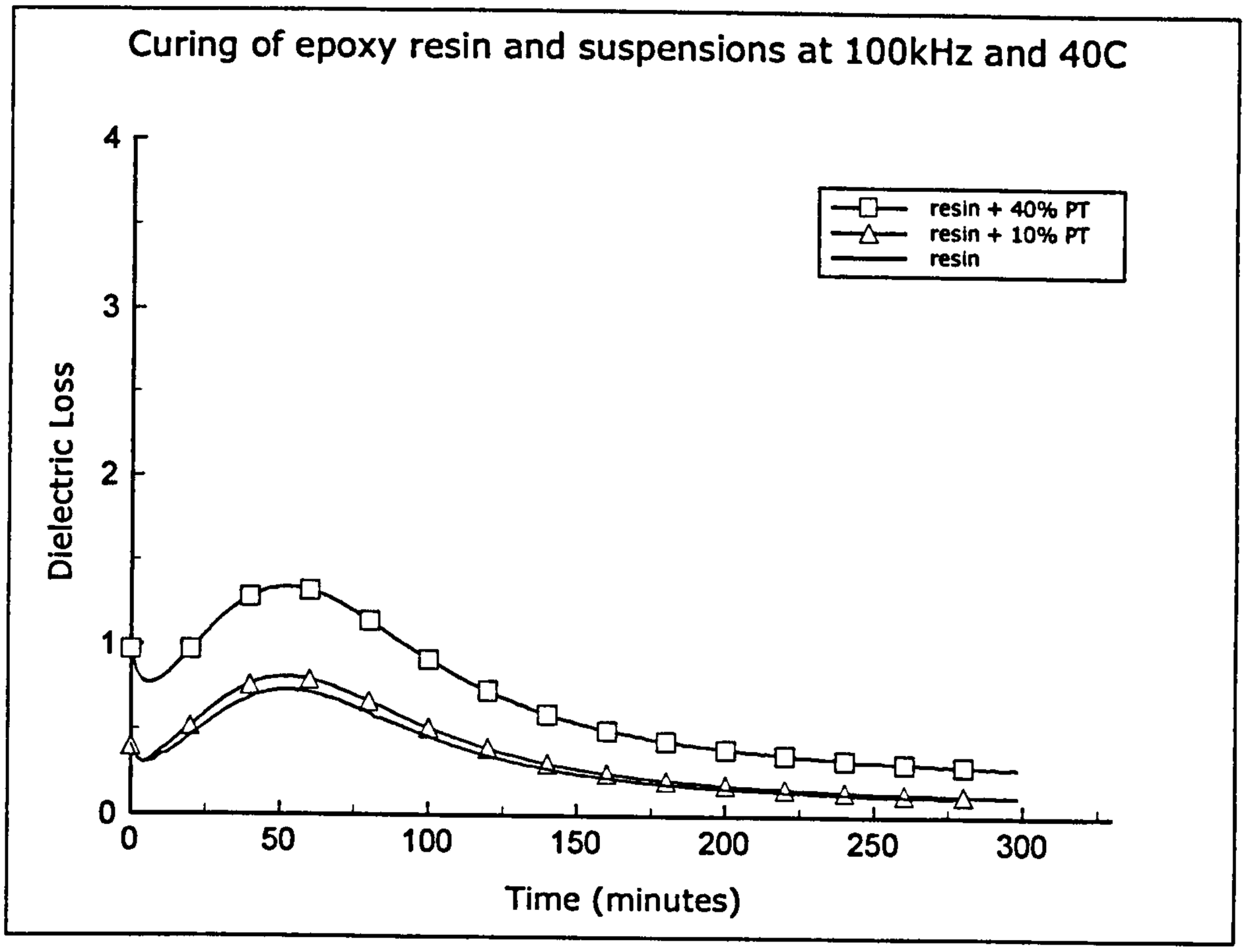

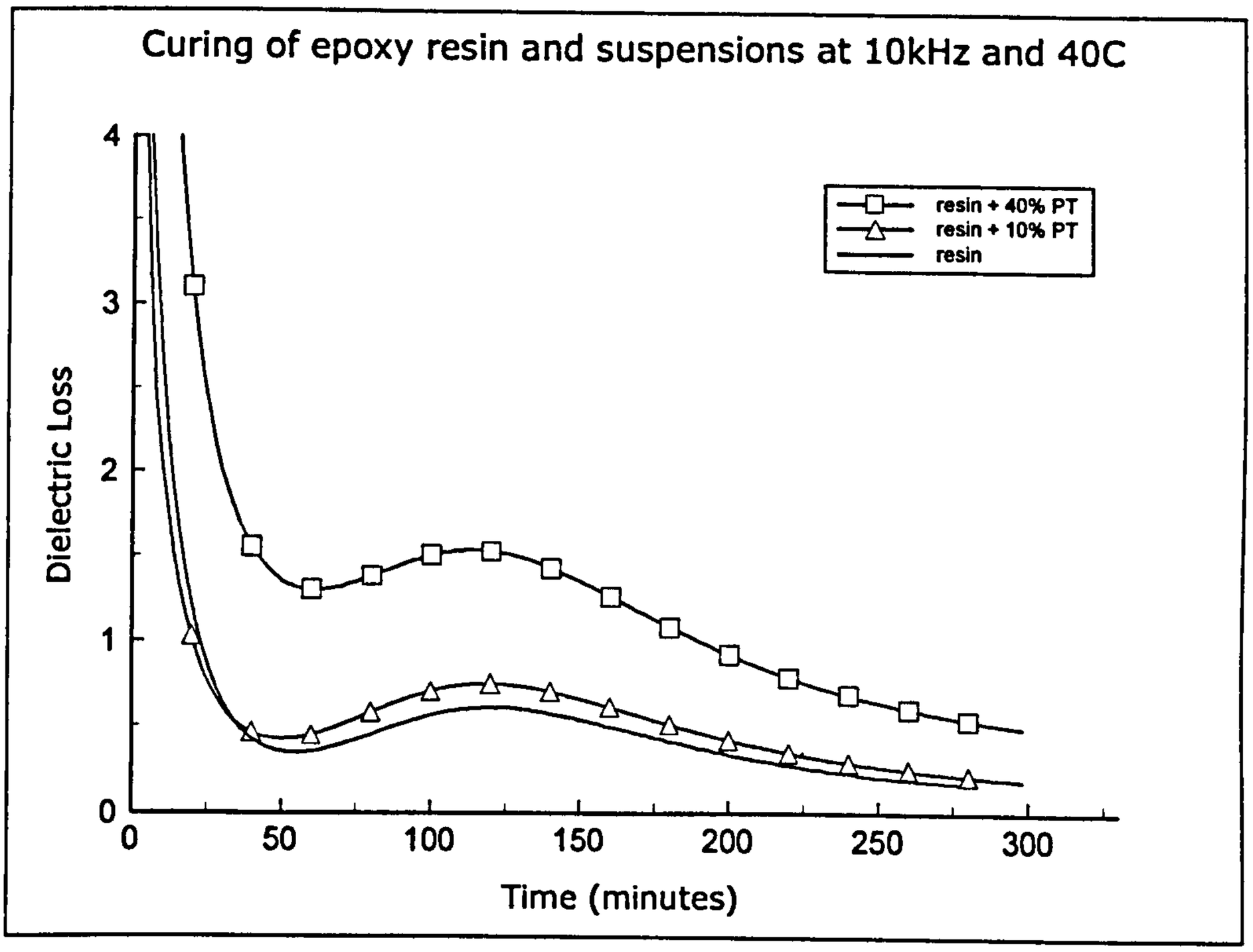

Figure 7.12: Dielectric cure monitoring of Epotek 302-3M epoxy resin and suspensions - time variation of permittivity at 10kHz and 100kHz.

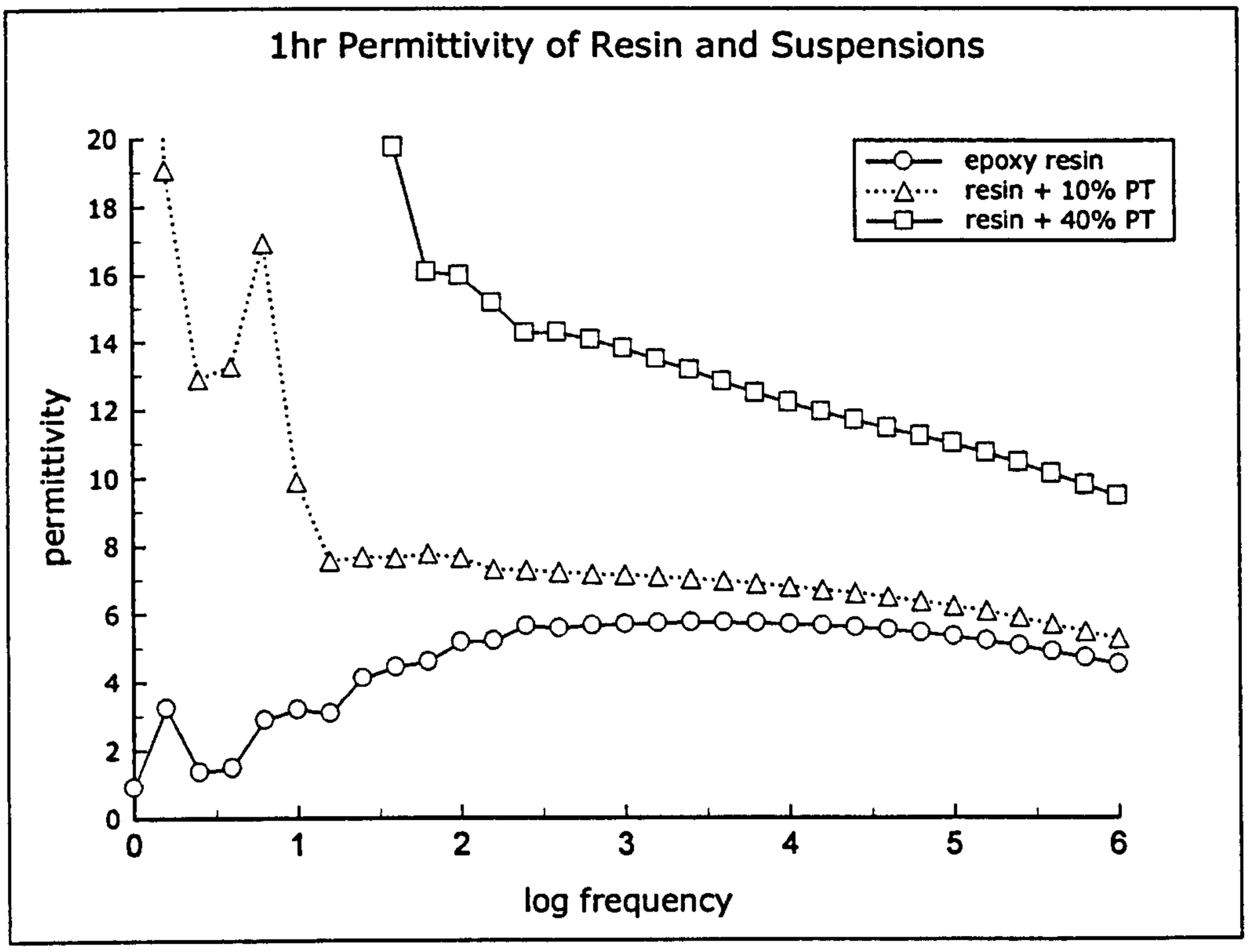

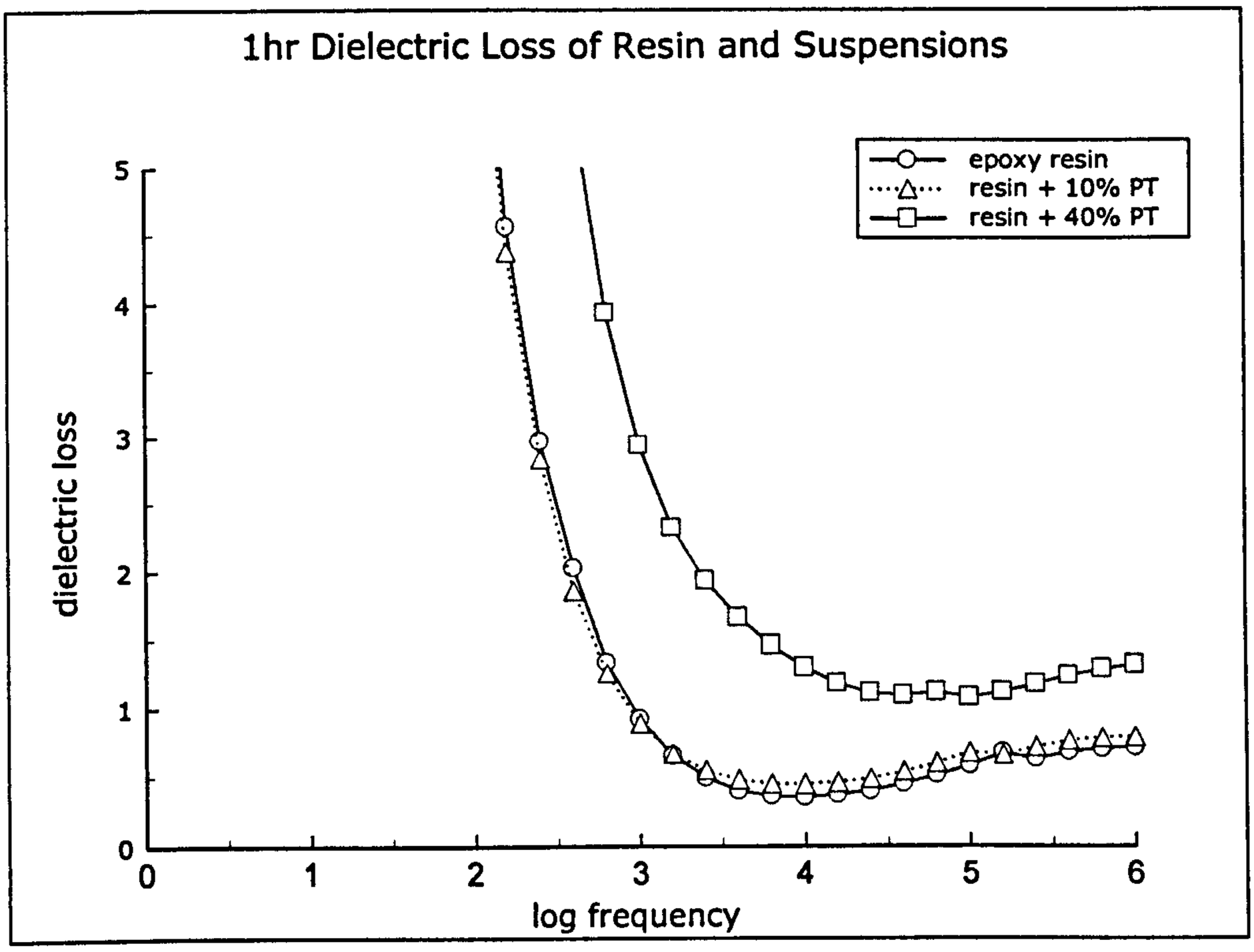

Figure 7.13: Dielectric cure monitoring of Epotek 302-3M epoxy resin and suspensions – permittivity and loss after 1hr at 40°C.

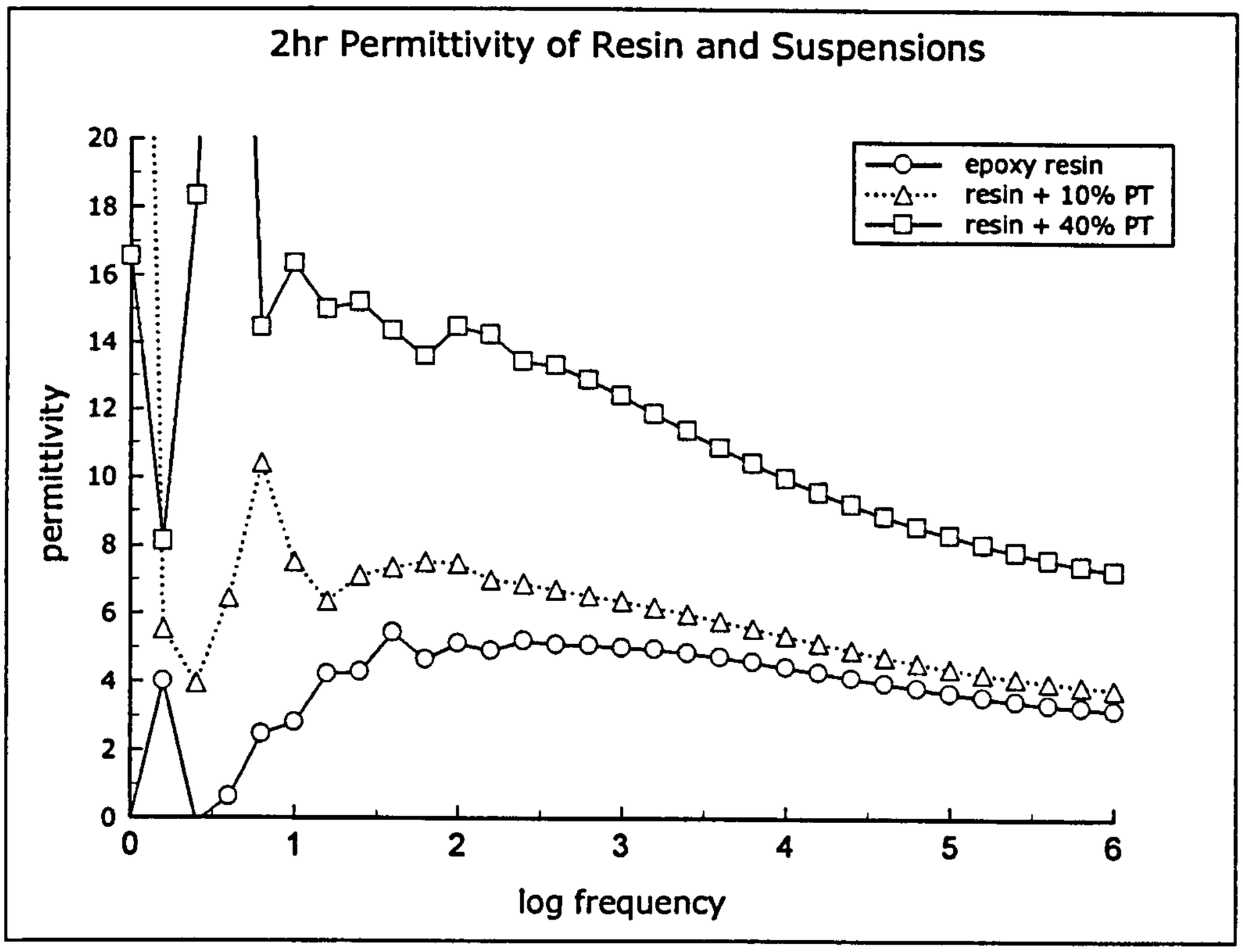

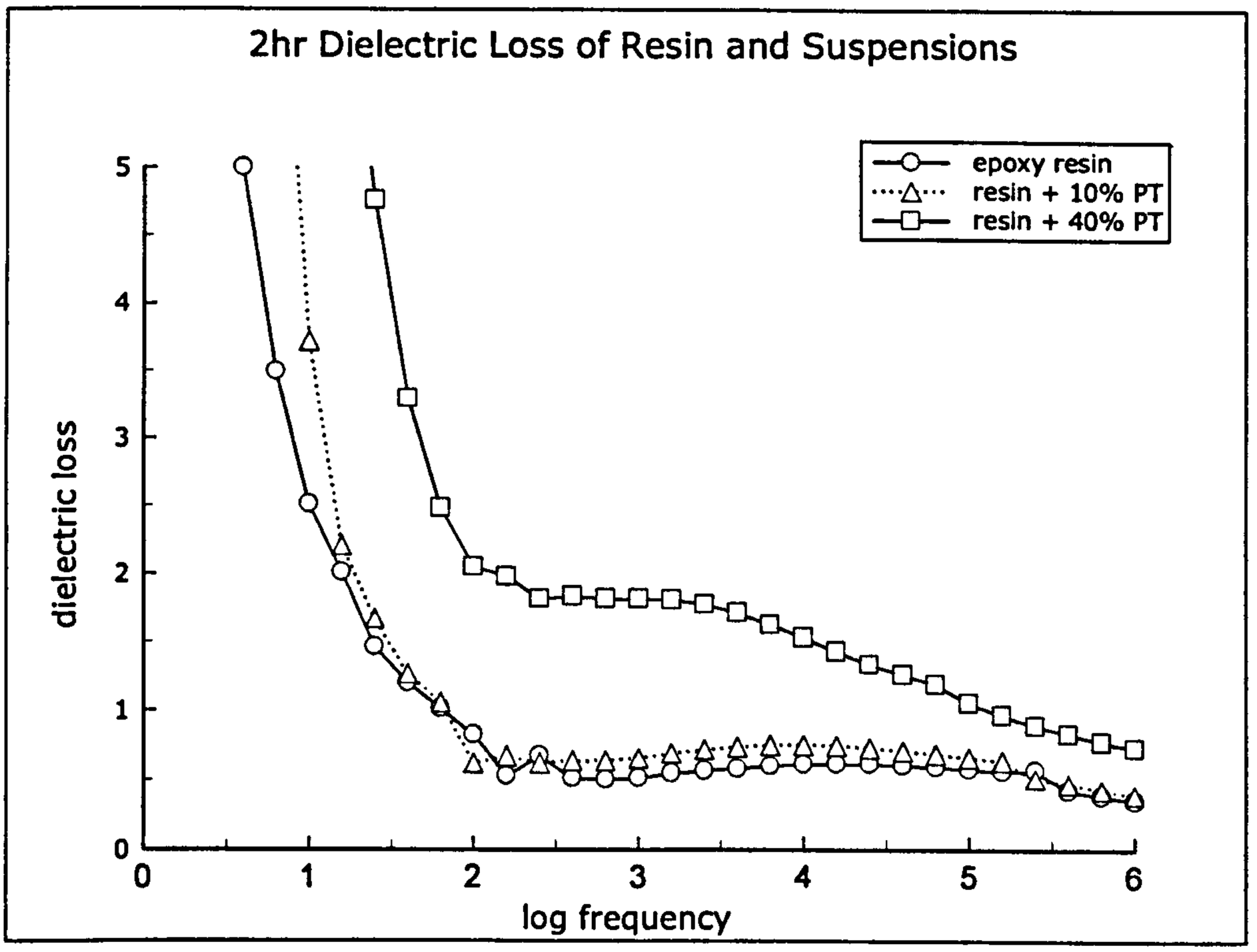

Figure 7.14: Dielectric cure monitoring of Epotek 302-3M epoxy resin and suspensions - permittivity and loss after 2hrs at 40°C.

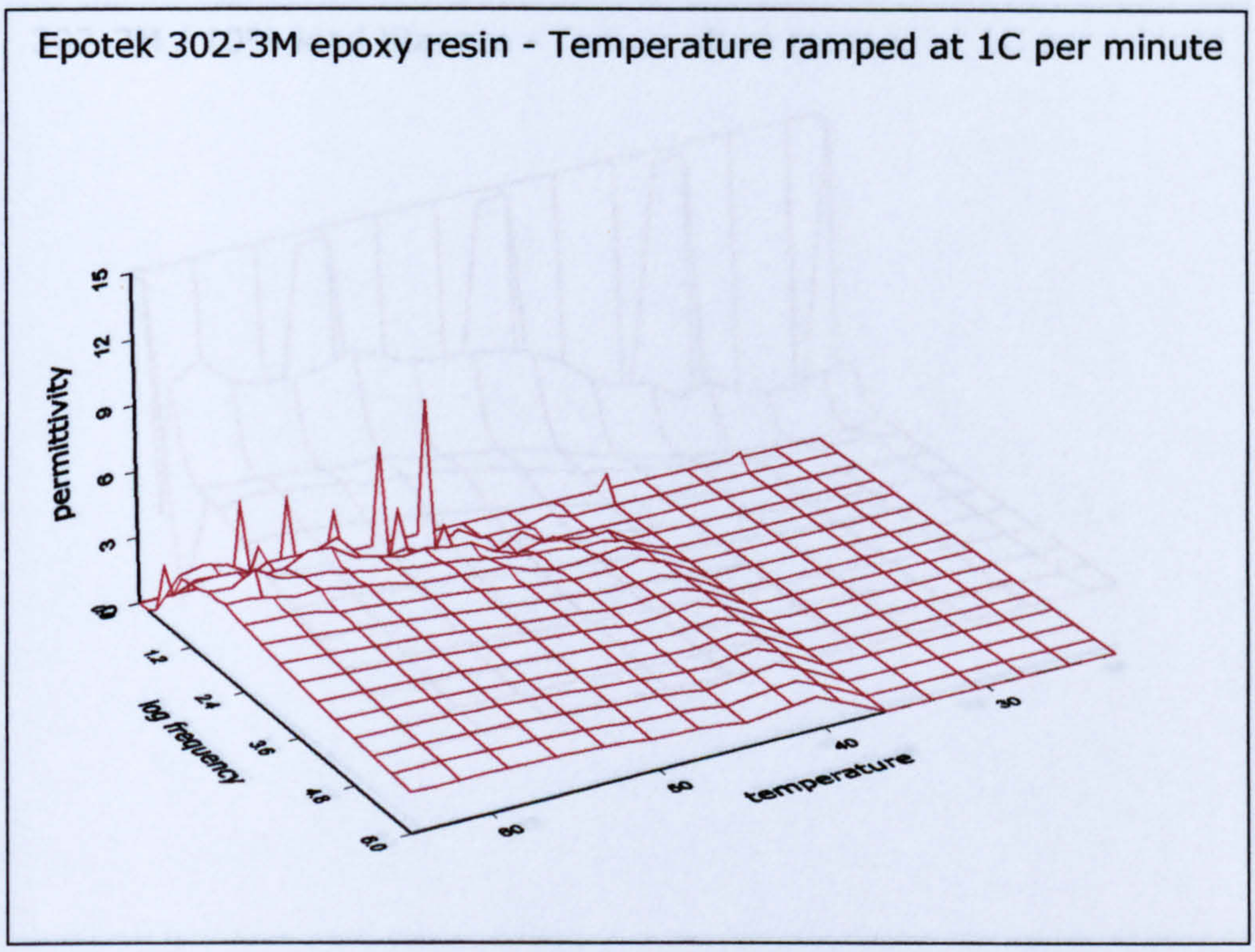

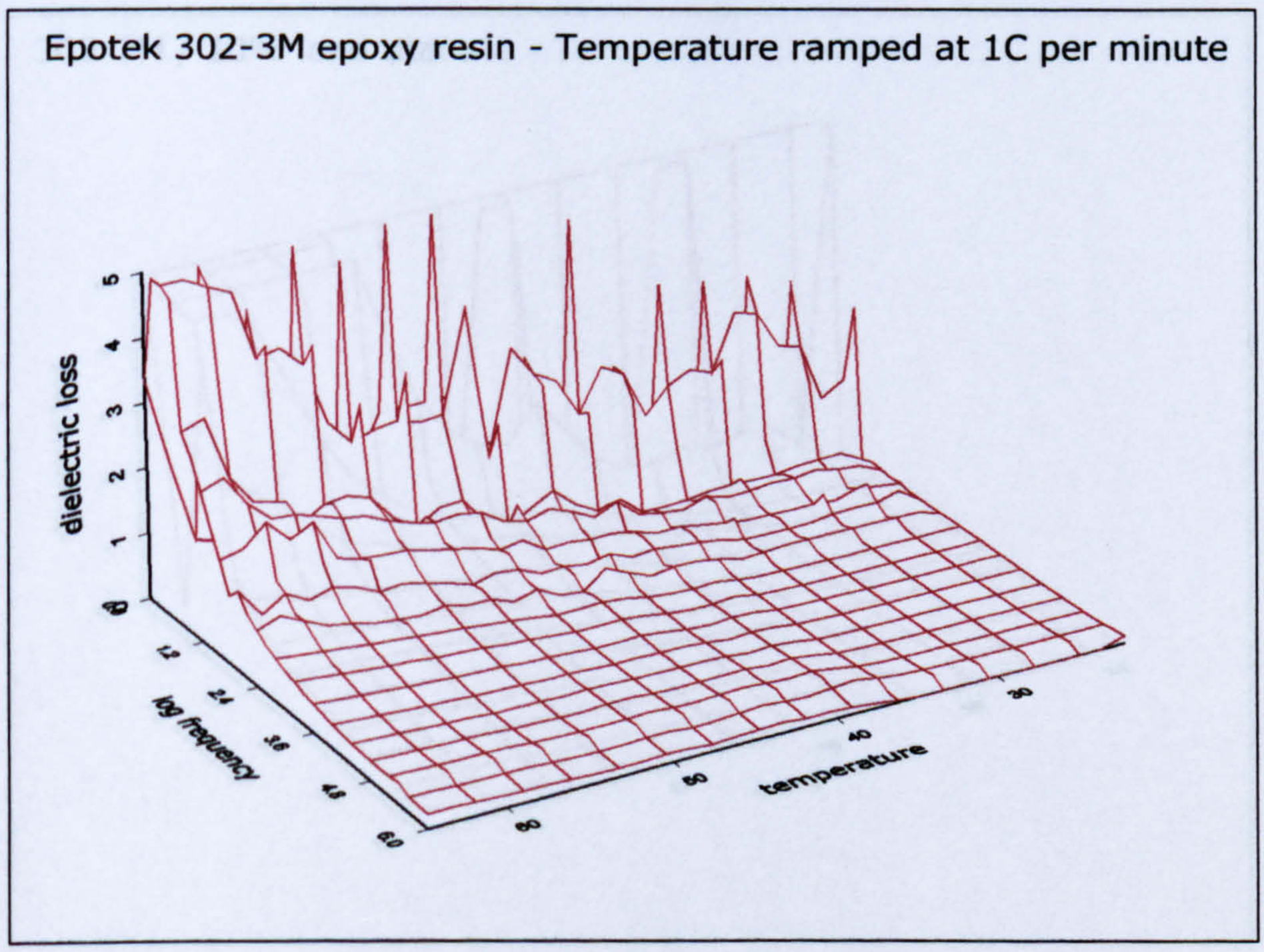

Figure 7.15 - Dielectric cure monitoring of Epotek 302-3M epoxy resin cured at 40°C. Temperature ramped at 1°C per minute.

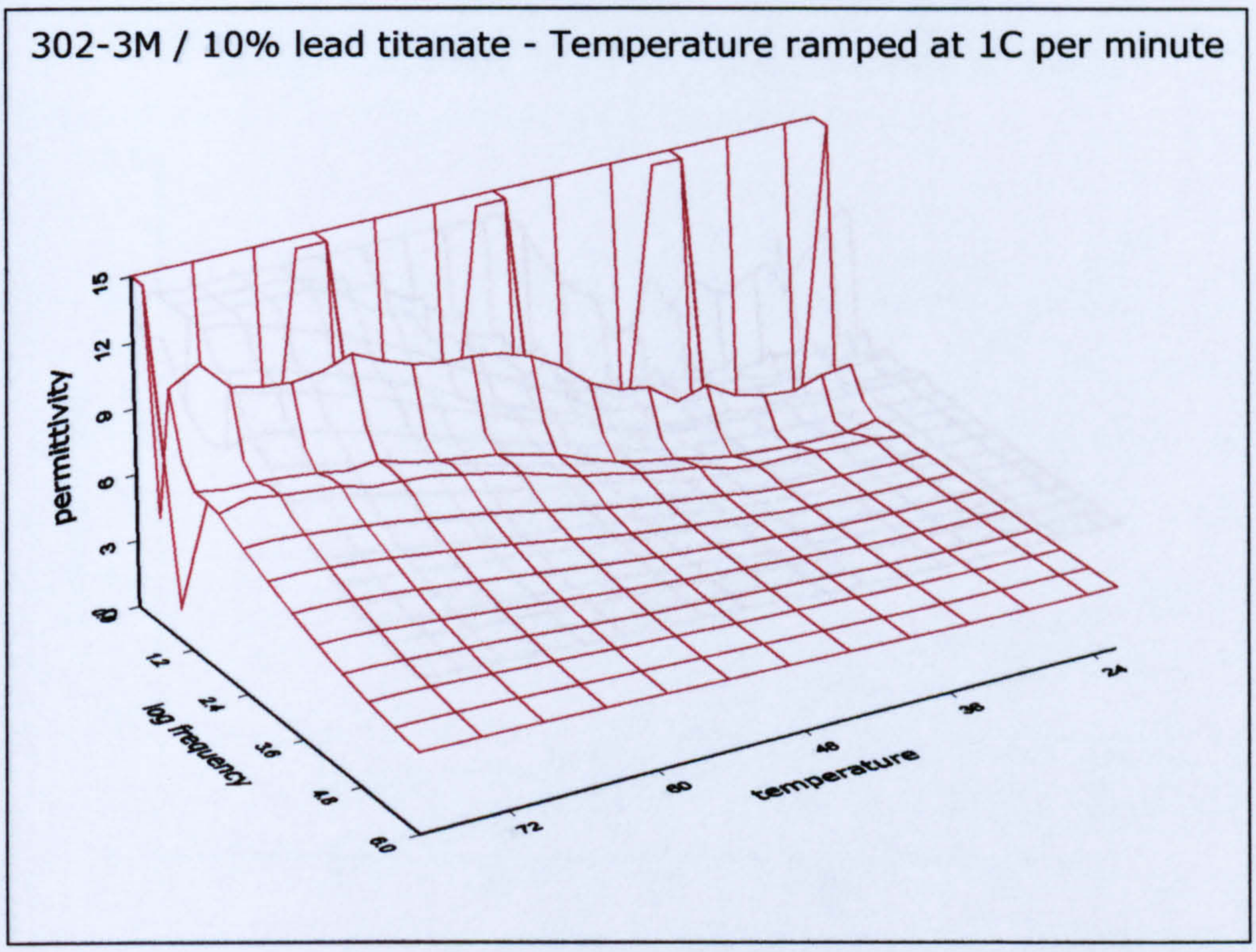

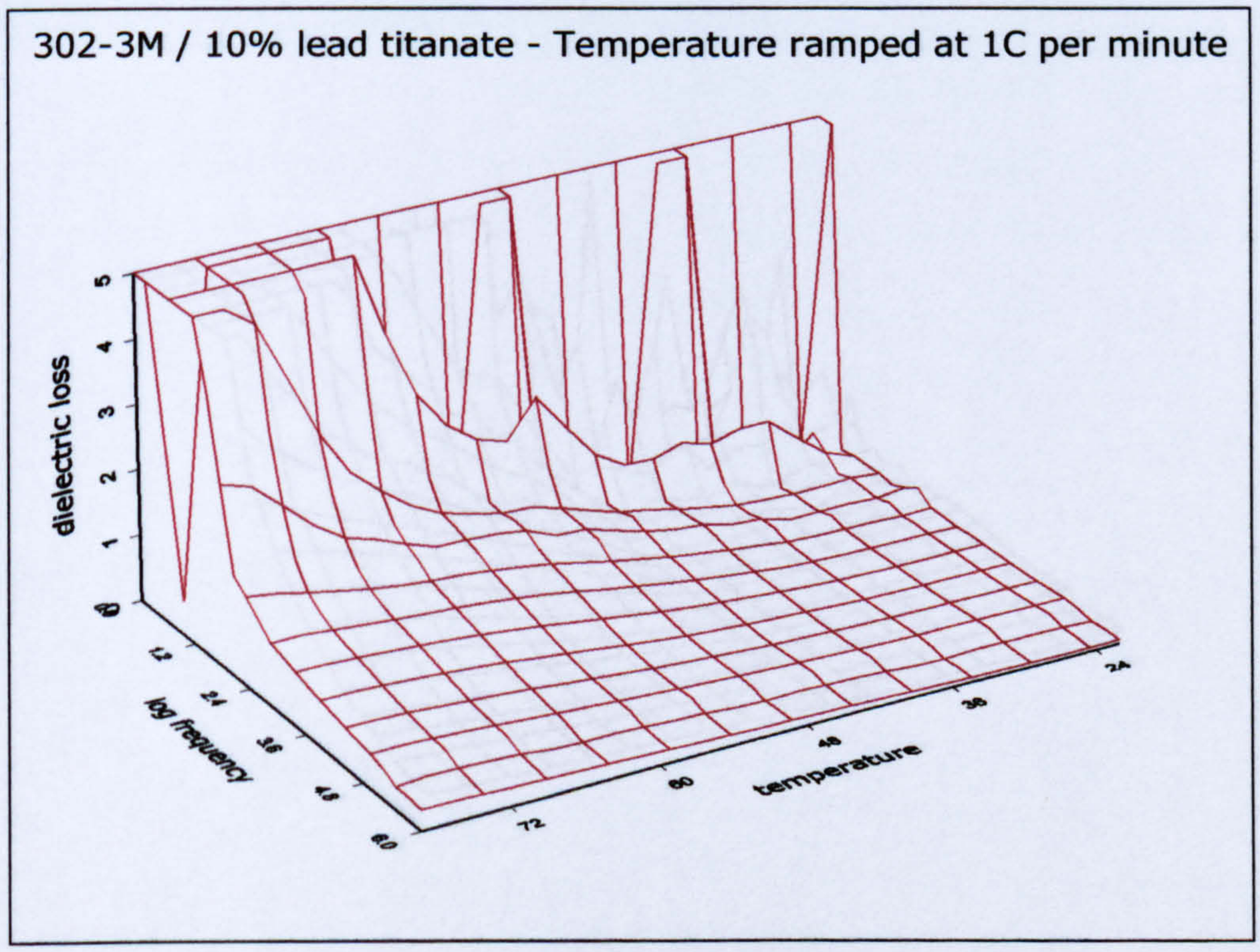

Figure 7.16 - Dielectric cure monitoring of Epotek 302-3M epoxy resin + 10% lead titanate. Temperature ramped at 1°C per minute.

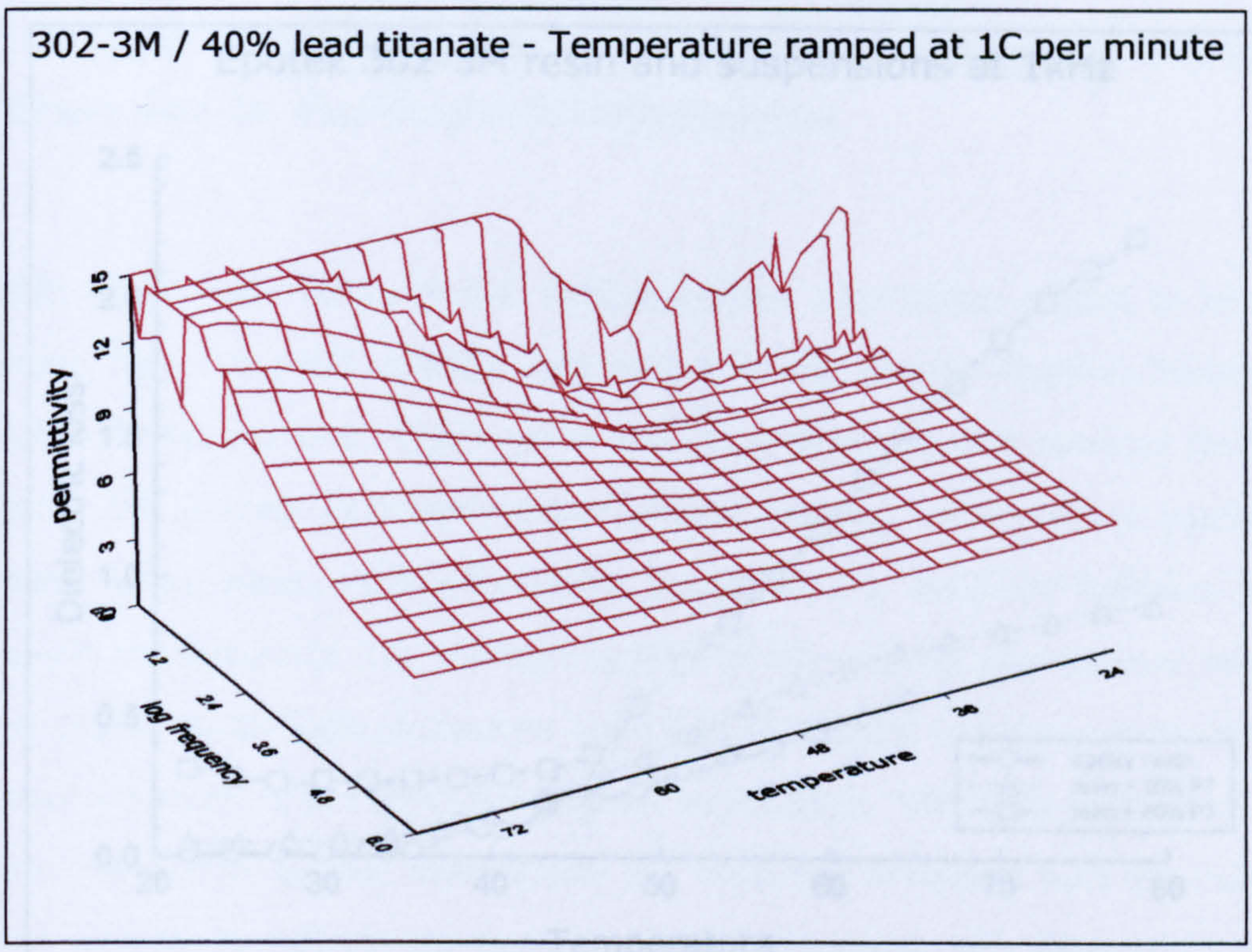

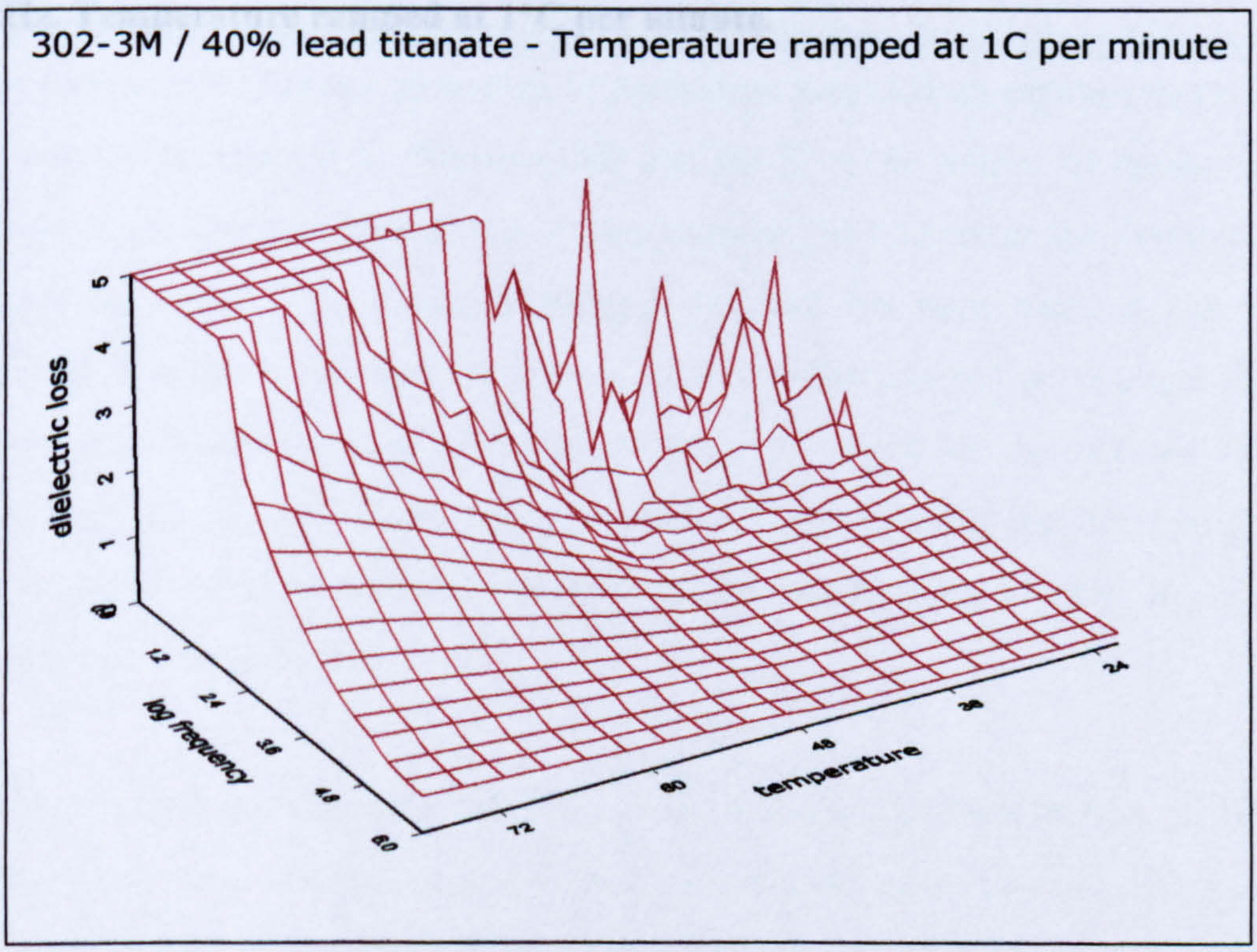

Figure 7.17 - Dielectric cure monitoring of Epotek 302-3M epoxy resin + 40% lead titanate. Temperature ramped at 1°C per minute.

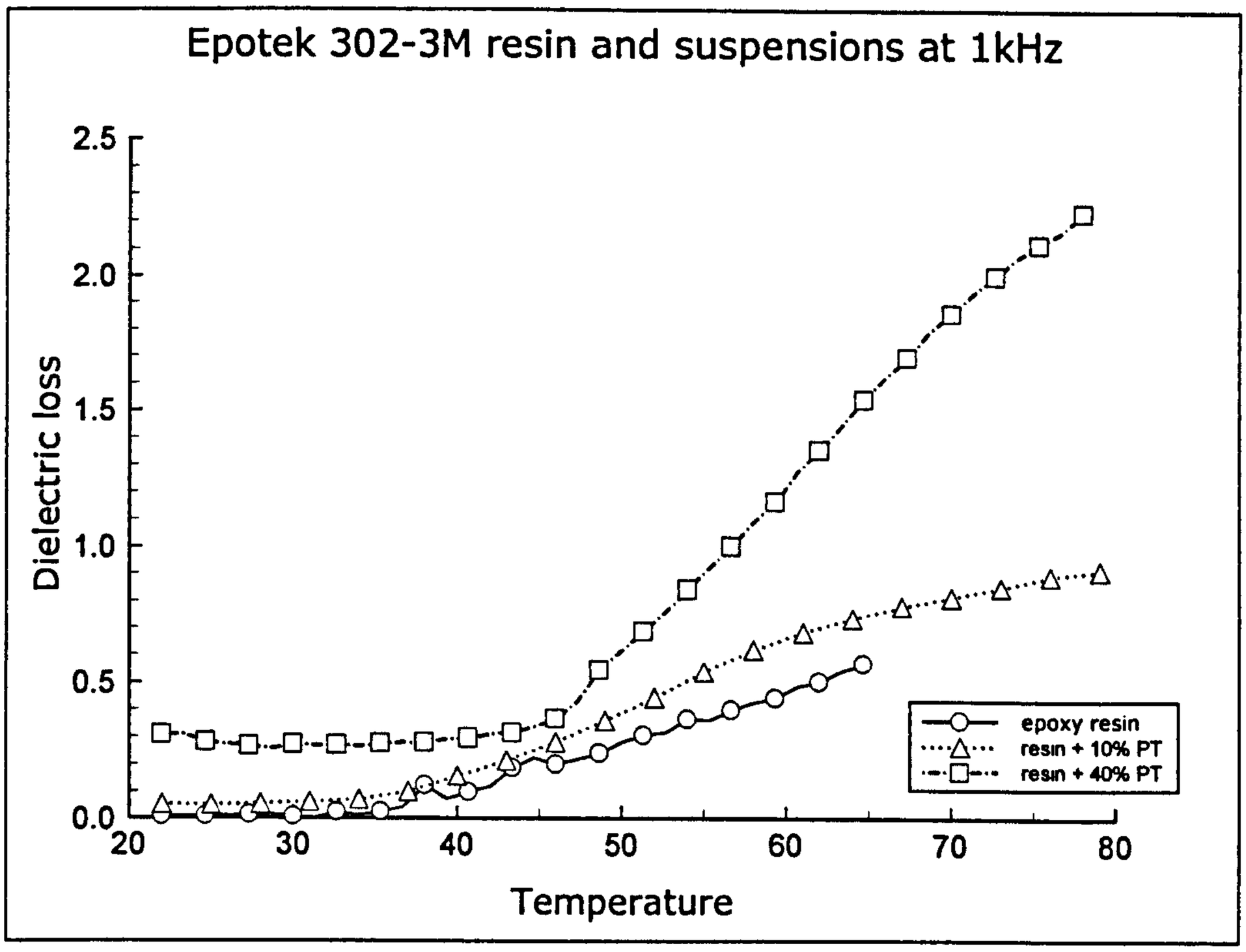

Figure 7.18 - Dielectric loss of Epotek 302-3M epoxy resin and suspensions at 1kHz. Temperature ramped at 1°C per minute.

8. Visual Observations of Electrically-Induced Structure Formation in Particulate Suspensions

Direct visual observations of low volume-fraction suspensions subject to an applied electric field can yield valuable information in the current context. Notably they provide further evidence, which can be used in conjunction with previous findings, to identify the process conditions under which chain-like structures of particles are formed. In particular, visual observation is used here to study the influence of field strength and frequency. The potential applied across a curing suspension is one of the more readily controllable parameters in the field structuring technique, and tailoring the applied waveform opens up a wide range of possibilities. Whilst this must await further study, some more general observations are made and compared with the findings of other workers to indicate the variety of useful composite structures which may be achieved.

8.1 Review of Structure Formation in Electrorheological Fluids

The formation of fibrillar structures in particulate suspensions exposed to an electric field was first reported by Winslow [80] and has been the subject of intense study in recent years. This has been due to strong commercial interest in the development of electrorheological (ER) fluids. Significant progress has been made in this regard, although it is fair to say that the level of understanding has not yet reached the stage where an all-encompassing model exists and the search for an optimal ER fluid continues [81-83, 37]. Nonetheless a great deal of attention has been paid to the formation of particle chains and some general rules have emerged which are the subject of the following discussion.

Small dielectric particles suspended in a fluid experience thermal motion, which tends to randomise their distribution and form a uniform dispersion. The suspended particles are also subject to the force of gravity, which can cause sedimentation. When the suspension is exposed to an electrical field the particles become polarized. The induced charge creates a dipolar field, which can be modelled in terms of a dipole moment (**d**):

$$\vec{\mathbf{d}} = \beta . a_d^3 . \varepsilon_f . \vec{\mathbf{E}}_{loc}$$

where β is the effective polarizability of the particle, a_d is its radius, ε_f is the dielectric permittivity of the fluid and $\mathbf{E}_{loc}$ is the local effective electric field acting on the particles [84].

There are long-range forces associated with the dipoles and the force between two identical spheres of radius a can be analysed as [81]:

$$\mathbf{F}_{el} = 12\pi\varepsilon_0\varepsilon_f a^2 \beta^2 E_0^2 \left\{ \left(\frac{a}{r}\right)^4 \left[\left(2f_{11}\cos^2\theta - f_{\perp}\sin^2\theta\right)\mathbf{e}_r + f_{\Gamma}\sin 2\theta\, \mathbf{e}_{\theta} \right] \right\}$$

here $\mathbf{F}_{el}$ is the electrostatic polarization force on a particle at the origin due to a particle located at r,θ where r is the separation of the particle centres and θ is the angle between the dipole moment vector and the centre to centre vector. The externally applied electric field has the form $\mathbf{E} = E_0\mathbf{e}_z$ where $\mathbf{e}_z$, $\mathbf{e}_r$ and $\mathbf{e}_\theta$ are the unit vectors pointed in the z, r and θ directions respectively. The f_{ii} are dimensionless functions of a/r and $\varepsilon_p/\varepsilon_f$ (ε_p is the particle dielectric permittivity). Values of f_{ii} have been calculated [85] for a range of $\varepsilon_p/\varepsilon_f$. A consequence of this expression is that particles exert an attractive force when a line connecting their centres is parallel to the field and a repulsion when the line of their centres is perpendicular to the field. Where the line of centres is at an angle of less than 55° to the field the particles experience a torque which attempts to align the centres with the field, thereby accounting for the tendency for particles to form 'pearl-chains' in dilute suspensions. In applying this expression, it should be acknowledged that certain assumptions have been made and its applicability is therefore limited, as discussed below. Nevertheless it serves to highlight some details of practical significance, namely the non-linear dependence of the polarization force on field strength, particle size and polarizability.

In real fluids it is essential to recognise that, owing to conduction, both bound and free charges are induced at the particle surfaces. An exact definition of the induced dipole moment then becomes more subtle. Jones has reviewed the concept of an '*instantaneous effective dipole moment*'. He points out that whereas a uniform electric field stimulates a dipolar response, a non-uniform electric field stimulates a multipolar response and this is very strongly dependent on particle size. [86]. Pohl [87] calculates that at interparticle separations equivalent to or less than the particle radius then higher order multipolar interactions will be equally as important as the simple dipolar interaction. In general, it is as well to remember that calculation of an exact instantaneous dielectrophoretic force is possible only if both the induced electrostatic potential and the spatial variation of the field are known.

An important point ought to be made regarding the polarizability parameter (β), which is occasionally used in research papers to describe real experimental conditions without due regard for its applicability. The parameter is defined as:

$$\beta = \frac{(\varepsilon_p - \varepsilon_f)}{(\varepsilon_p + 2\varepsilon_f)}$$

and this has been seen to be quoted at face value for AC and DC electric fields alike. However, in truth, the terms ε_p and ε_f should refer to the *complex* permittivities of the particles and fluid respectively, in recognition of the out-of-phase components of both polarizability and conductivity. These are of key importance in determining the frequency response of a particular system and are a major influence in the development of electric field induced structures. Pohl [87] has shown that where β assumes a positive value then movement of the particles is toward regions of higher field intensity, *positive dielectrophoresis*. Conversely, where β is negative then particle movement is toward regions of lower field intensity, *negative dielectrophoresis*.

parameter (ε_p^*-ε_f^*/ε_p^*+2ε_f^*) are given by [88]:

$$\mathrm{Re}[f(\varepsilon^*)] = \frac{(\sigma_p - \sigma_f)}{(1+\omega^2\tau^2)(\sigma_p + 2\sigma_f)} + \frac{\omega^2\tau^2(\varepsilon_p - \varepsilon_f)}{(1+\omega^2\tau^2)(\varepsilon_p + 2\varepsilon_f)}$$

and

$$\mathrm{Im}[f(\varepsilon^*)] = \frac{3\omega\tau(\varepsilon_p\sigma_f - \varepsilon_f\sigma_p)}{(1+\omega^2\tau^2)(\varepsilon_p + 2\varepsilon_f)(\sigma_p + 2\sigma_f)}$$

where $\tau = (\varepsilon_p + 2\varepsilon_f) / (\sigma_p + 2\sigma_f)$ and σ_p and ε_p denote the particle's effective, ie. frequency dependent, conductivity and permittivity respectively. The parameter (τ) is the Maxwell-Wagner time constant of the build-up of charges at the particle-fluid interface [89].

Continuing with this theme it can be said that particles subject to an applied AC field experience not only a dielectrophoretic force but also a rotational torque, both of which are functions of the induced dipole moment. An electrophoretic force is also experienced, which is a function of the net surface charge of the particle and this may be significant in the current context at low frequencies. Pethig [88] has shown that the time averaged dielectrophoretic force can be expressed as:

$$F(\omega) = 2\pi\varepsilon_f a^3 . \mathrm{Re}\left(\frac{\varepsilon_p^* - \varepsilon_f^*}{\varepsilon_p^* + 2\varepsilon_f^*}\right) . \left|\nabla E_{0RMS}^2\right|$$

and the simultaneous rotational torque as:

$$\Gamma(\omega) = -4\pi\varepsilon_f a^3 . \mathrm{Im}\left(\frac{\varepsilon_p^* - \varepsilon_f^*}{\varepsilon_p^* + 2\varepsilon_f^*}\right) . E_0^2$$

where E_o is the applied field. Pethig has applied this treatment with some success to explain the complex patterns formed when an electric field is applied to a suspension of living cells in an aqueous environment between interdigitated castellated electrodes. By using this arrangement he has demonstrated chains spanning the inter-electrode gap as a consequence of positive dielectrophoresis at high frequency and, with the same system, diamond shaped patterns in low field regions at low frequency, due to negative

a consequence of positive dielectrophoresis at high frequency and, with the same system, diamond shaped patterns in low field regions at low frequency, due to negative dielectrophoresis. The shape of these latter patterns appears to be related to the electrode geometry.

Khusid and Acrivos have formulated a statistical theory to describe the phase diagram of a low-conducting colloidal suspension subject to a uniform electric field and have subsequently gone on to use this to describe the interparticle interactions in such a suspension exposed to a non-uniform a.c. electric field.[67,90] Their treatment centres on the increase in electrical energy per unit volume of the suspension, due to the interaction of the particles with the applied field, as well as the long-range field-induced interactions between particles. The theory underpins the observed tendency toward particle chaining which results from positive dielectrophoresis. Furthermore they predict the formation of 'disklike aggregates' aligned perpendicularly to the electric field lines, to be the outcome of negative dielectrophoresis and that these are repelled from regions of higher field intensity. Where β is close to zero it is possible that no aggregation of particles will be observed. These predictions are broadly in line with the findings of Pethig et al and shed light on some of the pertinent electrohydrodynamic effects observed by Trau et al, which will be discussed at a later stage [92]. Khusid and Acrivos also postulate that there is a critical threshold for the field strength (E_{th}) which is required to trigger aggregation of particles and that this is dependent on the particle size. They calculate that in dilute suspensions: $E_{th}^2 \sim 1/\upsilon_p$ where υ_p is the particle volume.

Tao [84] uses an energy balance to determine a critical threshold when induced dipolar interaction between particles is strong enough to overcome the randomising effects of thermal motion. He calculates that the threshold electric field for aggregation is approximately:

$$E_{th}^2 = \frac{8\pi kT(1-\phi)}{\beta^2 \upsilon \phi \varepsilon_f}$$

where k is the Boltzmann constant, υ is the particle volume and ϕ is the volume fraction of particles in the system. He further postulates that the minimum energy configuration for such a system (assuming spherical particles) is a body-centred tetragonal (bct) solid and that there is a second critical field threshold. At constant temperature, the system therefore has two phase transitions. In the first of these the liquid begins to form chains spanning the electrodes and the distribution of the chains is random. Where the field intensity exceeds the level of the second threshold, the chains aggregate together to form thick columns, which have the bct lattice structure. This tendency is indeed observed in real fluids, however no insight is provided into the mechanism by which this transition may occur, and the dynamics of the system are such that the minimum energy configuration may be precluded. Clearly a full treatment must take into account not only the ratio of the polarization to thermal forces but also the ratio of the thermal to viscous forces, which act to retard structure formation. Melrose [92] has developed a non-equilibrium phase diagram of structures for ER fluids, which takes these aspects into account. Halsey in his review [35] explains that the force between chains is very different to that between individual particles. He ascribes the observed formation of columns to fluctuations in the electric field which are the result of thermal motion of the particle chains. The time-scale for column formation is usually very much greater than that associated with the assembly of individual chains.

In line with the preceding discussion, it is clear that a study of the polarization of suspensions can be successfully applied to explain the formation of ordered structures. However, there are further aspects of such a system to consider which may well prove to be critical if the technique is to be used to create useful composite materials. Firstly, as interparticle separation diminishes then dispersion forces (London-van der Waals), electrostatic forces (due to charged particles or distortion of the ionic double layer), and also steric hindrance, assume greater significance. Gast and Zukoski [93] have estimated the relative magnitudes of the interparticle interactions for a typical ER fluid and have concluded that the induced polarization and viscous forces completely overshadow the field-free van der Waals and electrostatic forces (by a factor of around

10000:1). Due consideration must be given to frequency effects / relaxation times and temperature, which may give cause to modify this view. Because of its complex nature, the polarizability parameter (β) may, for some systems, adopt a positive or a negative value or indeed zero, according to the applied field frequency. Furthermore, it must be recognised that there is a strong possibility that electrical barriers may be created either at the electrode surfaces or between particles, due to space charge build-up. This would have a screening effect acting to limit the field experienced by the particles and hence reduce their polarization at low frequencies. The electrode material, particle conductivity, surface conductivity and an increase in the field frequency are all factors to consider.

Overall, it should be recognised that the nature of the electrical contact between particles in strongly polarized suspensions is not especially well understood. Dielectric breakdown is sometimes observed, which suggests that below a certain field strength the particles are not in direct electrical contact. However, it may be useful to note that the field strengths employed are comparable to those used to perform certain electrochemical reactions [94]. For example, in the presence of suitable counter ions, chemicals such as pyrrole and phenol are known to undergo electrically-induced redox reactions leading to polymerization. As a consequence the possibility of some localised chemical modification, perhaps leading to ionization and charge build-up, should not be ruled out. (Note: A voltage of 1V would generate a field $20kVmm^{-1}$ across a 50nm thick dielectric layer).

Rattray [95] studied structure formation in ER fluids. He observed that initially the particles aggregated into clumps and small chains, and that these were distributed randomly throughout the fluid. The first stages of structuring thereby reflect the initial spatial distribution of the particles. Particle size influences their associated 'capture' distances and due to inertia, larger particles attract smaller. He also suggests that chains may seed from surface roughness on an electrode or a strongly localised field. Once formed, aggregates grew only from their tips, either by addition of isolated particles or by cluster coalescence. Where the induced structures were allowed to

reach their equilibrium configuration, full chains were formed. He observed that increasing the field strength resulted in a transition from many relatively diffuse columns, which did not span the entire gap between electrodes, to a similar number of densely packed columns, about half of which did completely straddle the gap. In a separate experiment he found that gradually increasing the field strength in a stepwise manner resulted in a much coarser structure, consisting of far fewer, thicker columns nearly all of which bridged the gap between electrodes. Interestingly, these columns are thin-waisted , exhibiting a higher packing density at their mid-points, ie. away from the electrodes. The chains are anchored at the electrodes, but have the freedom to move at their midpoints. This permits them to adopt the minimum 'close-packed' energy configuration. The overall effect provides firm evidence of the relative weakness of the lateral, chain coarsening forces, in comparison with the longer-range tip-to-tip forces of growing chains. The time-scale for column formation is correspondingly longer. These observations mirror Halseys' description. In all cases the field-induced structure persists after the field is removed.

Finally in this section, Figure 8.1 illustrates how electrode design could be used to control the field-induced microstructure. 8.1a) is a consequence of positive dielectrophoresis, whereby polarized particles have moved into the regions of highest field strength. Some are also seen to remain attached to the electrodes. 8.1b) is due to negative dielectrophoresis and particles have been repelled from the regions of highest field strength. 8.1c) is an intermediate pattern. The observed variations were achieved by Pethig et al in their experiments through manipulation of the conductivity of the fluid and also the applied field frequency, which were sufficient to bring about a change in the polarizability parameter (β) from positive to negative.

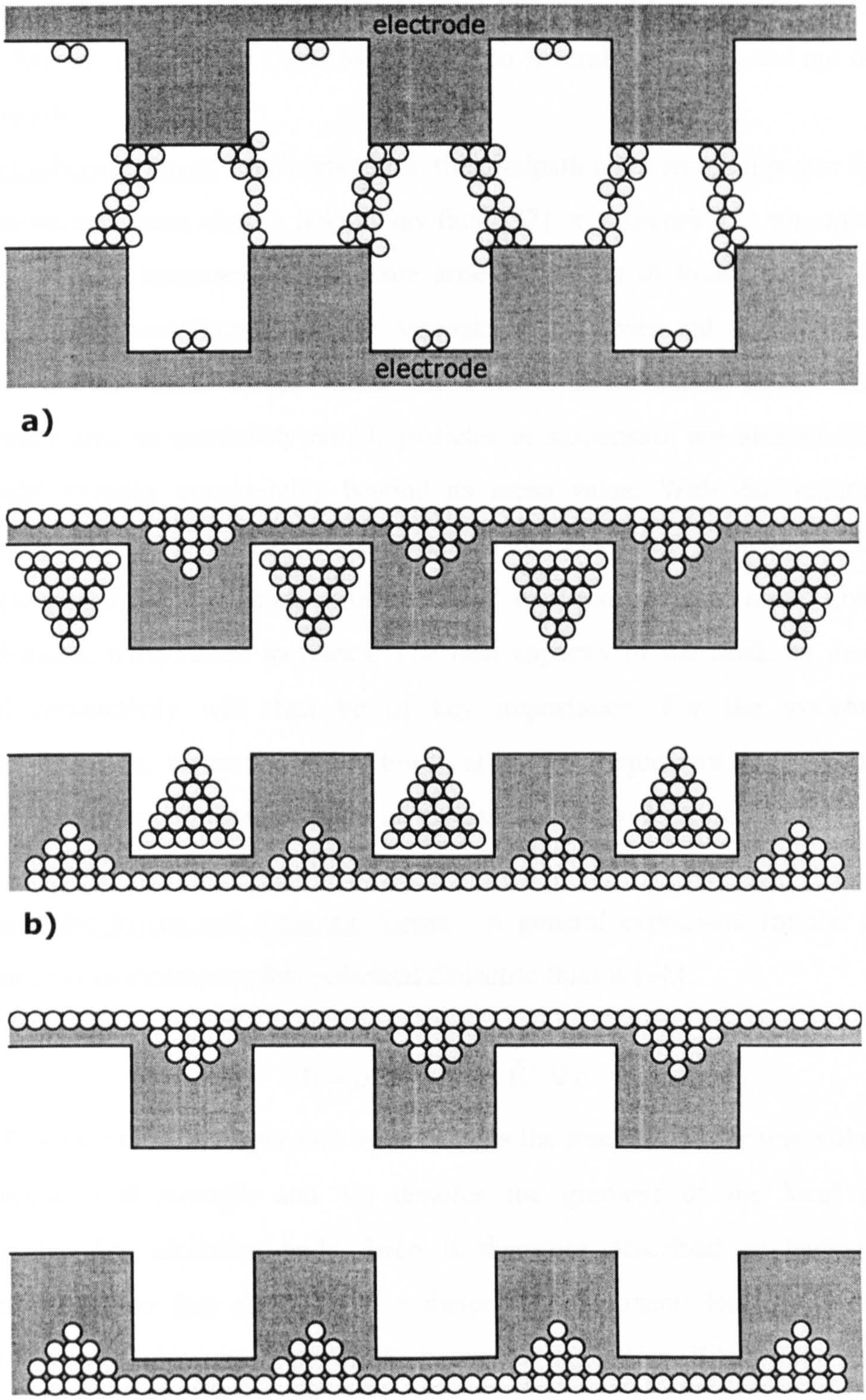

Figure 8.1: The use of patterned electrodes to manipulate the electric-field-induced microstructure (after Pethig) [88]

8.2 Electrohydrodynamic Forces

Electrical body-forces can cause fluid motion which is termed electrohydrodynamic (EHD) flow or 'streaming'. These forces fall into several categories and are described briefly below:

a). Electrothermal forces which arise from the dissipation of electrical power in a fluid. The non-instantaneous electric field in any fluid [87] or suspension is non-uniform and local temperature increases will therefore arise as a result of Joule heating. These, in turn, cause local variations in density, viscosity, permittivity and conductivity, which engender hydrodynamic forces within the fluid. The dissipated power has an E^2 dependence and, as previously noted, particles in suspension are able to distort the local field intensity considerably beyond its mean value. With due regard to the complexity of such a system, it may well be the case that relatively little power dissipation, confined in a small volume of fluid between particles, could give rise to quite dramatic temperature increases. The heat capacity of the fluid, its density and thermal conductivity will then be of key importance. For the systems under consideration here, dielectric loss is lower at higher frequencies and electrothermal forces are therefore expected to show an inverse frequency dependence.

b). Coulombic forces and dielectric forces. A general expression for the electrical body-force in an incompressible polarized dielectric fluid is [96]:

$$\vec{\mathbf{f}}_E = \rho_q \vec{\mathbf{E}} - \frac{1}{2}\varepsilon_0 . \vec{\mathbf{E}}^2 . \nabla \varepsilon$$

where $\mathbf{f}_E$ is electrical force per unit volume, ρ_q is the free charge per unit volume, **E** is the electric field strength and $\nabla\varepsilon$ denotes the gradient of the local dielectric permittivity. The electrical body force is therefore described as having both a coulombic (due to free charge) and a dielectric component. Both of these forces exhibit relaxation and are consequently frequency dependent. When polar liquids are subject to low frequency electric fields, turbulence is often observed which is sometimes referred to as 'electrophoretic streaming'.

c). Electroosmotic force. The phenomenon of electroosmosis is the complement of electrophoresis. Whereas electrophoresis refers to the movement (through a fluid) of charged bodies in response to an electric field, electroosmosis is used to describe the motion of the diffuse ionic layer adjacent to a fixed charged surface. This carries surrounding fluid along and the direction of flow is parallel to the fixed surface. Ramos et al [97] have pointed out that certain electrode geometries have non-uniform charge distributions on their surface and this can promote electroosmotic flow. The castellated arrangement illustrated in the previous section would be a typical example.

8.3 Electric-field-induced Effects in Emulsions and Immiscible Liquids

An interesting effect, which will be of considerable use in the assembly of composite materials, has been reported by Trau et al [91,98] concerning their experiment on electric-field-induced pattern formation in colloidal suspensions. They injected globules of a colloidal dispersion into a fluid through small holes in an electrode (Figure 8.2). Under the influence of an applied field they observed one of two effects and these were dependent on the conductivity of the dispersion. (**1**) When the conductivity of the dispersion exceeded that of the surrounding fluid then the globules were drawn

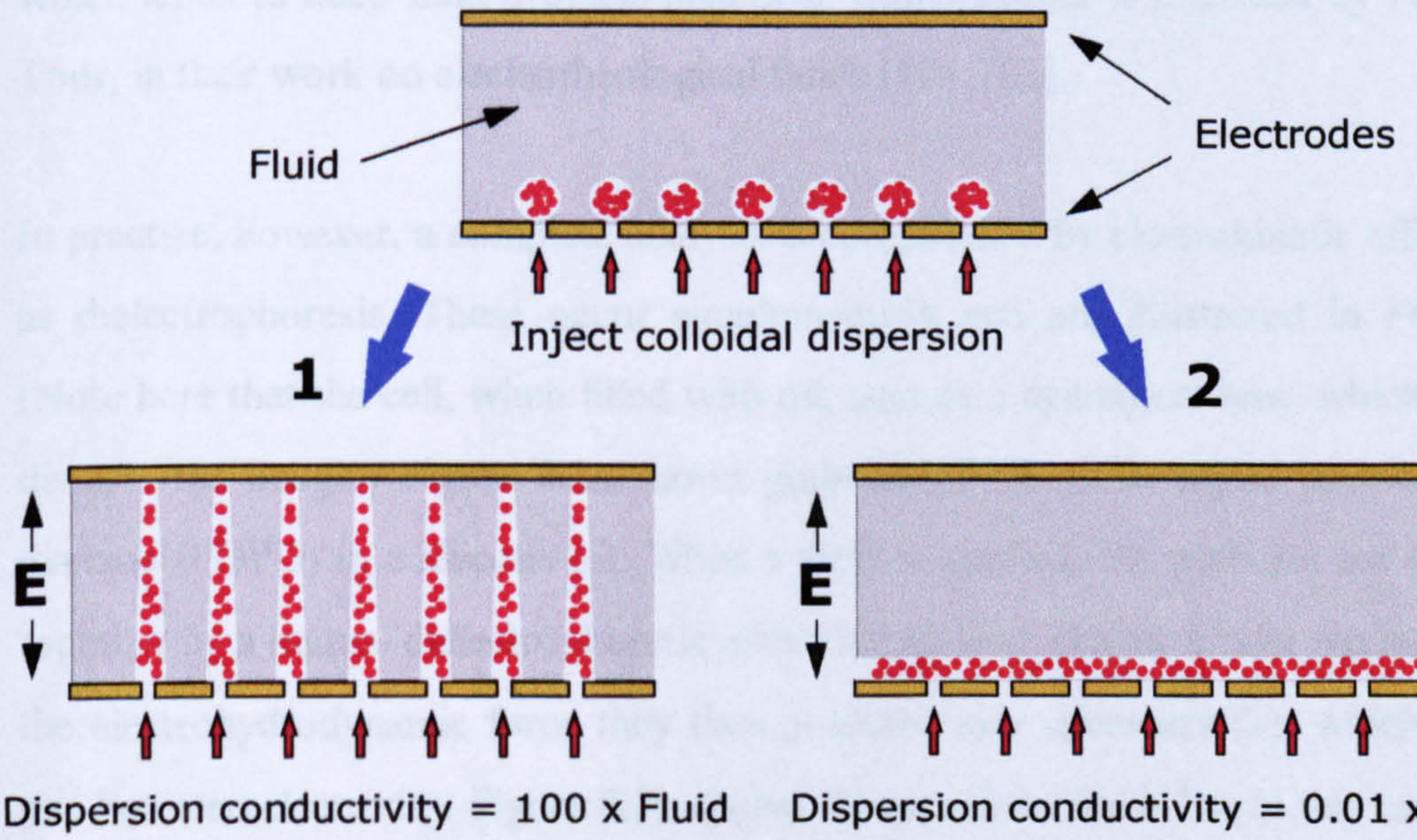

Figure 8.2: Electric-field-induced pattern formation in colloidal suspensions [91]

out in a direction parallel to the applied field. Taken to the limit, columns would form spanning the gap between electrodes. (2) When the conductivity of the dispersion was less than that of the ambient fluid then the globules were flattened and flowed perpendicular to the applied field. Ultimately a film would form adjacent to the electrode. These are electrohydrodynamic effects previously demonstrated by Rhodes et al. [99] in their work on continuous flow electrophoresis and predicted in theory by Landau and Lifshitz [96]. A limited mathematical analysis is presented by Saville [100] in terms of the flow field arising from the electrical body forces acting on the colloid. Note: It would be interesting to reassess the observed effect in terms of the polarizability parameter of the system. However, the published data are incomplete.

In the above experiment, the conductivity mismatch was created by dissolving unequal amounts of an organic salt in the surrounding fluid and in the dispersion. As the experiment progressed, the salt concentration headed towards an equilibrium value, by means of diffusion, and so the electrohydrodynamic effect was gradually lost. Clearly, if the two fluids were immiscible then this time-dependence could be avoided and the effect would become more controllable. Its usefulness in materials processing is then enhanced. A balance of forces would then need to include the effect of surface tension, which tends to keep fluid droplets spherical. Some insight is provided by Halsey and Toor, in their work on electrorheological fluids [101,102].

In practice, however, a complete analysis is complicated by electrokinetic effects, such as dielectrophoresis. These occur simultaneously and are illustrated in Figure 8.3. (Note here that the cell, when filled with oil, acts as a cylindrical lens, which optically distorts the image.) Figure 8.3a shows globules of the polar liquid poly-oxypropyl-diamine (POPD) in a silicone oil. When a field is applied, the globules are (1) drawn together by a mutual dielectrophoretic attraction to form chains. Under the influence of the electrohydrodynamic force they then coalesce into streamers (2), which span the gap between electrodes. Figure 8.3b shows the same two fluids but in this case a small amount of carbon black has been included in the (POPD). Initially

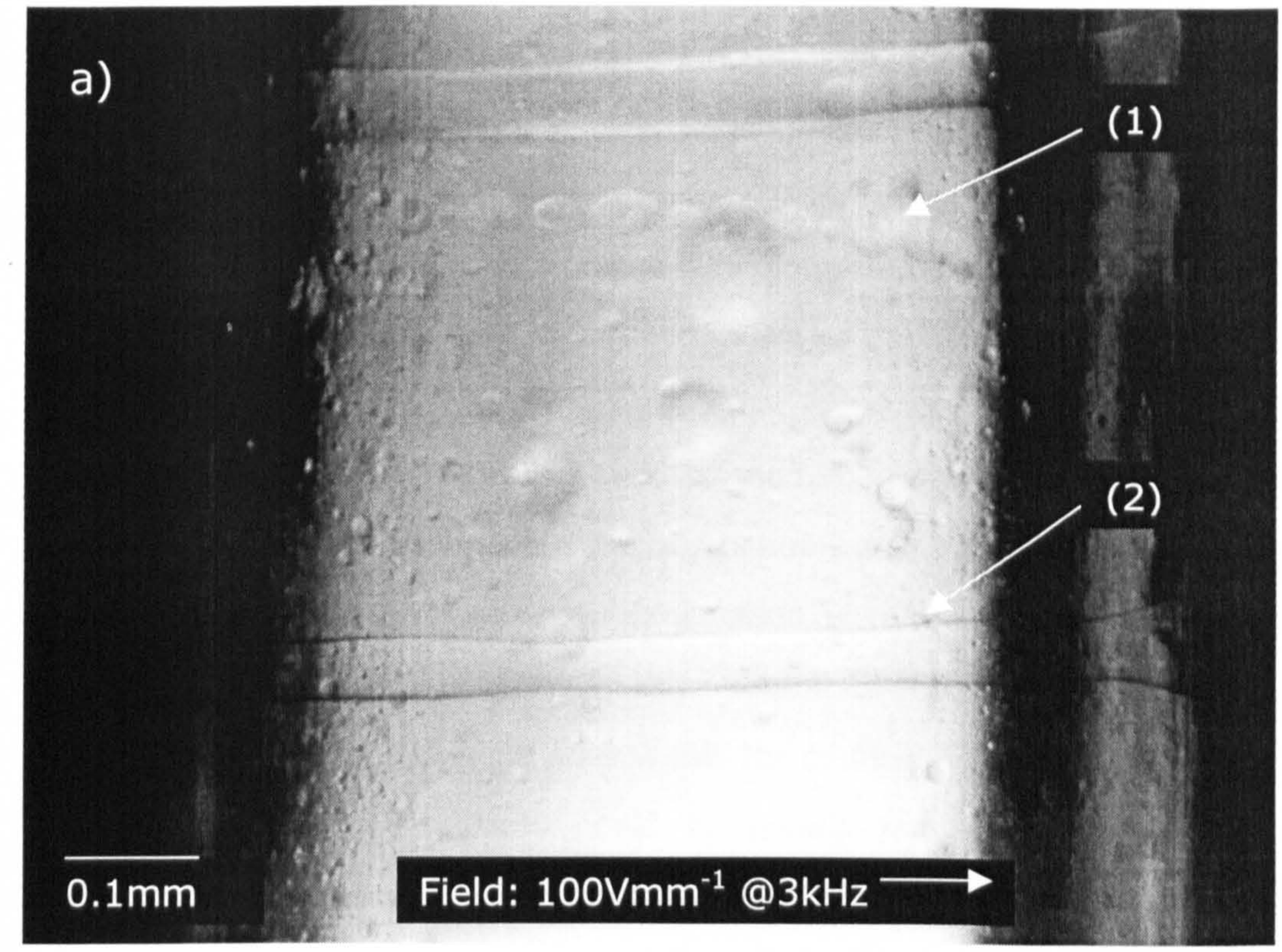

Figure 8.3: Electrohydrodynamic effects in immiscible liquids - a) polyoxypropyl-diamine in silicone oil; b) POPD with carbon black in silicone oil.

the carbon black chains form readily within the globules. This appears to create a conducting pathway, adjacent to the interface, which acts to inhibit the electric-field-induced flow within a globule and destroys the electrohydrodynamic effect. The globules are mutually attracted as they were before and coalesce, but no elongation is observed. The photograph also shows that globules of POPD on the surface adopt a toroidal shape (3). This may be a consequence of the flow pattern of the fluid within the globule. An overall reduction in internal pressure could explain this effect and surface tension at the interface would be modified accordingly. A further possibility may be that the fluid experiences electrostriction leading to a reduction in free-volume. No evidence leading to a precise explanation is offered here. Nevertheless, in the context of materials processing this 'double-dielectrophoresis' may be highly significant and by chaining particles within the confines of a second fluid the range of possible composite structures could be greatly enhanced. Furthermore, if it is recognised that several of the composite materials properties are likely to be influenced by an adsorbed interlayer on the particle surface, then it could be that an intermediate phase may be introduced to good effect. For example, where the electrical properties of the composite are determined by the presence of an adsorbed layer of an insulating matrix polymer then this could be replaced by generously 'pre-coating' the filler particles with a viscous solution of a lossy polymer in a polar solvent. Chaining and coalescence of the particle/polymer globules would then take place as previously observed (Figure 8.3a) in the matrix fluid and by adjusting the conductivity of the various components, it could be arranged that chaining of the particles within the globules also occurred. The polar solvent would finally be encouraged to diffuse out of the composite, leaving the filler particles coated with the lossy polymer and without insulating barrier layers of the matrix.

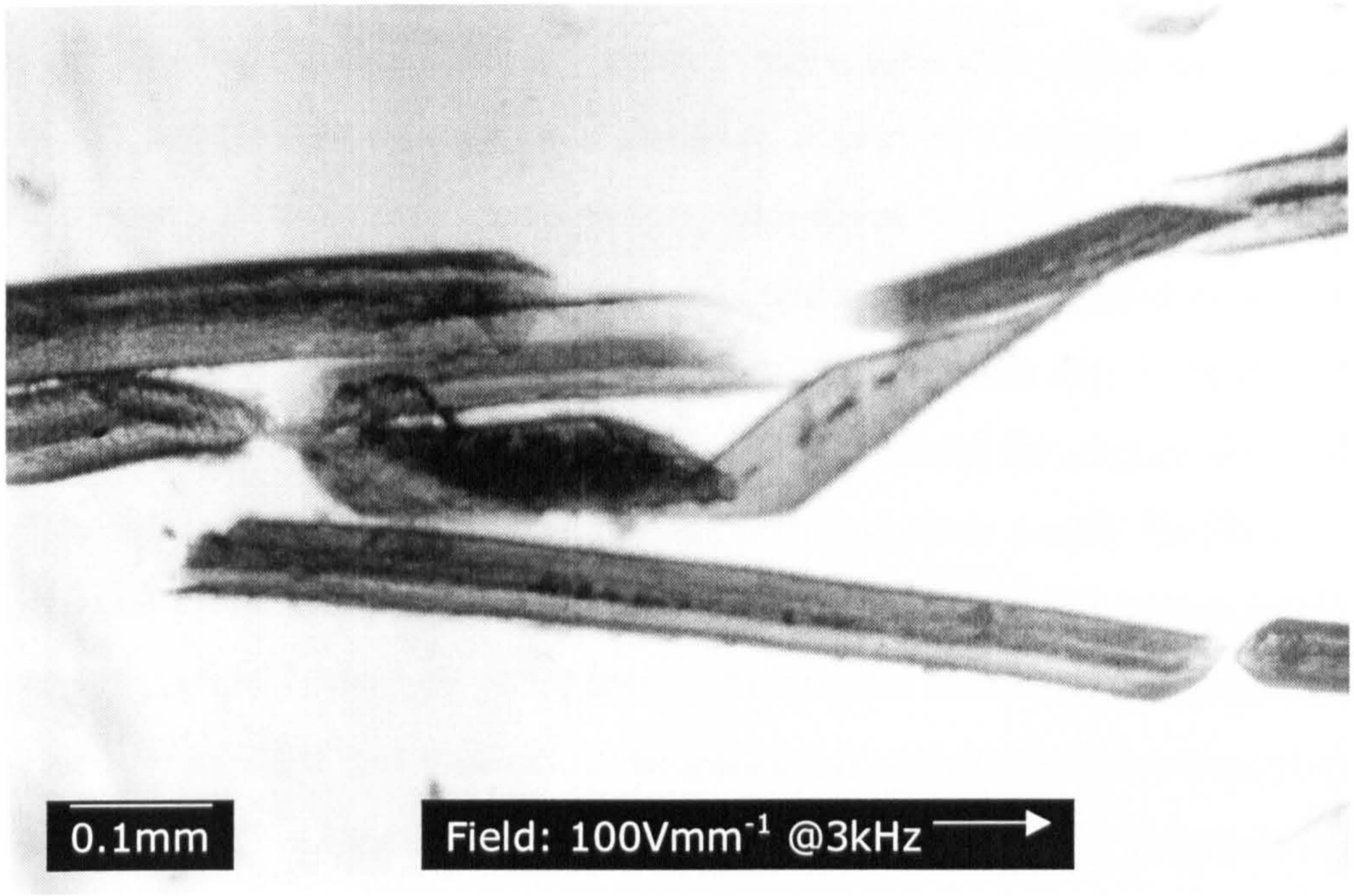

Figure 8.4: Natural fibres in silicone oil oriented parallel to an applied field.

8.4 Visual observations regarding the influence of particle shape on electrically-determined structures.

The theoretical arguments introduced in the preceding sections deal exclusively with spherical particles. In practice, however, filler materials will normally exhibit variations in particle shape and an overall distribution of particle sizes. Whilst variations in the size and distribution of spherical particles could be accommodated, for example in an assessment of the initial electrically-induced forces acting on a suspension, the effect of particle shape is much less quantifiable. As previously noted, the particles themselves determine spatial variations in the applied field and therefore, particle geometry, particle orientation and surface irregularity are all factors which influence overall behaviour. Distortion of the electrical double layer and free movement of charged species are further considerations and, at present, no mathematical treatment exists which can accommodate all of these variables. Nevertheless, some useful generalisations regarding particle shape can be made from direct visual observations.

Fibres and platelets: Figure 8.4 demonstrates the general rule that in positive dielectrophoresis high aspect ratio particles align with their major axes parallel to the applied field. In the photograph a close-up of part of a column of fibres is shown. There is some evidence of close-packing of individual fibres. It should also be noted that, in order to align, a randomly oriented fibre must have the freedom to rotate about its major axis. The 'swept volume' required to accomplish this is much greater than that of the individual fibre. To avoid entanglement, where the aligned microstructure is precluded, both the volume fraction of fibres and their length distribution must be controlled. Bowen et al [33] showed that PZT fibres could be aligned in a polyurethane matrix. Park and Robertson [103] reported that glass fibres oriented sluggishly parallel to the applied field and this would be consistent with their low polarizability. In all cases, the initial orientation of a fibre in relation to the field is a consideration, as this will affect the magnitude and the distribution of the induced polarization and hence the time-scale and the final pattern of the overall structure.

The same authors showed that mica platelets aligned with their major axes parallel to the field. There was no tendency for the linear strings so-formed to aggregate into full chains or into larger, columnar structures. This observation could be explained by an increased drag or stiffness that a string of platelets should exhibit when compared with a string of spherical particles. A further possibility may be more efficient screening of the induced dipoles by surface charge. Even though the fibres and platelets had a similar aspect ratio of around 60:1 the platelets were seen to respond far more rapidly to the field. Whilst the higher dielectric constant (and hence higher polarizability) of the mica was noted, it was also suggested that the geometry of the platelets may serve to reduce friction in some rotational modes. Miller and Jones [104] have carried out an analysis of the torque components due to the dielectrophoresis force for ellipsoidal particles and their frequency dependence. They have shown that alignment parallel to the field and also perpendicular to the field are both possible. Again the polarizability parameter is the principal controlling factor.

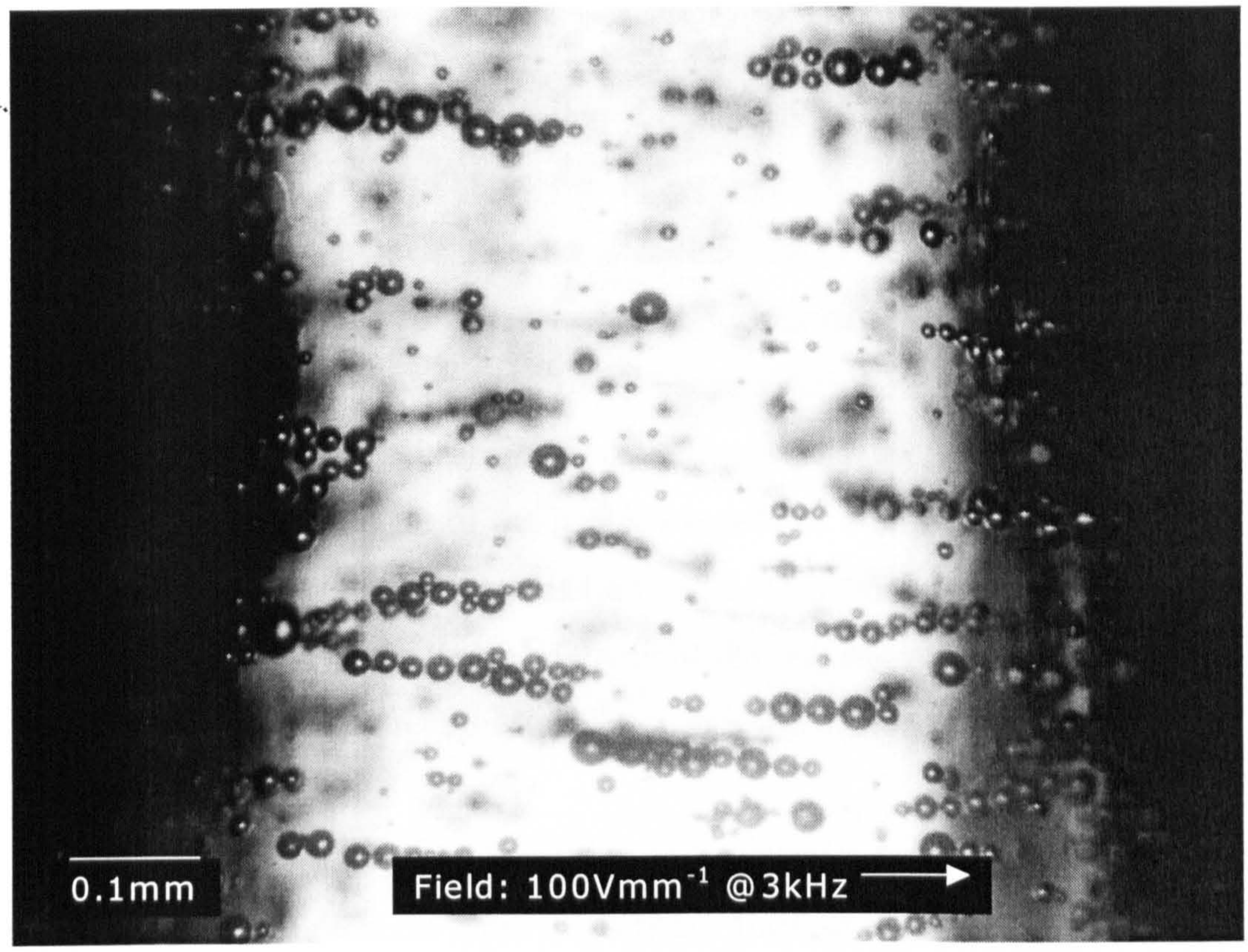

Figure 8.5: Field-induced strings of glass microballoons in silicone oil.

Glass microballoons: Figure 8.5 shows field-induced strings of glass microballoons in silicone oil. These formed slowly and there was no observed tendency for the strings to join into full chains.

Carbon black: As expected carbon black readily forms chains, at low field, in a curing epoxy resin. Where the applied field is too high then strings of carbon black aggregate into spherical clusters, these in turn aggregate into thick columns, which can form a conducting pathway between the electrodes. The tendency towards irreversible flocculation is thought to be due to van der Waals attractive forces at small particle separations and it may be avoidable by altering the chemistry of the suspension. When an ionic salt (CuCl) was added to the fluid, agglomeration was observed, but chaining did not occur. The ability to produce uniaxial conductors at low cost is technologically desirable and this topic would merit further study.

Bubbles: The behaviour of bubbles in an electric field has been studied extensively by Garton and Krasucki amongst others, who had identified them as a contributing factor to dielectric breakdown in insulating fluids such as transformer oils [105]. They concluded that the shape of bubbles in an applied field was a function of the mismatch in permittivities of the fluids. For the case where the permittivity of the bubble exceeds that of the ambient fluid by a factor of 20 and for conducting bubbles, then the bubble adopts an elongated 'prolate spheroidal' shape which lengthens with increasing field strength. Such a bubble has critical dimensions (and hence there is a critical field strength). When the length of the bubble exceeds its width (measured in terms of its major and minor axes) by a factor of 1.85 to 2.5, then the bubble becomes unstable and turbulence ensues. Where the permittivity of the bubble is less than twenty times that of the fluid the elongation of the bubble can increase indefinitely.

Mixtures of two particle types: An interesting phenomenon occurs when using a suspension of two different types of particles. Each of the different particle types can be said to have its own polarizability 'signature' and, because of this, separation of the two species is observed. Chains form which are comprised of either one type or the other. This has been observed both with a mixture of carbon black and PZT in a curing epoxy resin and also with a mixture of PZT and glass microballoons. Separation of different types of micro-organisms by dielectrophoresis has been investigated [106] and the technique has also been used to separate a mixture of different sub-micron sized latex spheres [107]. Ramos et al. have produced a review which is aimed at understanding the forces in aqueous suspensions using microelectrode structures [97].

Ionic crystals: NaCl crystals align readily at low field in silicone oil. Mixed chains of water droplets and NaCl crystals are possible. In this event the water droplets rapidly vaporise between the crystals, probably due to Joule heating.

8.5 Columns and Chains

In order to distinguish the characteristic types of structure which can be adopted by polarized particles in suspension under different process conditions, the term '*chain*' will consistently be used to describe a line of single particles. Typical chains are shown in Figure 8.5 and where appropriate a distinction will be made between 'partial' chains, ie. chain segments such as those illustrated and 'full' chains which completely span the gap between the electrodes. The term '*column*' refers to a wider cylinder composed of an aggregate of particles such as that shown in Figure 8.6.

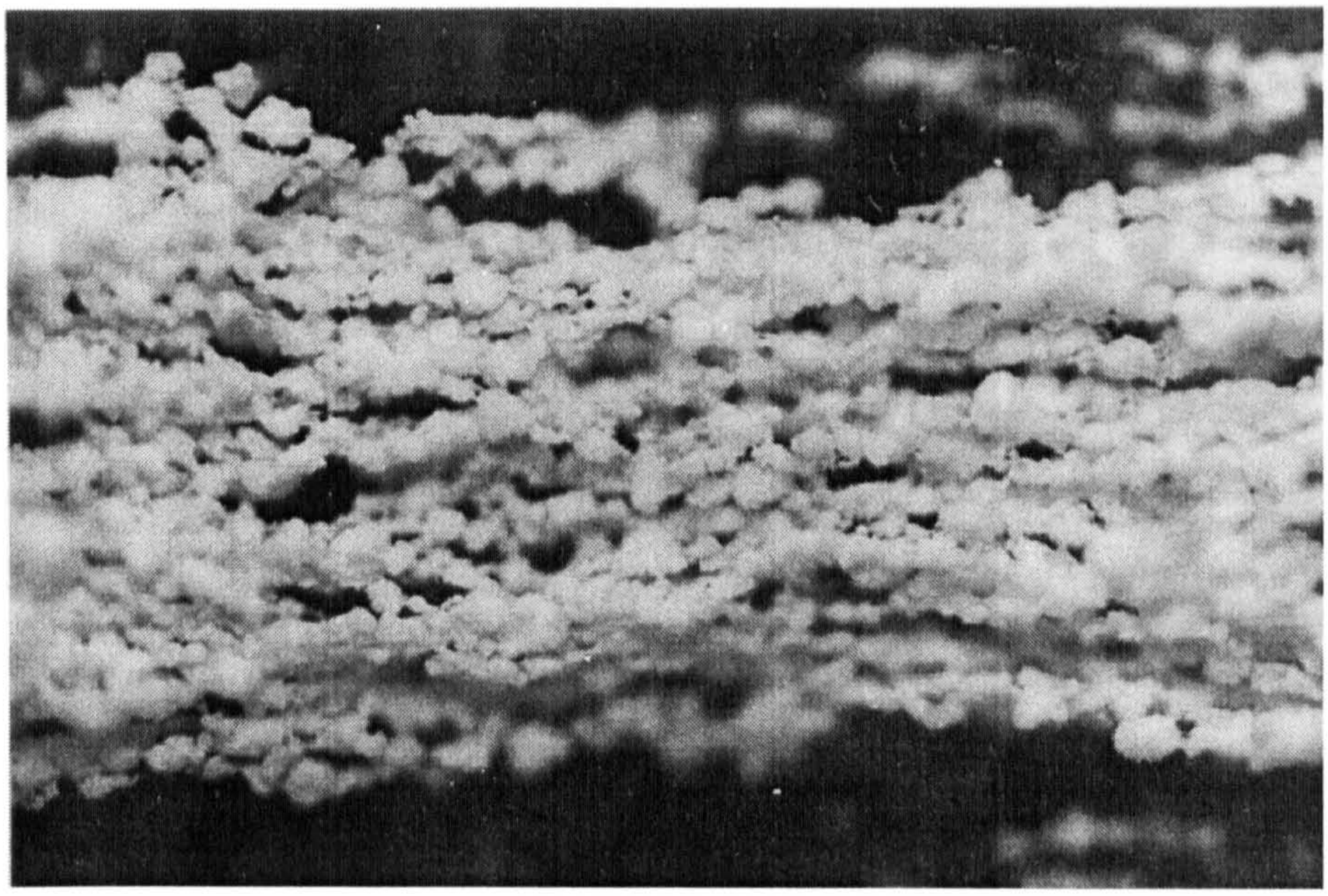

Figure 8.6: A 'column' of barium titanate particles in silicone oil (x25).

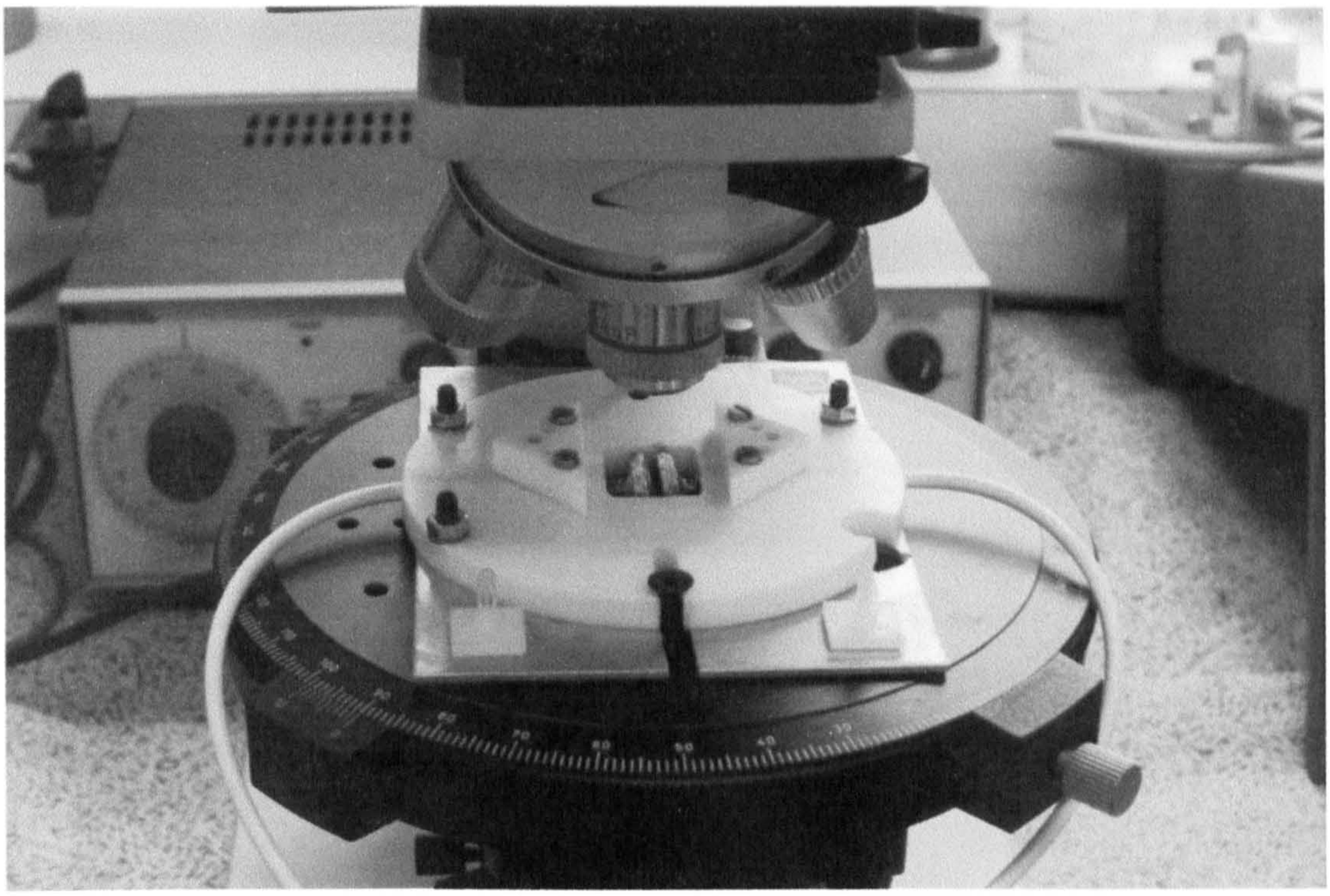

Figure 8.7: – Microscope attachment used for observation of low volume fraction suspensions under the influence of an electric field.

8.6 Direct Visual Observations of Field Structuring in Low Volume Fraction Suspensions of Lead Titanate in Epotek 302-3M Epoxy Resin.

An optical microscope was adapted to enable direct visual observation of the field-structuring effect. The arrangement is shown in Figure 8.7.

Low volume fraction suspensions (typically 2%) of pure lead titanate in Epotek 302-3M epoxy resin were introduced into the cell and an electric field was applied from a Trek 610C Power Amplifier in conjunction with a frequency generator. Field structuring was observed at different applied voltages / field strengths over a range of frequencies. This procedure was repeated at set time intervals as the resin cured at room temperature. The suspension was randomised by stirring between readings to ensure that it did not retain a 'history' of previous processing conditions. The electrically-induced structure of the suspension was conveniently described in terms of

the structure-types illustrated in Figure 8.8. Type I exhibits a weak dielectrophoretic force leading to a large number of randomly positioned short 'pearl-chains'. Type II consists of single strand chains which completely span the inter-electrode gap indicating a stronger dielectrophoretic attractive force. Some of these may be branched. Type III shows that chains have coalesced to form larger columnar structures.

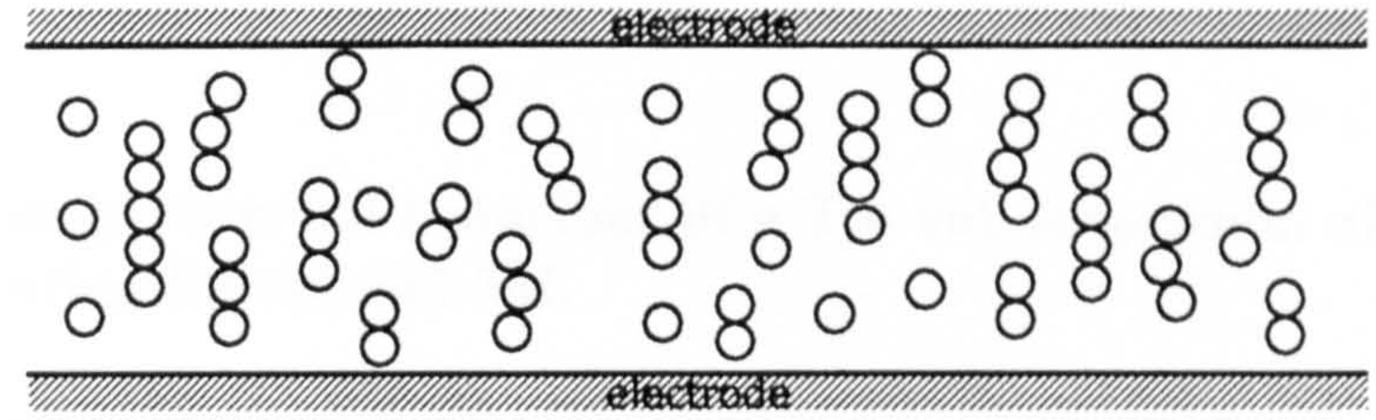

Type I) weak interaction of polarized particles - random chain fragments

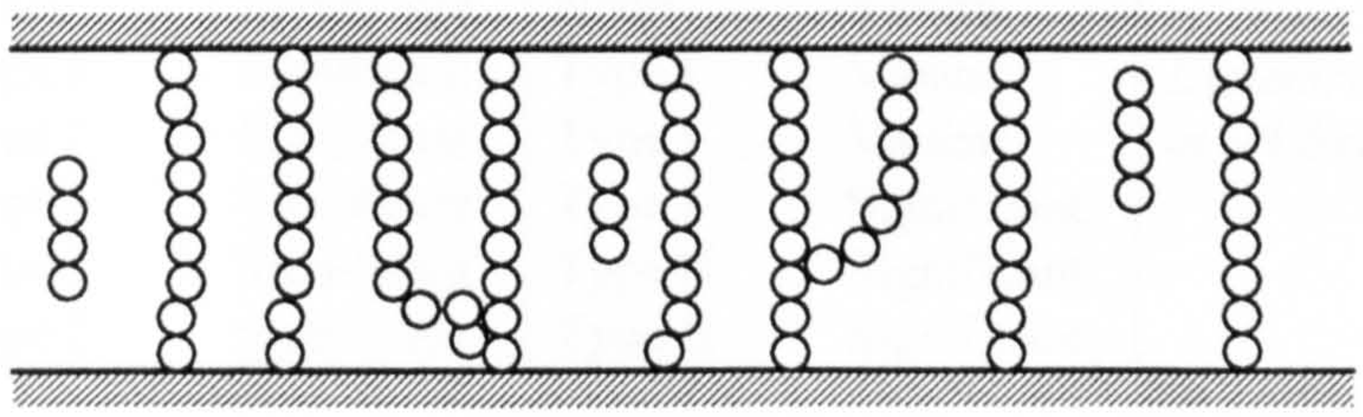

Type II) randomly located 'pearl chains'

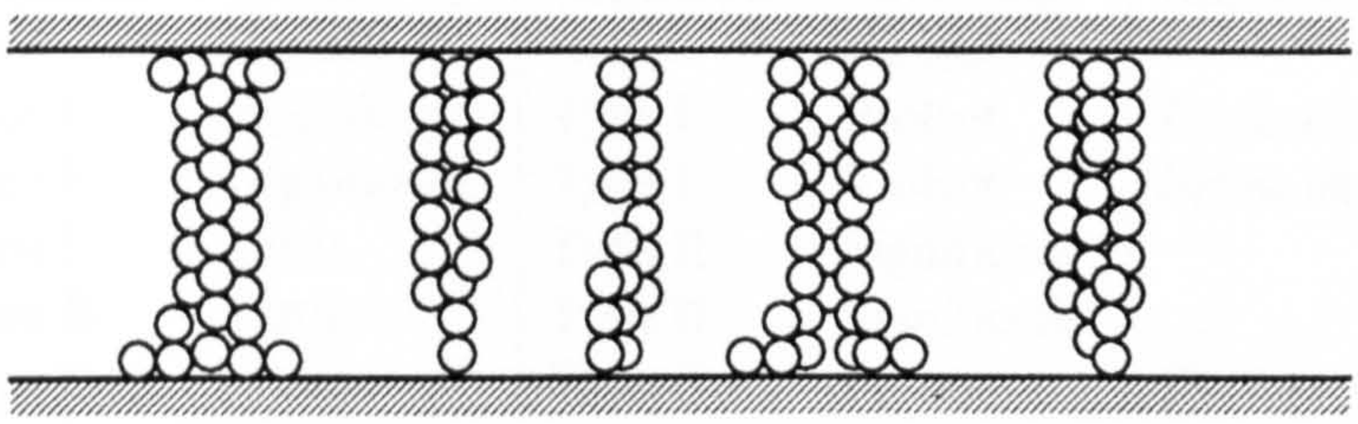

Type III) chains aggregate to form columns

Figure 8.8: Types of structure observed to form in low-volume fraction suspensions of lead titanate in a curing epoxy resin.

Table 8.1 shows the response of a 2% volume suspension of undried lead titanate in a curing epoxy resin (Epotek 302-3M). The resin was first degassed under vacuum at 50°C for 1 hour, the powder was added and the suspension degassed for a further 1 hour. The curing agent was added and thoroughly stirred before being introduced to the cell of the microscope attachment. Visual assessment was undertaken, at room temperature, 5 minutes after mixing and again after 30 minutes. The inter-electrode gap was 2mm. The experiment was subsequently repeated using dry lead titanate powder.

Table 8.1: Visually observed behaviour of a 2% vol. suspension of lead titanate (undried) in curing Epotek 302-3M.

a) - 5 minutes after mixing.

Frequency	Applied Field Strength (V/mm)					
	250		500		1000	
	Alignment	Streaming	Alignment	Streaming	Alignment	Streaming
100 Hz	None	Significant	None	Violent		
500 Hz	Type I	Significant	Type I	Violent	*Dielectric breakdown*	
1000 Hz	Type I	Significant	Type I	Violent	*at all frequencies*	
2000 Hz	Type I	Significant	Type I	Significant		
3000 Hz	Type I	Significant	Type II	Significant		
4000 Hz	Type I	Significant	Type II	Significant		

b) - 30 minutes after mixing.

Frequency	Applied Field Strength (V/mm)					
	250		500		1000	
	Alignment	Streaming	Alignment	Streaming	Alignment	Streaming
100 Hz	None	Significant	None	Violent		
500 Hz	Type I	Significant	Type I	Violent	*Dielectric breakdown*	
1000 Hz	Type I	Significant	Type I	Violent	*below 4kHz*	
2000 Hz	Type I	Little	Type II	Significant		
3000 Hz	Type II	Little	Type II	Significant		
4000 Hz	Type II	None	Type II	Little	Type I	Significant

At 250 V/mm the field strength is clearly sufficient for chains to form. Initially, at all frequencies, electrohydrodynamic flow of the fluid prevents full chains from forming. As time progresses (after 30 mins.) full chaining becomes possible at higher frequencies (≥3kHz).

At 500 V/mm fluid flow is initially violent. This is particularly the case at the lower frequencies, where turbulence prevents full chaining. At the higher frequencies full chaining starts to be observed despite significant fluid flow. After 30 minutes, fluid flow subsides at 4kHz and chaining readily occurs. After 40 minutes violent streaming returned at the higher frequencies, possibly due to exothermic heating; full chains formed rapidly and were immediately disrupted. After 1 hour under these conditions bubbles started to form in the resin and foaming ensued. The lead titanate particles clearly exhibited electrophoresis at lower frequencies.

At 1000 V/mm electrical breakdown occurred initially at all frequencies. Some evidence of chaining, at 4kHz, was observed after 30 minutes.

Table 8.2: Visually observed behaviour of a 2% vol. suspension of lead titanate (dried) in curing Epotek 302-3M.

a) 5 minutes after mixing.

Frequency	Field Strength (V/mm)					
	250		500		1000	
	Alignment	Streaming	Alignment	Streaming	Alignment	Streaming
100 Hz	Type I	Significant	None	Violent		
500 Hz	Type I	Significant	Type III	Significant		
1000 Hz	Type II	Little	Type III	Significant	*Discounted*	
2000 Hz	Type II	Little	Type III	Significant		
3000 Hz	Type II	Little	Type III	Little		
4000 Hz	Type II	Little	Type III	Little		

b) 30 minutes after mixing.

Frequency	Field Strength (V/mm)					
	250		500		1000	
	Alignment	Streaming	Alignment	Streaming	Alignment	Streaming
100 Hz	Type I	Significant	Type I	Significant		
500 Hz	Type I	Significant	Type II	Significant		
1000 Hz	Type II	Significant	Type II	Significant	*Discounted*	
2000 Hz	Type II	Little	Type III	Little		
3000 Hz	Type II	Little	Type III	Little		
4000 Hz	Type II	Little	Type III	Little		

c) 60 minutes after mixing.

Frequency	Field Strength (V/mm)					
	250		500		1000	
	Alignment	Streaming	Alignment	Streaming	Alignment	Streaming
100 Hz	Type I	Significant	Type I	Significant		
500 Hz	Type I	Significant	Type II	Significant		
1000 Hz	Type II	Little	Type II	Significant	*Discounted*	
2000 Hz	Type II	Little	Type III	Little		
3000 Hz	Type II	Little	Type III	Little		
4000 Hz	Type II	Little	Type III	Little		

Table 8.2 shows the same experiment repeated but this time using lead titanate powder which has been previously dried under vacuum for 2 hours at 75°C. Again chain formation is initially more favourable at the higher frequencies and, as time passes, at progressively lower frequencies. Overall, however, it can be seen that fluid flow is somewhat diminished and chains which form, as a consequence of polarization, are disrupted to a lesser extent. The presence of surface moisture would, therefore, be an important factor to consider when defining process parameters. It could be that the effect of drying is twofold. Clearly, by removing surface moisture the total number of charged ions is reduced. In addition, a number of reactive sites on the particle surfaces become available and ionic species may be adsorbed, thereby further reducing the number of free ions in the fluid. Note that for this experiment the highest field strength (1000V/mm) was omitted, by doing this, the possibility of contamination from the products of electrical breakdown was avoided. After 30 minutes a slight increase in fluid flow was observed at 1kHz and this might be explained by the observed increase in temperature due to the reaction exotherm.

8.7 Effect of applied field strength and field frequency on observed structure formation

The above observations, as expected, demonstrate the frequency dependence of electrohydrodynamic flow. They also give some insight into the amplitude of the applied field that will be required to produce a chained composite microstructure. They can be compared with the results of dielectric cure monitoring and a graph of the

frequency dependent dielectric loss for Epotek 302-3M curing at 20°C is shown as Figure 8.9.

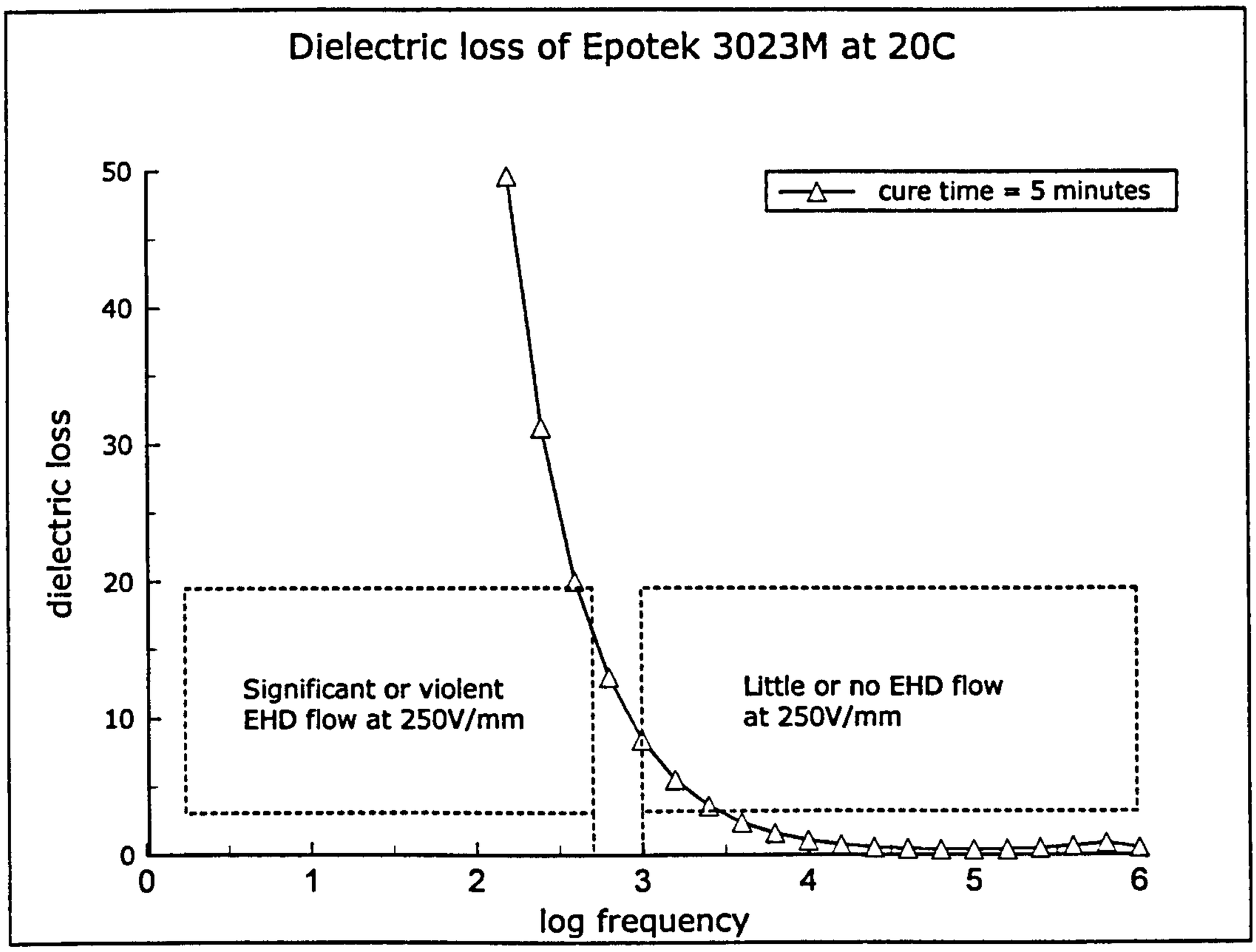

Figure 8.9: Initial dielectric loss of Epotek 302-3M epoxy resin at 20°C

From Table 8.2a) at 250V/mm there is a clear reduction in EHD flow which occurs between 0.5kHz and 1kHz. At 500V/mm, the same change is seen between 2kHz and 3kHz. The significance of this is apparent on the dielectric loss curve, as it corresponds to a range where, due to relaxation, the loss approaches its high frequency value. It has previously been demonstrated that initial dielectric loss is overwhelmingly dominated by the conduction term at these frequencies and in all probability we are seeing a conductivity-dominated effect. This is consistent with the observations that: i) the onset of streaming is at a higher frequency at the higher field strength and ii) that as time passes streaming occurs at progressively lower frequencies.

In order to define suitable field conditions for the assembly of composites it would be useful at this point to identify the field strength - frequency relationship, which highlights the onset of significant EHD flow. This could be related directly to measured conductivity and also to log (viscosity), which has been shown to mirror the extent of conversion of the reactants over the range in question. This model would then be extended to encompass a suitable range of temperatures. On the side of caution, there would be a question whether these parameters would accurately translate to higher volume fraction suspensions, where interfacial effects may assume greater prominence. Furthermore, there is an inherent danger that measurements made under low field conditions may not accurately reflect high-field behaviour. For the purposes of this study it can be said that suitable frequencies for composite assembly lie beyond the elbow in the dielectric loss curve. Further work would be needed to establish this with greater precision.

In the absence of EHD flow, visual observations show that full chaining occurs at 250V/mm. At 500V/mm columns form readily indicating a second threshold has been passed. The initial viscosity of the resin is 2.48Pas at 20°C.

A more complete data set is available for the resin and suspensions curing at 40°C and the results of cure monitoring are reproduced below as Figure 8.10. Figure 8.11 shows the changes that have occurred after 1 hour. Note that measurements relating to a suspension of 10% vol. lead titanate are little different from those of the resin alone. The effect of raising the temperature is twofold. Firstly, at a given field strength, a higher field frequency is required to suppress EHD flow because of increased charge mobility. However, the lower viscosity of the fluid will ensure that chaining is possible at lower field strengths. The initial viscosity of the resin is 1.13Pas at 40°C. This has significance because the viscous drag force scales linearly with viscosity, whereas the polarization force scales quadratically with applied field strength. Again, further work would be required to find where the applied field strength exceeds the threshold for chain formation and the corresponding field frequency at which EHD flow is suppressed.

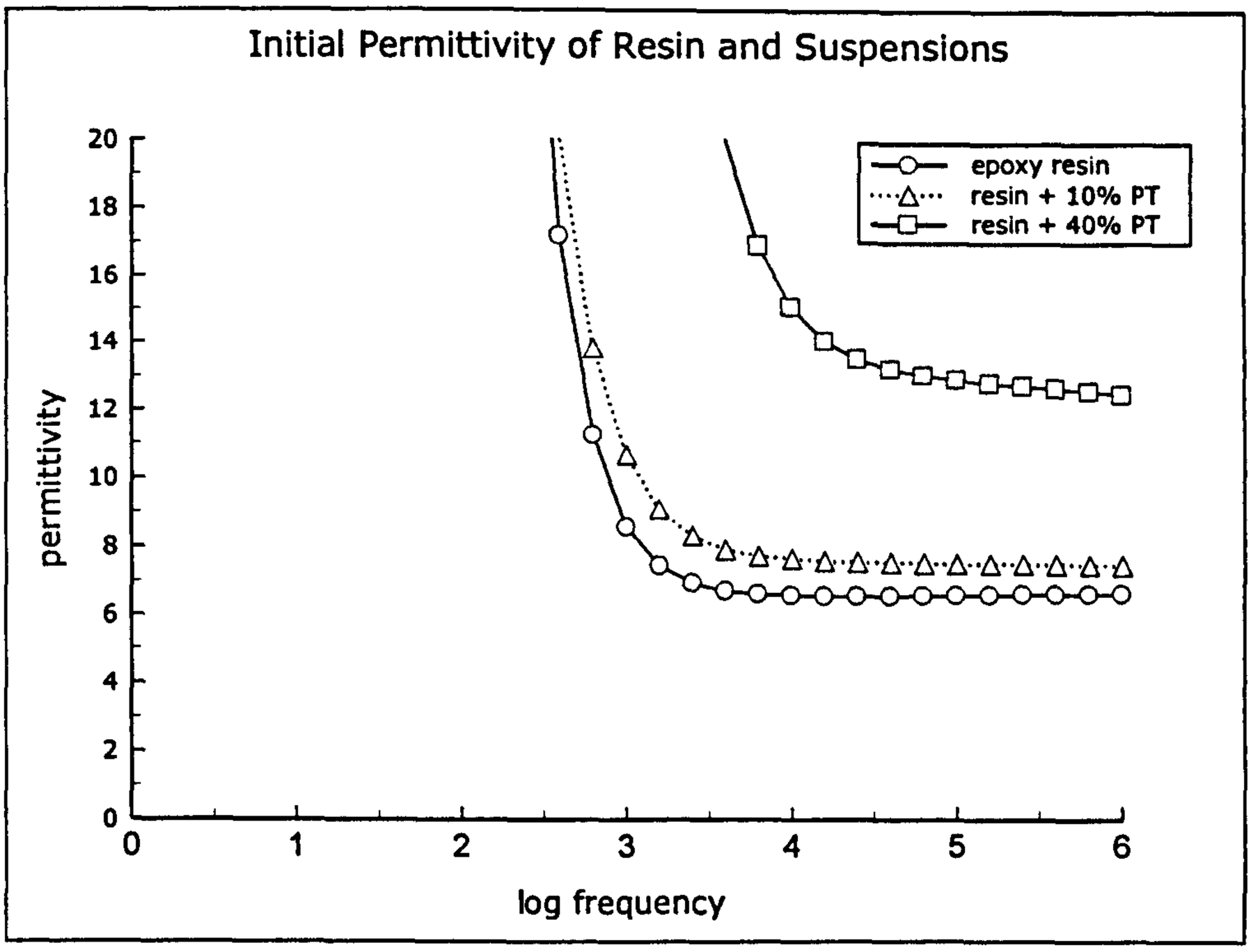

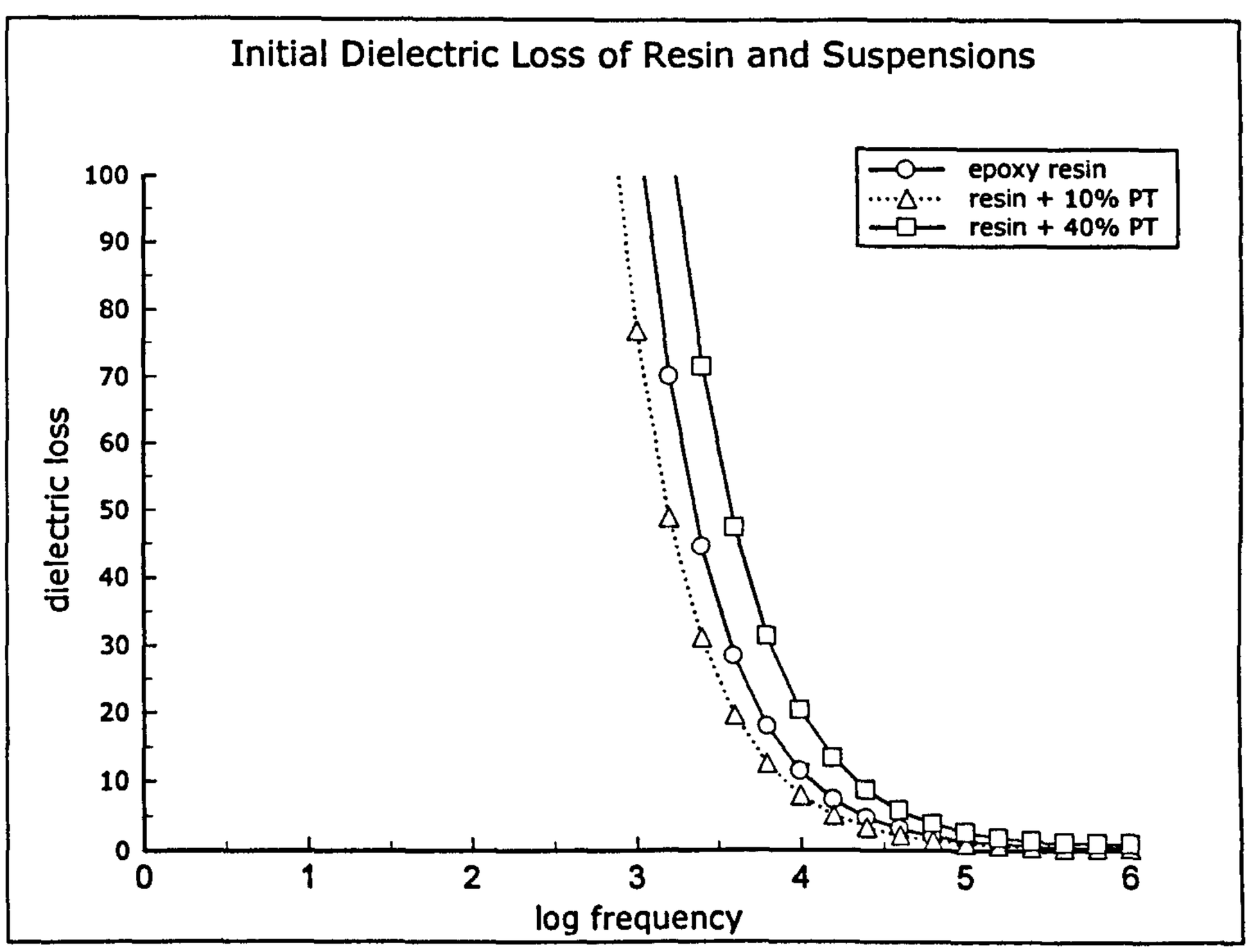

Figure 8.10: Dielectric cure monitoring of Epotek 302-3M epoxy resin and suspensions at 40°C

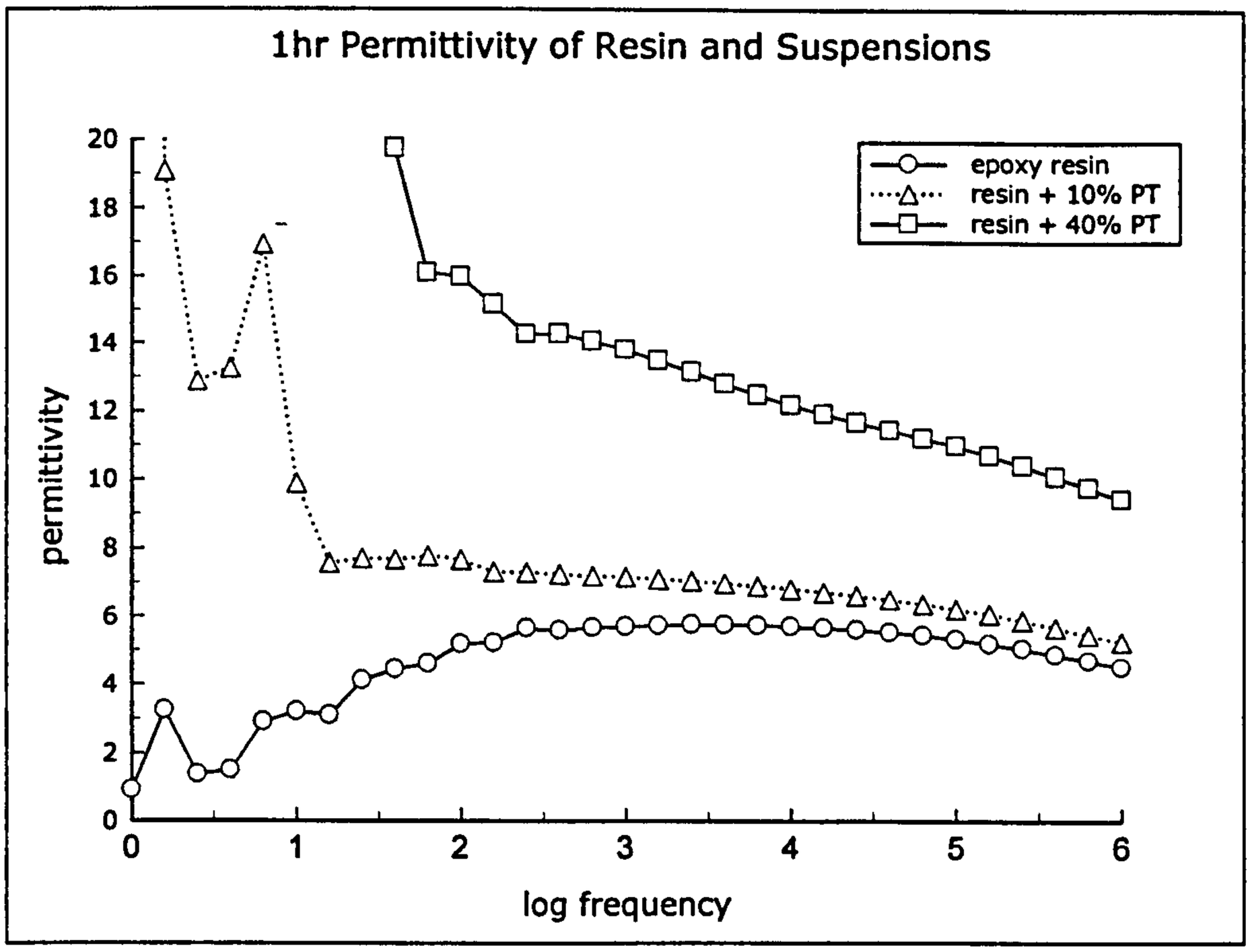

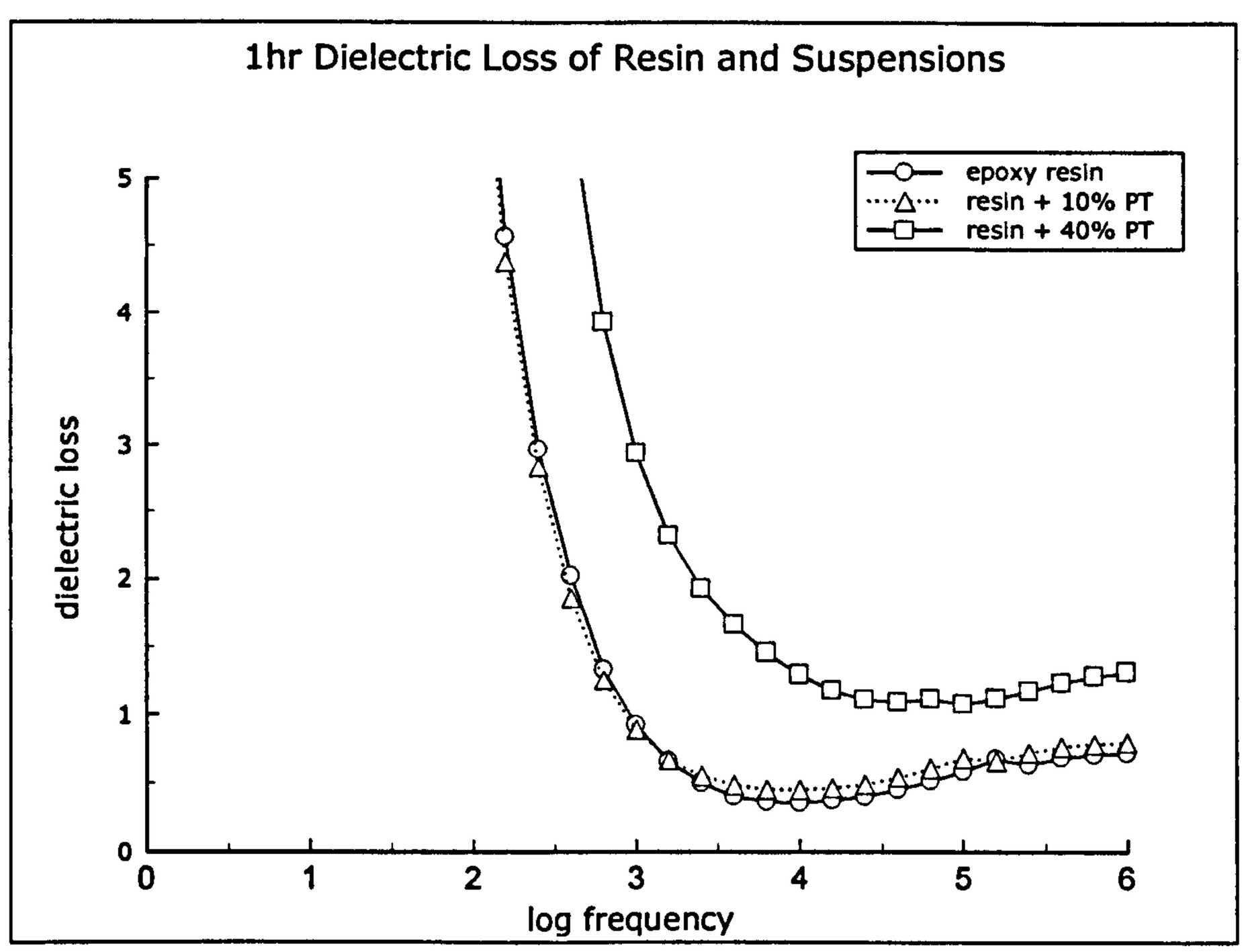

Figure 8.11: Dielectric cure monitoring of Epotek 302-3M epoxy resin and suspensions at 40°C

A further factor to consider in line with the above discussion is the frequency dependence of the polarizability parameter. Table 8.3a shows collected data and calculated values of the polarizability parameter in its complex form; it having a real part referred to as (Re [f (ε*)]) and an imaginary part (Im [f (ε*)]). The ideal, perfect dielectric, form of the polarizability parameter (β) is calculated for comparison. These values, over a range of frequencies, are calculated in Table 8.3b and plotted as Figure 8.12. The plot shows that the [Re f (ε*)] mirrors the form of the initial relative permittivity curve for the resin. The [Im f (ε*)] on the other hand mirrors the corresponding dielectric loss curve.

Interestingly, because (ε_p - ε_f) and (σ_p - σ_f) have opposite signs, the function (Re [f (ε*)]) passes through zero. This occurs at ≈1kHz and consequently the dielectrophoretic force is zero at this frequency. Below it the particles experience negative dielectrophoresis and above it positive dielectrophoresis. Given that the interparticle forces scale according to $(\beta)^2$, the point at which the traces of (Re [f (ε*)]) and (Im [f (ε*)]) cross may prove to mark a lower limit for composite assembly (2.5kHz).

This exercise has shown that, clearly, the ideal value of beta (β), quoted in some research papers, does not appear to be a true indicator of the dielectrophoretic force below c.10kHz.

Table 8.3a: Polarizability of a Dispersion of Lead Titanate in Epotek 302-3M curing at 40°C - Effect of Frequency

		@ 1kHz	@ 10kHz	@ 63kHz
Particle conductivity (σ_p)	S/m	10^{-11}	10^{-11}	10^{-11}
Fluid conductivity (σ_f)	S/m	6.11×10^{-6}	6.44×10^{-6}	7.09×10^{-6}
Particle permittivity (ε_p)	F/m	1.328×10^{-9}	1.328×10^{-9}	1.328×10^{-9}
Fluid permittivity (ε_f)	F/m	7.561×10^{-11}	5.808×10^{-11}	5.808×10^{-11}
Angular frequency (ϖ)	rad/s	6.2832×10^{3}	6.2832×10^{4}	3.9584×10^{5}
M-W time constant (τ)	s	1.211×10^{-4}	1.121×10^{-4}	1.018×10^{-4}
($\varpi^2 . \tau^2$)		0.579	49.61	1625.2
Polarizability ($\beta = \varepsilon_p - \varepsilon_f / \varepsilon_p + 2\varepsilon_f$)		0.8467	0.8794	0.8794
Re [f (ε^*)]		- 0.007	0.855	0.879
Im [f (ε^*)]		0.649	0.192	0.034

Table 8.3b: Calculated Initial Polarizability Parameter of a Dispersion of Lead Titanate in Epotek 302-3M curing at 40°C

log (frequency)	($\beta = \varepsilon_p - \varepsilon_f / \varepsilon_p + 2\varepsilon_f$)	Re [f(ε^*)]	Im [f(ε^*)]
3	0.847	-0.007	0.649
3.2	0.865	0.291	0.674
3.4	0.873	0.558	0.578
3.6	0.877	0.728	0.428
3.8	0.879	0.814	0.292
4	0.879	0.855	0.192
4.2	0.880	0.868	0.124
4.4	0.880	0.875	0.080
4.6	0.880	0.878	0.052
4.8	0.879	0.879	0.034
5	0.879	0.879	0.023

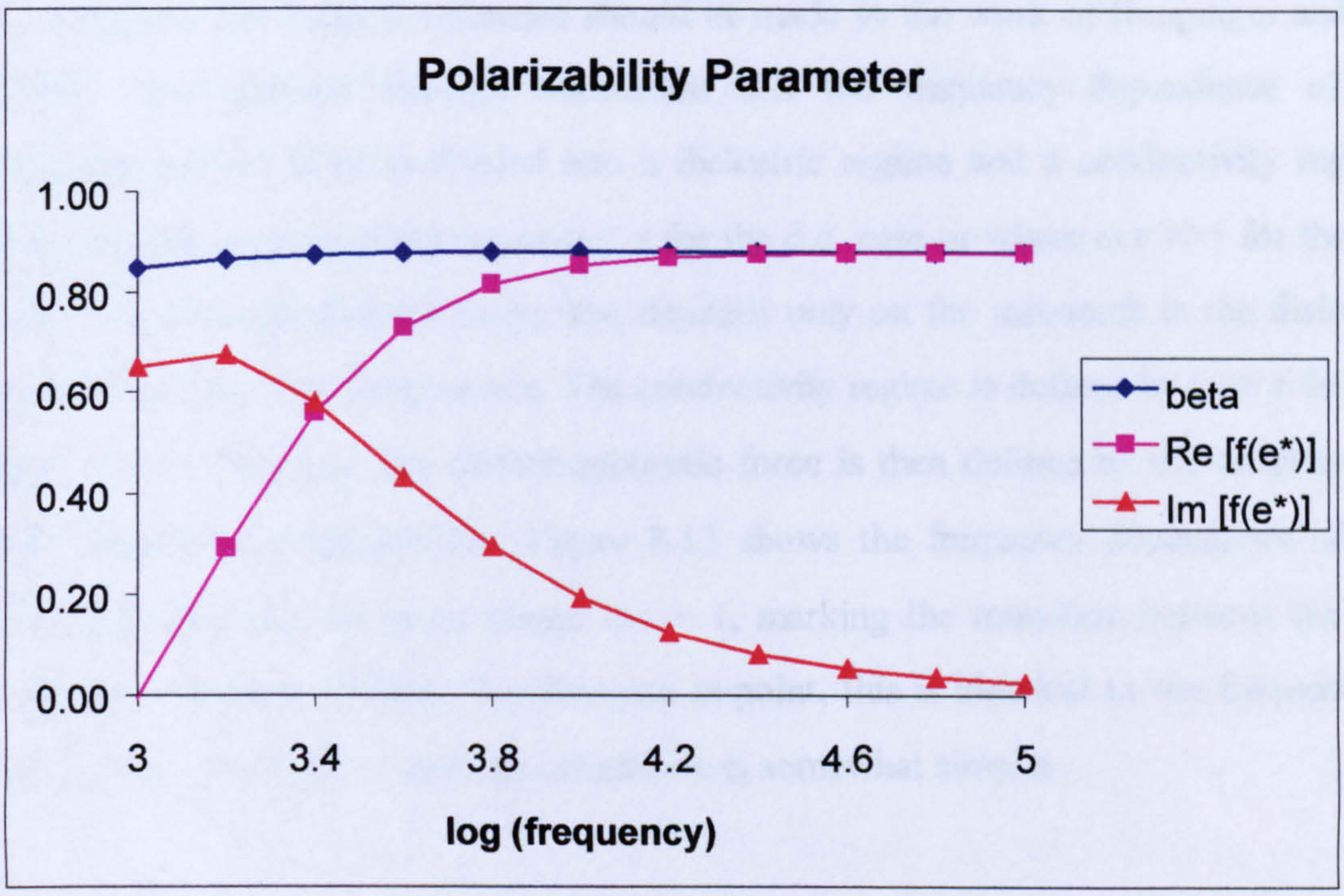

Figure 8.12: Initial Polarizability Parameter of a dispersion of Lead Titanate in Epotek 302-3M curing at 40°C

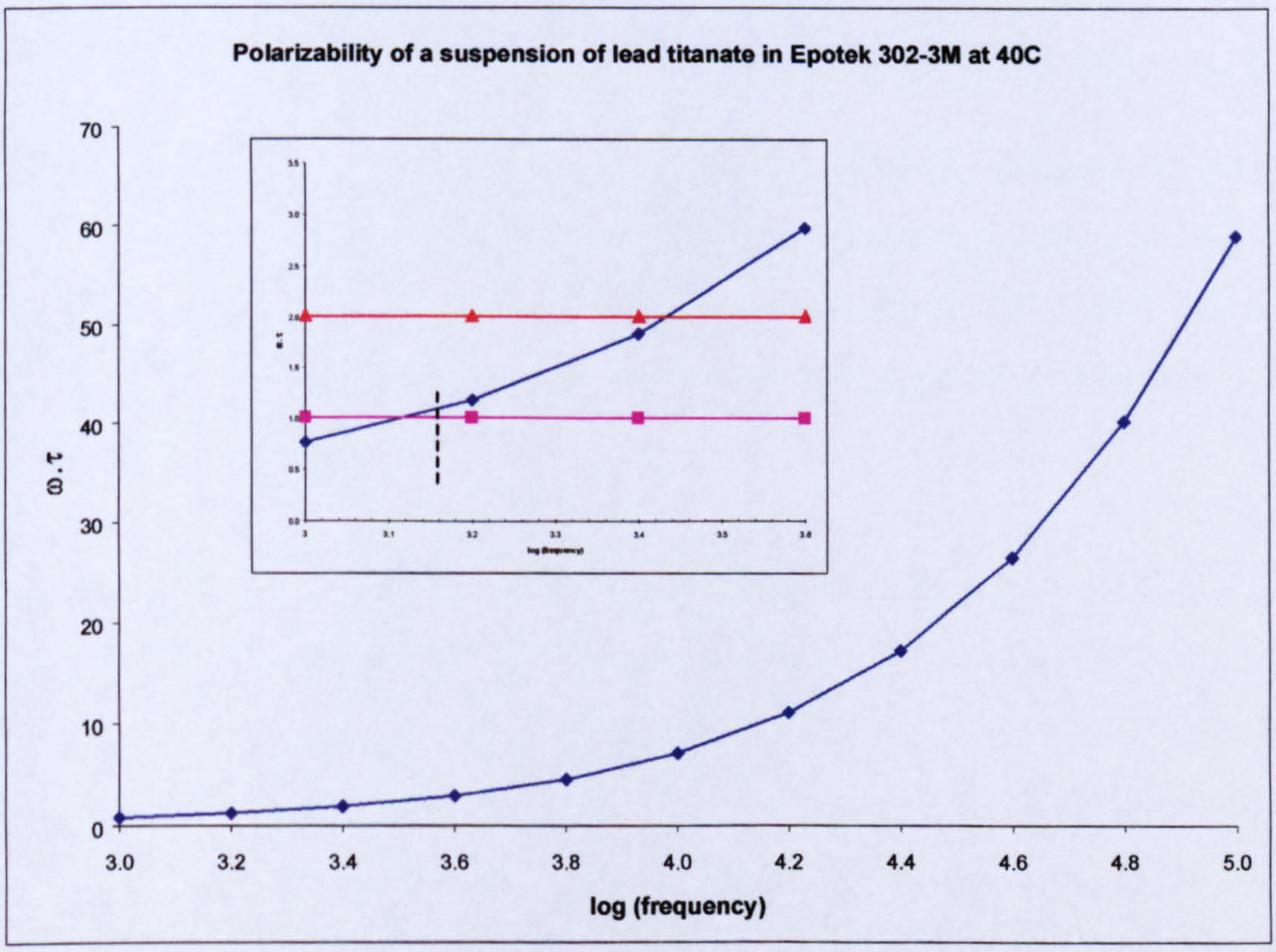

Figure 8.13: Polarizability of a dispersion of Lead Titanate in Epotek 302-3M curing at 40°C

To complete this section, reference should be made to the work of Benguigui and Lin [108]. They showed through calculation that the frequency dependence of the dielectrophoretic force is divided into a dielectric regime and a conductivity regime. The dielectric regime exists where $t << \tau$ for the d.c. case or where $\omega.\tau >> 1$ for the a.c. case. The dielectrophoretic force then depends only on the mismatch in the dielectric constants of the two components. The conductivity regime is defined by $t >> \tau$ for d.c. and $\omega.\tau << 1$ for a.c. The dielectrophoretic force is then defined by the difference in their respective conductivities. Figure 8.13 shows the frequency dependence of $\omega.\tau$ This indicates that the point where $\omega.\tau = 1$, marking the transition between the two regimes, occurs at 1290Hz. For the case in point, this is identical to the frequency at which $(\mathrm{Re}\,[\, f(\varepsilon^*)\,]) = 0$ and the calculation is somewhat simpler.

9. Processing of Structured Composite Materials

9.1 Definition of Processing Parameters

The preceding chapter has shown that, in order to form chains, there must be a net dielectrophoretic attraction between particles. A model of the process must include an assessment of the following: i) the induced dipolar or polarization force, which is a function of electric field strength and frequency; ii) the viscous drag force, which is time and temperature dependent; iii) sedimentation, which is again time and temperature dependent; iv) electrohydrodynamic forces, also a function of electric field strength and frequency; v) Brownian motion; vi) colloidal forces. From a materials' processing standpoint the first two of these can be said to be structure determining and the remainder are disruptive effects. Brownian motion is relatively small in comparison and can be ignored. Similarly, even though short-range colloidal forces may be overshadowed by the polarization force, the interfacial chemistry is an essential factor to be considered.

The basis of the technique is that an electric field is applied to a uniform dispersion of a filler material in a liquid pre-polymer. An electrically-determined structure forms and this is then fixed in place by gelation of the matrix. The chief processing variables, which must be defined are: a) time scale; b) temperature; c) electric field; d) electric field frequency.

For the matrix / filler combination under consideration, sedimentation is likely to be a limiting factor. The initial viscosity of the pre-polymer is 1.6 Pas at 25°C and falls to 0.97 Pas at 55°C. Under these conditions, the settling rates of a typical (8μm diameter) lead titanate particle, to a Stokes' Law approximation, are respectively 0.14 μm/s (at 25°C) and 0.25 μm/s (at 55°C). Given that the minimum total time required (handling time + early stages of cure) is of the order of 40minutes at 55°C and longer at 25°C, the conclusion is that sedimentation is indeed of major concern. A simple way of overcoming the problem is to cure the resin in stages. First the resin is allowed

to partially cure and then it is stirred once more to re-establish a uniform dispersion of particles. In this way a certain portion of the reactants are converted and, when a suitable cure temperature is adopted, viscosity cannot fall to its initial values. At 10 Pas it has been observed that the resin is still sufficiently fluid for chaining to occur. Previously gathered viscosity and dielectric cure monitoring data are used to outline a practical processing route. A step sequence of conditions was put down and this was subsequently refined by experiment.

The following conditions were used to process field structured composites:

1. Lead titanate powder was dried under vacuum for 16 hours at 80°C.
2. The powder was mixed with the resin and vacuum-degassed at 60°C for a minimum of 4 hours.
3. The curing agent was mechanically stirred into the resin under vacuum for 5 minutes at room temperature.
4. The mixture was allowed to stand at room temperature for 1 hour, then stirred again for 5 minutes under vacuum.
5. The mixture was transferred to a mould.
6. At a temperature of 35°C, an electric field of 250 V/mm at 3kHz was applied for 45 minutes.
7. The temperature was raised to 55°C, with the field applied, and held for 45 minutes to solidify the composite.
8. A post-cure of 1 hour at 120°C with the field applied could be performed to raise the T_g of the resin to 82°C. At 150°C the T_g of the resin rises to 96°C. Prior to post-curing an intermediate temperature of 80°C for 30 minutes might be applied as a precaution against electrical breakdown.

By way of an exercise, it is useful to estimate the polarization force acting on a typical lead titanate particle exposed to an applied voltage of 250 V/mm. For the condition where the interparticle separation is very much greater than the particle diameter, as

for example in a 2%vol. suspension, the polarization force is calculated as 1.45×10^{-11} N. In contrast, the weight of the submerged particle is 1.73×10^{-11} N. Similarly, the polarization force can be estimated for a range of interparticle separations (Table 9.1). The values chosen correspond to the mean interparticle spacing found in a range of typical, uniform particulate dispersions. Note that the estimation does not include a shape factor for the field intensification between particles and this is of most significance at separations of less than one particle diameter. The value of the exercise lies in its illustration of the general trend towards higher interparticle forces with decreasing separation.

Table 9.1 – Variation in the polarization force between particles.

Volume fraction of $PbTiO_3$ particles (%)	Mean interparticle spacing (μm)	Estimated interparticle polarization force (nN)
40	0.75	2950
20	3.03	1.11
10	5.90	0.72
5	9.50	0.12
2	15.75	0.014

9.2 Apparatus

To cover all aspects of composite materials assembly it was necessary to construct a processing unit (Figure 9.1). The design of this unit is such that it can: 1) emulate previous work which has been carried out in dielectrophoretic assembly and 2) act as a prototype production unit for the range of materials currently foreseen. In brief, the unit consists of an insulated cell with two copper electrodes. A voltage can be applied to either of these independently, up to a maximum of 8kV. The gap between the electrodes is variable to enable a range of sample thicknesses to be produced. A resistance network is use to limit the current drawn from the supply. A control unit is incorporated which can deliver: 1) d.c.; 2) pulsed d.c. with pulse times ranging from 0.2s to 12s; 3) a precise a.c. square wave at any frequency up to 1.5kHz. At 2.5kHz attenuation is 1.6%. A d.c. bias can be applied to an alternating field. The cell is temperature controlled by means of an air process-heater, to provide in-situ curing of

under a microscope. Electrical diagrams for the processing unit are included in Appendix B. A photograph of the processing chamber is shown as Figure 9.2 and a schematic of the cell as Figure 9.3. A Trek 610C high voltage amplifier, in conjunction with a frequency generator (Thurlby Thandar TG501) was also available to generate the required field.

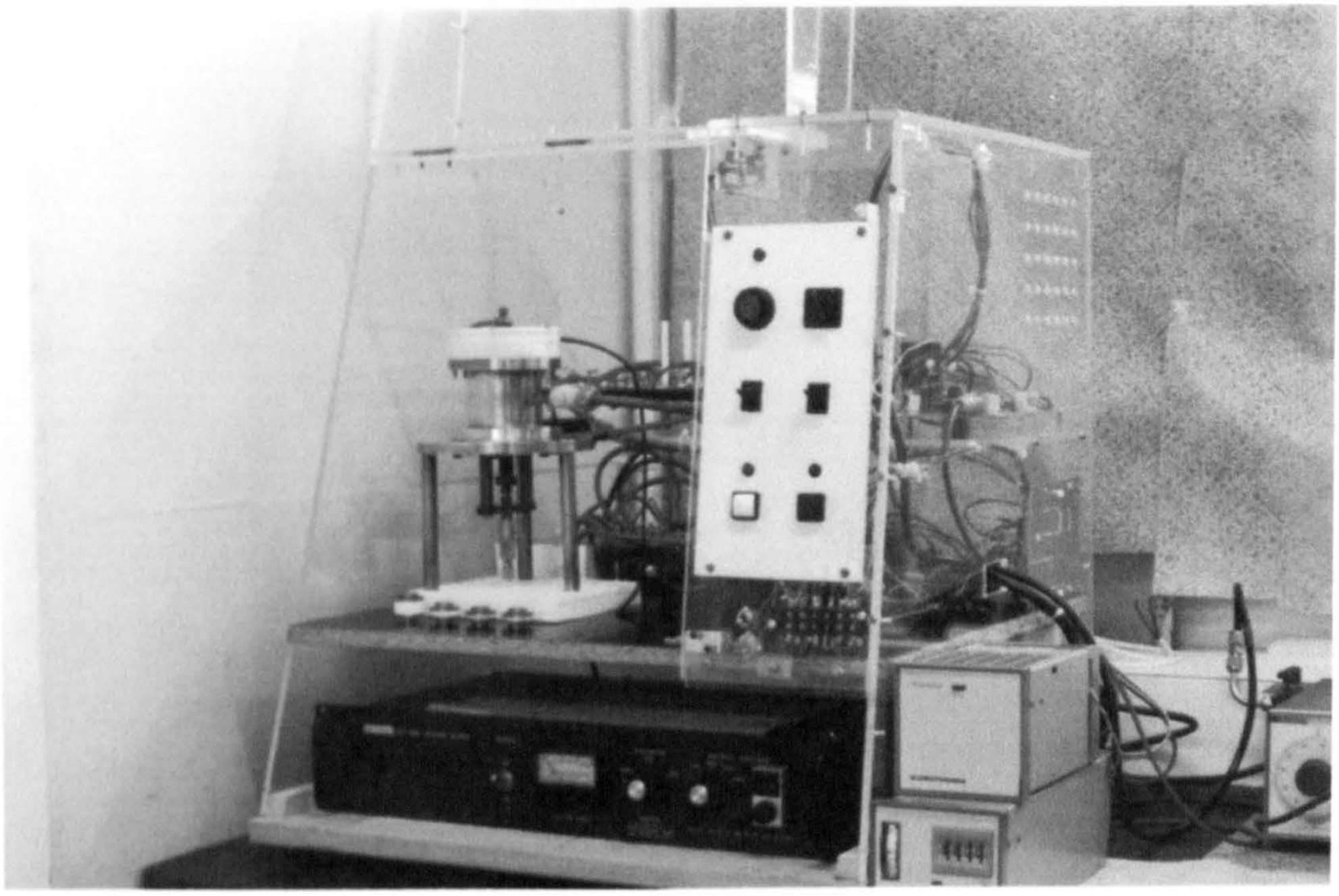

Figure 9.1: Structured composites processing unit.

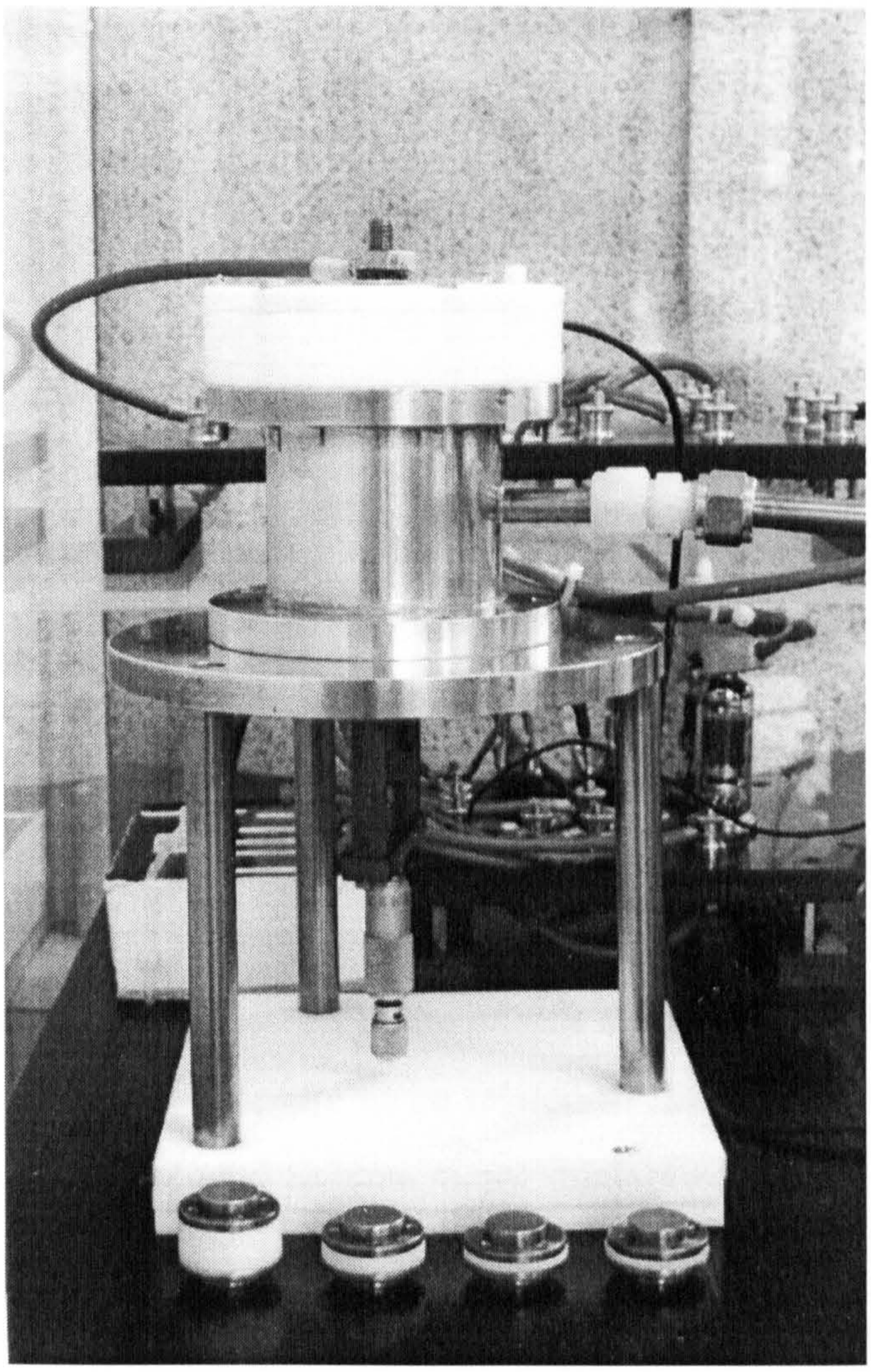

Figure 9.2: Insulated chamber for composite assembly.

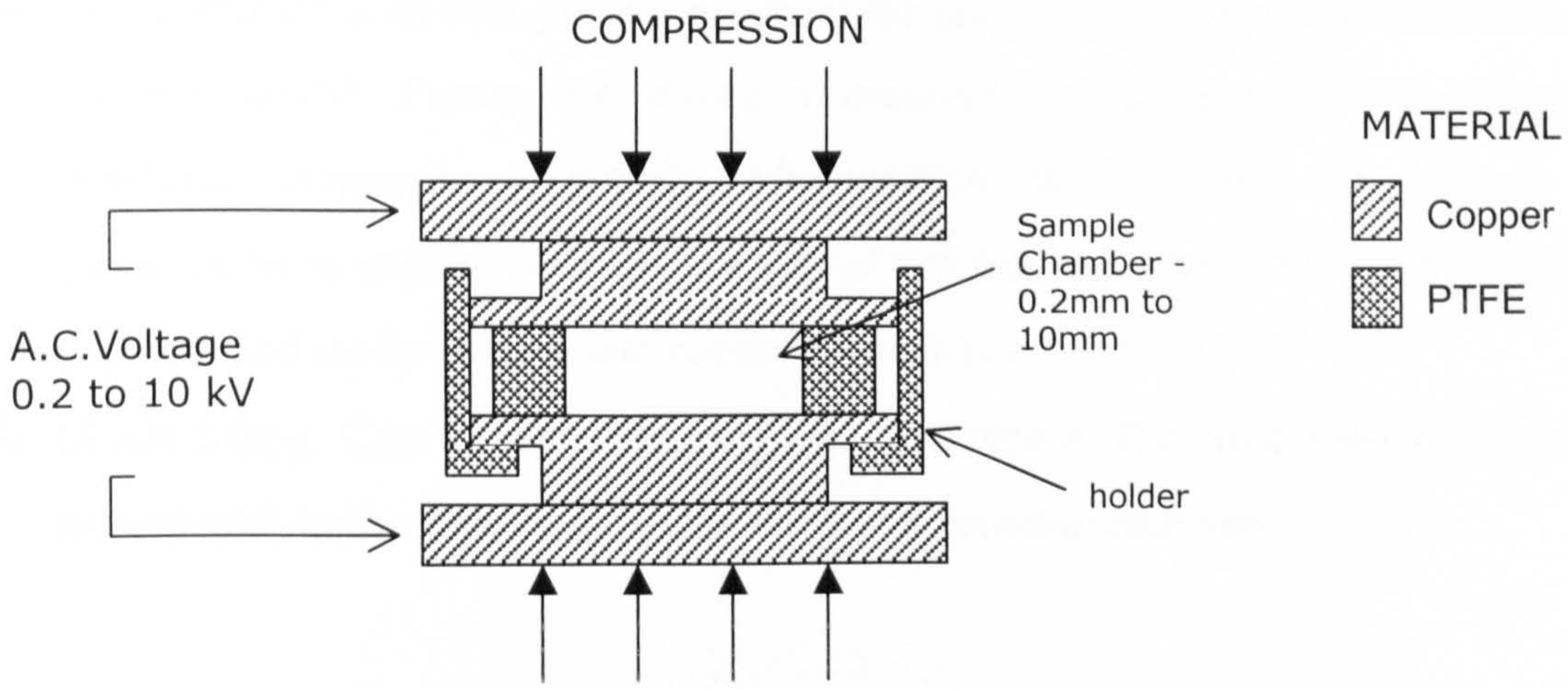

Figure 9.3: Schematic of a cell used for composite assembly.

9.3 Composite Materials Assembly – Practical

1) Degassing the resin. The minimum temperature at which this is effective is 60°C. Periods of upwards of 1 hour are required.
2) Mould release agents. A number of commercial release agents were shown to be effective. Two applications of Freekote were used on the electrodes for most of the samples prepared in this study.
3) Seals. Careful sealing of the mould is needed to prevent seepage of the resin. Cyanoacrylate adhesive proved to be effective.
4) Removal of the cured samples from the mould. A few minutes in the freezer compartment of a refrigerator was effective.
5) Gas pockets in the finished samples. Despite the precautions of thorough drying, degassing and stirring under vacuum, bubbles formed regularly. This may have been due to air being sucked into the mould as the resin shrinks or alternatively due to ionisation of the reactants in the intense electric field between particles. The distribution of porosity appears to be related to the volume fraction of ceramic. High volume fractions tend to have many small pores distributed throughout the sample. Lower volume fractions sometimes have one large gas pocket or void. If a void forms adjacent to an electrode then contact will be lost. An improved mould design would include the facility to cure the resin under pressure and to allow gas to diffuse away.
6) Sedimentation is an ever-present danger if the prescribed sequence of operations is not maintained. Figure 9.4 shows a cross-section of a lead titanate/epoxy structured composite in which sedimentation has occurred. A gradient in composition is evident between the top of the sample, where the chain-ends are exposed, and the bottom, where excess ceramic has collected.
7) Mould filling. Care is needed to avoid air entrapment. The fluid must make good contact with both electrodes. Excess resin is a potential problem.

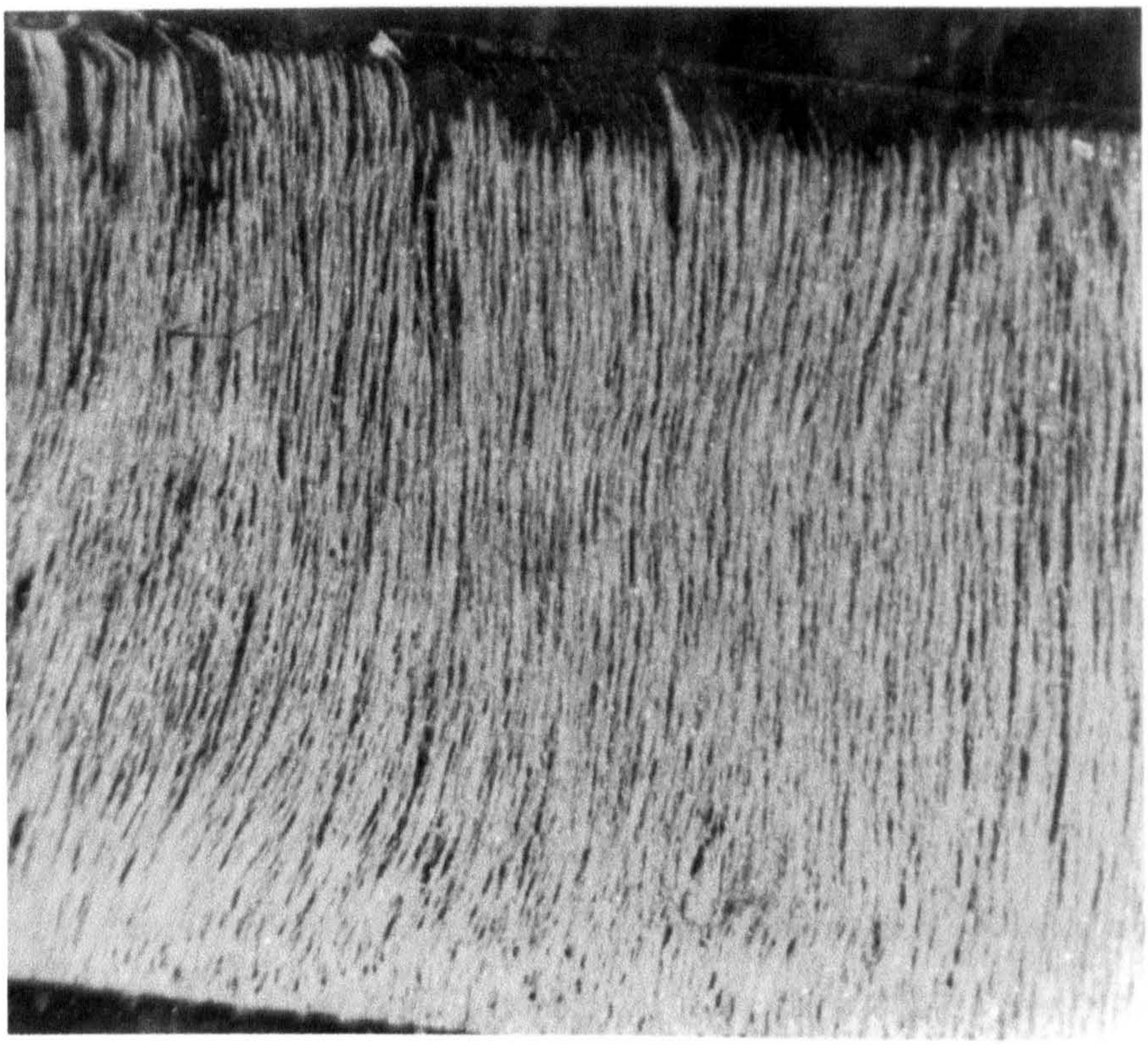

Figure 9.4: Sedimentation in a structured lead titanate / epoxy composite – particles have accumulated at the bottom of this section and the chains do not reach to the upper surface.

10 Properties of Field-Structured Composite Materials

10.1 Sample Preparation

Composites were prepared according to the exact method outlined in the previous chapter. A dispersion of known ceramic volume fraction was made up for each sample. This was divided into two identical parts. Whilst one portion was processed by field-structuring, the other was simultaneously put through an identical thermal cycle but with no field applied. After curing, a layer of material adjacent to each electrode was skimmed off to a depth of 250μm as a precaution against a build-up of impurities in that area. The density of each sample was measured by the Archimedes method and the volume fraction of the ceramic was calculated. This step was felt necessary to ensure that sedimentation had not caused the actual composition to drift away from its nominal value during handling. The composites were sectioned, using an annular saw (or diamond saw), both perpendicular and parallel to the applied field. Similar sections were made from the unstructured composites. The specimens were electroded with air-drying silver paint. A 1mm perimeter, around the edge of each specimen, was left exposed. The object of this was to minimise the effect of the fringing field when dielectric measurements were made. Dielectric measurements were made using an RLC bridge (GenRad 1689M Digibridge). Selected samples were poled and their piezoelectric properties were measured. Transmission light microscopy was used to reveal the chained microstructure in low volume fraction composites. A typical structured composite is shown in. Figure 10.1.

Preparation for microscopy is as follows: 1) A 1mm section is cut using a diamond saw. 2) This is potted in Buehler 'epo-thin' resin, which cures at room temperature in 24 hours. The resin provides mechanical strength when polishing. 3) The potted sample is hot-waxed to a microscope slide and both are hot-waxed to a glass block. 4) Excess resin is removed and the sample is polished down to a finish using 1μm diamond paste. The sample thickness is reduced in this process by the minimum amount possible. Samples that are too thin could distort. 5) The sample is turned and

the polished surface is glued to a microscope slide using an optically clear epoxy resin. 6) It can then be ground down to <100μm thickness and a suitable surface finish prepared. Hence the distribution of ceramic particles in the resin can be made visible by transmission light microscopy.

10.2 Dielectric Properties

Representative specimens were made from the structured samples both perpendicular and parallel to the applied field. These were compared with specimens, having the same dimensions, taken from unstructured composites. Dielectric measurements of capacitance and tan δ, the average of 20 readings, were made using the GenRad 1689M Digibridge (Appendix C). Values of relative permittivity (ε_r') were calculated, over the frequency range 0.5 - 100kHz, according to the standard relationship:

$$\varepsilon_r' = \frac{C_p . t}{A . \varepsilon_o}$$

where (C_p) is the measured capacitance, (A) is the electroded area, (t) the sample thickness and (ε_o) is the permittivity of free space (8.85 pFm^{-1}).

Dielectric loss (ε_r'') is calculated as :

$$\varepsilon_r'' = \tan\delta . \varepsilon_r'$$

When taking dielectric measurements it was frequently observed that the reading drifted over a period of time. In all cases the reading was allowed to stabilise before being recorded. This observation can be attributed to an absorption current. Herbert [109] identifies two possible causes: a) the movement of low-mobility defects such as protons and vacancies which drift from their equilibrium positions at low frequencies; impurities in the resin are known to accumulate at the ceramic / polymer interface and are the source of defects in the polymer network; b) the formation of barrier layers at the dielectric-electrode interface or at the ceramic / polymer interface. So-called

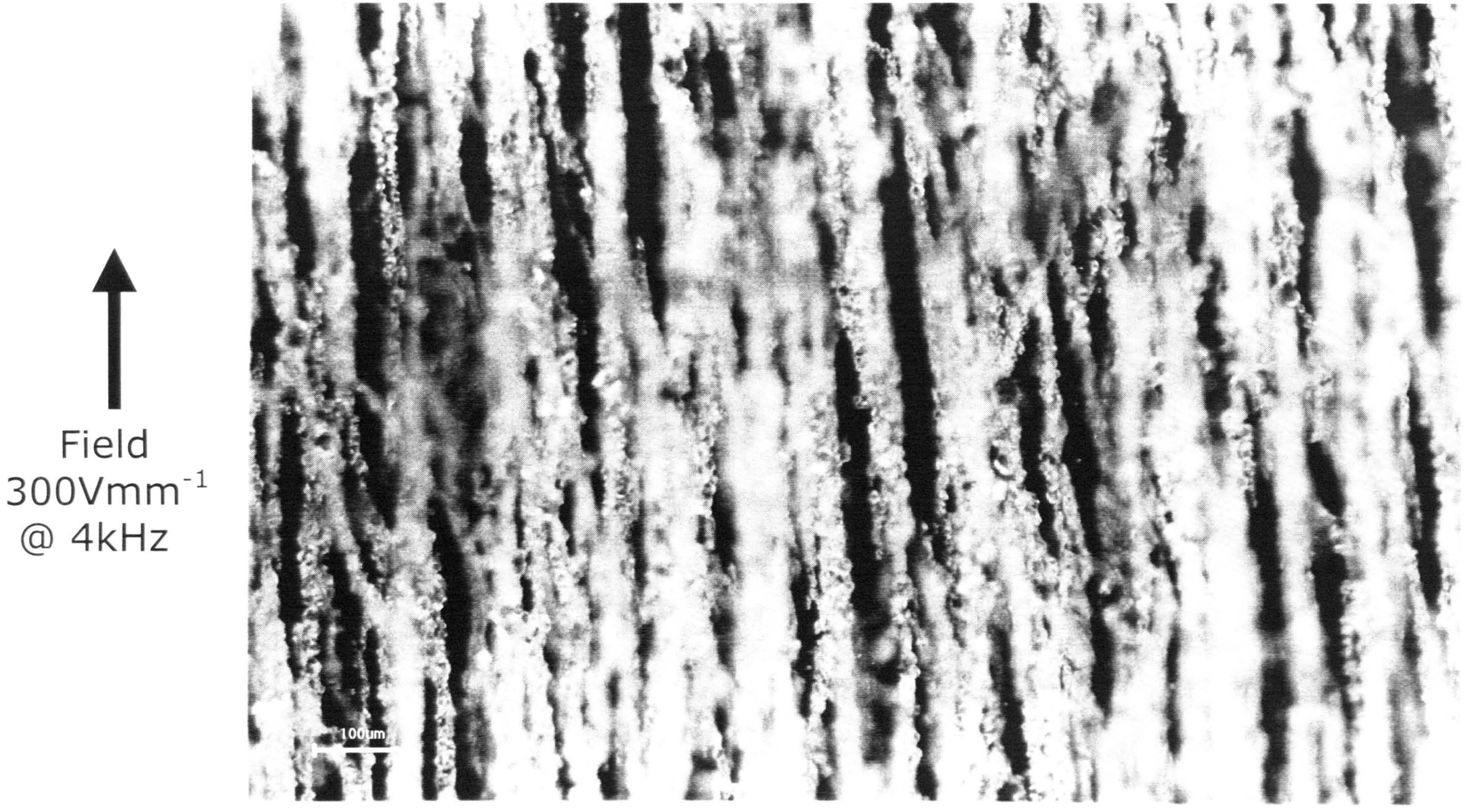

Figure 10.1 – 'Pearl chains' in a field-structured 10% vol. lead titanate / epoxy composite.

'blocking' electrodes are due to the formation of Schottky barriers, whereby electrons flow out from the dielectric to the electrode leaving a high capacitance depletion layer. Schottky barriers are of prime importance in thin films and high frequency applications. In this case, it is the nature of the electrode material (silver paint) to form blocking contacts as it forms a complex interface with the ceramic. The build-up and control of localised 'space-charges' in field-structured composites would merit further study. A range of space charge measurement techniques is presented by Ahmed and Srinivas in their review [110].

Measured values (GenRad Digibridge 1689) for the sample illustrated in Figure 10.1, 10% vol. lead titanate in Epotek 302-3M, are shown in Table 10.1. Clearly the field-structuring technique has lead to a significant increase in the dielectric permittivity due to a redistribution of the phases. Dielectric loss is also much higher parallel to the chain direction. The estimated accuracy is ±1%.

In the same way a range of composites having ceramic volume fractions of 10%, 20%, 30% and 40% was prepared and tested. Dielectric properties are shown in Figures 10.2 – 10.3. The properties of a 30% vol. composite are shown in Figures 10.4 – 10.5.

Table 10.1: Measured dielectric properties of structured and unstructured 10% vol. lead titanate / Epotek 302-3M epoxy resin composites.

Frequency (kHz)	Relative permittivity (ε_r')			Dielectric loss (ε_r'')		
	Structured ‖ to field	Structured ⊥ to field	Unstructured	Structured ‖ to field	Structured ⊥ to field	Unstructured
0.5	7.57	4.80	4.61	0.10	0.03	0.08
1	7.50	4.74	4.52	0.11	0.04	0.03
2	7.45	4.71	4.48	0.14	0.06	0.05
5	7.36	4.64	4.42	0.18	0.09	0.07
10	7.28	4.58	4.39	0.22	0.10	0.08
20	7.16	4.52	4.34	0.28	0.10	0.12
50	6.90	4.34	4.07	0.34	0.12	0.15
100	6.78	4.33	4.09	0.37	0.11	0.11

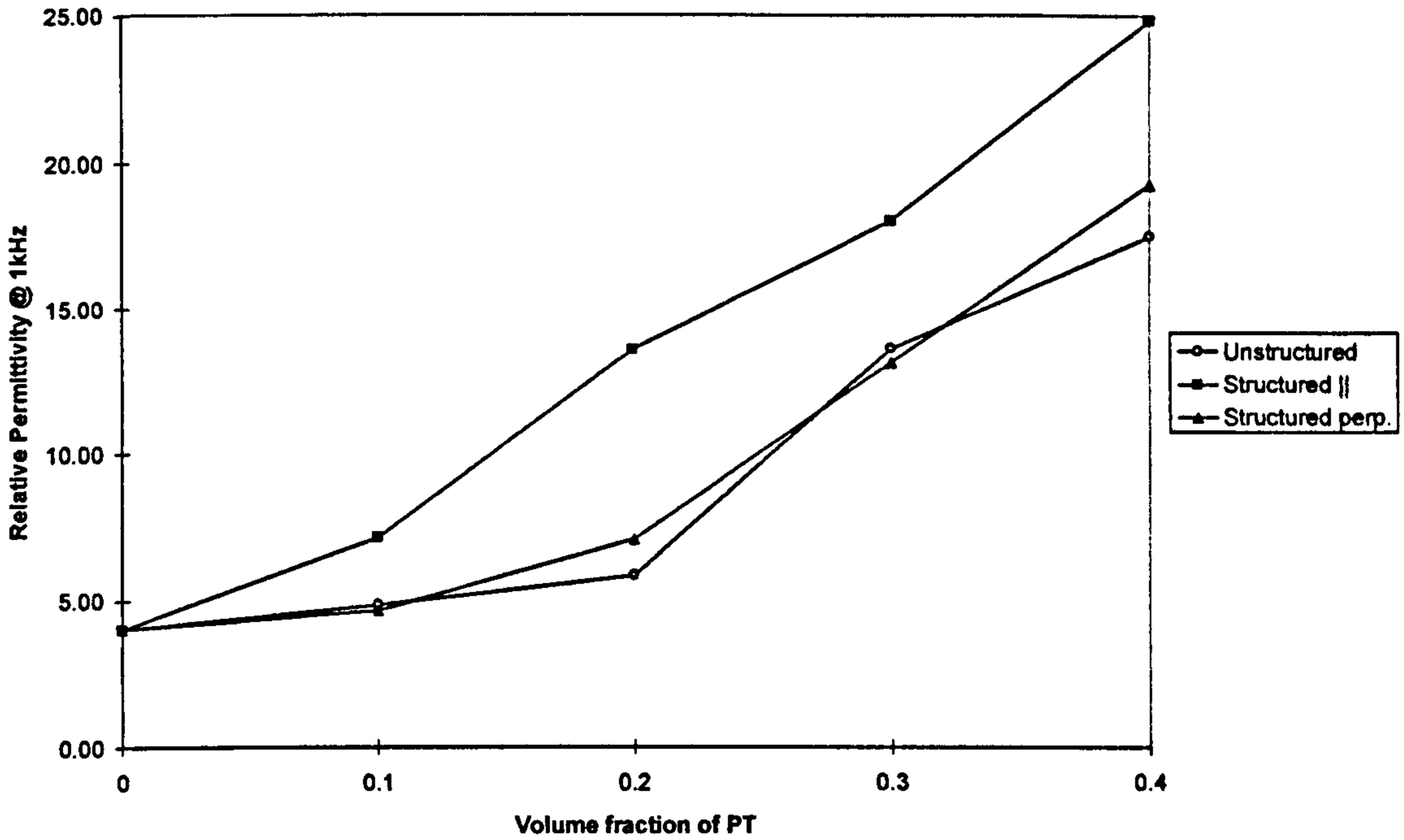

Figure 10.2: Relative permittivity (ε_r') of a range of unstructured and field-structured lead titanate / Epotek 302-3m epoxy composites.

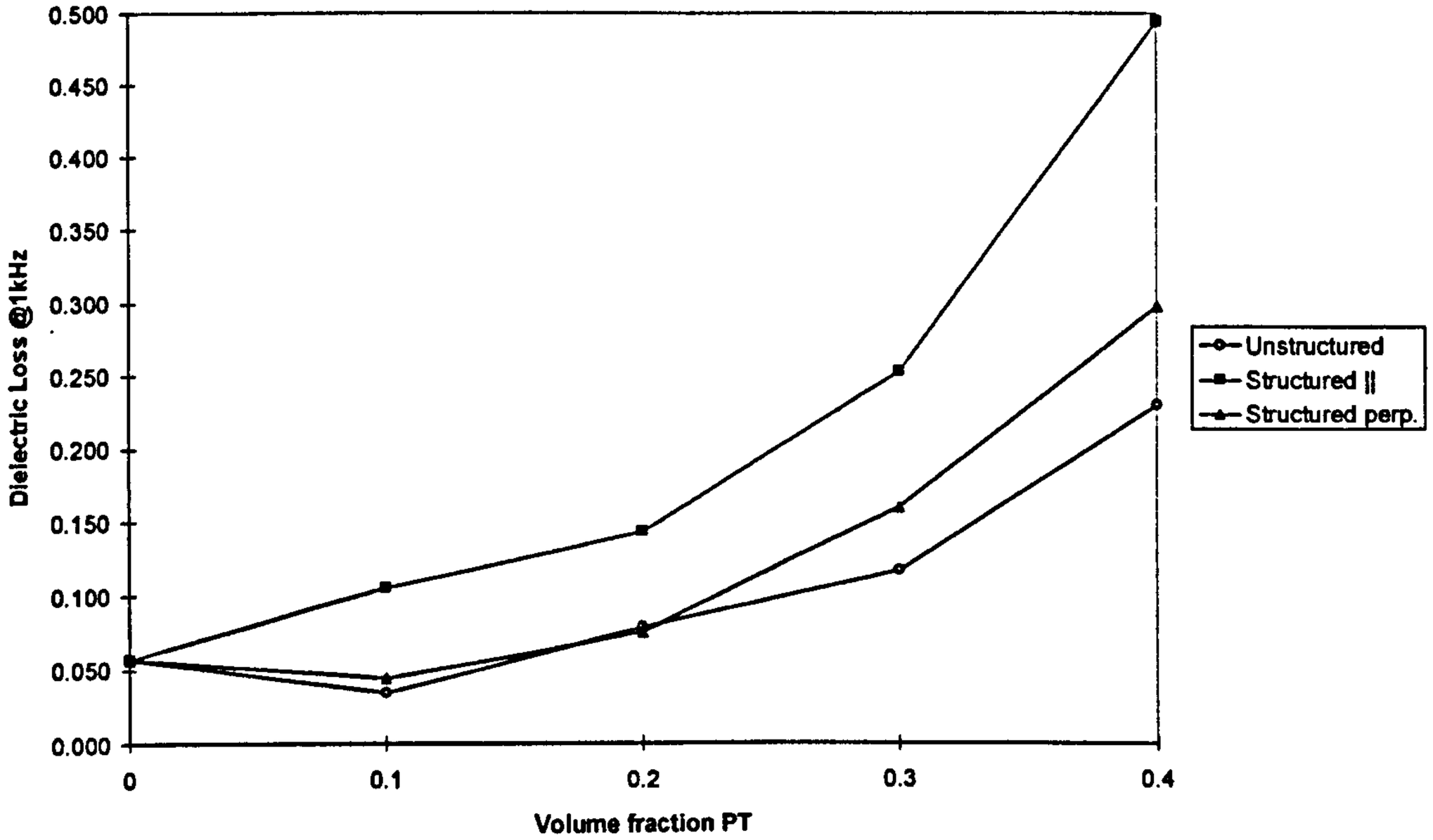

Figure 10.3: Dielectric loss (ε_r'') of a range of unstructured and field-structured lead titanate / Epotek 302-3m epoxy composites.

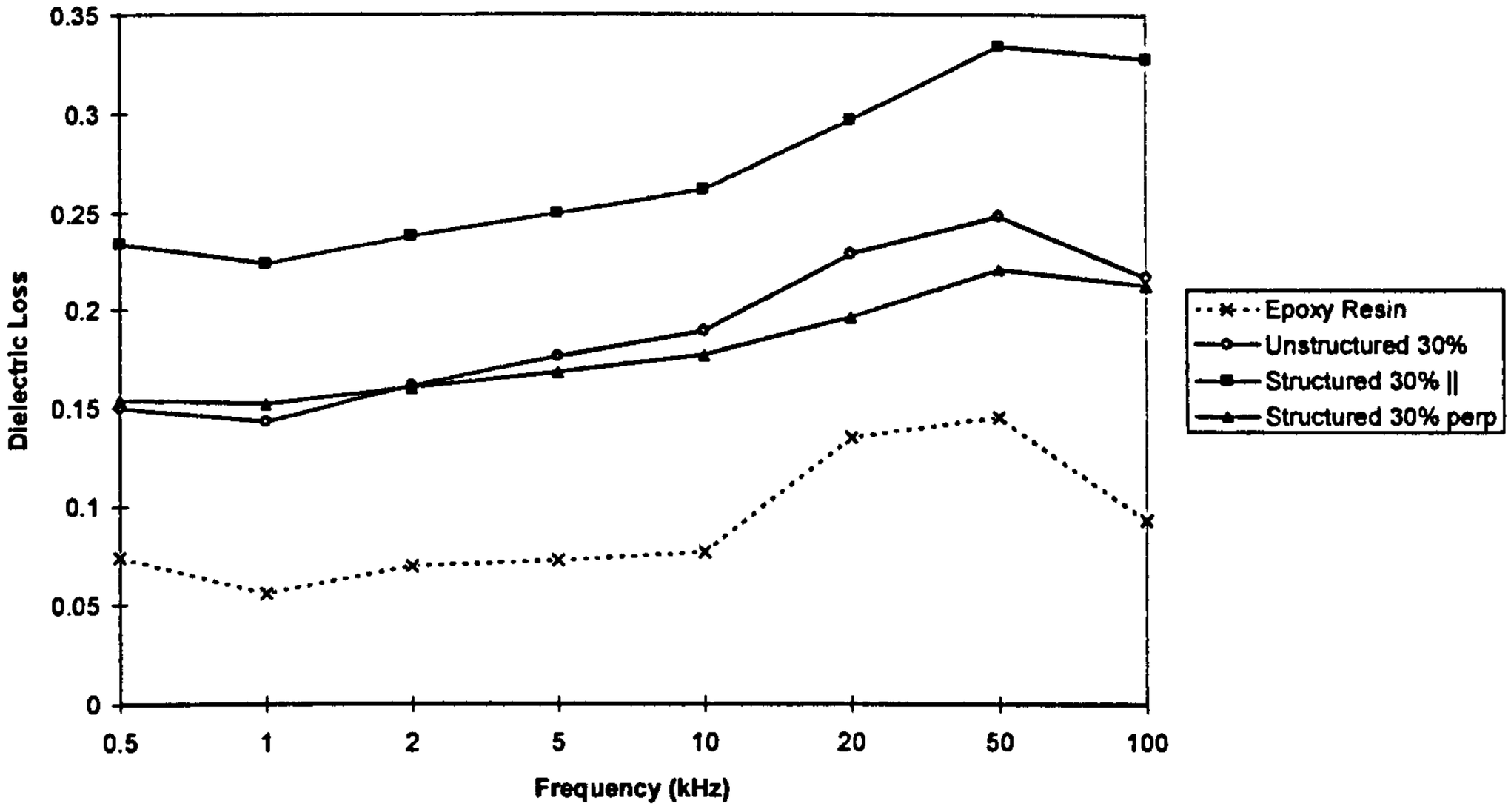

Figure 10.4: Dielectric loss (ε_r'') in Epotek 3023m epoxy resin and in a 30% vol. lead titanate / epoxy field-structured and unstructured composite.

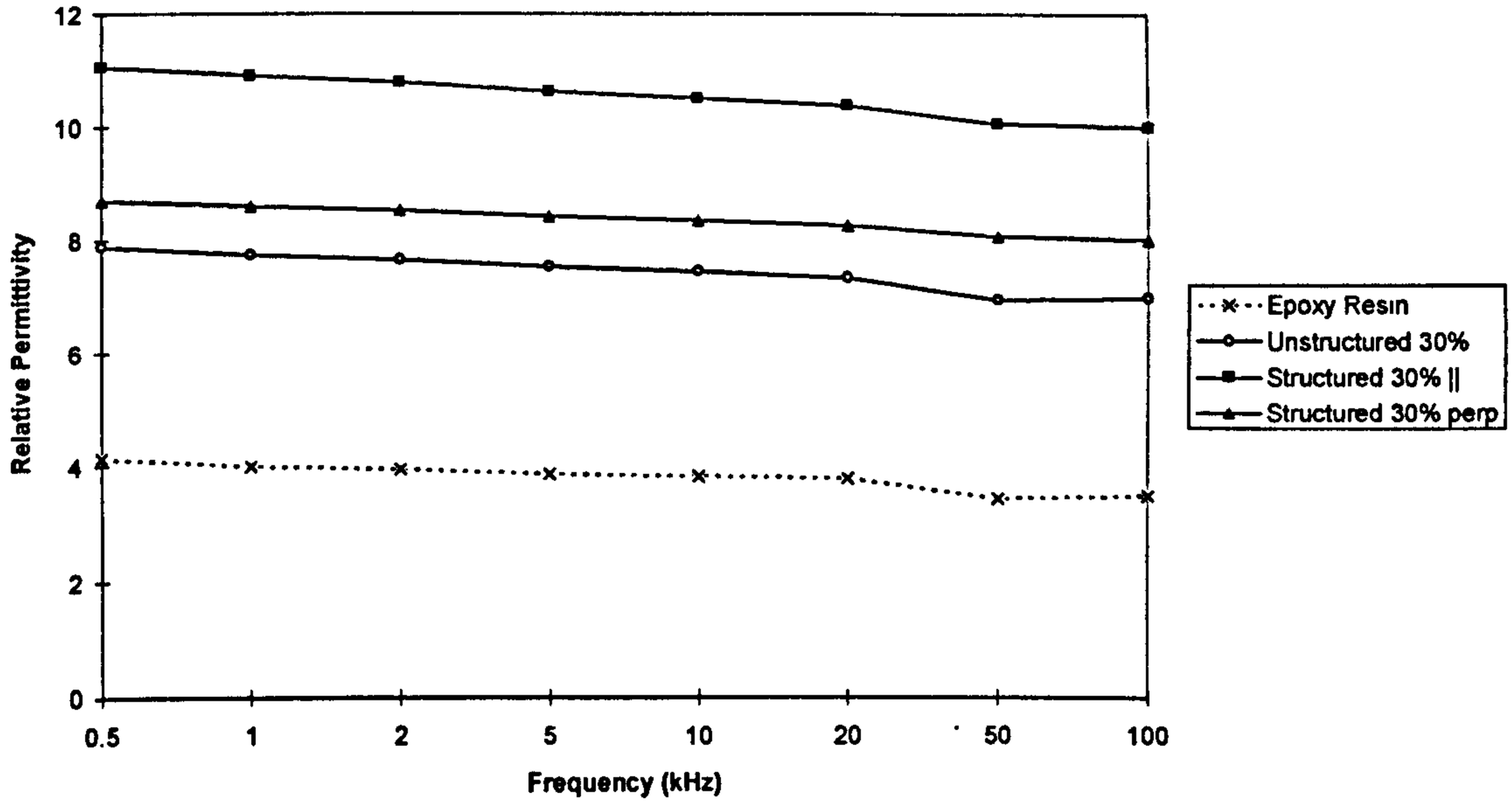

Figure 10.5: Relative permittivity (ε_r') of Epotek 3023m epoxy resin and in a 30% vol. lead titanate / epoxy field-structured and unstructured composite.

Figure 10.2 shows that field structuring markedly increases the relative permittivity of the composite parallel to the applied field, across the range, when compared with an equivalent unstructured material. The relative permittivity of the structured composite perpendicular the applied field can also exceed that of the unstructured material. This could be a consequence of chain branching. Consideration of dielectric loss (Figure 10.3) would seem to provide evidence of ordering in the perpendicular direction. Chain branching can occur where a particle size distribution exists. Larger particles, which polarize, are able to attract more that one smaller particle. Hence it is reasonable to suppose that at higher volume fractions of ceramic these ordered 0-3 composites should move away from a quasi 1-3 connectivity pattern and adopt a quasi 3-3 structure. The degree of chain-branching will then have a major influence on the measured properties of the composite. Figure 10.6 shows part of a chain in more detail to illustrate how chain branches can be formed.

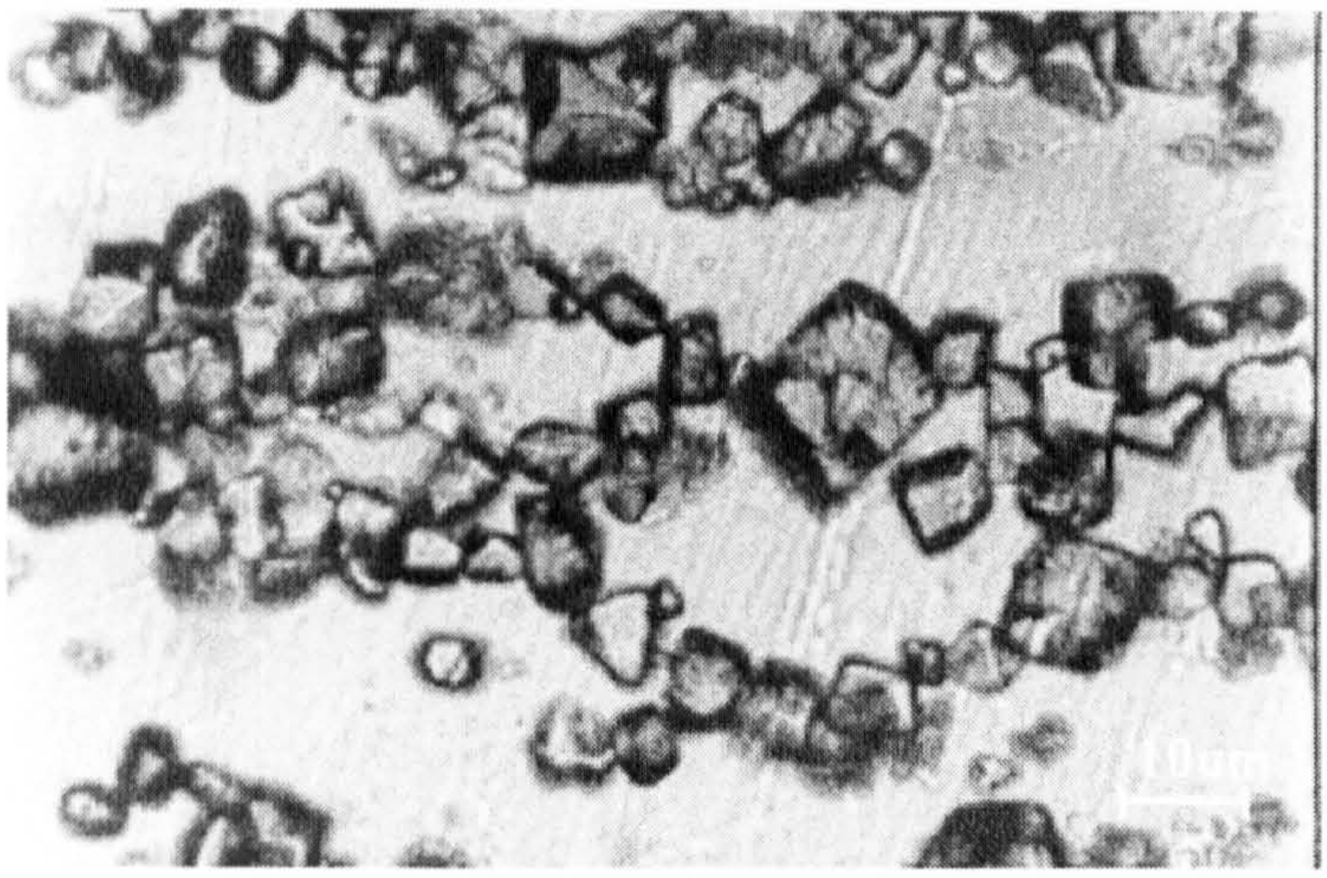

Figure 10.6: Chain branching in a lead titanate / Epotek 302-3M composite.

Figure 10.4 shows dielectric loss in the resin in 30% vol. lead titanate structured and unstructured composites across the frequency range 0.5-100kHz. The relaxation peak at around 40kHz, associated with the resin, is seen to be displaced in the ordered composite. Figure 10.5 shows the variation in relative permittivity over the same frequency range.

Table 10.2: Variability in dielectric properties of structured composites.

Measured volume fraction of ceramic (%)	Relative permittivity	Dielectric loss	Mean values
Structured ‖ to field			Structured ‖ to field
38.60	19.92	0.058	
38.16	17.73	0.050	Vol. fraction ceramic
38.78	15.23	0.047	= 38.07%
38.40	17.75	0.057	Relative permittivity
38.42	16.33	0.052	= 17.09
36.06	15.59	0.047	Dielectric loss =
0.0	2.87	0.008	0.052
Structured ⊥ to field			Structured ⊥ to field
39.22	15.83	0.040	Vol. fraction ceramic
38.39	12.62	0.039	= 38.62%
38.89	12.89	0.039	Relative permittivity
37.98	13.88	0.043	= 13.81
0.0	2.81	0.007	Dielectric loss =
			0.040

In order to assess the variability inherent in the process, a number of composites were prepared under identical condition, each having a nominal 40% vol. ceramic. These were sectioned and measured as before (Table 10.2). The Table also shows the mean values of like samples. Sources of variability would be: due to variations in the distribution of the ceramic phase, due to sedimentation or incomplete mixing and also due to any porosity that may be present. The size of the specimen will also be of significance. Below a certain thickness, samples will exhibit higher values of permittivity and loss. This is a consequence of the variability of the chains along their length.

The performance of the electrode is of major importance. If close contact is not made with the dielectric material, there will be a so-called 'parasitic' capacitance. A thin layer of low permittivity, between the electrode and the dielectric, inserts an additional, unwanted capacitance in series with the measuring circuit. Where high permittivity materials are concerned this can have a dramatic effect on the measured value. For field-structured composites, the electrode is in contact with the electroactive ceramic

only over a proportion of the total surface area and any variability in contact resistance across the surface is likely to be significant.

Two samples were prepared which had volume fractions of 45% and 55% of PZT5H powder in Epotek 302-3M. The PZT5H powder was prepared using the PbO:PbF2 flux growth technique outlined previously. At these high loadings the suspensions were difficult to handle. Dielectric properties were measured at 1kHz and are shown in Table 10.3. Structuring is in evidence in the 45% vol. samples, but not in the 55% vol. Note that the two specimens of 55% vol. composite were cut from the same sample and this should not be taken as reliable evidence that we have reached the upper limit for the technique. It may be that this one sample is not wholly representative. Surface-active agents are available which will improve the fluidity of such high volume-fraction dispersions and this will, in all probability, enable a field-structured material to be formed.

Table 10.3: Dielectric properties of PZT5H / Epotek 302-3M composites.

Nominal volume fraction of PZT5H (%)	Structured *(actual % v_f PZT5H)*		Unstructured *(actual % v_f PZT5H)*	
	Relative perm.	Dielectric loss	Relative perm.	Dielectric loss
45	23.81 *(45.86%)*	0.386	16.53 *(42.31%)*	0.165
45	21.30 *(42.15%)*	0.217	16.25 *(41.02%)*	0.161
45	21.32 *(44.74%)*	0.200	18.45 *(37.78%)*	0.252
55	21.12 *(54.32%)*	0.012	19.79 *(53.85%)*	0.012
55	21.24 *(54.32%)*	0.012	20.31 *(53.85%)*	0.012

A typical coupling agent is LICA 38 (Kenrich Petrochemicals Ltd., Bayonne, N.J.), which is a neoalkoxy-titanate. It acts to form a monomolecular organic layer on the inorganic ceramic surface and is specifically designed for use in composite materials which have a filler volume-fraction of ≈50%. Improvements in processing and in mechanical properties are claimed. Sample composites were prepared. The dielectric pemittivity of a 40% vol. PZT5H composite with 1% LICA 38 added was measured as 23.72. An equivalent 40% PZT5H composite with no added coupling agent gave a value of 20.2.

10.2.1 Modelling the dielectric properties of diphasic composite materials

The problem of modelling the dielectric properties of two-phase composite materials is by no means trivial. The significant variables are: i) the individual properties of the constituents; ii) the properties of the interface between them; iii) their respective volume fractions and iv) the spatial distribution of the phases in the bulk. Of these, the properties of the constituents and their volume fractions are easily determined. In contrast, the properties of the interface are often unlike those of either of the constituent materials, variations on a microscopic scale exist and build-up of space charges is commonplace. Furthermore, the included material itself determines the flux-density distribution, and hence the size of the inclusions in relation to the distance between them is all-important.

Many theoretical models have been tried, frequently with a caveat that they apply to low-volume fraction composites, to a specified uniform distribution or to a particular particle shape. These are reviewed along with several semi-empirical formulae by Van Beek [111]. More recently the problem has been considered specifically with reference to ferroelectric / polymer composites. Yamada derived a formula for ellipsoidal inclusions based on Maxwell's equations [112]. Banno developed the concept of 'modified cubes', based on the traditional parallel and series mixing rules [113]. A variant of Banno's model, which extends the concept to higher volume fraction materials, was introduced by Garner et al. [20]. Jayasundere, using a dispersion of spheres, modelled the interactions between particles [114]. Pardo et al. used a statistical treatment of randomly distributed particles having mixed 1-3 and 0-3 connectivity, although their predictions did not correlate closely with measured properties and they recognised the need for some refinement. Even so, their ideas would certainly merit consideration for modelling the properties of field-structured composites [115]. A theoretical treatment of a disordered dispersion of identical dielectric spheres by Geigenmüller and Mazur [116] is somewhat at odds with a related treatment by Felderhof, who has calculated the upper and lower bounds of the dielectric constant for such a mixture [117].

Figure 10.6 compares the measured dielectric permittivities of model field-structured and unstructured composites with the theoretical predictions of some of the models listed in Appendix D.

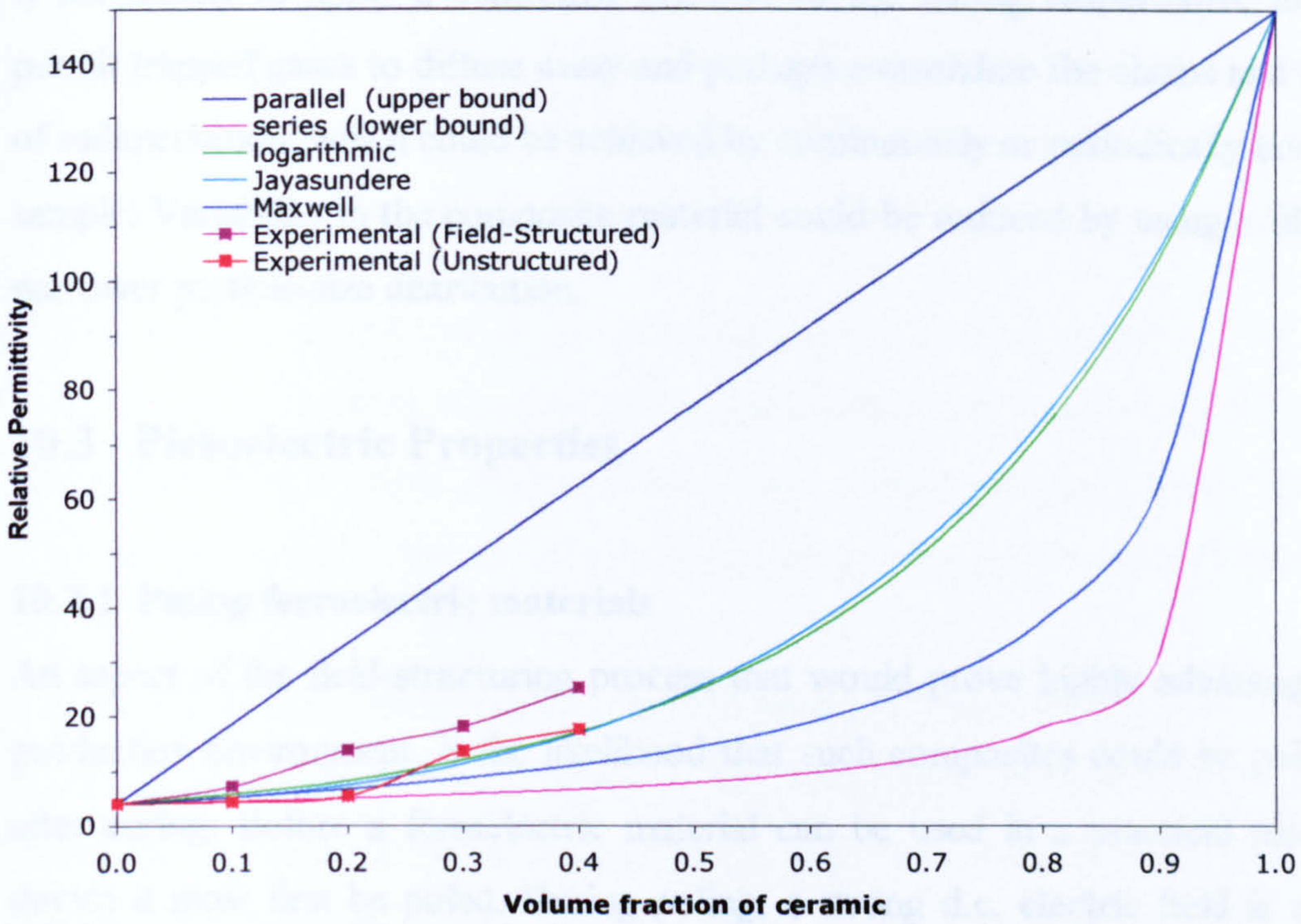

Figure 10.7 Theoretical models for the dielectric permittivity of the model lead titanate / Epotek 302-3M diphasic composite compared with experimental values for field-structured and unstructured materials.

10.2.2 Summary

To summarise, it is quite clear that the distribution of the phases in composites such as these has an important bearing on the measured dielectric properties. As a result of field-structuring, both relative permittivity and dielectric loss are increased parallel to the direction of the applied field. In the course of this study, structured composites were successfully made which had a volume fraction of 50% ceramic. By using suitable processing aids it may be possible to extend this still higher. As the upper limit approaches, the degree of anisotropy in the measured values will be smaller. As this work has progressed and a greater understanding of the field-structuring technique has emerged, so the shortcomings of the processing unit have become more obvious.

Significant variability has been observed between samples prepared under identical conditions. Some of this will be inherent in the process and some is undoubtedly due to the limitations of the equipment. The most important refinements that are needed are: i) the facility to apply a controlled pressure to the curing suspensions, in order to permit trapped gases to diffuse away and perhaps consolidate the chains and ii) control of sedimentation, which could be achieved by continuously or periodically inverting the sample. Variability in the composite material could be reduced by using a filler with a narrower particle-size distribution.

10.3 Piezoelectric Properties

10.3.1 Poling ferroelectric materials

An aspect of the field-structuring process that would prove highly advantageous in a production environment, is the likelihood that such composites could be poled in-situ after curing. Before a ferroelectric material can be used in a practical piezoelectric device it must first be poled. During poling, a strong d.c. electric field is applied to force the ferroelectric domains to re-orient along a particular axis. The process is normally carried out at elevated temperature, as this facilitates domain-wall movement. After poling, a remanent polarization persists in the direction of the applied field. The chief variables to consider are time, temperature and field strength. For a homogenous ceramic it is reasonably straightforward to prescribe these parameters, based on known properties. Where a two phase composite is concerned the situation is more complicated as the applied voltage is dropped unequally across the ceramic and the intervening polymer phases. The polymer phase shields the ceramic and only a fraction of the total applied field is effective in poling. Because of this, much higher fields are needed to pole 0-3 ceramic / polymer composites than for the ceramic alone. The final field distribution, after the first instant, is dependent on the relative conductivities of the two phases.

As has been stressed previously, the distribution of the phases is an important determining factor for local field intensity. Furthermore, any flaw can, in principle, lead

to an accumulation of localised space charges and hence an intensification of the field. The build-up of space charges should ideally be monitored as this can lead to breakdown [110]. In field-structured composites the ceramic / polymer interface is riddled with structural flaws and forms an intermittent pathway through the thickness of the material. Hence it may well be that these materials will have a low breakdown strength. In breakdown, a rapid discharge of electrical energy carbonises the polymer and a conducting pathway can be established.

Poling is often carried out in an insulating oil to prevent breakdown. An important point concerns the field intensification at the edges of the electrodes, which can limit the applied field strength. In the current work, a 1mm perimeter around the edge of each sample was left exposed and this is a useful precaution against edge-breakdown.

An alternative to conventional d.c. thermal poling is corona poling, whereby a corona discharge is sprayed over the surface of the ferroelectric material using a sharp metal point. This method has the advantage that, in the absence of a top electrode, localised charges are unable to accumulate and hence the incidence of breakdown is very much reduced. For large areas an array of needles can be used.

Useful studies have been published by: Schoch et al. regarding assessment of the degree of poling by x-ray methods [118]; Das-Gupta and Doughty and also Waller et al. on corona poling [119,120]; Setiadi et al. on step-wise poling of VDF/TrFE thin films [121]; Furukawa et al.on VDF/TrFE copolymers using a low-frequency a.c. poling technique [122]; and in standard texts.

An interesting technique was demonstrated by Zipfel [123], who suspended 30-40% vol. of ferroelectric single-crystals in a liquid polyurethane pre-polymer and applied both a hydrostatic pressure and an electric field. The crystals aligned with their polar axes in the field direction and the resin cured. This was reported to be a very efficient poling method.

10.3.2 Poling Technique

1. Ensure that good electrical contacts are made to the sample. Be aware of possible dielectric breakdown when electrodes are close to an electrical earth.
2. Before switching on the power, ensure that electrical cut-outs and safety devices are in place and the rig is safe from casual contact.
3. Ramp up the voltage in a stepwise fashion.
4. Where possible monitor the poling current, as this will reveal much about the integrity of the sample.
5. When the required time has elapsed, ramp down the voltage.
6. Short out the electrodes after the power is switched off to remove any capacitive charge. This is a real danger.
7. Allow oil to drain from the sample. Place on a conductive surface to cool. Note: the sample can be very hot.
8 Short out the electrodes overnight in a warm atmosphere to remove space charges.

10.3.3 Poling Practical

Poling of the composite samples was carried out in a temperature-controlled oil bath with a stirrer. The poling medium was Dow Corning 200/100cs filtered silicone oil or Aldrich 820-83-5 mineral oil. Power was provided from a Brandenburg regulated 15kV supply or a Brandenburg - Alpha series II 30kV supply. The experience of other workers suggested that the correct poling conditions for 0-3 lead titanate / polymer composites are a field of 10kV/mm at 80°C for around 15 mins. The piezoelectric charge coefficient of the poled samples was measured at a frequency of 115Hz using a Take Control PM35 Piezometer.

Early attempts to identify suitable poling conditions resulted in flashover between the electrodes at 7.5kV/mm and 80°C after as little as 3 minutes. Once breakdown has occured poling cannot be continued. This proved to be a significant problem due to the limited availability of the structured samples. Subsequently the temperature was

reduced to 60°C and the incidence of breakdown was somewhat reduced. Table 10.4 shows some early results.

Table 10.4: Initial poling studies on structured and unstructured lead titanate composites.

Sample	Applied field = 6kV/mm			
	Time / Temperature	d_{33} pC/N	Time / Temperature	d_{33} pC/N
30% PT unstructured	15 mins. @ 60°C	10	45 mins. @ 60°C	10
30% PT structured	15 mins. @ 60°C	15		
40% PT unstructured	15 mins. @ 70°C	14	30 mins. @ 70°C	14
40% PT structured	3 mins. @ 80°C	21		

It was noted that the dielectric properties of structured samples which had been poled and left overnight in an oven at 70°C could not be measured reliably until they had cooled and been left to stabilise at room temperature for several hours. This was attributed to humidity [28]. Unstructured samples did not exhibit this effect. For later work the samples were first dried in an oven at 70°C. Subsequently it was found that they were then able to withstand poling fields of 10 or 12 kV/mm.

A series of 40% vol. structured and unstructured composites was poled and the effect of poling on their piezoelectric properties is shown in Table 10.5.

Table 10.5: Development of piezoelectric properties in 40% vol. structured and unstructured composites during poling at 62°C

Time (mins.)	Poling field = 9.2kV/mm				Poling field = 10kV/mm			
	Struct. d_{33} (pC/N)		Unstruct. d_{33} (pC/N)		Struct. d_{33} (pC/N)		Unstruct. d_{33} (pC/N)	
	Sample1	Sample2	Sample1	Sample2	Sample3	Sample4	Sample3	Sample4
0	0	0	0	0	0	0	0	0
15	5.5	7.5	5	6	10	8.5	4.5	n/a
30	6.5	10	6	7	12	10	5.5	
45	8	11.25	7	7	16	12	6	
60	10	12.5	7	7	*Breakdn. (50mins)*	13	*Breakdn. (58mins)*	
75	13.5	15.5	7	7		14.5		
90	14	*Breakdn. (85mins)*				16		
105	*Breakdn.*							

The charge coefficients were found to have diminished slightly, in all cases, when the samples were remeasured two weeks after poling. This effect has been observed separately by others. An explanation has been suggested that the composites may not have been poled uniformly through their thickness.

A series of composites having different volume fractions of ceramic was prepared and poled at 60°C and 10kV/mm. The results are shown in Figure 10.8 and clearly highlight an increase, which has been brought about by field-structuring.

Structured and unstructured samples having a volume fraction of 50% lead titanate were poled in a step-wise manner as suggested by Setiadi [121]. The sequence was as follows:

1. Pole at 2kV/mm for 4 minutes. Pause for 1 minute.
2. Pole at 4kV/mm for 8 minutes. Pause for 2 minutes.
3. Pole at 6kV/mm for 8 minutes. Pause for 2 minutes.
4. Pole at 8kV/mm for 8 minutes. Pause for 2 minutes.
5. Pole at 10kV/mm for 8 minutes. Pause for 5 minutes.
6. Continue as Step 5 until fully poled.

In practice, the structured sample broke down after a total of 43 minutes (d_{33} was 23pC/N). The unstructured sample broke down after 48 minutes (d_{33} was 15pC/N). This step-wise technique is claimed to reduce the incidence of breakdown. However, these samples do not seem to show improvement over the direct approach.

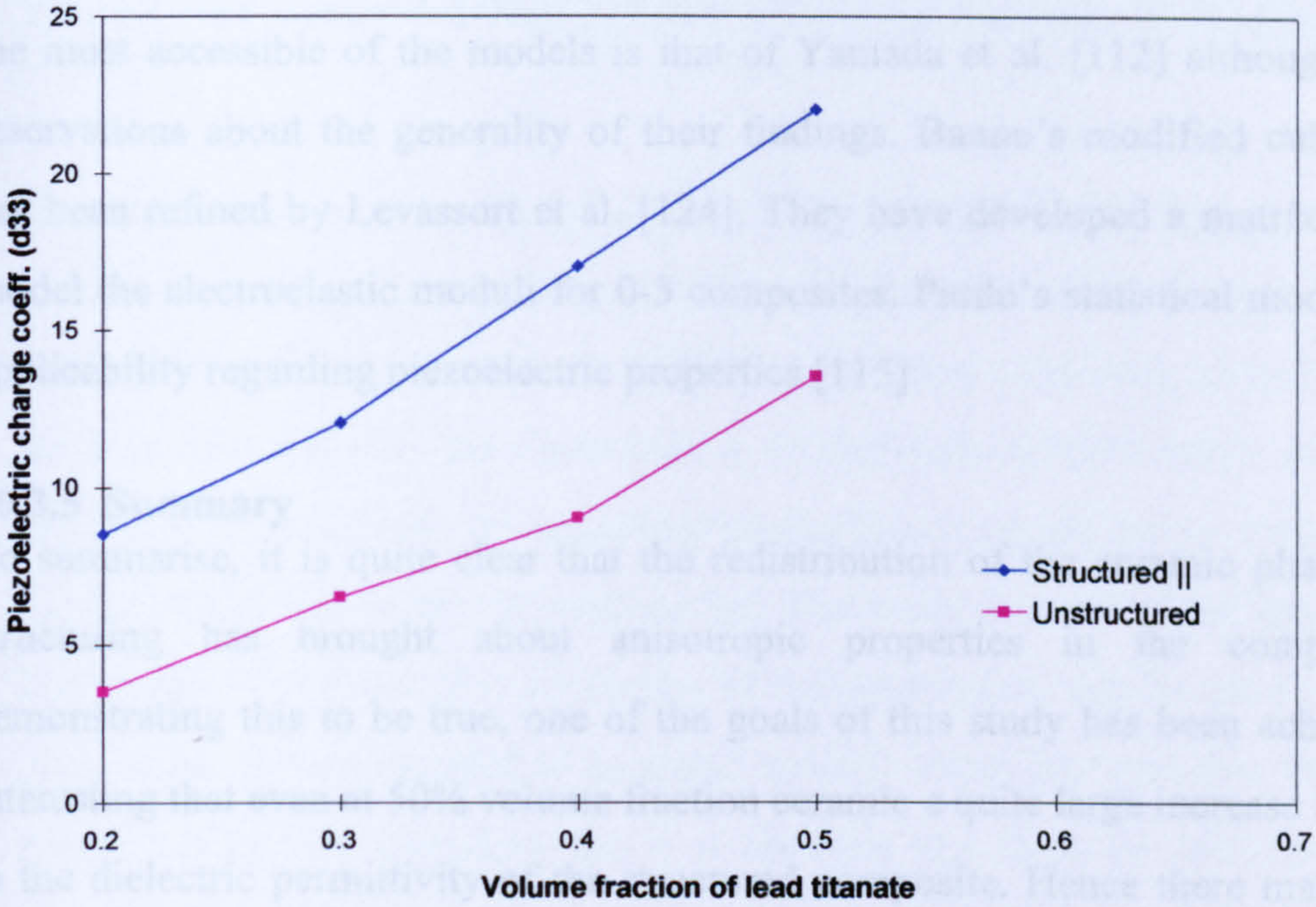

Figure 10.8: Piezoelectric charge coefficients of a range of structured and unstructured composites.

Composites were prepared with PZT5H ceramic and poled as before at 10kV/mm and 60°C. The results are shown in Table 10.6. The results were very disappointing and others have noted that ceramics made from this batch of PZT5H have also under-performed and it may have been substandard. However, the field-structuring technique is very much in its infancy and too little is known about the numerous variables to draw any firm conclusions.

Table 10.6: Piezoelectric properties of PZT5H structured and unstructured composites.

Vol. fract. PZT5H (%)	Piezoelectric charge coefficient – d_{33} (pC/N)					
	Field -structured			Unstructured		
	Sample 1	Sample 2	Sample 3	Sample 1	Sample 2	Sample 3
45	11	-	13	9	7	11
55	11	-	11	9	9.5	9

10.3.4 Modelling the piezoelectric properties of 0-3 composites

Models of dielectric properties of 0-3 composites outlined previously in this chapter have, in many cases, been extended to describe their piezoelectric properties. Perhaps

the most accessible of the models is that of Yamada et al. [112] although there are reservations about the generality of their findings. Banno's modified cubes method has been refined by Levassort et al. [124]. They have developed a matrix method to model the electroelastic moduli for 0-3 composites. Pardo's statistical model also has applicability regarding piezoelectric properties [115].

10.3.5 Summary

To summarise, it is quite clear that the redistribution of the ceramic phase by field structuring has brought about anisotropic properties in the composites. In demonstrating this to be true, one of the goals of this study has been achieved. It is interesting that even at 50% volume fraction ceramic a quite large increase is observed in the dielectric permittivity of the structured composite. Hence there may be scope for weight savings, obtaining equivalent performance from a less dense composite.

There are inherent problems in poling 0-3 composites and, in tandem with the limited availability of the structured composites, this has made it difficult to gather sufficient data for a thorough study. Even so, the results are encouraging. The model lead titanate / epoxy field-structured composites have exhibited the piezoelectric charge coefficients associated with higher volume fraction unstructured materials. Attempts to exploit the effect using PZT5H were unsuccessful in this case. As was found later, this may have been due to a substandard batch of ceramic powder. Nevertheless, the field-structuring technique has been shown to be effective and the work should be repeated. A corona poling rig has been constructed and this should enable results to be gathered more efficiently.

11. Short Range Interactions in Suspension Polarization

The polarization model, which describes the forces in dielectric suspensions exposed to an electric field, has been used successfully to describe the movement of particles and hence their ordering into various chain-like and other structures. It has been validated through research into the development of electrorheological fluids and also in the separation of living cells by dielectrophoresis. Electric fields are now routinely used in biotechnology and in genetic engineering. The work presented here has shown that a knowledge of the dielectric properties of the constituents can be used to estimate the process parameters required to assemble ordered composite materials. Despite this the model has certain limitations and it is essential that these be addressed if the field structuring technique is to be used to produce technologically useful materials.

The key issue lies in the assumption that particle polarization is the result of an accumulation of bound and free charge in a vanishingly thin layer between the two phases. In reality, particles develop a surface charge which both promotes the adsorption of counter-ions and also causes a redistribution of ions in the surrounding fluid to form a diffuse electrical double layer. This layer has a finite thickness, commonly referred to as the Debye length ($1/\kappa$). There is an associated pressure due to the local ion distribution, known as the osmotic pressure. Although the role of these factors in colloidal suspensions is well documented, the same cannot be said of their behaviour in polarized suspensions such as ER fluids.

11.1 Interactions between adjacent particles in field-free suspensions

Briefly, the principal interactions which influence field-free suspension microstructure are as follows:

i) Van der Waals interactions. These are fundamental physical forces, which result from the quantum mechanical coupling of dipoles in the electron clouds of adjacent

bodies. They are effective at particle separations below about 100nm. The maximum van der Waals attractive energy (V_{att}) felt by two spheres is:

$$V_{att} = -\frac{A.a}{12.r_{min}}$$

The magnitude of the Hamaker coefficient (A) depends on the dielectric response of both the particle and the suspending medium. In general, it increases with particle density. (a) is the particle radius and (r_{min}) is the minimum surface to surface separation. Van der Waals forces can be substantial for typical colloidal particles, in the range 400-15000 kT; where kT approximates to the thermal energy of the particles [126]. The forces are therefore sufficient to enable irreversible aggregation of particles to occur.

ii) Electrostatic repulsion. When like-charged particles approach sufficiently close for their ionic double layers to overlap they experience an electrostatic repulsion. The viscosity of a suspension, in particular, is strongly dependent on electrostatic interactions between particles and shows a non-linear increase with increased volume fraction of particles.

The electrostatic repulsion between identical particles of low surface potential is given by the approximation:

$$V_E = \frac{4.\pi.\varepsilon.\varepsilon_0.\psi_0^2.a^2}{r}.\exp\left[-a.\kappa\left(\frac{r}{a}-2\right)\right]$$

where V_E is the electrostatic interaction energy, ε is the dielectric permittivity of the fluid, ε_0 the permittivity of free space, ψ_0 the particle surface potential, a is the particle radius and r the surface to surface separation [126].

The total interaction energy between particles underpins much work on colloidal stability and is referred to as the DLVO model (Derjaguin-Landau-Vervey-Overbeek).

It can be approximated as the *sum* of the electrostatic and van der Waals energies:

$$V_{tot} = -\frac{A.a}{12.r_{min}}.\left(1-\frac{24.\pi.\varepsilon.\varepsilon_0.\psi_0.r_{min}}{A}\right)$$

where r_{min} again denotes minimum separation.

Two techniques which are commonly used to exercise control over colloidal stability, are both relevant to the current study. Firstly, van der Waals interactions can be shielded by steric stabilisation. Polymer molecules are used which adsorb onto the particle surface, their long chains prevent close encounters thus mitigating the attractive forces. Secondly, the electrostatic repulsion between particles can be increased by increasing the ionic strength of the surrounding fluid; thereby reducing the Debye length.

iii) Solvation/hydration forces. In recent years, short range repulsive forces (1nm) have been reported which are associated with the hydration shells of surface-adsorbed ions [127]. These forces again shield the van der Waals interactions, however, because of their limited range they are unlikely to dominate except where nanoscale particles are concerned. Note that van der Waals forces scale up with increasing particle size.

In addition to the above it should be mentioned that there have been several reports of *attractive* forces between like-charged particles, which cannot easily be explained by the standard DLVO treatment outlined above. These are found to occur in concentrated suspensions and are thus of interest. It has been suggested that these forces result from a redistribution of the electrical double layer of ions and counterions, although the subject remains controversial [128].

11.2 Interactions between adjacent polarized particles in suspension

When polarized particles are separated by a distance greater than one particle diameter, the net interaction between them can be described in terms of: i) the polarization force,

As the inter-particle separation diminishes, multibody interactions assume greater importance and below one particle diameter the polarization force is best described in terms of a coupled multipolar rather than a dipolar response [Jones]. Simple geometry shows that the average inter-particle separation (r) is less than one particle diameter (2a) for all uniform suspensions containing more than 6.54% vol. solid spherical particles (Figure 11.1) where:

$$r = \left(\frac{1.612}{\sqrt[3]{v_f}} - 2 \right) .a$$

The polarization force overshadows the field-free inter-particle forces and at separations equivalent to or less than the Debye length, there are electrostatic and mechanical effects to consider due to displacement and diffusion of ions, when the double layer becomes distorted.

The distance of closest approach between strongly polarized particles is uncertain. An estimate of 4 - 7nm has been made for the spacing between particles in an ER fluid [129]. It may be that strongly adsorbed ions screen the induced polarization and prevent direct electrical contact. At such small separations steric factors such as particle shape and surface roughness are clearly important. If an electric current is established between the particles, either by direct contact or by surface ion migration, the polarizing field will be disturbed. Osmotic pressure may then reassert, leading to fluctuations in the distance between particles. Local temperature gradients, field-induced ionisation and tunnelling are factors to consider. A dynamic situation exists and although the basic polarization model can be refined to incorporate variations in particle size, shape and spatial distribution, there are significant technical difficulties in applying it at very small inter-particle separations, where a number of additional effects are likely to be in competition.

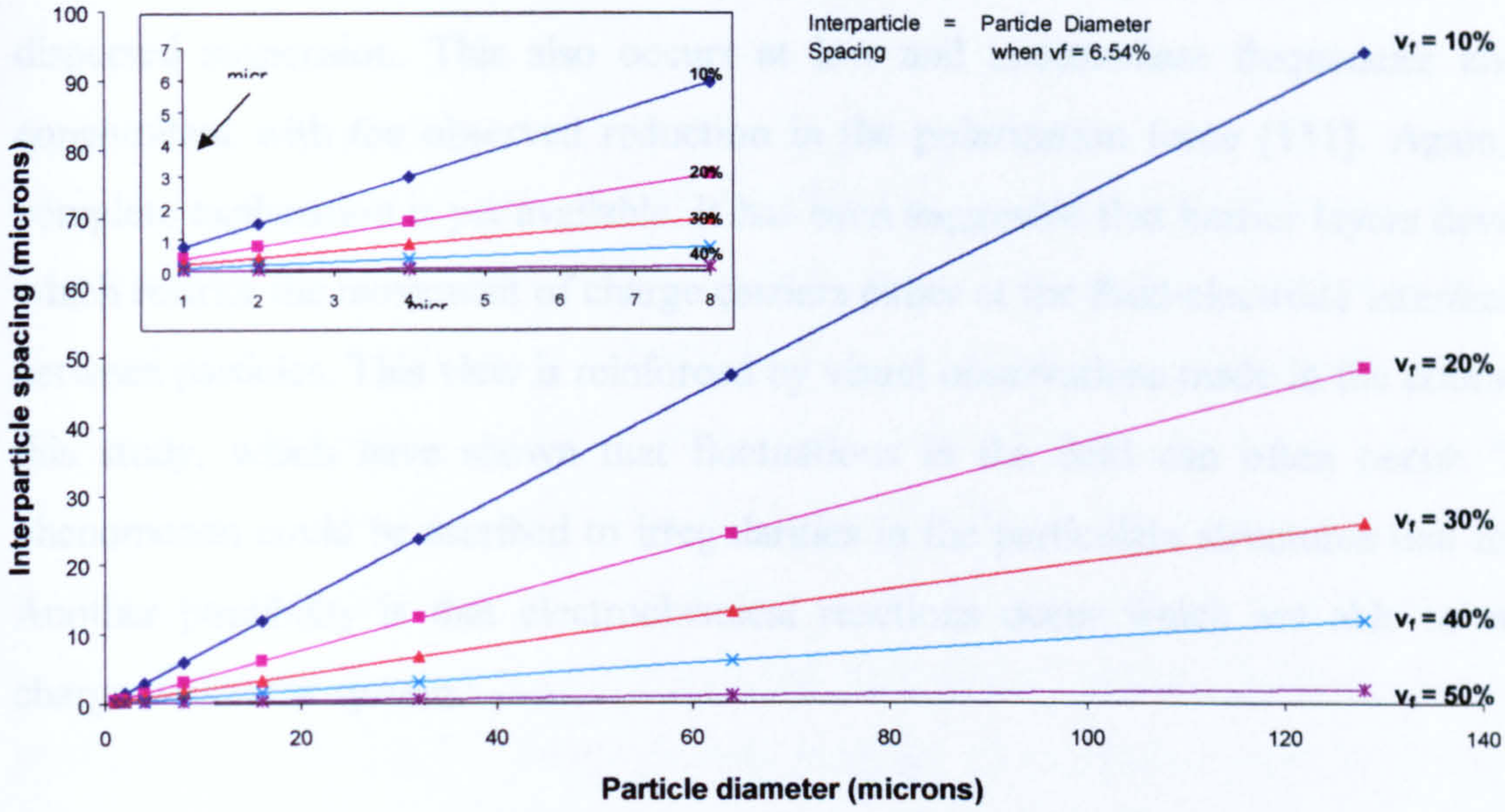

Figure 11.1: Average separation between spherical particles in suspensions

11.3 Consequences for electric-field structuring of composites

Where particles are closely packed, the bulk dielectric properties of suspensions are difficult to predict and often differ from those expected. Two frequently observed phenomena, which result from particle interactions, have consequences for the electric-field structuring technique. The first of these is the marked reduction in the polarization force, typically seen in ER fluids, when field frequency is increased in the range 10Hz-1kHz [130].This is a consequence of dielectric relaxation and is volume fraction sensitive. It occurs even though neither the fluid nor the solid phase exhibits relaxations in this range. A definitive explanation for this is uncertain and the wide distribution of relaxation times indicates that no single process is responsible, but rather that it results from interfacial polarization in its broadest sense. It is probable that spatial polarization of the double layer gives rise to a large effective permittivity. Where the volume fraction of the dispersed phase increases to the point where interparticle separation is less than the Debye length this cannot occur and the bulk properties of the suspension become dominated by particle and surface dielectric properties [37].

A related phenomenon, also typical of ER fluids, is the large increase in the permittivity of a field-structured suspension in comparison to that of an otherwise identical, well-dispersed suspension. This also occurs at low and intermediate frequencies and is concomitant with the observed reduction in the polarization force [131]. Again, no complete explanation is yet available. It has been suggested that barrier layers develop which restrict the movement of charge carriers either at the fluid-electrode interface or between particles. This view is reinforced by visual observations made in the course of this study, which have shown that fluctuations in the field can often occur. This phenomenon could be ascribed to irregularities in the particulate structures that form. Another possibility is that electrochemical reactions occur which are able to store charge within the system.

Overall there are several points to note, which fall outside the scope of the basic polarization model:

i). It has been demonstrated that the electric-field structuring technique is capable of bringing particles into very close proximity, where the influence of short-range forces cannot be ignored. A good illustration that van der Waals forces have an influence on field-structured composite microstructure, can be found by contrasting the field-induced behaviour of lead titanate in an epoxy pre-polymer with that of carbon black. Lead titanate adopts the classic 'pearl-chain' structures spanning the electrodes, carbon black forms into sizeable clumps or flocs, which remain stable when the field is removed.

ii). The field-structured composites prepared here show an increased dielectric loss in comparison with their unstructured equivalents. The reason for this is at present unknown and it may be inherent in the structuring technique. Ionic species could become trapped at the particle-matrix interface forming a layer with particular electrical properties. It is known that ions trapped at defects in the polymer network can promote the accumulation of space charge.

iii). Furthermore field-structured composites could develop in-built residual stress when the polarizing field is removed.

11.4 Zeta Potential

Zeta potential measurements can give a useful insight into the probable nature of the interaction between particles and can be used to point the way to improvements. The zeta potential of a particle in suspension is a feature of the ionic double layer and represents the electrical potential that exists at the surface of shear between the charged particle and the surrounding fluid. The location of the shear-surface depends on the size and concentration of the surface adsorbed ions and the amount of solvent which is associated. Thus it can be a strong indicator of surface chemistry. It can be evaluated by tracking the electrophoretic mobility of suspended particles under the influence of a moderate electric field (3V/mm at 1kHz). The viscosity of the fluid, pH and dielectric constant must be known and the zeta potential is computed using the Smoluchowski relationship. The instrument used for this study was a Malvern Instruments – Zetasizer 3000. Viscosity was measured using a Gilmont Instruments falling-ball viscometer, Size No.1 (0.2 to 10cP).

In the current context there are several important points to note regarding the applicability of the results which can be obtained. The first of these is the caveat that measurements made under low field may not necessarily relate directly to the high field conditions which are used in the structuring of composites. The second point concerns the practical difficulty of obtaining useful measurements on a curing thermoset. Although viscosity is relatively constant for a period at room temperature, there is the problem of subsequently cleaning the optical components for reuse and the cost, in this case, is prohibitive. Furthermore, because of the high density of the solid being used, sedimentation is a problem and there is some difficulty in obtaining a suitable suspension. It is not known whether the Smoluchowski relationship, used in the computation extends to liquid polymers.

In the absence of measurements on the curing resin, some information can be derived from a study of the ceramic suspended in the curing agent (poly-oxypropyl-diamine). The commercial (Vernitron) PZT5H powder was chosen because it provided a narrow particle size range in the sub-micron range and therefore a sufficiently slow rate of sedimentation. One sample of PZT5H was coated with LICA38, a coupling agent, which is discussed in the following section. Glass microballoon and untreated carbon black suspensions were prepared for comparison. All powders were dried in a vacuum oven for 16hrs at 80°C before use. The dielectric permittivity of the POPD was measured at 6.08 and its pH 13.38 at 21°C. The suspensions were allowed to stand overnight to ensure full development of the zeta potential (Table 11.1). The results were as follows:

Table 11.1: Zeta potential of poly-oxypropyl-diamine suspensions at room temperature.

Temperature Viscosity of POPD (cP)	21°C 9.58	35°C 6.49	45°C 5.33	55°C 4.03
	Zeta Potential (mV)			
1. 0.5%vol. PZT5H in POPD	-2.1 ± 0.4	-3.0 ± 0.3	-3.8 ± 0.2	-5.1 ± 0.3
2. 0.5%vol. PZT5H in POPD + 1%LICA38	-2.5 ± 0.7	-3.8 ± 0.4	-4.7 ± 0.4	-6.4 ± 0.5
3. 1%vol. glass microballoons in POPD	-2.6 ± 0.1	-3.8 ± 0.2	-4.5 ± 0.2	-5.7 ± 0.3
4. 0.5%vol. carbon black (untreated) in POPD	-3.1 ± 0.2			-7.2 ± 0.3

In a separate experiment three suspensions of PZT5H (1%vol.) were compared: the first of these was made as before using dry PZT5H; the second with PZT5H saturated in deionised water; and the third was made up using PZT5H coated in an ionic salt. Coating was achieved by adding dry PZT5H to copper II chloride, which had previously been dissolved in acetone. The acetone was subsequently evaporated away. The quantity used was 50μmol $CuCl_2.2H_2O$ per g PZT5H. No appreciable difference was detected between the values of zeta potential measured for the three suspensions.

The most interesting points to emerge from these results are firstly, that the zeta potential is negative and secondly, that it is in all cases low. Little variation is noticeable between the various suspensions. One possible explanation is that molecules

of the fluid, poly-oxypropyl-diamine, are preferentially adsorbed on to the particle surfaces. The zeta potential is dependent on the pH of the surrounding fluid; hence it can be altered by the addition of an ionic salt. Small amounts of copper II chloride were shown to be soluble in POPD and could be used effectively to reduce its pH. By doing this it could reasonably be supposed that the zeta potential would be made less negative, the potential barrier between particles would therefore be reduced and this may be a valuable tool to use in field-structuring. The results shown here do not lead to any firm conclusion in this regard and it is probable that the effect is very dependent on the salt concentration. In a separate experiment, visual observation of field-structuring using graphite in Epotek 302-3M showed that a filamentary network formed. This occurred at lower field strengths than were needed for lead titanate. Addition of a small amount of copper II chloride caused clumps or flocs to form as previously demonstrated with carbon black. More work would be needed to establish the usefulness of this technique. Furthermore, due regard would have to be given to the possibility that large concentrations of an ionic salt may influence the electrical and mechanical properties of a finished composite. In particular, a rise in the conductivity of the resin could be expected which would be undesirable in a piezoelectric composite. To explore this the dielectric properties of Epotek 302-3M epoxy resin modified by additions of copper II chloride were measured:

Table 11.2: Dielectric properties of Epotek 302-3M modified with $CuCl_2$.

Sample	Relative permittivity	Tan δ
Epotek 302-3M	3.94	0.009
Epotek 302-3M + 20mmol/l $CuCl_2(2H_2O)$	3.72	0.009
Epotek 302-3M + 40mmol/l $CuCl_2(2H_2O)$	3.83	0.006
Epotek 302-3M + 80mmol/l $CuCl_2(2H_2O)$	3.42	0.008
Epotek 302-3M + 320mmol/l $CuCl_2(2H_2O)$	4.22	0.020
Epotek 302-3M + 640mmol/l $CuCl_2(2H_2O)$	4.52	0.095

Interestingly no variation in the zeta potential was seen between wet and dry PZT5H, which suggests that the surface water present may have been absorbed into the fluid. Similarly, surface coating the PZT with the ionic salt had no effect on zeta potential suggesting that the salt may have been displaced preferentially by diamine.

11.5 Coupling Agents

Coupling agents are widely used in composites processing to improve properties by some modification of the interface between filler and matrix. A number of different types exist, with silanes being perhaps the most common. For this study we decided to concentrate on an organo-metallic compound which had been recommended for use in piezoelectric composites. This was LICA38 (Kenrich Petrochemicals Inc., Bayonne, N.J.), neoalkoxy-dioctyl-pyrophosphato-titanate. This is a surface-active coupling agent, applied by solvent evaporation (isopropanol) on to the dry ceramic powder prior to use.

a) Visual observation of field-structuring of 1%wt.LICA38-coupled lead titanate and PZT5H. No discernible variation in the required frequency or field strength was observed. The coupled ceramic powders ordered as before.

b) Dielectric cure monitoring. Cure monitoring was performed, for comparison, using coupled and uncoupled PZT5H in Ciba-Geigy Araldite CY1300/HY1300 at 60°C. Relative permittivity and dielectric loss under these conditions are shown in Figures 11.2 and 11.3 respectively. Two notable effects appear when the LICA 38 coupling agent is used. The first is the order of magnitude reduction in the relaxation frequency, shown clearly in the dielectric loss curves. Secondly, there is a marked reduction in both permittivity and loss in the range 0-1kHz. As this is the result of surface modification, it is clear evidence to support the view that interfacial polarization dominates in this frequency range. Whether this is due to steric hindrance by 'hairy' particles or to chemical adsorption is not known.

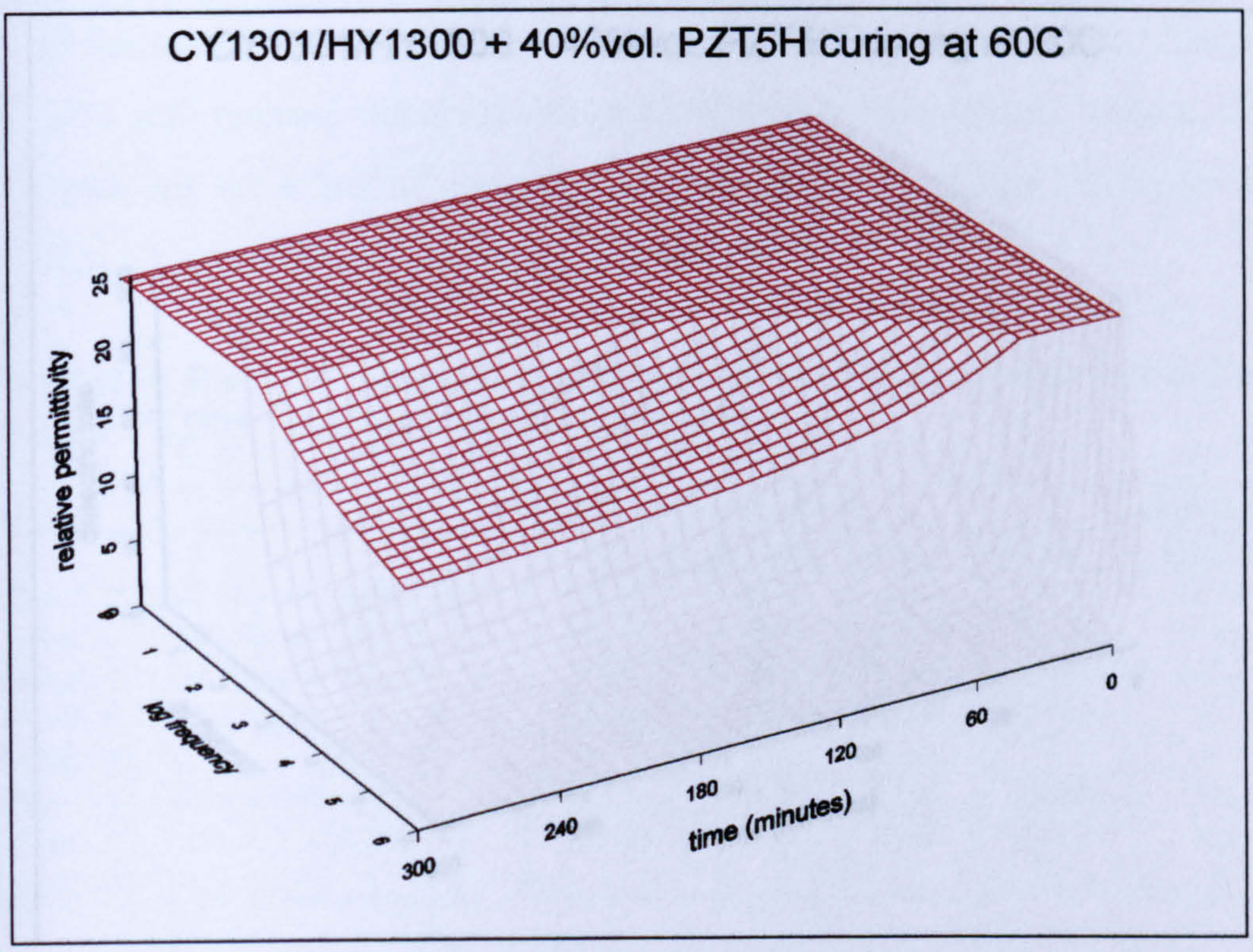

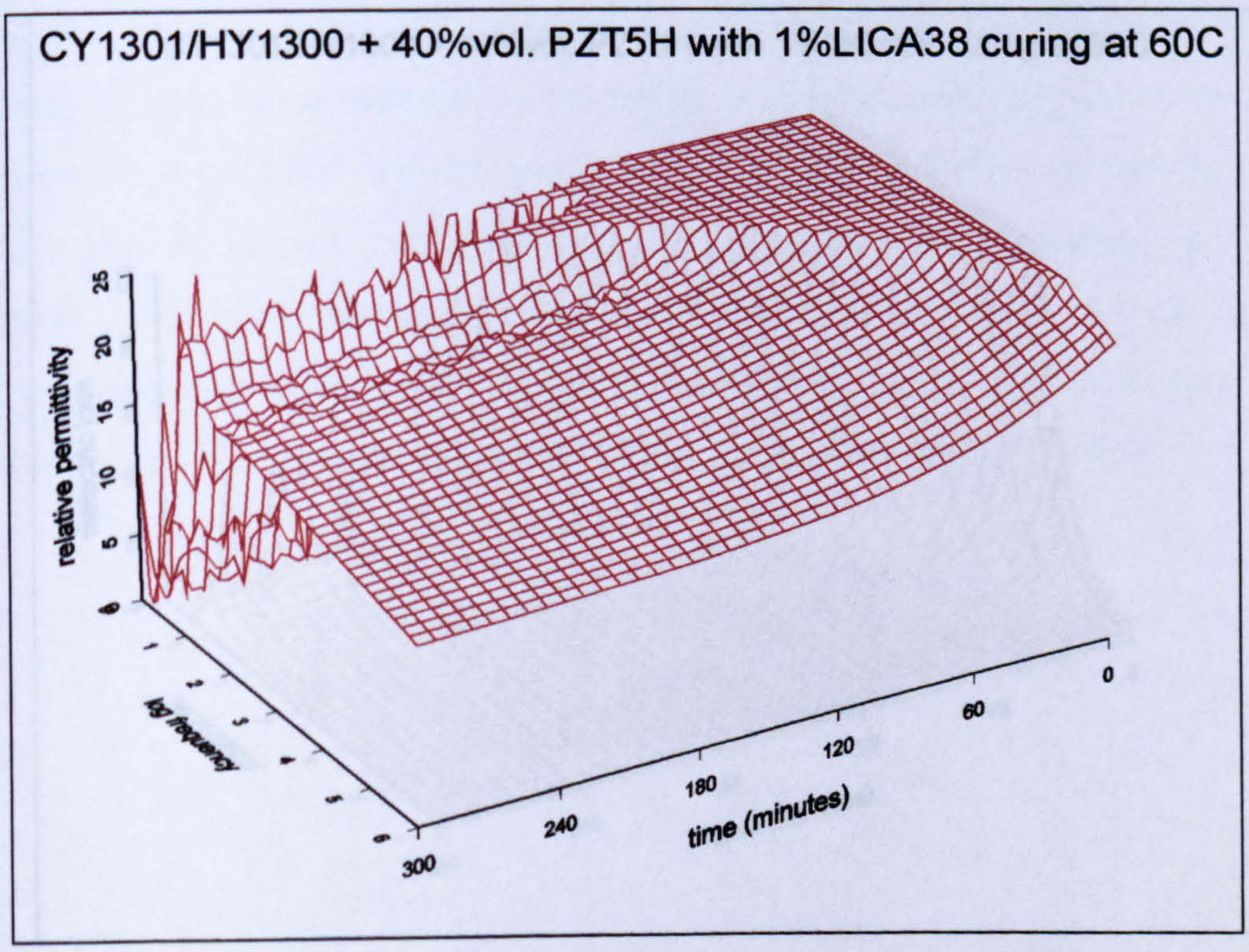

Figure 11.2: Dielectric cure monitoring of Araldite CY1301/HY1300 - Effect of coupling agent LICA38 on relative permittivity.

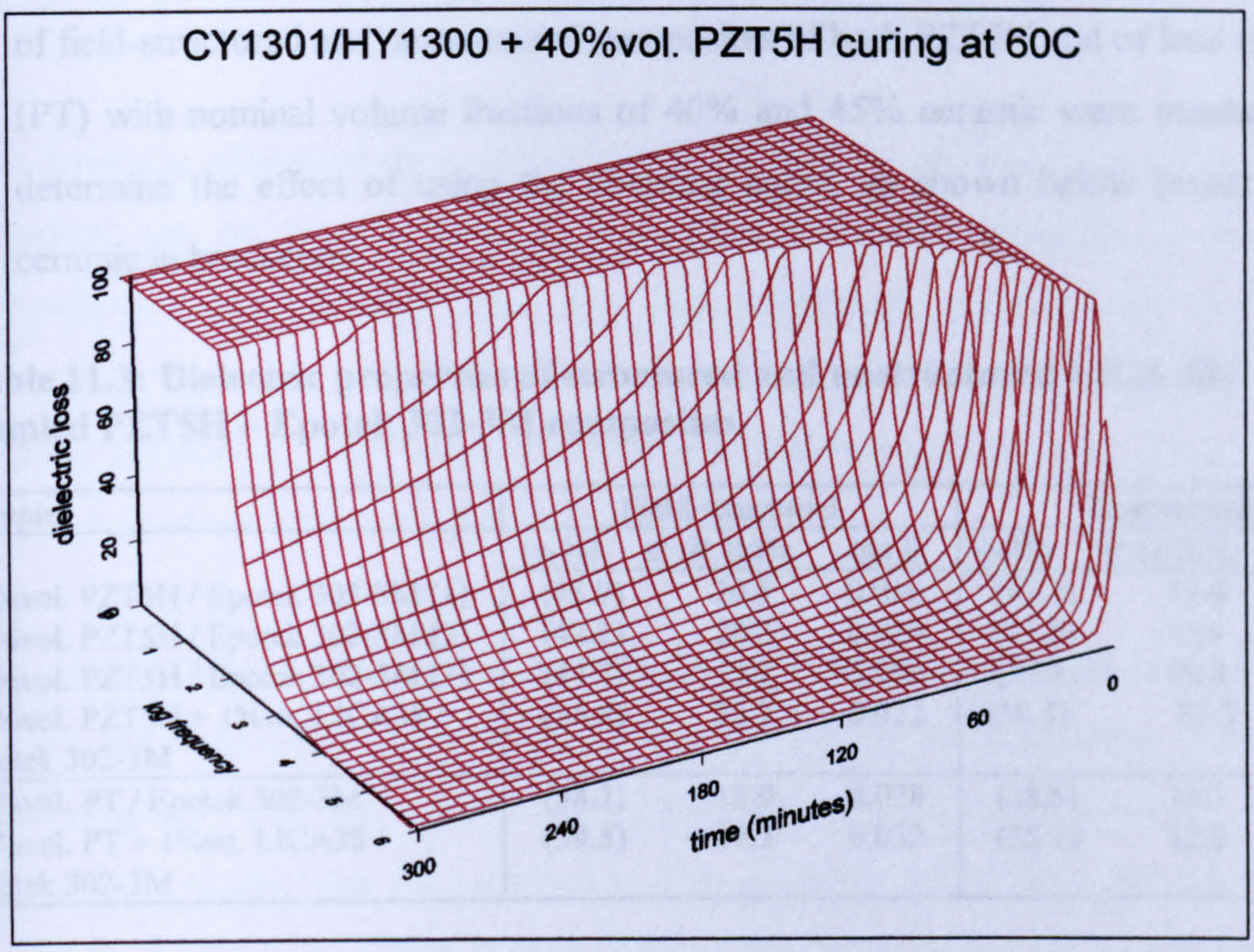

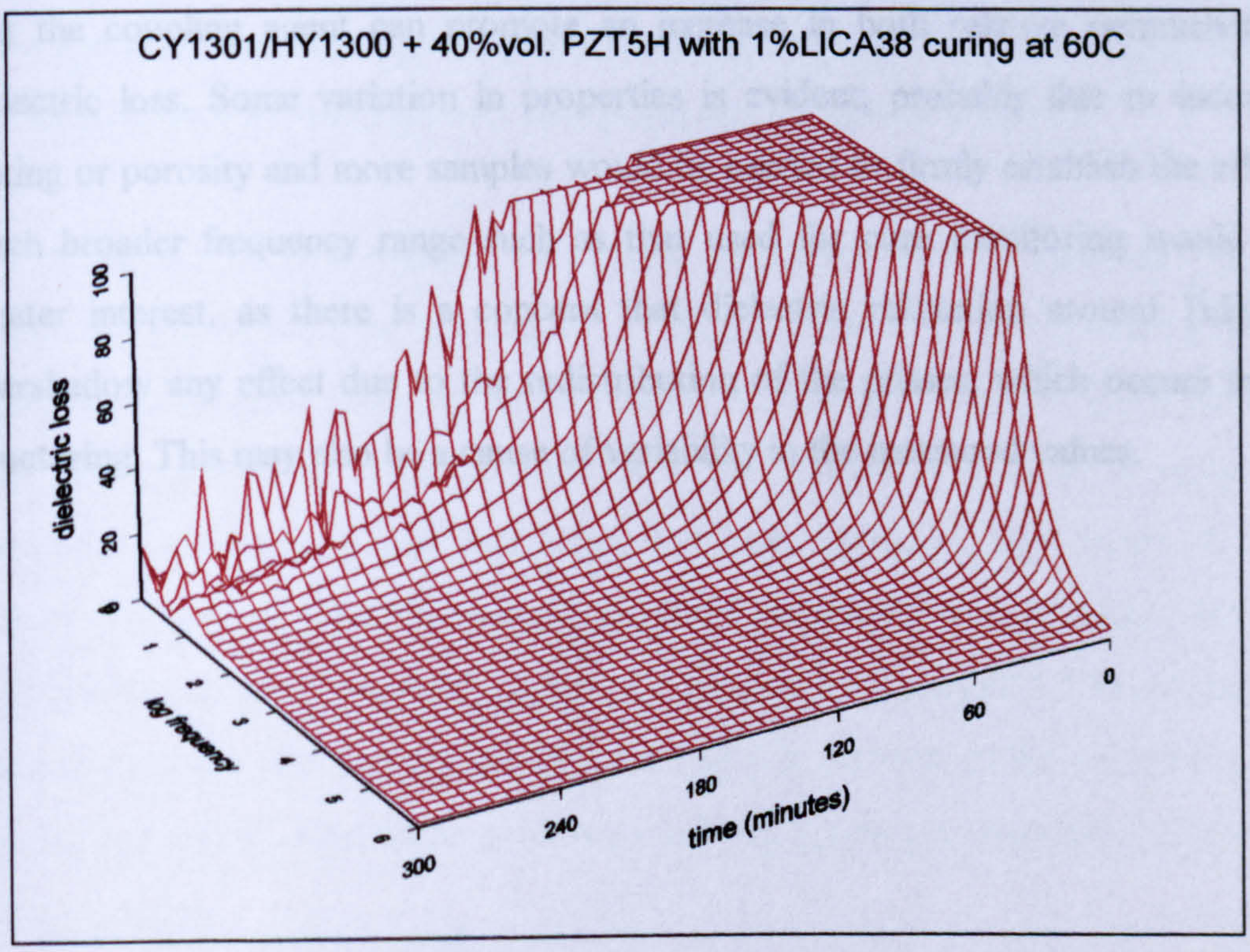

Figure 11.3: Dielectric cure monitoring of Araldite CY1301/HY1300 - Effect of coupling agent LICA38 on dielectric loss.

c) Properties of LICA38-coupled lead titanate composites. The dielectric properties of field-structured and unstructured composites of both PZT5H and of lead titanate (PT) with nominal volume fractions of 40% and 45% ceramic were measured to determine the effect of using the coupling agent, as shown below (exact vf % ceramic in brackets):

Table 11.3: Dielectric properties of structured and unstructured LICA 38-coupled PZT5H – Epotek 302-3M composites.

Sample	Field-structured			Unstructured		
	(v_f%)	ε' @ 1kHz	tan δ	(v_f%)	ε' @1kHz	tan δ
45%vol. PZT5H / Epotek 302-3M (1)	(45.9)	20.8	0.016	(42.3)	15.4	0.010
45%vol. PZT5H / Epotek 302-3M (2)	(42.2)	20.2	0.010	(41.0)	15.9	0.010
45%vol. PZT5H / Epotek 302-3M (3)	(44.7)	19.1	0.009	(37.8)	19.5	0.014
40%vol. PZT5H + 1%wt. LICA38 / Epotek 302-3M	(35.8)	23.7	0.022	(38.5)	23.5	0.086
40%vol. PT / Epotek 302-3M	(38.3)	18.0	0.028	(38.6)	14.3	0.025
40%vol. PT + 1%wt. LICA38 / Epotek 302-3M	(39.5)	19.5	0.032	(35.1)	12.8	0.023

Table 11.3 shows that the results are somewhat inconclusive, but do seem to indicate that the coupling agent can promote an increase in both relative permittivity and dielectric loss. Some variation in properties is evident, probably due to incomplete mixing or porosity and more samples would be needed to firmly establish the effect. A much broader frequency range such as that used for cure monitoring would be of greater interest, as there is a concern that dielectric relaxation around 1kHz may overshadow any effect due to the redistribution of the phases, which occurs in field-structuring. This may also be a cause of variability in the measured values.

12. Discussion

This work has addressed the central question of whether the electric-field structuring technique can be used to produce technologically useful materials. It has been demonstrated, for the first time, that dielectrophoresis can be used to induce anisotropic dielectric and piezoelectric properties in 55%vol. fraction ceramic / polymer composites. Previously it had been assumed that the technique was applicable only to low volume-fractions of filler [132].

This development has been made possible by considering the process in basic detail, using a model composite system of pure lead titanate powder suspended in an epoxy resin. Suspensions of the ceramic in the epoxy pre-polymer were monitored, as they were curing, to establish the variation in their dielectric properties. This information was used in conjunction with visual observations, made under the microscope, and viscosity measurements, to establish suitable processing conditions for the composite. The experience has been used to gain a deeper knowledge of this promising technique and its prospects for making novel two-phase and multiphase materials.

The formation of field-induced particulate structures from a randomly dispersed suspension can be modeled in terms of : i) the polarization force; ii) viscous drag; iii) electro-hydrodynamic force; iv) sedimentation; v) Brownian motion. When the applied field strength exceeds a certain threshold, the polarization force is sufficient to overcome viscous drag and suspended particles aggregate into 'pearl chains' or 'fibrils'. If the field strength exceeds a second threshold, then adjacent chains may coalesce into larger 'columnar' structures. Increasing the applied field strength in a step-wise fashion also favours the formation of thin-waisted, stable columns spanning the electrodes [34]. Alternating fields are preferred in order to suppress electrophoresis of the particles.

During the course of this study it has emerged that the applied field frequency used for structuring composites is likely to differ from the 'ideal alignment frequency' referred to in previous published work [2,31]. In practice, the correct frequency to use relates to the state of cure of the fluid and therefore is time and temperature dependent. The surface electrical properties of the particles are a further important consideration. Ions from the fluid are adsorbed onto the particle surfaces and this will result in some volume fraction and particle size dependence. Initial conductivity has been seen to be lower in 10% vol. suspensions of the model system compared to the neat resin.

The 'ideal alignment frequency' corresponds to the maximum dielectrophoretic force, measured using a rotational viscometer, [2] which is then taken to be the optimum frequency for structure formation. Whilst this approach is understandable, the method has an important weakness. It fails to recognise that in a weakly conducting fluid, such as a curing resin, two forces are acting which both contribute to the measured total, but are not compatible with for structure formation. The polarization force is structure-determining, but the electro-hydrodynamic force is responsible for fluid flow and is therefore disruptive. In addition, it is known that the dielectric properties of a suspension are strongly dependent on shear-rate (flow-modified permittivity) and hence the above method may not translate accurately to composites' production where the bulk of the fluid remains static. A reduction in the dielectrophoretic force at frequencies greater than the 'ideal alignment frequency' has been noted in many electrorheological fluids and has been ascribed to a relaxation of interfacial polarization.

To produce a field-structured composite it is important to suppress electrically-induced flow in the fluid. Electro-hydrodynamic flow is a function of the concentration of free-charge in suspension and the strength of the applied field. Hence it can be seen that the field strength and the field frequency used in structuring cannot be considered independently. As the resin cures, charge mobility is restricted and the upper frequency limit for flow to occur is progressively lowered. The dielectric loss curve of a suspension, measured under low field conditions, can be examined to reveal the

frequency range where EHD flow occurs, at any given time during the cure cycle. It is thus a valuable tool in predicting a suitable alignment frequency.

The optimum field frequency for chain formation is more difficult to assess, given that the ultimate goal is to establish useful properties in the composite. A reliable estimate can be gained by using the dielectric properties of the components to plot the frequency dependence of the polarization parameter. Chaining is favoured when the real part of the polarizability parameter approaches its maximum positive value. The estimated frequency can be substantiated by direct visual observations on low volume fraction suspensions. Calculations of the polarization force between particles, taken from published literature on electrorheological fluids, demonstrate that it increases dramatically as interparticle separation diminishes. It is therefore reasonable to assume that the field strength required to maintain the particulate structures that have formed is much lower than that required for their assembly from a random suspension. Hence chaining could better be regarded as a two stage process. The first stage is the development of the field-induced structure and the second is a holding phase, probably at a reduced field strength. During the holding phase, if surface chemistry is controlled, modification of the interlayer between particles may be possible; this might be achieved by dielectric or joule heating.

The interaction between strongly polarized particles at their minimum (sub-micron) separation is poorly understood. The field is uncertain, although it can clearly be very intense and it may well fluctuate. Electrochemical reactions, local temperature gradients, field-induced ionisation and tunnelling are factors to consider. Surface chemical and electrical properties are likely to assume prime importance, as they do in determining the material properties of the composite. Surface chemistry should therefore be viewed as another variable in the process. The surface-active coupling agent, LICA 38 has been shown to affect the properties of field-structured composites, but appears to have little influence on the structuring process. Gas is evolved where moisture is present and can lead to porosity in the composite.

Charged surfaces are known to attract counter-ions in solution. Although the zeta-potential of the particles in the model system appears to be low, ions will be attracted to the region between two polarised particles, and as a consequence, barrier layers of polymer may form. Surface contaminants, such as acetic acid, are known to accelerate the cure of epoxy resins and may also promote the formation of unwanted barrier layers.

One of the major pitfalls associated with the field-structuring technique is sedimentation. Sedimentation will occur to an unacceptable extent if the viscosity of the fluid is allowed to fall too low. In this study field-structuring is performed at a low temperature (40°C-55°C), allowing viscosity to rise gradually as the resin cures. This has the penalty of being relatively slow and it would be desirable to operate at a higher temperature to shorten the cure-time. An increase in temperature could take place during the 'holding' phase, mentioned above, paying due attention to the effect that raising the temperature has on polarization. For precise control it will be necessary to monitor temperature and to know the time/temperature/viscosity relationship of the resin in the early stages of cure. The observation that log viscosity is related linearly to the extent of conversion of the reactants (up to ~35%) [36] could be used to good effect. The reaction exotherm is a significant factor to consider.

There is a concern that irregularities in the chains that form will always lead to variability in the properties of field-structured composites. The variations are a consequence of the initial spatial distribution of particles in suspension and of the particle-size distribution, which can lead to chain branching. A narrow particle size distribution is clearly of benefit. A method of producing a PZT powder with a narrow particle size range (5-10 microns), by flux growth has been shown to be effective. The properties of this powder have not been studied in detail. Porosity has been a persistent problem in the composites produced to-date and is certainly the cause of some variability in the measured properties. Controlled application of pressure should be used to expel trapped or evolved gases.

Electrode design can be use to control field-induced microstructure. Patterned electrodes, which modify the spatial distribution of the applied field, are known to be an effective means of positioning chains to form an array. They may also prove effective in addressing the problem of variability. Switched electrode arrays could be used in an extension of the basic field-structuring process. These would detect the expected rise in current or capacitance associated with formation of a chain and exercise local control over the applied field. The rise in current is interfacial in origin. The same technique could be used to 'flip' individual fibres into a predetermined position and orientation. An ohmic contact at the fluid-electrode interface is desirable to limit the build-up of space-charge layers.

The chief problem with the composites produced to-date is that their relative permittivity (ε' = c.25) and piezoelectric coefficient (d_{33} = c.22pC/N) are lower than required. The presence of insulating layers of polymer between the particles is thought to be a significant limiting factor. The application of strong pressure during the holding phase may well be of benefit in breaking down these barriers. A more ambitious, though useful, approach would be to attempt to modify the barriers by using particles coated in a lossy thermoplastic, such as PVDF. Although this may be difficult to achieve technically, such a material would be very interesting. Amundson [133] has shown that a bulk alignment of microstructure can be induced in a diblock copolymer, polystyrene - poly (methyl methacrylate), by application of an electric field while cooling though the order-disorder transition temperature. Under suitable conditions electrostatic forces align the microstructure such that the lamellar surfaces are orientated parallel to the direction of the applied field. By the same analysis it is predicted that lamellae of PVDF could also be aligned. If it could be arranged that the c-axis lay in the direction of the applied field, the optimum orientation to achieve the maximum piezoelectric response, then the usefulness of the composite would be enhanced. PVDF has a low surface energy and it is also possible that some modification of the inter-layers might be achieved through dielectric heating.

Direct visual observations of the field-induced behaviour of suspensions have raised the possibility of a variety of novel two phase and multiphase materials. Chained structures can be formed within the confines of a second, immiscible fluid, which itself can form columns or stable streamers. This technique has been termed 'double dielectrophoresis'. Under certain conditions, shell-like structures can be formed. 'Pearl chains' can be made to form globally, in the field direction, around bubbles. Where particles of two different materials are mixed in a suspension, each material has its' own 'polarization signature'. When a field is applied segregation often occurs, each material forming separate chains.

12.1 Conclusion

At present there is comparatively little published literature regarding the electric-field structuring of composite materials, also referred to as 'dielectrophoretic assembly', although a large body of work exists in associated subject areas, such as electrorheological (ER) fluids, dielectrics and colloids. As a consequence, the technique has not yet received the attention it deserves and its potential has not been fully revealed.

This study has served to highlight that electric-field structuring is a highly complex technique. A large number of variables are involved and these do not have the same time, temperature and field frequency dependence. When considering the process as a whole it is important to remain focused on the requirement for improved properties in the composite. It is insufficient to simply concentrate on using the applied electric field to redistribute particles into an aligned or 'chained' microstructure. To define a processing schedule it is helpful to consider the procedure from two different standpoints and to reconcile the requirements of each. Firstly, by considering the basic polarization model it becomes relatively straightforward to determine the correct alignment field strength and frequency and to integrate these conditions into a typical cure-cycle. The question of predicting the material properties of the field-structured composites is more problematic. Hence the second standpoint concerns surface and interfacial chemistry. This relates not only to the initial components, but extends to

surface adsorption of ions from solution, adsorption onto polarized particles and to the use of surface-active coupling agents. These two standpoints share common ground regarding the surface electrical properties of the particles and the influence this may have on the redistribution of the phases. The study has highlighted that once structures are formed it is most probable that the magnitude of the applied field can be reduced and a holding phase commenced. For greatest efficiency, both field frequency and strength should be under active control.

Electric fields are a highly controllable and cost-effective energy source, which can be used to induce anisotropic properties in composite materials. It seems certain that their usefulness will extend beyond electrokinetic redistribution of the phases and that electrochemical reactions and localised dielectric heating will also prove to be important. A wide range of new dual-phase and multiphase materials can be expected. Hence it may well be that the term 'dielectrophoretic assembly' will come to be seen as one aspect of the more general description 'electric-field structuring'.

13. Further work

There is little doubt that a wide variety of field-induced structures can be formed using the field-structuring technique. A large number of material combinations will be possible. However, much remains to be done regarding the development of useful properties in the composites. The key areas to concentrate on are:

1. Surface chemistry and interlayers between particles. Thickness and chemical composition of barrier layers. Does this differ from the bulk? The use of surface-active agents and coated particles. Surface adsorption of ions onto polarized particles.
2. Controlled application of pressure during cure.
3. Patterned electrodes, which control the spatial distribution of the applied field.
4. Processing conditions. Given an accurate model, the field-structuring process will be readily adaptable to computer control. Applied field strength, frequency, applied pressure and temperature could all come under active control during the cure-cycle. A complete data set would be needed for the polymer regarding the time/temperature/viscosity relationship and how this relates to the extent of conversion of the reactants. Further investigation will reveal how this is modified by varying the volume fraction of the particulate phase. The data would then need to be related to the dielectric spectra of the resin and suspensions gathered under low voltage conditions and these further related to continuous current/voltage measurements made under processing conditions. The information could be used to establish the influence of temperature on particle polarization/chain formation and should eliminate the need for direct visual observations.
5. The properties of aligned PZT fibre/epoxy piezoelectric composites should be investigated. Field-aligning or 'flipping' fibres into a predetermined configuration could be achieved using a switchable electrode array as outlined in the preceding discussion. This could prove to be a significant method of manufacturing 1-3 fibre composites.

6. Field-structured composites will possess a range of anisotropic properties. Directional electrical, thermal, acoustic, electromagnetic and structural properties, amongst others, will be possible. Applications that would benefit from this new approach to processing should be sought out and actively pursued.
7. Corona poling of the piezoelectric composites should be investigated. It is uncertain whether dielectric breakdown during poling is exacerbated in the field-structured composites.
8. Development of novel materials and the 'double dielectrophoresis' technique.

In addition to the above there is a large body of published work which may profitably be considered with regard to future applications or to extending current knowledge of the process. Some useful references include Chen et al, on the properties of nanocrystalline PT powder and PT/ P(VDF-TrFe) 0-3 nanocomposites [134]; Newnham on 'smart' electroceramics [135] and the extensive amount of recent literature on conductive composites. Shiga has explored an electroviscoeleastic effect in polymer blends [136]. Hagenbuchle has studied chain formation and chain dynamics in a dilute magnetorheological fluid [137]. Hajimichael has conducted work into the development of epoxy foams [138]. Wu has introduced some interesting filler materials in his work on alumina-coated hollow glass spheres and alumina composites [139]. The topic of fluid / fluid interfaces has been studied by Carroll [140], Hajiloo [141], Boucher [142] and Bayramli [143]. Several interesting and imaginative applications of the use of electric fields in materials processing can be found in the work of Aksay [144], Trau [145] and Kim [146].

References

[1] Newnham R.E.; Skinner D.P.; Cross L.E. 'Connectivity and Piezoelectric-Pyroelectric Composites.' *Mat. Res. Bull.* 13 pp525-536 (1978)

[2] Randall C.A.; Bowen C.P.; Shrout T.R.; Messing G.L.; Newnham R.E.; 'Dielectrophoretic Assembly: A Novel Concept in Advanced Composite Fabrication'. *Proc. 4th Int. Conf. on Electrorheological Fluids 1993* (R.Tao, ed.) pp516-525 (1994), World Scientific Publ.

[3] Pohl H.A.; *J.Appl.Phys* 22 pp869- (1951); see also Pohl H.A. *Dielectrophoreseis: The Behaviour of Neutral Matter in Non-Uniform Electric Fields*, Cambridge University Press (1978)

[4] *An American National Standard* IEEE Standard on Piezoelectricity, ANSI/IEEE Std. 176-1987

[5] Newnham R.E.; Safari A.; Sa-gong G.; Giniewicz J.; 'Flexible Composite Piezoelectric Sensors'. *1984 IEEE Ultrasonics Symposium Proceedings*, Publ. IEEE, New York

[6] Tien T.-Y.; Carlson W.G. *J. Amer. Ceram. Soc.*, 45 pp567-571 (1962)

[7] Goodman G.; *J. Amer. Ceram. Soc.*, 36 pp368-372 (1953)

[8] Chilton J.A.; Goosey M.T.; 'Electroactive Polymer Composites'. *Polymer Composites* 3 No.2 pp71-88 (1990)

[9] Klicker K.A.; Biggers J.V.; Newnham R.E.; 'Composite of PZT and epoxy for hydrostatic transducer applications'. *J. Amer. Ceram.* Soc. 64 pp5- (1981)

[10] Klicker K.A.; Schultz W.A.; Biggers J.V.; 'Piezoelectric composites with 1-3 connectivity and a foamed polyurethane matrix'. *J. Amer. Ceram. Soc.* 65 C208 (1982)

[11] Haun M.J.; 'Transverse reinforcement of 1-3 and 1-3-0 PZT/polymer composites with glass fibres'. M.S. Thesis, Penn State University Pa. (1983)

[12] Savakus H.P.; Klicker K.A.; Newnham R.E.; 'Piezoelectric Transducers: A simplified fabrication procedure.' *Materials Research Bulletin* 16 pp677-680 (1981)

[13] Shorrocks N.M.; Brown M.E.; Whatmore R.W.; Ainger F.W.; 'Piezoelectric Composites for underwater transducers.' *Ferroelectrics* 54 pp215- (1984)

[14] Sa-gong S.; Safari A.; Jeng S.J.; Newnham R.E.; 'Poling Flexible Piezoelectric Composites.' *Ferroelectric Letts.* 5 pp131- (1986)

[15] Pauer L.A.; 'Flexible Composite Materials'. *IEEE Int. Conf. Rec. 1.* (1973)

[16] Banno H.; Saito S.; 'Piezoelectric Properties of Composites of Synthetic Rubber and $PbTiO_3$ or PZT'. *Jap. J. Appl. Phys.* 22 (Suppl. 22-2) pp69- (1983)

[17] Monroe D.L.; Blum J.B.; Safari A.; 'Sol-gel derived $PbTiO_3$ Piezoelectric Composites'. *Ferroelectrics Letts.* 5 pp39- (1986)

[18] Ting R.Y.; 'Composite Piezoelectric Materials for Transduction'. *Applied Acoustics* 41 pp325-355 (1994)

[19] Das-Gupta D.K. and Dias C.; 'Piezoelectric Properties of 0-3 Ceramic/Polar Polymer Composites'. *Mat. Res. Soc. Symp. Proc.* 276 pp25-29 (1992)

[20] Garner G.M.; Shorrocks N.M.; Whatmore R.W.; Goosey M.T.; Seth P.; Ainger F.W.; '0-3 Piezoelectric Composites for Large Area Hydrophones'. *Ferroelectrics* 93 pp169-176 (1989)

[21] Yamashita Y.; Yokoyama K.; Honda H.; Takahashi T.; Jap. *J. Appl. Phys.* 20 (Suppl. 20-4) pp183-187 (1981)

[22] Takeuchi K.; Damjanovic D.; Gururaja T.R.; Jang S.J.; Cross L.E.; 'Electromechanical Properties of Calcium Modified Lead Titanate Ceramics'. Materials Research Laboratory, The Pennsylvania State University, University Park, PA 16802

[23] United States Patent. No. 5169551 (Dec.8th 1992)

[24] Galgoci E.C.; Runt J.; 'Interfacial Adhesion in PZT-Epoxy Composites'. *Ferroelectrics* 70 pp205-212 (1986)

[25] Lee Y.H.; Huan M.J.; Safari A.; Newnham R.E.; 'Preparation of $PbTiO_3$ for a flexible 0-3 piezoelectric composite'. *Proc 6th IEEE Int. Symp. on Applications of Ferroelectrics* pp318-322 (1986) IEEE, N.Y.

[26] Giniewicz J.R.; Newnhan R.E.; Safari A.; Moffat D.; '(Pb,Bi)(Ti,Fe,Mn)O_3 /Polymer Composite for Hydrophone Applications'. *Ferroelectrics* 73 pp405-417 (1987)

[27] Chilton J.A.; Garner G.M.; Whatmore R.W.; Ainger F.W.; '0-3 Composite Sensitivity'. *Ferroelectrics* 109 pp217-222 (1990)

[28] Chilton J.A.; Garner G.M.; Twiney R.; Whatmore R.W.; 'High Moisture Resistant Electroactive Composites'. *Ferroelectrics* 127 pp197-202 (1992)

[29] Randall C.A.; Miyazaki S.; More K.L.; Bhalla A.S.; Newnham R.E.; 'Structure-Property Relationships in Dielectrophoretically Assembled $BaTiO_3$ Nanocomposites'. *Materials Letters* 15 pp26-30 (1992)

[30] Miller D.V.; Randall C.A.; Bhalla A.S.; Newnham R.E.; Adair J.H.; 'Electrorheological Properties of $BaTiO_3$ Suspensions', *Ferroelectrics Letters* 15 pp141-151 (1993)

[31] Bowen C.P.; Bhalla A.S.; Newnham R.E.; Randall C.A.; 'An Investigation of the Assembly Conditions of Dielectric Particles in Uncured Thermoset Polymers'. *J. Mater. Res.* 9 No.3 pp781-788 (March 1994)

[32] Bowen C.P.; Shrout T.R.; Newnham R.E.; Randall C.A.; 'A Study of the Frequency Dependence of the Dielectrophoretic Effect in Thermoset Polymers'. *J. Mater. Res.* 12 No.9 pp2345-2356 (Sept.1997)

[33] Bowen C.P.; Newnham R.E.; Randall C.A.; 'Dielectric Properties of Dielectrophoretically Assembled Particulate-polymer Composites'. *J. Mater. Res.* 13 No.1 pp205-210 (Jan.1998)

[34] Blackwood K.M.; Block H.; Rattray P.; Tsangaris G.; Vorobiev D.N.; 'The Polarization Structuring and Rheology of ER Fluids'. *Proc. 4th Int. Conf. on Electrorheological Fluids 1993* (R.Tao, ed.) pp3-21 (1994), World Scientific Publ.

[35] Halsey T.C.; 'Electrorheological Fluids'. *Science* 258 pp761-766 (Oct.30th 1992)

[36] Maistros G.M. and Bucknall C.B.; 'Modelling the dielectric behaviour of epoxy resin blends during curing'. *Polymer Engineering and Science* 34 No.20 pp1517-1528 (!994)

[37] Block H.; Kelly J.P.; Qin A.; Watson T.; 'Materials and Mechanisms in Electrorheology'. *Langmuir* 6 pp6-14 (1990)
[38] Xu Y.; 'Ferroelectric Materials and their Applications'. (1991) North Holland, Elsevier Science Publ., Amsterdam
[39] Moorthy S.G.; Kumar F.J.; Balakumar S.; Subramanian C.; 'Growth of Lead Titanate Single Crystals and their Characterization'. *J. Kor. Phys. Soc.* 32 ppS1214-1216 (Feb. 1998)
[40] Sun B.N.; Huang Y.; Payne D.A.; 'Growth of Large $PbTiO_3$ Single Crystals by a Self-flux Technique'. *J. Crystal Growth* 128 pp867-870 (1993)
[41] del Olmo L.; Calzada M.L.; 'Electromechanical Behavior of Pure PbTiO3 Ceramics'. *Ultrasonics Int. 89 Conf. Proc. pp600-605* (1989)
[42] Lee Y.H.; Haun M.J.; Safari A.; Newnham R.E.; 'Preparation of $PbTiO_3$ Powder for a Flexible 0-3 Piezoelectric Composite'. Materials Research Laboratory, The Pennsylvania State University, University Park, PA 16802
[43] Kamiya K.; Honda H.; Nasu H.; 'Sol-gel Processing of $PbTiO_3$ Ceramic Fibers'. *Nippon Seramikkusu Kyokai Gakujutsu Ronbunshi* 98 pp759-764 (1990)
[44] Kim C.E.; Park Y.I.; Lee H.W.; 'Preparation of $PbTiO_3$ Fibres using Triethanolamine-complexed Alkoxide'. *J. Mats. Sci. Letts.* 16 pp96-100 (1997)
[45] Jaffe B.; Cook W.R.Jr.; Jaffe H.; *Piezoelectric Ceramics* (1971) Academic Press, London
[46] Fushimi S.; Ikeda T.; 'Phase Equilibrium in the System $PbO-TiO_2-ZrO_2$'. *J. Amer. Ceram. Soc.* 50 No.3 pp129-132 (1967)
[47] Takahashi S.; 'Sintering $Pb(Zr,Ti)O_3$ Ceramics at Low Temperature'. *Jpn. J. Appl. Phys.* 19 No.4 pp771-772 (1980)
[48] Clarke R.; Whatmore R.W.; 'The Growth and Characterisation of $PbZrTi_{(1-x)}O_3$ Single Crystals'. *J. Crystal Growth* 33 pp29-38 (1976)
[49] Scott B.A.; Burns G.; 'Crystal Growth and Observation of the Ferroelectric Phase of $PbZrO_3$'. *J. Amer. Ceram. Soc.* 55 No.7 pp331-333 (July 1972)
[50] Kingon A.I.; Clark J.B.; 'Sintering of PZT Ceramics: I Atmosphere Control, II Effect of PbO Content on Densification'. *J. Amer. Ceram. Soc.* 66 No.4 pp253-260 (1983)
[51] Sandonnini C.; *Atti Reale Accad. Sci. Torino* 22 [I] pp959- (1914)
[52] Yoshikawa Y.; Selvaraj U.; Moses P.; Witham J.; Meyer R. Shrout T.; '$Pb(Zr,Ti)O_3$ [PZT] Fibers – Fabrication and Measurement Methods'. *J. Intell. Mats. Syst. And Struct.* 6 pp152-158 (March 1995)
[53] Kimura T.; Takenaka A.; Mifune T.; Hayashi Y.; Yamaguchi T.; 'Preparation of Needle-like $TiZrO_4$ and PZT Powders'. *J. Mats. Sci.* 27 pp1479-1483 (1992)
[54] Wen W.; Tam W.Y.; Sheng P.; 'Fabrication of PZT Microspheres for Application in Electrorheological Fluids'. 17 pp419-421 (1998)
[55] Enns J.B. and Gillham J.K.; *J. Appl. Pol. Sci.* 'Time-Temperature-Transformation (TTT) Cure Diagram: Modeling the Cure Behavior of Thermosets'. 28 pp.2567-2591 (1983)
[56] DiBenedetto A.T. in Neilsen L.E.; *J. Macromol. Sci., Rev. Macromol. Chem.* 69 C3 (1969)

[57] Smith I.T.; 'The Mechanism of the Cross-linking of Epoxide Resins by Amines'. *Polymer* 2 pp95-108 (1961)
[58] Shechter L., Wynstra J. and Kurkjy R.P.; *Ind. Eng. Chem.*, 48 pp94- (1956)
[59] Wisanrakkit G. and Gillam J.K.; 'The Glass Transition Temperature (T_g) as an Index of Chemical Conversion for a High T_g Amine/Epoxy System: Chemical and Diffusion-Controlled Reaction Kinetics'. *J. Appl. Pol. Sci.* 41 pp2885-2929 (1990)
[60] Williams M.L., Landel R.F. and Ferry J.D.; *J. Am. Chem. Soc.*, 77 pp3701-(1955) also [66]
[61] Havilcek I. and Dusek K. in *Crosslinked Polymers,* Eds. Sedlacek B.and Kahovic J.; pp417-424 Walter de Gruyter, N.Y. (1987)
[62] Roller M.B.; 'Rheology of Curing Thermosets'. *Polym. Eng. Sci.* 26 pp432-(1986)
[63] Tajima Y.A.; Crozier D.G.; 'Thermokinetic Modeling of an Epoxy Resin 1. Chemoviscosity'. *Polymer Engineering and Science* 23 No.4 pp186-190 (1983)
[64] Tajima Y.A.; Crozier D.G.; 'Chemorheology of an Amine-Cured Epoxy Resin'. *Polymer Engineering and Science* 26 No.6 pp427-440 (1986)
[65] Flory P.J.; *Principals of Polymer Chemistry,* (1953) Cornell University Press, Ithaca, N.Y.
[66] Ferry J.D.; *Viscoelastic Properties of Polymers* 3rd Edition (1980) Wiley, N.Y.
[67] Khusid B.; Acrivos A.; 'Effects of Conductivity in Electric-field-induced Aggregation In ER Fluids'. *Journal of Physics: Physical Review E* 52 pp1669-1693 (1995)
[68] Tabellout M.; Randrianantoandro H.; Emery J.R.; Durrand D.; Hayward D.; Pethrick R.A.; 'Real-time Dielectric Studies of network Formation in Thermally Activated Epoxy-Amine and Isocyanate-Triol Systems'. *Polymer* 36 No.24 pp4547-4552 (1995)
[69] Lairez D.; Emery J.R.; Durrand D.; Hayward D.; Pethrick R.A.; 'Real Time Dielectric Measurements of Network Formation in a Crosslinked Epoxy Resin System'. *Plastics, Rubber and Composites Processing and Applications* 16 pp231-238 (1991)
[70] Kranbuehl D.E.; Delos S.E.; Jue P.K.; 'Dielectric Properties of the Polymerization of an Aromatic Polyamide'. *Polymer* 27 pp11-18 (Jan.1986)
[71] Kranbuehl D.E.; Senturia S.D.; Sheppard N.F.; *Adv. Polym. Sci.* 80 1- (1986)
[72] Kranbuehl D.E.; Delos S.E.; Hoff M.; Haverty P.; Freeman W.; Hoffman R.; Godfrey J.; ' Use of the Frequency Dependence of the Impedance to Monitor Viscosity during Cure'. *Polymer Engineering and Science* 29 No.5 pp285-289 (mid-March1989)
[73] Scaife B.K.P.; *Principles of Dielectrics* (1989) Oxford Science Publications
[74] McCrum N.G.; Read B.E.; Williams G.; *Anelastic and Dielectric Effects in Polymeric Solids* (1967) John Wiley
[75] Day D.; Lewis T.J.; Lee H.; Senturia S.; *J. of Adhesion*, 18 pp73- (1985)
[76] Kao K.C. and Hwong W.; *Electric Transport in Solids* (1981) Pergamon Press
[77] North A.M.; Pethrick R.A.; Wilson A.D.; *Polymer* 'Dielectric Properties of Phase-separated Polymer Solids'. 19 pp913-930 (1978)

[78] Böttcher C.J.F.; *Theory of Electric Polarization* (1978) Elsevier Scientific
[79] Tsangaris G.M.; Psarras G.C.; Kouloumbi N.; 'Electric Modulus and Interfacial Polarization in Composite Polymeric Systems'. *Journal of Materials Science* 33 pp2027-2037 (1998)
[80] Winslow W.M.; 'Induced Fibrillation of Suspensions'. *Journal of Applied Physics* 20 pp1137-1140 (Dec.1949)
[81] Zukoski C.F.; 'Material Properties and the Electrorheological Response'. *Ann. Rev. Mats. Sci.* 23 pp45-78 (1993)
[82] *Proceedings of the 4th International Conference on Electrorheological Fluids* - Ed. R.Tao (1994) World Scientific
[83] *Proceedings of the 5th International Conference on Electrorheological Fluids, Magnetorheological Suspensions and Associated Technology* - Ed. R.Tao (1996) World Scientific
[84] Tao R.; 'Order parameters and phase transitions in ER fluids' in *Proceedings of the 3rd International Conference on Electrorheological Fluids* - Ed. R.Tao (1992) World Scientific
[85] Klingenberg D.J.; van Swol F.; Zukoski C.F.;'The Small Shear-rate Response of Electrorheological Suspensions –I Simulation in the Point Dipole Limit, II Extension beyond the Point Dipole Limit.' *J. of Chem. Phys.* 94 pp6160-6178 (1991)
[86] Jones T.B.; 'Multipole Corrections to the Dielectrophoretic Force'. *IEEE Transactions on Industry Applications* 1A-21 No.4 pp930-934 (July-Aug.1985)
[87] Pohl H.A.; *Dielectrophoresis* (1978) Cambridge University Press
[88] Pethig R.; Huang Y.; Wang X-B.; Burt J.P.H.; 'Positive and Negative Dielectrophoretic Collection of Colloid Particles using Interdigitated Castellated electrodes'. *J. Phys. D: Appl. Phys.* 24 pp881-888 (1992)
[89] Hanai T.; *Kolloid Z.* 171 pp23-31 (1960)
[90] Khusid B.; Acrivos A.; 'Effects of Interparticle Interactions on Dielectrophoresis in Colloidal Suspensions'. *Journal of Physics E: Phys.Rev.* 54 No.5 pp5428-5435 (Nov.1996)
[91 Trau M.; Sankaran S.; SavilleD.A; Aksay I.A.; 'Electric-field-induced Pattern Formation in Colloidal Dispersions' *Nature* 374 pp437-439 (30th Mar.1995)
[92] Melrose J.R.; *Mol.Phys.* 76 pp635- (1992)
[93] Gast A.P.; Zukoski C.F.; 'Electrorheological Fluids as Colloid Suspensions'. *Advances in Colloid and Interface Science* 30 pp153-202 (1989)
[94] Gardner J.W.; Bartlett P.N.; 'Potential Applications of Electropolymerised Thin Organic Films in Nanotechnology'. *Nanotechnology* 2 pp19-32 (1991)
[95] Rattray P.; 'Pulsed Flow and Time-resolved Dielectric Spectroscopy of Electrorheological Fluids'; PhD Thesis, Cranfield University, U.K. (1994)
[96] Landau L.D.; Lifshitz E.M.; *Electrodynamics of Continuous Media* 2nd Ed.. (1984) Pergammon Press N.Y.
[97] Ramos A.; Morgan H.; Green N.G.; Castellanos A.;'AC Electrokinetics: A Review of Forces in Microelectrode Structures.' *J. Phys. D: Appl. Phys.*, 31 pp2338-2353 (1998)

[98] Trau M.;Sankaran S.; Saville D.A.; Aksay I.A.; 'Pattern Formation in Nonaqueous Colloidal Dispersions via Electrohydrodynamic Flow'. *Langmuir* 11 No.12 pp4665-4672 (1995)

[99] Rhodes P.H.; SnyderR.S.; Roberts G.L.; 'Electrohydrodynamic Distortion of Sample Streams in Continuous Flow Electrophoresis'. *J. of Coll. and Int. Science* 129 No.1 pp78-90 (Apr.1989)

[100] Saville D.A.; 'Electrodynamic Deformation of a Particulate Stream by a Transverse Electric Field'. *Physical Review Letters* 71 No.18 pp2907-2910 (1993)

[101] Halsey T.C.; Toor W.R.;'Structure of Electrorheological Fluids'. Phys.Rev.Letts. 65 No.22 pp2820-2823 (1990)

[102] Toor W.R.; Halsey T.C.;'Bulk and Surface Energies of Dipolar Lattices'. Physical Rev.A 45 pp8617-8623 (1992)

[103] Park C.; Robertson R.E.;'Aligned Microstructure of some Particulate Polymer Composites obtained with an Electric Field'. *J.of Materials Science* 33 pp3541-3553 (1998)

[104] Miller R.D.; Jones T.B.; 'Frequency -dependent Orientation of Ellipsoidal Particles in AC Electric Fields'. *9th Ann. IEEE-EMBS Conf.-Boston* (Nov.1987)

[105] Garton C.G.; Krasucki Z.;'Bubbles in Insulating Liquids: Stability in an Electric Field'. *Proceedings of the Royal Society of London* 280A pp211-226 (1964)

[106] Pethig R.; *Critical Rev. Biotech.* 16 pp331-348 (1996)

[107] Green N.G.; Morgan H.; 'Separation of Submicrometer Particles using a Combination of Dielectrophoretic and Electrohydrodynamic Forces'. *J. Phys. D: Appl. Phys.* 31 L25-L30 (1998)

[108] Benguigui L.; Lin I.J.; 'The Dielectrophoresis Force'. *Amer. J. Phys.*, 54 (5) pp447-450 (1986)

[109] Herbert J.M.; *Ceramic Dielectrics and Capacitors* (1985) Gordon and Breach Science Publishers, O.P.A. (Amsterdam) B.V.

[110] Ahmed N.H.; Srinivas N.N.; 'Review of Space Charge Measurement in Dielectrics'. *IEEE Transactions on Dielectrics and Electrical Insulation* 4 No.5 pp644-655 (1997)

[111] van Beek L.K.H.; 'Dielectric Behaviour of Heterogenous Systems'. *Progress in Dielectrics* 7 pp69-114 (1967)

[112] Yamada T.; Ueda T.; Kitayama T.; 'Piezoelectricity of a High-Content Lead Zirconate Titanate / Polymer Composite'. *J. Appl. Phys.* 53(6) pp4328-32 (1982)

[113] Banno H.; Saito S.; 'Piezoelectric Properties of Composites of Synthetic Rubber and $PbTiO_3$ or PZT'. *Jap. J. Appl. Phys.* 22 suppl.22-2 pp67-69 (1983)

[114] Jayasundere N.; Smith B.; *J. Appl. Phys.* 73 pp2462-2466 (1993)

[115] Pardo L.; Mendiola J.; Alemany C.; 'Theoretical Treatment of Ferroelectric Composites using Monte Carlo Calculations'. *J. Appl. Phys.* 64 (10) pp5092-5097 (1988)

[116] Geigenmüller U.; Mazur P.;'The Effective Dielectric Constant of a Dispersion of Spheres'. *Physica* 136A pp316-369 (1986) Elsevier Science Publ. B.V.

[117] Felderhof B.U.; 'Bounds for the Effective Dielectric Constant of a Suspension of Spherically Symmetric Particles'. and 'Bounds for the Effective Dielectric Constant of a Suspension of Uniform Spheres'. *J. Phys. C : Solid State Physics* 15 pp3943-3951 and pp3953-3966 (1982)
[118] Schoch Jr. K.F.; Partlow D.P.; Krause R.F.;'Assessment of the Degree of Poling in 0-3 Piezoelectric Composites by X-ray Methods'. *Ferroelectrics* 77 pp39-46 (1988)
[119] Das-Gupta D.; Doughty K.; *J. Appl. Phys.* 49 pp4601-4603 (1978)
[120] Waller D.; Igbal T.; Safari A.; *J. Amer. Ceram. Soc.* 72 pp322-324 (1989)
[121] Setiadi D.; Regtien P.; Wübbenhorst M.;'The Step-wise Poling of VDF/TrFE Copolymers'. *Ferroelectrics* 186 pp255-258 (1996)
[122] Furukawa T.; Lovinger A.; Davis G.; Broadhurst M.; *Macromolecules* 16 pp1885-1890 (1983)
[123] Zipfel G.G.; *Bell Labs.Rec.* (11-13 April 1983)
[124] Levassort F.; Lethiecq M.; Certon D.; Patat F.; 'A Matrix Method for Modeling Electroelastic Moduli of 0-3 Piezo-Composites'. *IEEE Transactions on Ultrasonics, Ferroelectrics and Frequency Control* 44(2) (1997)
[125] Miller K.T.; Zukoski C.F.; '*The Mechanics of Nanoscale Suspensions*' in *Studies in Surface Science and Catalysis* 103 pp23-55 (1996) Elsevier Science B.V.
[126] Russel W.B.; Saville D.A.; Schowalter W.R.; *Colloidal Dispersions* (1989) Cambridge University Press
[127] Israelachvili J.N.; *Intermolecular and Surface Forces*-2nd Ed. (1992) Academic Press
[128] Bowen W.R.; Sharif A.O.; 'Long-Range Electrostatic Attraction Between Like-Charged Spheres in a Charged Pore'. *Nature* 393 pp663-665 (also Grier D.G.; pp621-623) (18thJun1998)
[129] Block H.; '*A Dielectric Study of Order in Electric Field Aligned Dispersions and its Application to Electrorheology*' EPSRC Report GR/K15947 (1999)
[130] Boissy C.; Foulc J.N.; Atten P.; 'Influence of the Electric-Field Frequency on the Properties of Electrorheological Fluids'. *Proc. Int'l. Conf. on ER Fluids 1993* Ed.R.Tao. pp453-462 World Science (1994)
[131] Shahidi M.; Hasted J.B.; Jonscher A.K.; *Nature* 258 pp595- (1975)
[132] Janas V.F.; Safari A.; 'Overview of Fine-Scale Piezoelectric Ceramic/Polymer Composite Processing.' *J. Amer. Ceram. Soc.* 78 pp2945-2955 (1995)
[133] Amundson K.; Helfand E.; Davis D.D.; Quan X.; Patel S.S.; 'Effect of an Electric-Field on Block Copolymer Microstructure'. *Macromolecules* 24 pp 6546-6548 (1991)
[134] Chen Y.; Chan H.L.; Choy C.L.; 'Properties of Nanocrystalline PT Powder and PT/P(VDF-TrFE) 0-3 Nanocomposites.' *Proceedings of IEEE Int. Symp. On the Applications of Ferroelectrics (ISAF '96)* (1997) IEEE, N.Y.
[135] Newnham R.E.; Ruschau G.R.; 'Smart Electroceramics'. *J. Amer. Ceram. Soc.* 74 pp463-480 (1991)
[136] Shiga T.; Okada A.; Kurauchi T.; 'Electroviscoelastic Effect of Polymer Blends Consisting of Silicone Elastomer and Semiconducting Polymer Particles'. *Macromolecules* 26 pp6958-6963 (1993)

[137] Hagenbüchle M.; Liu J.; 'Chain Formation and Chain Dynamics in a Dilute Magnetorheological Fluid'. *Applied Optics* 36 No.30 (20thOct.1997)
[138] Hajimichael M.; Lewis A.; Scholey D.; Simmonds C.; 'Investigation and Development of Epoxy Foams'. *British Polymer Journal* 18 No.5 pp307-311 (1986)
[139] Wu S.J.; De Jonge L.C.; 'Alumina-coated Hollow Glass Spheres / Alumina Composites'. *Journal of Materials Science* 32 pp6075-6084 (1997)
[140] Carroll B.J.; Lucassen J.; 'Effect of Surface Dynamics on the Process of Droplet Formation from Supported and Free Liquid Cylinders'. *J. of the Chem. Soc. – Faraday Transactions I* 70 pp1228-1239 (1974)
[141] Hajiloo A.; Ramamohan T.R.; Slattery J.C.; 'Effect of Interfacial Viscosities on the Stability of a Liquid Thread'. *J. of Coll. And Interface Science* 117 No.2 pp384-393 (Jun.1987)
[142] Boucher E.A.; 'Capillary Phenomena: Properties of Systems with Fluid/Fluid Interfaces'. *Rep. Prog. Phys.* 43 pp497-546 (1980)
[143] Bayramli E.; Abou-Obeid A.; van de Ven T.G.M.; 'Liquid Bridges between Spheres in a Gravitational Field'. *J. of Coll. And Interface Science* 116 No.2 pp490-502 (Apr.1987)
[144] Aksay I.A.; Trau M.; Manne S.; Honma I.; Yao N.; Zhou L.; Fenter P.; Eisenberger P.M.; Gruner S.M.; 'Biomimetic Pathways for Assembling Inorganic Thin Films'. *Science* 273 pp892-898 (16thAug1996)
[145] Trau M.; Saville D.A.; Aksay I.A.; 'Assembly of Colloidal Crystals at Electrode Interfaces'. *Langmuir* 13 pp6375-6381 (1997)
[146] Kim E.; Xia Y.; Whitesides G.M.; 'Polymer Microstructures Formed by Moulding in Capillaries'. *Nature* 376 pp581-584 (17thAug1995)

Appendix A.

Comparison of the properties of candidate transducer materials for hydrophone devices (published work).

Material	Density kgm^{-3}	ε_r	d_{33} pCN^{-1}	g_{33} mVN^{-1}	d_h pCN^{-1}	g_h mVm^{-1}	$d_h.g_h.10^{15}$ m^2N^{-1}	Ref. No.
PZT	7900	1800	450	28	40	2.5	100	[5]
$PbTiO_3$	7500	230	53	26	47	23	1080	[6]
$PbNb_2O_6$	6330	225	85	42	67	33	2200	[7]
PVDF	1800	12	-30	-280	-10	-100	1000	[8]
1-3 Composite PZT/Epoxy	1370	54	150	313	27	56	1536	[9]
1-3 Composite PZT/ PU foam	930	41	180	495	73	210	15330	[10]
1-2-3 Comp. PZT/PU-foam/ Glass reinforced	1250	104	213	231	203	220	44700	[11]
Diced PZT/ 25% Epoxy		330	290	100	52	18	935	[12]
Diced PZT/ 25% Epoxy Glass reinforced		640			136	24	3264	[13]
0-3 Composite PZT/ Carbon / Epoxy		120	55	155	30	90	2700	[14]
0-3 Composite PZT/PU		26	10	43	2	8	10	[15]
0-3 Composite PT/Chloroprene		45	65	163	40	100	4000	[16]
0-3 Composite PT/Epoxy		48	60	141	42	96	4032	[17]
0-3 Composite PT/Rubber 'Piezorubber'	5537	37	46		41	124	5084	[18]
0-3 Composite Ca-modified PT/PVDF	6890	207			62	33	2066	[19]

Appendix B.

Structured Composites Processing Unit – Electrical Diagrams.

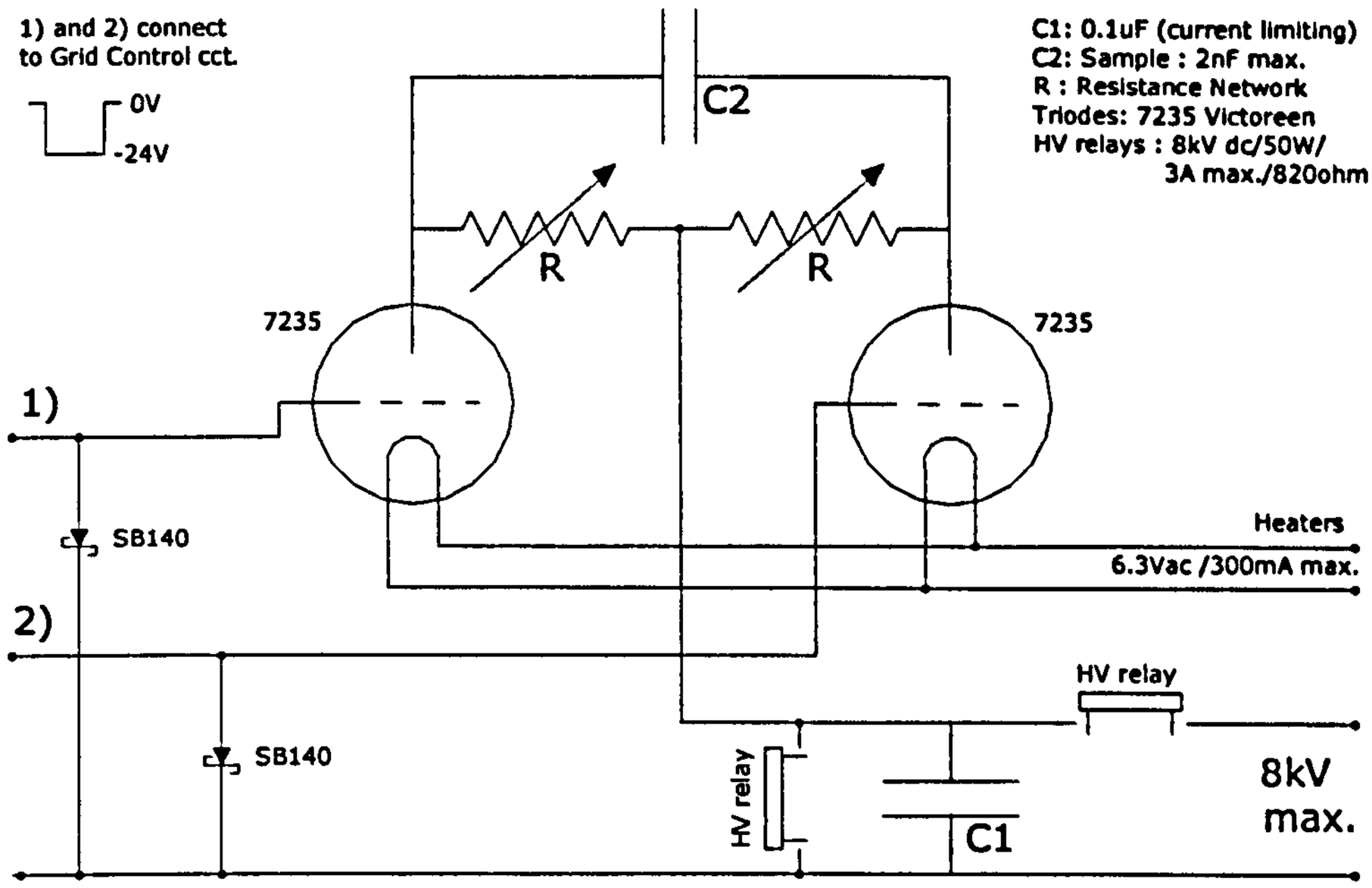

Figure B1: Structured Composites Processing Unit - High Voltage Switching Circuit.

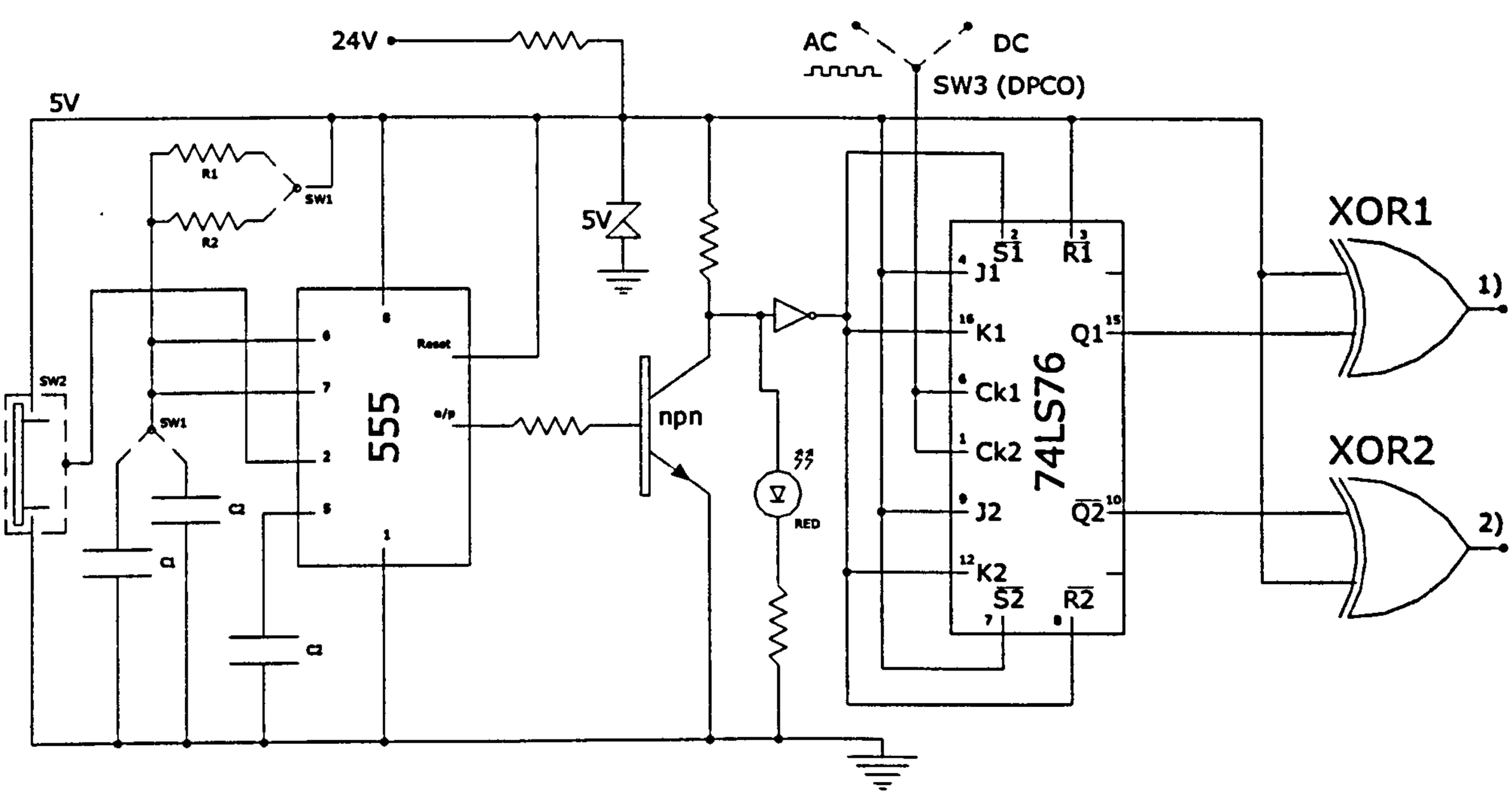

Figure B2: Structured Composites Processing Unit - Grid Control Circuit.

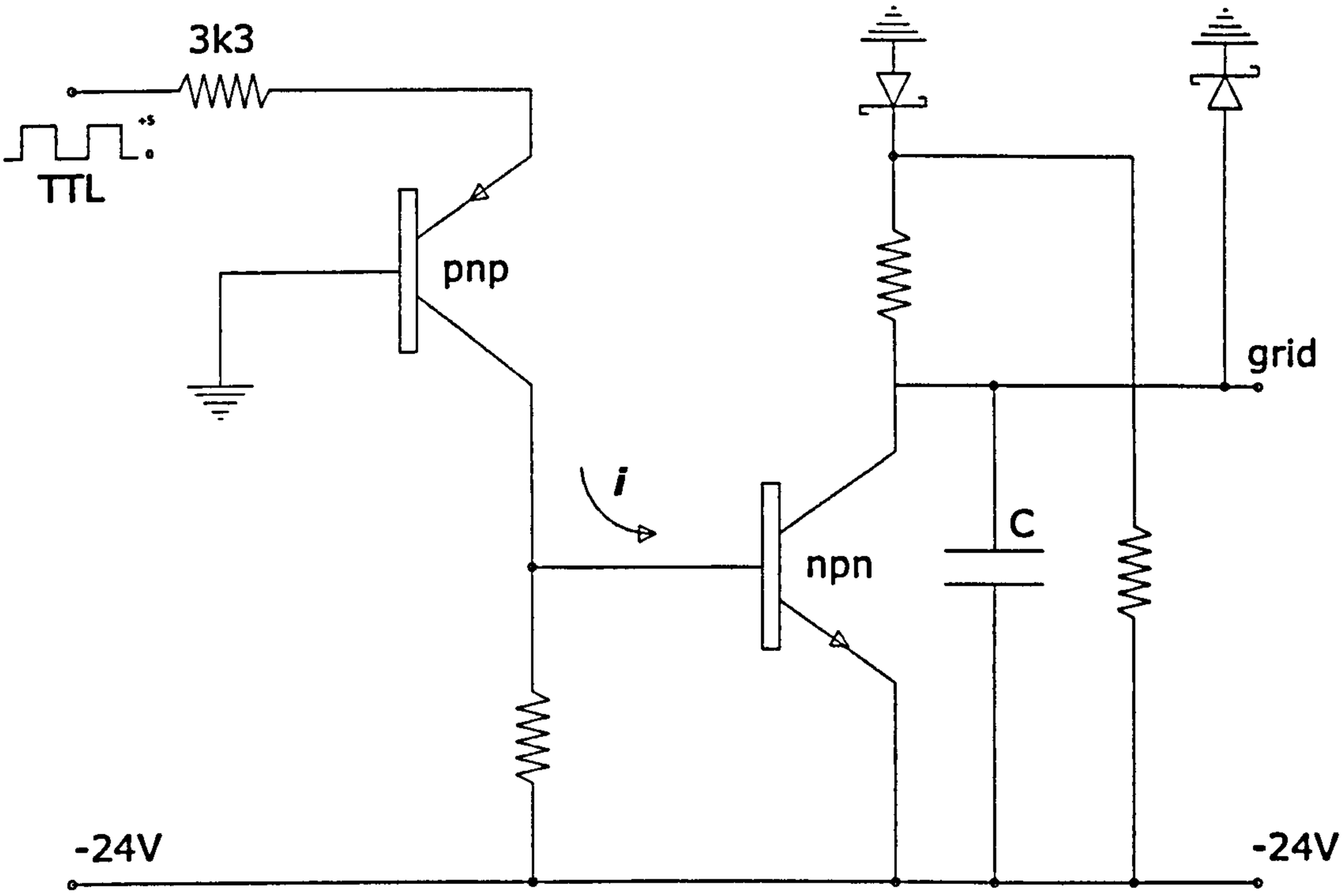

Figure B3: Structured Composites Processing Unit - Grid Triggering Circuit.

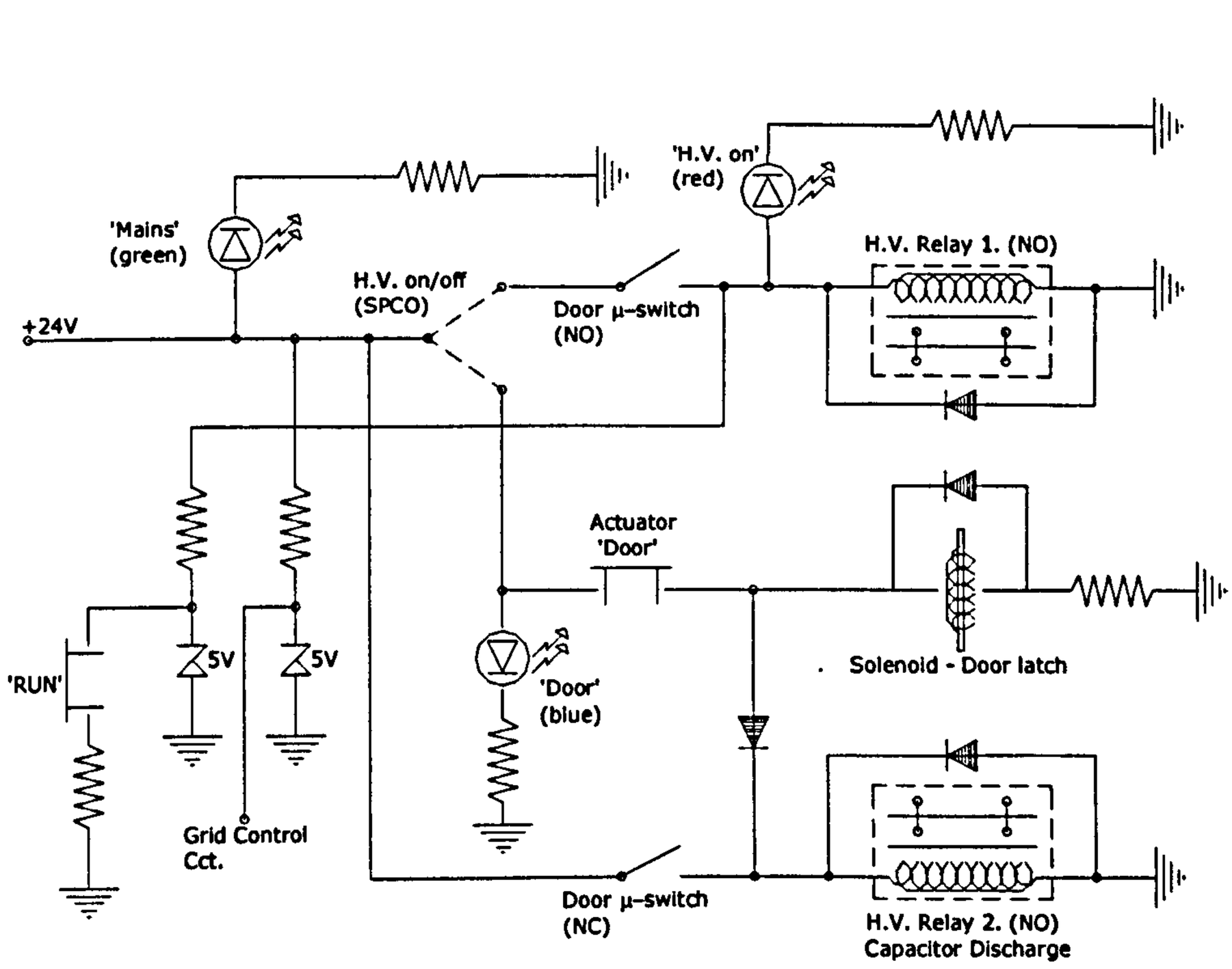

Figure B4: Structured Composites Processing Unit - Operation and Safety Switching Circuit.

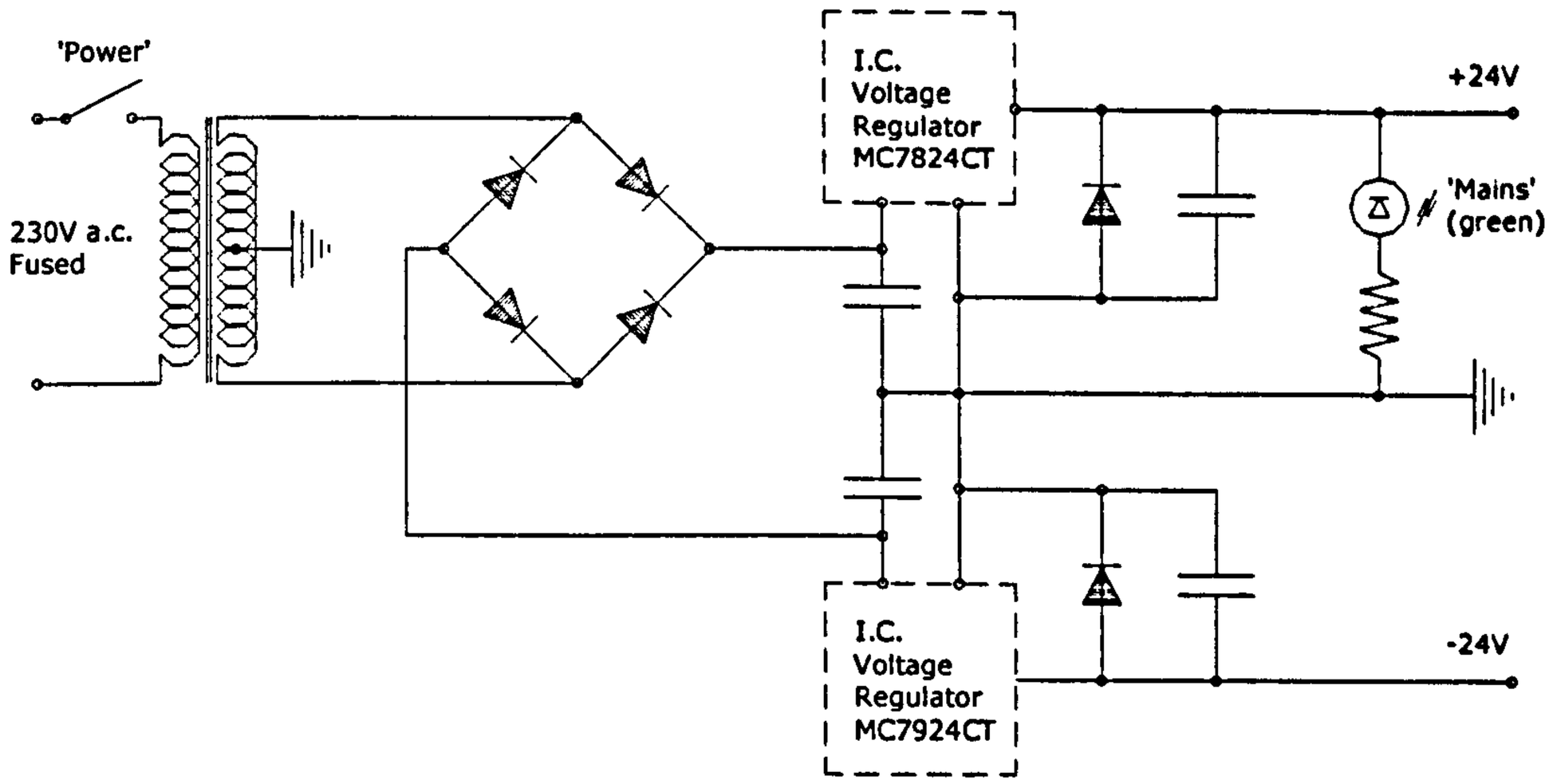

Figure B5: Structured Composites Processing Unit - Split Low Voltage Power Supply Circuit.

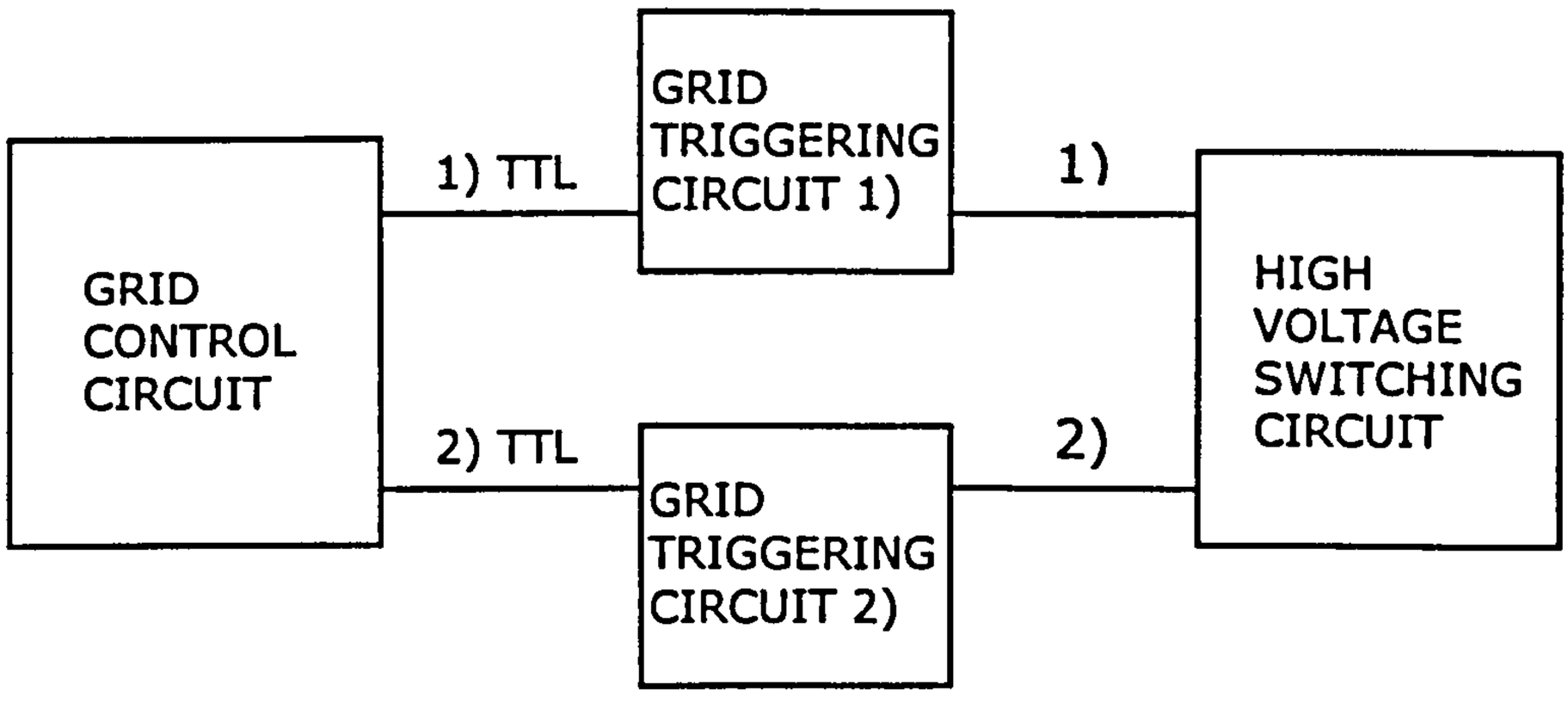

Figure B6: Structured Composites Processing Unit - Block Diagram Interconnection.

Appendix C.

GenRad 1689M Precision RLC Digibridge

The RLC Digibridge is a microprocessor-controlled test unit, which utilises a phase sensitive detector to measure the voltage across a DUT (device under test). To do this, the test circuit places the DUT in series with a standard internal resistor, such that both carry the same current. The phase sensitive detector then generates four reference signals, at precise 90° intervals, which are compared against a test signal. The vector components of the voltage across the DUT and the standard resistor are measured and are used to calculate the unknown impedance. The unit allows the operator to select any one of 503 preprogrammed frequencies in the range 12Hz to 100kHz. A test voltage of 0.005 to 1.275V is also selectable. Different values of the result can be diplayed depending on whether the DUT is represented as a lossy inductor or capacitor or equally if its' equivalent circuit approximates most closely to series or parallel.

Operation

All measurements were carried out at a test voltage of 1V. Prior to measurement the bridge must be 'zeroed'. The resistance of the test circuit and any stray capacitance or inductance, due for example to electrical connections are first evaluated. The unit subsequently subtracts these values from those measured. To do this the open circuit and short circuit values are first measured at 1kHz, with the DUT removed.

Accuracy

The impedances of the internal components are set at the factory calibration frequency of 1Khz and are computed for other test frequencies. These computed values are used in the calculation of any measured value. Manufacturers values for accuracy are given as 0.06% @ 12Hz; 0.04% @ 100Hz; 0.02% @ 1kHz; 0.17% @ 10kHz; 0.34% @ 100kHz. Compensation for variations in ambient temperature cannot be taken into account.

Note: Kijlstra, J. et al, [*Langmuir* 9 (7) pp1625-1633 (1993)] have stated that, at frequencies below 800Hz, this type of unit is not capable of giving reproducible results with a high impedance DUT. A similar view is held by previous workers at Cranfield and confirmed by the U.K. distributor, although they have indicted that satisfactory results are achievable above 150Hz. The problem appears to be that the signal-to-noise ratio at low frequencies can fall below a critical level, such that the test signal cannot be distinguished from the background (eg. thermal noise or Johnson noise). Efforts to isolate the effect and compensate have not been effective. Accordingly, for this work, measurements below 500Hz have been ignored. The quoted results are an average of twenty measurements and have been shown to be reproducible.

Appendix D.

Calculation of effective dielectric permittivity for diphasic composites using simple theoretical models.

Simple expressions for the effective dielectric permittivities of composite materials can be derived by considering the capacitance of the individual phases. Referring to Figure 1.1 (reproduced below) the 1-3 type composite can be thought of as an arrangement of individual capacitors acting in parallel. The capacitance of the composite is then given by the sum of the capacitances of the two phases:

$$C_p = C_1 + C_2 \quad \textit{and therefore} \quad \frac{A.\varepsilon_o.\varepsilon_c}{t} = \frac{n_1.A_1.\varepsilon_o.\varepsilon_1}{t} + \frac{n_2.A_2.\varepsilon_o.\varepsilon_2}{t}$$

where ε_1 and ε_2 refer to the dielectric permittivities if the matrix and the included phase respectivly; n_1 and n_2 denote the numbers of individual elements of the two phases; A_1 and A_2 are the cross-sectional areas of the two types of element. Hence it can be seen that, *for parallel connected phases*, the effective dielectric permittivity of the composite (ε_c) has the form:

$$\varepsilon_c = V_1\varepsilon_1 + V_2\varepsilon_2$$

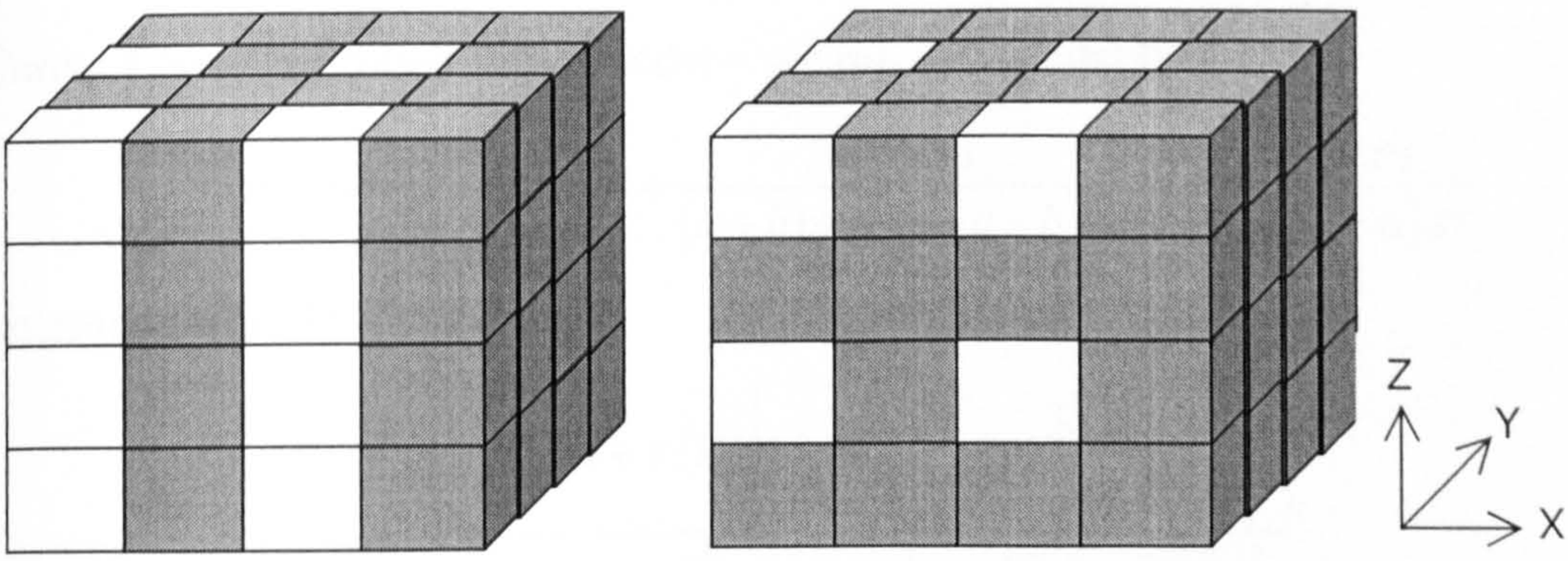

Figure 1.1 Schematic diagram of 1-3 type (left) and 0-3 type connectivity patterns for two-phase composites (see note).

Similarly, the 0-3 type composite can be thought of as an arrangement of elemental capacitors in series. In this case the capacitance of the composite is taken to be:

$$\frac{1}{C_s} = \frac{1}{C_1} + \frac{1}{C_2}$$

This gives an expression *for series connected phases*:

$$\frac{1}{\varepsilon_c} = \frac{V_1}{\varepsilon_1} + \frac{V_2}{\varepsilon_2}$$

In the current study the parallel and series cases can be taken to be a first approximation for the upper and lower bounds of the dielectric permittivity of the model composite system. Some more of the common theoretical models are listed below:

Maxwell [73]:

$$\varepsilon_c = \varepsilon_1 \left(\frac{2\varepsilon_1 + \varepsilon_2 + 2V_2.(\varepsilon_2 - \varepsilon_1)}{2\varepsilon_1 + \varepsilon_2 - V_2.(\varepsilon_2 - \varepsilon_1)} \right)$$

Lichtenecker (Logarithmic) [111]:

$$\log \varepsilon_c = V_1.\log \varepsilon_1 + V_2.\log \varepsilon_2$$

Yamada (Energy model) [112]:

$$\varepsilon_c = \varepsilon_1 \left(1 + \frac{n.V_2.(\varepsilon_2 - \varepsilon_1)}{n.\varepsilon_1 + (\varepsilon_2 - \varepsilon_1).V_1} \right)$$

Banno (Modified cubes model – see ref. for details) [113]:

$$\varepsilon_c = \frac{a^2.(a + (1-a).n)^2.\varepsilon_1.\varepsilon_2}{a.\varepsilon_1 + (1-a).n.\varepsilon_1} + \left(1 - a^2.(a + (1-a).n)\right).\varepsilon_2$$

Garner ('New' modified cubes model – see ref. for details) [20]:

$$\varepsilon_c = \left(1 - a^2 - 2ab\right).\varepsilon_1 + \frac{a^2.\varepsilon_1.\varepsilon_2}{(a+b).\varepsilon_1 + (1-a-b).\varepsilon_2} + \frac{2ab.\varepsilon_1.\varepsilon_2}{a.\varepsilon_1 + (1-a).\varepsilon_2}$$

Jayasundere [114]:

$$\varepsilon_c = \frac{\varepsilon_1.V_1 + \varepsilon_2.V_2.\left[\frac{3\varepsilon_1}{(\varepsilon_2 + 2\varepsilon_1)}\right].\left[1 + \frac{3V_2(\varepsilon_2 - \varepsilon_1)}{\varepsilon_2 + 2\varepsilon_1}\right]}{V_1 + V_2.\left[\frac{3\varepsilon_1}{(\varepsilon_2 + 2\varepsilon_1)}\right].\left[1 + \frac{3V_2(\varepsilon_2 - \varepsilon_1)}{\varepsilon_2 + 2\varepsilon_1}\right]}$$